AGARD-CP-392

AGARD-CP-392

AGARD

ADVISORY GROUP FOR AEROSPACE RESEARCH & DEVELOPMENT

7 RUE ANCELLE 92200 NEUILLY SUR SEINE FRANCE

AGARD CONFERENCE PROCEEDINGS No.392

Interior Ballistics of Guns

NORTH ATLANTIC TREATY ORGANIZATION

DISTRIBUTION AND AVAILABILITY
ON BACK COVER

C

NORTH ATLANTIC TREATY ORGANIZATION

ADVISORY GROUP FOR AEROSPACE RESEARCH AND DEVELOPMENT

(ORGANISATION DU TRAITE DE L'ATLANTIQUE NORD)

AGARD Conference Proceedings No.392

INTERIOR BALLISTICS OF GUNS

Papers presented at the Propulsion and Energetics Panel 66th (B) Specialists' Meeting,
held in Florence, Italy, 9—11 September 1985.

THE MISSION OF AGARD

The mission of AGARD is to bring together the leading personalities of the NATO nations in the fields of science and technology relating to aerospace for the following purposes:

— Exchanging of scientific and technical information;

— Continuously stimulating advances in the aerospace sciences relevant to strengthening the common defence posture;

— Improving the co-operation among member nations in aerospace research and development;

— Providing scientific and technical advice and assistance to the North Atlantic Military Committee in the field of aerospace research and development;

— Rendering scientific and technical assistance, as requested, to other NATO bodies and to member nations in connection with research and development problems in the aerospace field;

— Providing assistance to member nations for the purpose of increasing their scientific and technical potential;

— Recommending effective ways for the member nations to use their research and development capabilities for the common benefit of the NATO community.

The highest authority within AGARD is the National Delegates Board consisting of officially appointed senior representatives from each member nation. The mission of AGARD is carried out through the Panels which are composed of experts appointed by the National Delegates, the Consultant and Exchange Programme and the Aerospace Applications Studies Programme. The results of AGARD work are reported to the member nations and the NATO Authorities through the AGARD series of publications of which this is one.

Participation in AGARD activities is by invitation only and is normally limited to citizens of the NATO nations.

Published January 1986

ISBN 92-835-0388-0

Printed by Specialised Printing Services Limited
40 Chigwell Lane, Loughton, Essex IG10 3TZ

RECENT PUBLICATIONS OF THE PROPULSION AND ENERGETICS PANEL

Conference Proceedings

Testing and Measurement Techniques in Heat Transfer and Combustion
AGARD Conference Proceedings No.281, 55th *A* Meeting, May 1980

Centrifugal Compressors, Flow Phenomena and Performance
AGARD Conference Proceedings No.282, 56th *B* Meeting, May 1980

Turbine Engine Testing
AGARD Conference Proceedings No.293, 56th Meeting, Sep/October 1980

Helicopter Propulsion Systems
AGARD Conference Proceedings No.302, 57th Meeting, May 1981

Ramjets and Ramrockets for Military Applications
AGARD Conference Proceedings No.307, 58th Meeting, October 1981

Problems in Bearings and Lubrication
AGARD Conference Proceedings No.323, 59th Meeting, May/June 1982

Engine Handling
AGARD Conference Proceedings No.324, 60th Meeting, October 1982

Viscous Effects in Turbomachines
AGARD Conference Proceedings No.351, 61st *A* Meeting, June 1983

Auxiliary Power Systems
AGARD Conference Proceedings 352, 61st *B* Meeting, May 1983

Combustion Problems in Turbine Engines
AGARD Conference Proceedings 353, 62nd Meeting, October 1983

Hazard Studies for Solid Propellant Rocket Motors
AGARD Conference Proceedings 367, 63rd *A* Meeting, May/June 1984

Engine Cyclic Durability by Analysis and Testing
AGARD Conference Proceedings No.368, 63rd *B* Meeting, May/June 1984

Gears and Power Transmission Systems for Helicopters and Turboprops
AGARD Conference Proceedings No.369, 64th Meeting October 1984

Heat Transfer and Cooling in Gas Turbines
AGARD Conference Proceedings No.390, 65th Meeting, May 1985

Smokeless Propellants
AGARD Conference Proceedings No.391, 66th *A* Meeting, September 1985

Working Group Reports

Aircraft Fire Safety
AGARD Advisory Report 132, Vol.1 and Vol.2. Results of WG11 (September and November 1979)

Turbulent Transport Phenomena (in English and French)
AGARD Advisory Report 150. Results of WG 09 (February 1980)

Through Flow Calculations in Axial Turbomachines
AGARD Advisory Report 175. Results of WG 12 (October 1981)

Alternative Jet Engine Fuels
AGARD Advisory Report 181. Vol.1 and Vol.2. Results of WG 13 (July 1982)

Suitable Averaging Techniques in Non-Uniform Internal Flows
AGARD Advisory Report 182 (in English and French). Results of WG 14 (June/August 1983)

Lecture Series

Non-Destructive Inspection Methods for Propulsion Systems and Components
AGARD LS 103 (April 1979)

The Application of Design to Cost and Life Cycle Cost to Aircraft Engines
AGARD LS 107 (May 1980)

Microcomputer Applications in Power and Propulsion Systems
AGARD LS 113 (April 1981)

Aircraft Fire Safety
AGARD LS 123 (June 1982)

Operation and Performance Measurement of Engines in Sea Level Test Facilities
AGARD LS 132 (April 1984)

Ramjet and Ramrocket Propulsion Systems for Missiles
AGARD LS 136 (September 1984)

3-D Computation Techniques Applied to Internal Flows in Propulsion Systems
AGARD LS 140 (June 1985)

Other Publications

Airbreathing Engine Test Facility Register
AGARD AG 269 (July 1981)

THEME

This meeting provided scientists, development engineers and application specialists with a broad overview of advancing technology and experimental techniques in interior ballistics of liquid and solid propellant guns. A comparison of these technologies with interior ballistics of rockets was also drawn.

The meeting was originally be divided into ten sessions, Overview; Liquid Propellant Guns; Characteristics of Solid Gun Propellants; Gun Barrel Erosion; Low Vulnerability Propellant for Guns; Experimental and Test Techniques in Interior Ballistics; Gun Ignition Systems; New Problems in Guns; Traveling Charge Gun Theory; and Comparison of Interior Ballistics of Guns and Rockets. The last session was cancelled.

* * * *

La réunion proposée a permis aux scientifiques se consacrant à la recherche, aux ingénieurs chargés de développements et aux spécialistes des applications d'avoir une vue générale des progrès de la technologie et des techniques expérimentales dans le domaine de la balistique interne des canons à propergol liquide et solide. En outre, des comparaisons ont été établies entre ces technologies et la balistique interne de fusées.

La réunion était à l'origine divisée en 10 séances: Aspect Général; Canons à Propergol Liquide; Caractéristiques des Propergols Solides pour Canons; Erosion Interne des Canons; Propergols pour Canons, à Faible Niveau de Vulnérabilité; Techniques d'Expériences et d'Essais en Balistique Interne; Systèmes de Mise à Feu de Canons; Problèmes Liés aux Canons; Théories du Déplacement de la Charge à l'Intérieur du Tube; Comparaison entre la Balistique Interne des Canons et celles des Roquettes. Cette dernière séance a été annulée.

PROPULSION AND ENERGETICS PANEL

PROGRAMME COMMITTEE

HOST NATIONAL COORDINATOR

PANEL EXECUTIVE

ACKNOWLEDGEMENT

The Propulsion and Energetics Panel wishes to express its thanks to the Italian National Delegates for the invitation to hold this meeting in Florence, Italy, and for the facilities and personnel which made the meeting possible.

CONTENTS

*Issued in classified publication CP 392 (Supplement).

*Issued in classified publication CP 392 (Supplement).
†Discussion only. Paper not available at time of printing.

TECHNICAL EVALUATION REPORT

by

J.M.Frankle
7408 Kalton Court
Baltimore, Maryland 21208
USA

1. SUMMARY

This meeting was intended to provide scientists, development engineers, and applications specialists with a broad overview of advancing technology and experimental techniques in interior ballistics of liquid and solid propellant guns. A comparison of these technologies with interior ballistics of rockets was to have been drawn. The material presented in the 21 technical papers and the discussions which followed these presentations served to accomplish these objectives. The comparison of gun and rocket interior ballistics was limited.

It is concluded that:

- there must be a constant interchange between modelers and experimentalists
- although liquid propellant gun activity is at a high level, much basic work remains to be done before a weapon system, even of the regenerative type, can be developed and fielded
- investigations of mechanical properties of solid propellants must be emphasized to support the efforts to increase the interior ballistic performance of such guns
- development of multi-dimensional, multi-phase, interior ballistics codes will be expensive in terms of money and time
- development of low vulnerability ammunition can be approached in different ways but underlying mechanisms important to countering the same threats must be related
- there is an encouraging balance between research to improve vented tube ignition systems and research to develop new methods, such as lasers
- the good technical progress is being made at an evolutionary rate; no really new ideas for guns with dramatic increases in performance were discussed

It is recommended that:

- cooperative arrangements be explored in the areas of liquid propellant guns; multi-dimensional, multi-phase, interior ballistic codes; and low vulnerability ammunition
- plans be made to hold another meeting on the interior ballistics of guns in 1990

2. INTRODUCTION

Prof. C. Casci, Director of Department of Energy, Milan Polytechnic, Italy, originated the idea for the 66th B Specialists' Meeting on the Interior Ballistics of Guns and his proposal received much support. Although there have been many new developments in interior ballistics of guns, there had been no AGARD symposium in this area for 20 years. Examples of new developments included results from studies of two-phase flow with combustion, properties of materials at high temperature, and mechanical properties of propellants. Prof. Casci

served as Chairman of the Program Committee as well as a Session Chairman.

The meeting was expected to provide research scientists, development engineers, and applications specialists with a broad overview of advancing technology and experimental techniques in interior ballistics of liquid and solid propellant guns. A comparison of these techniques with interior ballistics of rockets was to have been drawn. Ten sessions, with 24 papers were planned and scheduled as detailed in the list of References which is appended to this report. Three papers were withdrawn (Papers 16, 23, and 24). The US work with gun simulators (Paper 16) which paralleled the French studies (Paper 15) was not submitted. Traveling charge gun theory was limited to the French accomplishments (Paper 22) with the US program status, modeling studies, and summary of efforts to obtain safe, fast burning propellants (Paper 23) not provided. Comparison of interior ballistics of guns and rockets was restricted to the comments in Prof. M. Summerfield's overview (Paper 1) with the Italian description of the interior ballistics of closed breech guns, recoilless guns, and rockets (Paper 24) not furnished; consequently, there was no Session X.

3. CONTENTS OF MEETING AND EVALUATION

3.1 SESSION I - OVERVIEW

The overview (Paper 1) by Summerfield, US, contained some observations that were referred to periodically by the presenters that followed. This paper offered mainly speculation; there was no intent to provide technical details. The objectives of his point-of-view were to focus attention on the possibilities for solution of practical design problems through research in propellant combustion and flow processes and to stimulate discussion of the possibilities for innovative experiments and innovative theoretical approaches.

As a preface, Summerfield made the general observation that computer models are accepted in place of factual information when they are but speculation. He stressed the dangers of such assumptions and of the need to redirect efforts to perform clever laboratory measurements to discover the facts.

Eight topics of current interest in interior ballistics were listed and issues of uncertainty were raised; Summerfield had time to touch on only half of these in his presentation but his written paper addresses all of the following:

- Exothermic Gas Phase Reactions Behind the Projectile
- Complexities in the Burning Mechanism of Solid Propellants
- Ignition of Gun Charges with Special Reference to Lasers
- Combustion in a Liquid Propellant Gun
- Sensitivity, Hazards, and Initiation Mechanisms
- Investigations in Zero-Gravity Laboratory
- The Potential for Higher Projectile Velocities
- Nonintrusive Experimental Methods Applicable to Guns

After his litany of observations and concerns, Summerfield closed with a forward look in anticipation of a future meeting at which results of experiments on these various phenomena will be discussed.

3.2 SESSION II - LIQUID PROPELLANT GUNS

US research and development efforts on liquid propellant guns were described (Paper 2) by Morrison as focused on hydroxl ammonium nitrate (HAN) based monopropellants in a regenerative gun. Advantages of HAN-based liquid propellants include efficient logistics, low cost, high volumetric impulse, resistance to ignition unless heavily confined, low toxicity, low vulnerability,

and flexibility in packaging and vehicle stowage. Current studies are concerned with contamination of the liquid propellant and the effects of temperature on both the propellant itself and its interior ballistic behavior.

One of the engineering concepts developed by the General Electric Co. generates an annular liquid jet. Design parameters can be adjusted so that the injection and combustion rates of the propellant balance the volume increases resulting from the motions of the piston and the projectile to produce a flat-top, pressure-time curve.

Muzzle velocity reproducibility was generally poor in experimental firings of 25-mm and 30-mm fixtures and high-frequency pressure oscillations were present. Extensive spectral analysis of the pressure oscillations has not yet provided a full understanding of their origin. Oscillations were also present in 105-mm data but the muzzle velocity standard deviation of 0.33 per cent is a level comparable to that obtained in the 105-mm howitzer with a solid propellant charge.

The primary differences in the four computer models for simulation of interior ballistic performance of regenerative liquid propellant guns are in the way the combustion process and barrel flow are treated. Morrison agrees with Summerfield's asssessment of the lack of knowledge of the droplet combustion process.

In the future, automatic loading, zoning, and control of the ballistic process will be addressed along with the development of durable seals in an effort to achieve a 155-mm brassboard demonstration for an artillery system. If successful, a program to develop a tank gun system will follow.

Melchior presented (Paper 3) the French study of hypergolic liquid bipropellants for guns. These propellants have greater forces and lower flame temperatures than classical propellants. The 30-mm firing system used to test the injection of propellants during combustion had two concentric reservoirs and a differential area piston. Chamber pressure records were essentially smooth with some instabilities of the first tangential mode. Proper redesign of the injector will eliminate these. A series of 12 firings gave a standard deviation in muzzle velocity of 0.4 per cent.

Parametric experimental studies were conducted to optimize the piston area ratio, modify the piston configuration, design for a low temperature effect on pressure and velocity, and test two injector designs.

A digital computer model of the operation of this gun concept was developed. It contained the mechanical details and typical lumped parameters for the interior ballistics part. Calculated performance compares well with experimental. The model was used to calculate the performance for a 155-mm with a specified maximum pressure and muzzle velocity.

The UK liquid propellant gun program is based on the regenerative-injection design and will use a HAN-based monopropellant. Cook presented (Paper 4) the results of experiments to characterize the ignition, combustion, and physical properties of liquid propellants at gun pressures. Otto Fuel II and inert silicone fluid were investigated in these tests as HAN has not yet been developed in the UK. A lumped parameter, liquid propellant gun code is being carefully validated by means of the experimental results.

Results from compressibility tests of silicone fluid, up to 600 MPa, in a new liquid propellant test vessel showed that the bulk modulus increased with the rate of pressure rise. There was also a hysteresis effect which is thought to be due to compression heating of the liquid and of heat transfer to the

vessel. The compressibility of Otto Fuel II was measured at a rate of compression of 140 MPa per ms. It ignited and partially decomposed. The cause was not clear but compression ignition or friction is suspected.

A pyrogen igniter , firing down into bulk liquid propellant, breaks it up into fine droplets and gives good ignition and rapid, complete, combustion. The Force Constant was determined to be 0.833 MJ/kg for Otto Fuel II when a heat loss correction determined for solid propellants is applied.

Liquid ejection tests with silicone fluid showed that there was no difference between the ejection time for a single 2-mm hole and four 1-mm holes. To predict the times with the interior ballistics model required that the orifices be reduced to 80 per cent of the actual diameters, as expected for small, sharp edged, circular orifices.

Following further tests of the compressibility of Otto Fuel II, fast ejection of inert liquid will be investigated. Closed vessel firing tests and compressibility measurements will be made for other liquid propellants as they become available. Vented vessel and 30-mm gun testing will then be conducted with this versatile apparatus. This is not a regenerative injection gun; a solid propellant charge will still be used to drive the piston and inject liquid into the combustion chamber. The UK program is satisfying the need for basic data to improve the computer models.

3.3 SESSION III - CHARACTERISTICS OF SOLID PROPELLANT GUNS

Development of modern propellants and combustible cartridge cases for high performance gun ammunition in Germany was reviewed (Paper 5) by Knobloch. Improvement of gun ammunition includes reduction of erosion, increase of muzzle velocity, reduction of temperature coefficients, reduction of costs, and replacement of propellant charge bag material and metal cartridge cases by better containers including those manufactured from combustible material. Also addressed are improved mechanical properties for propellants, particularly at low temperature, combustible igniters, low vulnerability propellants, modular charges, and unit modules. Charge design for new ammunition for existing systems is of concern as well for new weapons systems.

Approaches include adjusted geometries (19-perforation propellant and rosette grains, for example) and solventless triple base propellant to increase the performance for conventional propellants.

Combustible cases provide for lower weight, lower vulnerability ammunition with the elimination of the spent-case toxicity problem. Combustible igniters have been made for the 120-mm tank gun and other weapons. Typical problems include the need for debris-free combustion and high mechanical strength. A multifelting process has made it possible to deal with these concerns. The composition and porosity can be varied throughout the length and thickness of the combustible case. Mechanical properties can be increased where needed. Erosion-reducing additives can be incorporated in the case.

Considerable work has been done to reduce the temperature gradient usually experienced with hot charges. Propellants with granules of double base propellant in a matrix of single base propellant have been studied. Surface treatment of propellant with silicone oil also produced negative temperature gradients.

New propellant compositions with nitric esters (BTN and MTN) and nitramines (RDX and HMX) were tested. One of the advantages of the new multibase propellant compositions is the avoidance of highly erosive nitroglycerine. Increases in velocity were realized for the 20-mm, 40-mm, and the 120-mm guns.

At the beginning of the 1980s in Germany, some incidents with granular propellant charges led to more intensive studies of the interior ballistics of guns. Pressure waves due to bad igniter functions and their consequences were addressed. One such consequence is the heavy dynamic loading of the propellant grains, especially near the projectile base. Zimmermann described (Paper 6) special test devices which were constructed to simulate the dynamic forces on gun propellant grains during shots at ambient and low (-40 deg C) temperatures. With these devices, the dynamic stress at failure, the type of fragmentation, and other correlated physical characteristics of several propellant types were measured.

For tests under real gun conditions (20-mm, 25-mm, and 105-mm), a total pressure gage, based on a piezoelectric foil, was developed and used in connection with a gas pressure gage to derive grain pressure on the projectile base. A second method for measuring the load on propellant grains was to install strain gages in hollow cylindrical grains made of steel and put them on the projectile base. Grain pressure is decreased by the following factors: lower loading density, larger grains, shorter combustion chambers, lower igniter gas velocity, lower igniter gas pressure (but high enough for good ignition), and higher grain stiffness.

A test device was developed to measure dynamic stress-strain curves for single and multiple grains and to see the grain break-up and fragmentation patterns afterwards. Both longitudinal and lateral compression tests of M30 and JA2 propellants were carried out at loading rates comparable to those experienced in a gun.

Results from the experiments described permit the determination of the safety margin between the maximum stress the propellant grains are subjected to and their stress at fracture under gun conditions. For existing propellants, charges must be designed and assembled to minimize the stress on the grains. New propellants must be tougher at ambient and extreme temperatures.

Parameters which affect the quality of triple base propellant for the 155-39-mm field artillery gun were investigated in Italy. Di Lorenzo described (Paper 7) additional analyses, not in the production specifications, which were conducted to evaluate technological process parameters and nitrocellulose characteristics. These included microscopic examination of the propellant; gel-permeation, high-performance liquid chromatography; closed vessel and interrupted combustion tests; and internal ballistic evaluation by means of computer-aided simulation.

Initially, process parameters were optimized to meet propellant density. A propellant sample, which met all laboratory specifications, was fired in the gun and did not meet the ballistics requirements. Guided by the added analyses listed, more propellant samples, with nitrocelluloses having different characteristics, were manufactured and fired. A nitrocellulose blend of high and low nitrogen content with high polidispersity, high weight and number average molecular weights, gave the best results. Also, propellants which shown burning rate anomalies before 65 per cent burned in closed vessel tests have internal defects that will compromise ballistic acceptance.

3.4 SESSION IV - GUN BARREL INTERACTIONS

A UK theoretical study of the interaction of pressure waves generated during the internal ballistics cycle with the vibrations of a tank gun barrel was described (Paper 8) by Crowley along with the possible effects on accuracy and structural integrity. Both a lumped parameter interior ballistics model and a gas dynamics model were used in the study to provide input forcing functions for the gun barrel vibrations code. Two theoretical guns were considered; one was a

100-mm gun and the second was a heavier 125-mm gun more characteristic of a modern tank weapon. Two propellant charges were selected to give maximum pressures typical of current high-velocity guns and of the next generation of such weapons. Three igniter configurations were used in the gas dynamic model calculations to simulate different levels of pressure waves.

Results showed that the use of a gas dynamics model to calculate the pressure forces on the gun leads to significant changes in the pattern of barrel vibrations. In particular, the muzzle jump may be completely reversed with a consequent effect on accuracy. The higher frequencies excited by pressure waves would probably have an adverse effect on the fatigue life of the gun barrel. It is, therefore, important that gas dynamic effects be considered in future work on gun dynamics.

An investigation of erosion in German high-performance tank gun tubes was discussed (Paper 9) by Krumm. Depending on the type of gun and its particular use, either fatigue or wear determines the useful life of the barrel. For example, the life of the 120-mm smoothbore gun installed in the Leopard 2 Main Battle Tank was limited by wear. Measures were taken to improve wear by effectively coating the bore surface with hard chromium. Very difficult and extensive work resulted in a plating that is able to resist the intense thermal, mechanical, and chemical loads. The wear life of the 120-mm now approaches the fatigue life. Gun performance and accuracy are almost constant throughout its life.

Very descriptive pictures of the bore of the 120-mm were shown to illustrate types of chrome plating failure. Crumbling, excavation, spalling, thermal shock cracks, melting of the chrome surface, blistering, chipping, and large scaling with cavitation were all seen. The bore area at the fume extractor was a critical location.

Erosion, ammunition cookoff, and gun tube bending and strength are all strongly dependent on bore surface temperature and heat transfer. Fast response, 1-microsecond, eroding thermocouples were described (Paper 10) by Lawton who also presented typical results from measurements made during 40-mm gun firings in the UK. The thermocouples, which are available commercially, can tolerate up to 3 mm wear and pressures up to 2000 bar. It is to be noted that high-performance guns operate at two to three times this maximum pressure. They will withstand steady state temperatures of 600 deg C and flash temperatures of 1500 deg C.

The temperature begins to rise before the projectile clears the thermocouple. Lawton feels that gas leakage past the shot is more likely to have caused this observation than friction. While he points out that an improved design of the driving band may reduce barrel erosion due to the gas leakage and subsequent temperature rise, no tests with obturators were carried out to verify the hypothesis.

A simple theory is proposed for calculating the maximum bore temperature and the total heat transfer and this theory is validated by measurements on 14 different rounds made up by using three propellants and various charge masses and grain geometries.

3.5 SESSION V - LOW VULNERABILITY PROPELLANTS FOR GUNS

The status of the US Low Vulnerability Ammunition (LOVA) program was outlined (Paper 11) by Rocchio. It became apparent in the early 1970s that the most effective way to defeat an armored vehicle, particularly a tank, was to initiate the gun propellant in on-board ammunition stores. After defining the

primary threat (behind-armor-spall generated by the penetration process for shaped charge and kinetic energy warheads) faced by M60-series tanks and their ammunition, the dominant physical mechanism (conductive thermal ignition) involved in the initiation process was determined. Compartmentalized ammunition storage in the M1 and M1A1 tank systems changes the focus to reduction of the potential for cook-off and warhead-propelling charge coupling.

The current LOVA propellant formulation, which is in the final stages of development for the 105-mm tank gun, is 76-per cent RDX, 12-per cent cellulose acetate butyrate polymer system, 8-per cent acetyl triethyl citrate plasticizer, and 4-per cent nitrocellulose. This first generation LOVA is producible and provides acceptable interior ballistic performance for the standard 105-mm HEAT and APFSDS cartridges. Variability matches that of the M30 propellant it replaces now that an improved primer has been developed.

High-energy LOVA propellants (HELOVA) are being developed for use in 120-mm ammunition and the higher performance 105-mm ammunition under development. Research goals are energetic polymers and plasticizers, improved mechanical properties, and better processing characteristics. Initial members of this second generation of low vulnerability formulations have given good results in recent tests.

The French program on desensitization of propelling charges was covered (Paper 12) by Mesnil. As recognized by Rocchio in his paper, tank vulnerability can be significantly reduced by decreasing the ammunition vulnerability. Whereas US LOVA propellant consists of an energetic material in an inert matrix, the French desensitized charges are composed of energetic propellant in an inert foam matrix. Since there are lots of spaces between the 19-perforation grains in 105-mm charges, single perforation propellant is added and the remaining space is filled with a binder.

Tests were conducted by firing shaped charges through armor plate into a propelling charge backed up by a lead witness plate. Photodiodes were inserted at three locations in the charge to attempt to measure the reaction rates. A conventional, bulk loaded charge detonated as shown by case fragments in the lead plate. There was no reaction when the desensitized charge was subjected to the same test procedure. The jet went right through the cased charge. No rate data were obtained due to the lack of a reaction. In the two repeat shots with the same residual jet energy, there were low level rates recorded but their meaning is uncertain as there were no reactions. The test was continued by decreasing the armor thickness until detonation of the desensitized charge resulted. The threshold of the detonation energy for the ammunition was increased from 10 kJ for a conventional charge to over 40 kJ for a desensitized charge.

The interior ballistic performance of the desensitized rounds was preserved and the temperature behavior of such charges was examined. Differences in maximum pressures of the two gages used were cited as small and indicative of low pressure waves. This was clarified later when it was explained that point-by-point differences between the two pressure-time records showed no negative differences.

3.6 SESSION VI - EXPERIMENTAL AND TEST TECHNIQUES IN INTERIOR BALLISTICS

Thermal stress cycling during firing constitutes a major mechanism for erosion, wear, and fatigue in gun barrels. Three computer models were coupled to provide for the prediction of spatial and temporal temperature distributions at the inner surface of and through the barrel wall and in the gas dynamic flow of the interior ballistic cycle. These models are described (Paper 13) by The along with the results from preliminary experimental firings of a caliber 0.50-in. gun in the Netherlands.

A one-dimensional, heat conduction model is used to calculate the temperature distribution in the barrel wall. It was validated by comparison with published 20-mm data. After matching the temperature-time profile at the depth nearest the barrel surface, the code predicts the distributions at other depths very well. The core flow is calculated with a one-dimensional, two-phase gas dynamic model. This does not treat ignition and flame spreading; the calculation is started at a relatively high pressure (80 MPa in an example which has a maximum pressure of 310 MPa). Heat loss is accounted for by adjustment of mass, momentum, and energy after the boundary layer calculation at each time interval. The boundary layer model is two-dimensional, quasi-two-phase, viscous, compressible, and turbulent. Coupling is complex since the different numerical solution methods have different stability criteria.

Comparison of measured and calculated results gave encouraging agreement according to the authors. However, maximum pressure agrees because it is matched; calculated pressure-time after maximum pressure is much higher than measured and the 7-per cent higher calculated muzzle velocity follows. The calculations start after the most meaningful early portion of the pressure difference-time profile. Future work on ignition, flame spreading tube emptying, and experimental measurements should improve the code which is at a relatively early stage of development.

Belgian research in heat transfer and the cook-off phenomenon in a small caliber weapon was discussed (Paper 14, Part One) by Meymans and then, in Part Two of the same paper, Celens presented results of studies of a thermodynamic model, powder parameters from closed vessel tests, and the ignition phenomenon.

Cook-off is defined as an unintended function of the propellant of a cartridge. It results from heat transfer between an overheated barrel or chamber and the propellant. The critical temperature is the highest temperature to which a propellant can be exposed without cooking off. If exposed to a temperature greater than the critical temperature, a propellant will cook-off after an induction time. Induction times and critical temperatures were measured during salvo-firings in a 5.56-mm rifle. A number of different tests were carried out and the results were compared to those predicted by means of a theoretical model. Some extremely difficult experimental methods were used to determine the physico-chemical parameters needed in the model. In tests where the gun was heated by salvo-firings, the temperature distribution in time and space was complex. Special tests were conducted in which the gun was uniformly heated at a fixed temperature by an external heat source. Comparison of theoretical results with these experimental measurements was very good.

Better determinations of the physico-chemical propellant parameters are expected through the use of newly developed equipment. The mathematical model will be further refined by the results of a study of small arms weapons characterized by other geometries and new generation propellants and ammunition.

The thermodynamic model for calculating the interior ballistic performance in small caliber weapons was summarized. Because funds are not available to develop a very expensive model, like a two-dimensional code, a very simple model is being used. There are still problems in obtaining input parameters. A large number of simplifications have been made; for example, there is no relation between breech and base pressure. When bore friction is obtained by fitting to experimental velocity data to get an adjusted projectile mass, the adjustment includes the missing pressure gradient. Celens is interested in hearing from other laboratories concerning his method for deducing muzzle velocity from the times of arrival of the projectile at the several pressure gages. Maximum pressure and muzzle velocity are matched by using propellant vivacity and force as fitting parameters. This was before closed vessel measurements became available for these propellant properties. The predictive power of the model is limited as a result of the simplifications.

A great number of closed vessel tests have been made to obtain good values for force, covolume, and burning rate for various propellants. The universal problems in determining these properties for deterred ball propellants was naturally experienced. To improve the model, the ignition phase is being studied in experiments in a transparent, polycarbonate combustion chamber.

To improve our knowledge of the phenomena associated with the ignition and combustion of propelling charges for large caliber ammunition, three visualization devices have been developed in France. Berthommier described (Paper 15) the gun simulators, the instrumentation used, and presented the results from typical tests. The 105-mm tank gun can be studied with or without a projectile and the 155-mm artillery weapon can be investigated with a projectile. Translucent fiberglass tubes which rupture at 100 MPa and polycarbonate tubes which rupture at 30 MPa make it possible to visualize what's happening in detail. Instrumentation consists of high-speed (8,000 frames/sec) cinematography, flash radiography, strain gages, piezoelectric pressure gages, accelerometers, pressure probes in the projectile, camera velocimetry of the projectile, and a timing system.

In the first test, the performance of a metal primer containing black powder was compared with that of a combustible igniter containing a black powder detonating cord. The simultaneous ignition over two-thirds of the charge, the smooth pressure development with no waves, and the gradual acceleration of the 105-mm projectile are clearly seen for the detonating cord igniter. In the second test, the device without a 105-mm projectile was used to study the differences between simultaneous and programmed ignition of six igniters placed at three longitudinal positions in the charge.

In addition to the demonstrated value for the study of ignition systems, the visualization devices are an important tool for obtaining detailed knowledge of pressures, flame front progression, propellant bed displacement, and projectile motion for use in the validation of interior ballistics computer codes.

Considerable progress has been made in recent years in probing the gun interior ballistic cycle and subsequent muzzle flow dynamics. Klingenberg, Germany, presented (Paper 17) a survey of experimental research capabilities as well as the limitations and constraints encountered in ballistic environments. The experimental diagnostics described were primarly spectroscopic techniques for measuring the temperature and gas velocity in reacting two-phase flows produced by the combustion of both solid and liquid propellants. These techniques were the emission and/or absorption methods, reversal and Abel inversion methods, and laser Doppler spectrometry. In particular, a novel intrusive emission gage technique was described which permitted the thermetric probing of optically thick propellant gases in highly pressurized combustion chambers.

A detailed review of fundamentals of spectroscopy preceded the description of techniques. Temperature measurements made in gun muzzle flash studies, including alkali salt additives for suppression, enhanced the understanding of gun interior and transitional ballistic flows. However, the diagnosis and quantitative characterization of non-equilibrium conditions in chemically reacting muzzle flows and the chemical inhibition of gun muzzle flash is still an unsolved problem. The objective of current work is to investigate two-phase, chemically reacting flows that simulate those in a real gun but which are transparent. A gas gun driven by the combustion of a prepressurized mixture of hydrogen and oxygen diluted with helium is used.

Klingenberg feels that Summerfield's clever experiments are difficult in real gun flows and that nonintrusive techniques fail for in-bore flows. He fully understands and supports the contention that the development of theoretical and computational methods for predicting real ballistic flows must be conducted interactively with experimental investigations.

A UK mathematical model which predicts the flow and heat transfer in a gun barrel was described (Paper 18) by Rhodes. In particular, the model was used to investigate the effects of talcum powder additives in the combustible cartridge case of a 120-mm tank gun. The transient, two-dimensional code, which includes a turbulence model but no combustion capability, was developed to simulate shock tube experiments with clean and dusty flows. Since the model appeared to be well-validated, it was decided to test it in the more complex real gun situation.

Assumptions in the code were unrealistic in some cases. While detailed treatment was included for initial leakage past the driving band and past the forward stabilizer band, a version of the Baer-Frankle lumped parameter interior ballistics code was used to provide the fraction of the propellant and case burned at each point in time. The stick propellant charge and case were assumed to remain in place in the chamber.

The model gives a good prediction of ballistic performance and of heat transfer in the gas and to the wall when no particles were present. The expected magnitude of reduction in heat transfer when particles were present was not predicted and the cooling effect of the particles was even reversed in some calculations. Clearly, much work remains to be done to make this a useful tool for guiding the development of improved erosion-reduction additives.

3.7 SESSION VII - GUN IGNITION SYSTEMS

In recent years, there has been a trend towards steadily rising gun pressures, especially in direct fire weapons, and this has caused many functional problems to arise with conventional vent tube ignition systems. To overcome these problems and to allow the process of gun development to continue, the UK has been carrying out a program of research into a number of novel ignition systems for large caliber guns. Bowden detailed (Paper 19) this program and the results obtained to date.

Spark ignition, laser ignition, and electrical impulse ignition are being explored. Criteria specified for new igniter concepts were a minimum of 250 rounds of repeated ignitions, ignition despite considerable variations in propelling charge location relative to the breech, and capability for igniting charges now in service.

Spark ignition has been shown to be feasible and several ceramic materials have been identifed as promising. Further improvements are being sought with the encapsulation of the insulator/central electrode into a strong metal support. Laser ignition of commonly used gun ignition materials has been demonstrated and Neodynium laser parameters have been established for reliable ignition. A sapphire window design has been defined which is expected to withstand the gun environment and stay debris-free. When penetration of charge containment materials is demonstrated, laser ignition will be the only new igniter being considered that will work with existing charges. In the electrical impulse igniter category, electromagnetic coupling shows much more promise than either capacitive or magnetic coupling.

An overall assessment is that a laser ignition system shows the most potential. This research directly, and apparently successfully, addressed one of Summerfield's concerns. On the other hand, the basic premise that current vent tube ignition systems represent the design limit is challenged by Penner's design which follows.

Modern high-performance cartridges are designed for high loading densities of propelling charges. The requirement for improved primers is a obvious consequence. Following his tutorial on ignition systems, Penner described (Paper 20) a new series of German primers that are suitable for tank gun ammunition with consolidated propellant charges and for ammunition with upgraded performance. An ideal primer must be designed to produce hot matter, transfer it to the propellant, distribute it throughout the propelling charge, and heat the propellant surface up to the decomposition temperature. These steps are discussed in detail and the conclusion is drawn that hot gas primers are unsuitable for use. High flow rate primers are also considered a potential problem since surface layers of nearby propellant grains may be eroded away without heat transfer to the remainder of these grains. The eroded material may undergo a detonative reaction similar to a dust explosion.

The new primers, which contain molded and stacked pellets of boron and potassium nitrate, were designed to avoid the following shortcomings of existing primers: the flame temperatures of ignition fumes is too low, the flow rate is too high, the interior pressure is too high, the time-dependent pattern is too irregular, the mass ratio of gases and condensed or condensable reaction products is not optimal, and the reaction times are not optimal. The primers have been tested without problems in the 105-mm tank gun even with triple-base propellants which are susceptible to brittle fracture at low temperatures. Some additional work remains to be done.

3.8 SESSION VIII- NEW PROBLEMS IN GUNS

Future high-performance guns require propellants capable of developing high pressure while maintaining the integrity of their mechanical and physico-chemical properties. To assure predictible behavior of conventional and nitramine propellants in guns, very high pressure tests must be conducted in manometric bombs. Comparisons between theoretical calculations and experimental measurements of the maximum pressures in these tests showed discrepancies of as much as 50 per cent at 1500 MPa. Samirant, France, described (Paper 21) the efforts to determine the causes for these large divergences.

Three laboratories in France and Germany carried out a series of pressure measurements in the 400-650 MPa range in their different bombs. The gages were used successively by each laboratory and the same lot of BTu 85 propellant was used. Results were perfectly comparable but the measured maximum pressures were 17 per cent lower than theoretical values at 600 MPa. Combustion gases were analyzed by mass spectroscoy and chromatography and the measured results were in good agreement with the theoretical calculations. By means of high-resolution laser Doppler velocimetry, the dimensional variations of the bomb were measured during the test, and a purely elastic behavior model was validated. The correction to the bomb volume variation reduced the discrepancy to 8 per cent. US calculations showed that a 3-per cent reduction in molecular radius under pressure was sufficient to make theory and experiment agree. Confirmatory studies of this likely possibility are underway in France. The volume correction has been integrated into the procedure for measuring propellant characteristics in high pressure bombs.

3.9 SESSION IX - TRAVELING CHARGE GUN THEORY

The traveling charge concept seems attractive for obtaining very high projectile velocities (greater than 2 km/s) as it makes it possible to reduce the energy losses resulting from the fact that in a conventional gun, the combustion gases must be accelerated as well as the projectile. Very high charge-to-mass ratios are needed to approach such high velocities in a conventional gun. Dervaux discussed (Paper 22) the traveling charge modeling work that has been carried out in France.

A preliminary study with a lumped parameter interior ballistics code demonstrated that extremely high burning rates are needed to achieve the desired effect. Such values, as well as those of the pressure variation which takes place in the combustion area of the traveling charge, will induce extremely high interior stresses in the solid propellant grain. These may well be greater than the propellant can withstand and combustion is likely to take place as the propellant is fragmented. Therefore, it was necessary to modify a one-dimensional, two-phase code to deal with the traveling charge concept.

Calculations were carried out for a 30-mm weapon. As expected, pressure and velocity distributions were very much different than those for conventional guns. The kinetic energy of the gases was calculated to be much lower than for conventional guns. While it is true that these are results from a computer model, Mesnil is confident that the experimental program should be able to be carried out. On the other hand, Summerfield made a somewhat pessimistic assessment of the concept in his overview and the US research on the traveling charge gun concept has been centered on the development of a safe, very high burning rate propellant for years. However, a suitable propellant may now be available.

4. CONCLUSIONS AND RECOMMENDATIONS

Prof. Summerfield's remarks in his opening paper served to provide a framework for modelers and experimentalists to interact. He was probably a bit hard on the interior ballistics modelers but all those in attendance certainly realize that there must be a constant interchange between the two disciplines. The results of one provide guidance and validation for the other. Some papers supported Summerfield's concerns; others described significant achievements in understanding of interior ballistic processes in guns.

Activity in liquid propellant guns is at a high level. However, much basic work remains to be done before a weapon system, even of the regenerative type, can be developed and fielded. Cooperative programs are being carried out between some of the countries. These arrangements should be maintained and others initiated.

High quality investigations of the mechanical properties of solid propellants under gun environmental conditions are being pursued in several countries. The emphasis on increased interior ballistic performance in solid propellant guns requires an attendant acceleration in this area.

It appears that each organization is determined to develop its own multi-dimensional, multi-phase, interior ballistics code. There may be some justification for this but it is an expensive proposition in money and in time. If the code development process serves to teach realism to the researchers involved, it may be worth the price. Intensive interaction between code developers should supported.

Two separate approaches to the development of low vulnerability ammunition were presented. Underlying mechanisms that are important in countering the same threats must be related. Cooperative investigations in these areas of basic understanding are indicated.

Improved vented tube ignition systems for guns are being developed while new methods, such as lasers, are the subjects of considerable research. The balance is encouraging.

The only negative aspect of the meeting was that there was no discussion of really new ideas for guns with dramatic increases in performance. All the good technical progress is being made at an evolutionary rate.

Mr. Zeller, Société Nationale des Poudres et Explosifs, France, made concluding remarks in Prof. Casci's absence. The papers were of an excellent scientific and technical level as were the discussions which followed the presentations. It was clear that this meeting was justified and another one should be held a few years in the future. In agreement with Mr. Zeller, it is recommended that plans be made to hold another meeting in 1990.

INTRODUCTION
INTERIOR BALLISTICS OF GUNS

by

Prof. Corrado Casci
Politecnico di Milano
Piazza Leonardo Da Vinci, 32
20133 Milan
Italy

The interest of AGARD-PEP in interior ballistics problems should not be surprising. Solid propellant burning in rockets and guns features similar physical and chemical properties.

The motivations to propose a Symposium on 'Interior Ballistics of Guns' are the following:

- AGARD has not held a Symposium on this subject since 1966, i.e. 19 years ago.
- There has been considerable technical development in the interior ballistics field in that time, which deserves discussion among engineers, scientists, and users. Two very significant examples are: (a) better scientific and technical understanding of instabilities and consequent gun damage in high muzzle velocity, light weight weapons; (b) development of liquid propellant guns, still on an experimental basis.
- Conventional warfare (non-nuclear, non-strategic) has become an important subject in the military defense of Western Europe.
- Engineering superiority in gun development is essential for the NATO powers, much more than for the Warsaw Pact powers, because of the well-known imbalance of European forces.

Importance of interior ballistics and recent developments of its technology have made obsolete all of the above studies. Indeed, three new factors have entered ballistics theory in the past decade, each having flowed from a stream of science unrelated to interior ballistics:

- First is the detailed treatment of combustion of the solid propellant, including particularly the ignition and flame-spreading phases at the start of the combustion cycle and the associated nonsteady gas flow, all of which have reached an advanced state of development in the field of rocketry.
- The second is the formulation of the dynamical fluid flow equations in two-phase flow form with appropriate relations for the interactions of the two phases.
- The third is what made it possible to incorporate the first two factors, namely, the use of advanced computers to solve the partial differential equations describing the nonsteady two-phase flow system with simultaneous burning of the solid propellant granules. Ballistic theory augmented in this manner with two-phase flow theory and combustion theory has brought new insight to the ballistician.

Moreover, other important problems are related to:

- properties of the materials required to stand high temperatures and chemical erosion;
- performance reliability of mechanical components, in particular in small arms where shooting frequency is very high;
- mechanical problems connected with high energy propellants.

I hope that this meeting, thanks to both the papers presented and the discussions which followed, will answer most if not all of the questions posed by the science and the technique of interior ballistics of guns.

AN OVERVIEW OF SOME SCIENTIFIC PROBLEMS IN THE INTERIOR BALLISTICS OF GUNS

by
Martin Summerfield
President, Princeton Combustion Research Laboratories, Inc.
and
Professor Emeritus, Princeton University
475 U.S. Highway One
Monmouth Junction, N.J.
08852
U.S.A.

SUMMARY

The objective of this overview of some of the current problems of interior ballistics of guns is two-fold, one, to focus attention on the possibilities for solution of practical design problems through research in propellant combustion and flow processes, and two, to stimulate discussion of the possibilities for innovative experiments and innovative theoretical approaches. Therefore, the paper offers mainly speculation rather than a detailed review of factual data and results.

Observations are offered in this paper on eight topics of current interest in interior ballistics. These are (1) The role of exothermic gas-phase reactions in the main flow behind a projectile; (2) Complexities in the burning mechanism of nitrocellulose base and nitramine propellants; (3) The mechanism of ignition of a solid propellant with special reference to the role of radiation as an ignition source; (4) The mechanism of combustion in a liquid propellant gun; (5) Sensitivity of gun propellants, initiation mechanisms, and explosion hazards; (6) Modern nonintrusive diagnostic methods, mainly spectroscopic, and the information obtainable under gun conditions; (7) Investigations that might be performed in microgravity (spacelab) conditions; (8) Speculations as to techniques for achieving high muzzle velocity. We may anticipate that many of the papers in this meeting will dwell on these issues.

PREFACE

One general observation can be made. It seems that the science of ballistics has been altered unconsciously over the past decade by the increasing variety of analytical models that can be solved on a modern computer. In many instances, such computer models are accepted in place of factual information, in spite of the lack of the necessary physical information on which many of the individual equations should be based. If such models or codes were labelled truthfully as speculation, the situation would be harmless, but there is a strong tendency to place a much greater belief in their validity than the few facts would justify. This can be seriously misleading. Adjustable parameters, often included in large numbers in such models, can be adjusted to make a few computed results fit the few available observables. What is needed is a realistic assessment of the assumptions and the redirection of efforts to perform clever laboratory measurements to discover the facts. Modern non-intrusive methods which are also fast offer a means to this end,but the physicists who are responsible for such spectroscopic developments then have to understand what the important questions are. Unfortunately, there is still a great gap between the researches of the gun ballistician and the applied spectroscopists interested in combustion and flow phenomena. This intellectual gap has to be narrowed or closed.

EXOTHERMIC GAS PHASE REACTIONS BEHIND THE PROJECTILE

The main goal of ballistic computation is to predict, in the design concept phase of gun development, before actual firing tests, the muzzle velocity of the projectile for a given propellant charge and the peak pressure in the chamber of the gun. A secondary goal that was not attainable before the advent of modern theories of interior combustion ballistics is to predict or explain pathologies of ballistic performance. Such pathologies usually manifest themselves as anomalous pressure waves or pressure spikes during the peak pressure regime. Prior to 1970, the theoretical framework was based on a lumped combustion process, and the two-phase flow with burning was ignored, even though ballisticians knew that the propellant grains were swept along with the gas flow during the ballistic cycle and that burning took place all along the barrel. After 1970, however, theories that included two-phase flow and burning of granules while traveling down the barrel were developed. These theories, in one-dimensional form, displayed solutions that remarkably exhibited not only the expected muzzle velocities and peak pressures but also the pathologies mentioned above. The most useful form or code, as it was called, was the Nova Code, and it is widely employed today.

Still, the basic theory represented the burning process in a rather simplified form, and admittedly there was scant evidence to support the basic postulates. For example, one important postulate is that the propellant burning process can be described mathematically by the well-known steady-state burning-rate law, the linear rate being proportional to the pressure raised to the nth power. But this is a steady-state law and the gun cycle is very

very non-steady. It was argued that the steady-state law applies nevertheless because the high pressure makes the characteristic time of the thin flame zone very short compared with the characteristic time of the gun cycle. How do we know this? The justifying theoretical argument was based on theories of solid propellant flames that were deduced from experiments with ammonium perchlorate rocket propellants, not for gun propellants made of nitrocellulose or nitramines. In fact, there is abundant contrary evidence that indicates that gun propellants exhibit flames with much longer characteristic times, perhaps long enough even at gun pressures to destroy the steady-state assumption. Unfortunately, because we lack the necessary physical and chemical information concerning such flames, we do not know what else to do. It would be worthwhile to verify the assumption, since it is so fundamental to ballistic theory.

The problem is even more complicated. If the gaseous flame is as slow as the limited evidence suggests, then there is a good possibility that the gas behind the projectile is not all burned, as the Nova Code says. If it were still reacting exothermically, then we might look to the gas as a source of such combustion anomalies as pressure waves and spikes, and not to the solid granules; and we might search for different kinds of remedies in design. Unfortunately, we know nothing about the state of reactedness of the gas that flows in the gun behind the projectile. We can speculate that, if a substantial fraction of the heat release occurs in the gas, there could be instabilities of a type familiar to liquid rocket engineers.

All of these uncertainties in our basic knowledge of the combustion process indicates that there is a need for clever experiments.

COMPLEXITIES IN THE BURNING MECHANISM OF SOLID PROPELLANTS

We have already remarked on the possibility of slow gas phase reactions as a potential source of inaccuracy in the theory of interior ballistics as it exists today. Such slow gas phase reactions can alter greatly the picture of the gas flow behind the projectile and also the response of the burning process to rapid changes in pressure. This is the problem of dynamic burning.

But the burning process in nitrocellulose propellants is further complicated by observations that there are significant sub-surface exothermic reactions in the condensed phase. The present highly developed dynamic burning rate theory, associated by some with the name of Zeldovich, would be invalid for a burning propellant that undergoes significant sub-surface reactions, and we have no other theory or dynamic burning rate law. Mainly, this state of affairs is due to our lack of systematic knowledge from experiments as to the nature of the burning surface region. This could have a profound effect on the ballistic anomalies we mentioned. Perhaps it was simple good fortune that experimental research on burning of solid propellants started with ammonium perchlorate propellants compounded with a non-energetic binder. Early spectroscopic observations revealed that the gaseous flame is very thin and examination of extinguished surfaces revealed that there are no significant subsurface reactions. It was a straightforward matter to make use of these facts to develop today's form of non-steady burning rate theory. What would have happened if we had done our earliest experiments on nitrocellulose base propellants and found thick gaseous flames and extensive sub-surface exothermic reaction? It might have directed theoreticians in a different direction.

The catalog of complexities is not yet complete. We have discussed slow gas phase reactions and sub-surface reactions. We hasten to add erosive burning, a complicated boundary-layer phenomenon. It has been recognized experimentally for at least forty years that cross-flow of hot gas can affect the burning rate by a very substantial amount, perhaps a 20 to 50% increase. Some experiments have even indicated a decrease in burning rate under certain flow conditions. What takes place in a gun chamber? We tend to ignore the erosive burning factor, mainly because we know nothing about it under gun conditions of pressure and flow, and partly because the existing predictive codes can be adjusted to fit the observed pressure-time traces without taking it into account. If we did take it into account, what erosive burning law would we use? Can we simply borrow the erosive burning law painstakingly developed by rocket engineers, mostly with AP propellants at much lower pressures? Even if we accept some correlation equation for the purpose, if we do not know the underlying physical process of combustion and fluid mechanics that causes the observed change in burning rate, can we safely apply it to other situations?

Putting all this together, gas phase reactions in the gun, thick gaseous flames in the burning zone, sub-surface reactions, and erosive burning, we have a picture of a complex subject, made more so by the difficulties of doing fast experiments at very high pressure.

IGNITION OF GUN CHARGES WITH SPECIAL REFERENCE TO LASER IGNITION

The conventional way to ignite a gun charge is to employ an igniter in the form of a bayonet or center-core tube, if it is a large caliber charge, or a small ignition cup in the case of small arms. These work in a manner similar to the ignition system of a solid propellant rocket, that is, the igniter generates hot gas, hot particles, and some radiation, all of which serves to heat the exposed propellant surface and, very important, also to raise the pressure during the first stage of flame. In the rocketry field, it was thought about twenty years ago that a radiation source could be used to measure the energy

flux required for ignition of a propellant, and perhaps the science could be applied to develop a suitable technology, perhaps replacing the bulky powder igniter with a small laser device that would apply the same level of energy flux.

Unfortunately for such hopes, it did not work out that way, and for good reason. A radiation source suffers from several inherent disadvantages, and until ways are found to overcome these disadvantages, either for rockets or for guns, then it will not be practical. Research on the mechanism of ignition, using hot gas sources, radiation sources, and hot wires in contact with propellant disclosed that radiation flux is far less effective than either conductive or convective flux for three reasons: (1) Radiant energy inevitably penetrates the surface of the propellant and thus does not deposit the energy in a concentrated region; (2) Radiant energy may heat the exposed propellant, but the adjacent gas, which has to support the burning process in the gas phase, starts out cold, not hot; and (3) The initial pressure rise associated with the firing of the ignition charge, which assists the ignition of the propellant charge, is unfortunately absent in the case of a laser igniter.

These disadvantages are substantial, and so laser igniters are difficult to reduce to practical use, whether in guns or in solid propellant rockets. Perhaps these disadvantages can be overcome. Research was useful in identifying these processes; it may be possible through fundamental research to find a way around these obstacles.

COMBUSTION IN A LIQUID PROPELLANT GUN

Liquid propellant guns can take one of several possible forms. First of all, the propellant can, by analogy with the most prominent form of rocket motor, be a bi-propellant system, and going further into the analogy, the bi-propellant combination can be either self-igniting or non-self-igniting. The latter requires an auxiliary ignition device. Alternatively, by analogy with a prominent form of gas generator, it can be a monopropellant liquid, instead of a bi-propellant liquid combination. Then, it can be a bulk-loaded design, similar to the earlier forms of liquid propellant gun, and similar also to the conventional solid propellant gun, in which the entire charge is placed in the combustor before the start of the combustion process; or it can be a direct-injection device, similar in principle to the liquid propellant rocket motor. If it is a direct-injection device, it is most likely to be a so-called regenerative type, one in which the required high pressure pumping is achieved by allowing the combustion pressure to act on a movable piston. This scheme of pumping is not the only one possible, but is the one that has been adopted in the USA for development. The principle of direct-injection with regenerative pumping was first patented in the USA by Colin Hudson; the patent has long ago become a public property.

Both types of LP gun, bulk-loaded or direct-injection, depend for their successful operation on rapid combustion, just as the liquid propellant rocket depends on rapid combustion. In the gun, this is aided by the prevailing high pressure of operation, typically 10 or even 100 times greater than that of a liquid propellant rocket. But a distinctly unfavorable feature is the high throughput that is necessary in the direct-injection LPG. For illustration, an LP gun is required to accept an injection throughput rate that is about 20 to 50 times greater than that of the highest performance liquid propellant rocket motor in operation, expressed as flow rate per unit cross-sectional area of the combustion chamber.

As a consequence, the practical problems of the combustion process have outstripped our theoretical understanding. We have a good theoretical understanding of the combustion process of a single droplet burning in a large quiescent atmosphere. We have some understanding of the "weak interaction" process of spray combustion, an array of burning droplets affecting each other. There is some speculative theory of a dense array of droplets burning in an oxidizing atmosphere, so-called group combustion. But in the case of such high throughputs, ca. 2 to 5 kg/sec.-sq.cm., we do not know how to describe the physics even in non-analytical terms. Is the injected liquid in the form of a spray, which would appeal to the theoreticians because it would permit them to apply current theories of droplet combustion to the process, or is it in the form of irregular filaments, or is it more nearly a foam, that is, an inside-out form of spray? We do not know whether all the liquid propellant burns up in the combustion chamber or whether some of the burning liquid travels behind the projectile, burning all the way along the barrel. This question impacts the description of the flow process in the gun barrel: Is it two-phase flow or essentially one-phase, hot burned gas?

These questions have a direct bearing on the design: How to shape the injector, how to decide on the diameter of the chamber, how long to make the barrel, and how to scale up from small-scale bench experiments to a full-size LP gun. Clever diagnostic experiments are required to explore these essential questions. Unfortunately, the mathematical modeling on which we rely for design and for scale-up is far beyond our knowlege of the processes involved.

SENSITIVITY, HAZARDS, AND INITIATION MECHANISMS

Our knowledge of the fundamental processes that govern the sensitivity of gun propellants, explosives, pyrotechnics, and high energy materials in general to energetic stimuli is very rudimentary. On the one hand, we wish to initiate the exothermic reaction as reliably as possible and without the necessity of employing large or complex igniters. On the

other hand, we wish to make these materials as safe as possible against unexpected stimuli, hostile stimuli, or accidental stimuli.

These stimuli can take several forms, either singly or in combination. Heat or elevated temperature can initiate the exothermic reaction, and the material keeps reacting after iniation because it generates its own hot reaction zone or hot products. Shock waves or rapidly applied high pressure can initiate the reaction; in some cases, we believe that the effect is to cause high temperature, so that initiation in this case is really the first case. The effect of friction, either at the interface with another sliding material, or internally in the form of shear, is more obscure; one prominent thought is that such friction is really a form of heating, and so the process really reverts to the first case again. Less is known about the role of intense optical radiation, particularly in the visible or ultraviolet region of the spectrum, where photon energies are comparable to some bond energies. Electrostatically caused sparks are another obscure form of initiation. Impact by fragments or projectiles may involve heat, pressure waves, friction, and internal shear associated with rapid deformation, all at the same time; it is a matter of speculation as to which of these ignition mechanisms is the principal agent to start the reaction.

On a more basic level, we believe that there is no necessary connection between propellant sensitivity and propellant energy or performance, just as in the field of chemical reactions, there is no necessary connection between chemical thermodynamics and chemical kinetics. There are correlations between energy of reaction and some sensitivity index, but these correlations display only a general trend and leave the observer with the belief that there exist many exceptions to the trend. This leads one to believe that we do not understand the basic process of initiation. Physical chemists have only recently begun to investigate the field of shock chemistry, that is, the chemical reactions and the rate processes that occur when a shock wave passes through a condensed medium. It is apparently not as simple as merely the heating effect associated with the rapid compression. Perhaps the change in density causes a change in the forces between molecules that then allows rapid reaction to occur.

At a practical level, gun designers still use a black powder type bayonet primer or a center-core tube igniter filled with black powder or a similar composition. There is some advantage in using such materials. The ignition temperature of black powder is relatively low compared with smokeless compositions, so it starts readily and propagates the flame rapidly; and its products offer a good combination of hot gas, hot solids and intense radiation. Attempts to find alternative ignition materials have been frustrated by our lack of knowledge as to which type of stimulus is important and what level is needed.

An appealing form of ignition would be a light-weight, compact, laser delivering an intense radiation beam on the propellant surfaces to be ignited. It has not worked out in a practical way yet. There are some basic processes in initiation that we still do not understand. The search for low vulnerability propellants has focused on nitramine type mixtures, but we know nothing about why a nitramine is relatively insensitive to heat in spite of its high output of energy. The search for so-called insensitive high explosives has similarly been frustrated by a lack of knowledge of the basic processes involved. Clever experiments are needed, properly aimed at the basic phenomena. It is still a very empirical field.

INVESTIGATIONS IN ZERO-GRAVITY LABORATORY

I invite the audience to speculate as to what research might be done usefully in the field of interior ballistics or gunnery in general in a spacelab or in zero-gravity conditions. The age of utilization of space is here, and we have the opportunity now to make use of the conditions of outer space.

An orbital space lab offers various conditions not readily available in earth-bound laboratories: zero gravity and, through the use of on-board spinning platforms, partial gravity; very high vacuum and correspondingly very rapid pump-out speeds; a wide range of radiations unimpeded by the earth's atmosphere; a sustained high velocity platform; the absence of atmospheric drag, etc. The USA and the USSR have long had orbital laboratory capability, and the European community participates in the space capability of the USA through the operation of its Spacelab, carried into orbit by the Space Shuttle. The costs of experimentation in space are rapidly coming down as experience is gained. The opportunities are thus available.

What can usefully be done in Spacelab or on the Space Shuttle itself? As we ask this question, in order to challenge thought, it should be noted that, for simply zero gravity without any of the other outer space characteristics (ultra-high vacuum, etc.), there exist several free-fall towers in the USA, in Japan, and elsewhere, for short-duration experiments; and for intermediate-durations, there are facilities for high-altitude, arching aircraft flight, employing specially trained pilots and special aircraft equipped as laboratories. The gun research community has not made use of these novel opportunities.

In a gun, the experimental conditions for making measurements are difficult for various reasons, among them being high temperature, high pressure, short duration, and thick steel tubes. But the problem of short duration can, in some cases, be neutralized by the absence of gravity. Nowhere in the analysis of an interior ballistic problem is gravity taken into account; the effect is negligible because of the short time of action.

However, if an idealized experiment is attempted on earth, and if the process is planned because of instrumentation so as to require a significant amount of induction time or observation time, then gravity interferes with the experiment.

One place where gravity would not interfere would be an orbital space laboratory. Thus, a two-phase flow process cannot be performed for detailed study on earth because the granules suspended in the gas flow would tend to settle out; but in a gun there is no settling because the time is so short, and in a space lab there is no settling because gravity is absent. Another example is the effect of cavitation in the rapid liquid propellant flow of an LP gun on the hazard of unwanted explosion in the liquid; duplicating such bubbles and making detailed observations is impossible on earth, where the bubbles rapidly separate from the flow field, but in a space lab, such separations would not occur. As another example, the nature of the combustion process of a solid propellant is determined in part by measurements made on the gaseous flame, but in complex geometries, such flames are distorted by the earth's gravity, thus distorting the results. In a space laboratory, such interference by gravity is eliminated. Buoyancy, a gravitational effect, interferes with certain experiments on radiative ignition; in a space laboratory, there would be no such interference. There are other examples that one might consider.

If the purpose of this conference is indeed to stimulate new thoughts about interior ballistics, the physics, the fluid mechanics, the thermodynamics, etc., then the availability of a novel type of laboratory ought to be considered.

THE POTENTIAL FOR HIGHER PROJECTILE VELOCITIES

Examination of an energy balance for a typical gun reveals that only about one-third of the chemical energy or internal energy released by the combustion of the propellant is transformed into useful kinetic energy of the projectile. Greater fractions of such useful transformation are possible, as in any heat engine, by enlarging certain design parameters, e.g., the pressure can be raised by increasing the charge mass to projectile mass ratio, the volumetric expansion can be raised by increasing the length of the barrel, and so on, but there are practical limits to the various increases. However, several tricks are possible. The most common trick is the sub-caliber munition, which represents a means to impart the same kinetic energy to a projectile of lower average density, thus achieving higher muzzle velocity. For some applications, this trick works very well.

Examination of the losses (about two-thirds of the internal energy of the propellant) shows where it goes, and one of the most difficult problems is to reduce those losses. The thermodynamic loss, heat remaining in the expanded gas, seems insurmountable by any practical improvement in the thermodynamic cycle. The heat loss to the chamber and barrel represents a large fraction of the available combustion energy, about 20% in many instances, but it may require durable, refractory, shock-resistant ceramic liners to minimize this loss. We will continue to observe the efforts of the engineers concerned with internal combustion reciprocating engines, where an identical problem exists; perhaps we will be able to adapt their solutions.

Within the domain of direct chemically energized guns, the traveling charge concept has recently been revived. As an interesting suggestion, it had lain unexploited for about 30 years or more, since the time of World War II and before, when the idea was advanced in the literature. Efforts are being made to see whether this concept can be exploited for higher projectile velocities. It is not clear whether shifting some of the propellant mass from the conventional chamber over to the projectile, in an effort to minimize the loss of driving pressure pushing the projectile, works always to an advantage. It is one form of a rocket-assisted projectile. Much depends on how it is done. Thus, if the additional metal mass required to hold the transported propellant and contain the combustion process is counted as useful projectile mass, then one conclusion can be reached. If this extra mass is considered a penalty, then a different, more pessimistic conclusion can be reached. There is also, in the fluid-mechanical analysis, the question of how the transported propellant releases its combustion gas in the barrel and whether the pressure at the exit of such a device helps significantly the acceleration of the projectile. It is a case of a rocket with high back pressure. In brief, there is a penalty associated with shifting some fraction of the available propellant charge from the chamber to the projectile, but there is a gain at the projectile, which thereby possesses a part of its propulsion in itself. The balance, gain over loss, depends on how it is done. All of these considerations are apart from the problems of regulation of the combustion process to match the gun cycle and the propellant structural problem, which have not been solved.

In brief, the field of interior ballistics of guns is waiting for new ideas. Perhaps the discussions at this meeting will bring forth some useful suggestions.

NONINTRUSIVE EXPERIMENTAL METHODS APPLICABLE TO GUN PROCESSES

Nonintrusive methods of observation of the processes inside a gun can take several forms - photography, spectroscopy, radiometry, magnetism, X-ray shadowgraphy, radioactive tracers, and to a limited degree, conventional pressure gauges and wall thermocouples; but the class of techniques that has developed the most rapidly in the past decade has been the spectroscopic type. The advent of high-intensity laser sources, easily controlled, and tunable in frequency, has revolutionized the field. Before the laser, the use of

spectroscopy was limited to absorption or emission spectral registration, and the determination of details of the combustion and/or flow structure required a kind of laborious tomography, to convert from 2-D to 3-D information. Also before the laser, spectral purity was achieved only by severe reduction of light intensity, which limited the phenomena that could be observed. The laser now provides spectrally pure radiation, narrowly focused, with wavelengths that can be chosen almost at will to excite the target gases in a special way. The availability of high intensities in narrow spectral ranges made possible also the use of Raman type excitation or fluorescence type excitation, with yields of easily measured signal strengths. This made possible spatial resolution not achievable previously, by crossed beam methods. The purity of wavelength made possible also the doppler velocimeter, which makes use of small shifts of wavelength due to particle or scatterer velocity, shifts that ordinarily could not be observable without the spectral purity of a laser.

As these tools became available, the hope has grown that they could be aimed at the pressing problems of combustion and flow of interior ballistics. Some of the more important questions have been indicated in the earlier sections of this paper. But this required advancement of the techniques beyond that ordinarily employed for the study of, for example, the gas turbine combustor. Not only does the gun field require windows to permit observations into the combustor or barrel, or in the laboratory, into a similar high pressure, high flow rate device, but the kinds of questions to be answered demand narrow spatial resolution without loss of accuracy due to the short time of the process and the small diameter of the beam. Intense lasers have made this possible. Spatial resolutions as small as 100 microns and even smaller are now being employed; and measurement times counted in milliseconds are feasible even with such slender beams. It is possible to think now of resolving some of the more important questions mentioned above. For example, are significant exothermic chemical reactions taking place in the flow field of a gun, and what is the spatial distribution of products and reactants in the gaseous layer called the flame surrounding a propellant granule? The processes occurring in the flame boundary layer under erosive burning conditions now become accessible. We can thus look forward with anticipation to some future meeting at which results of experiments on these various phenomena will be discussed.

DISCUSSION

P.Ramette, Fr

You talked about increasing the velocity of projectiles. Could you give us some numerical values of what you feel being realistic as far as the velocity of this projectile in the future?

Author's Reply

The higher velocity, and I mentioned two possibilities in the last section of my paper, is for the sub-calibre munition or the saboted projectile and for the travelling charge. The answer is I cannot offer a number in each case. But, I'm not sure that was the exact question so let me just discuss them for a moment. The travelling charge is an especially complicated problem because there are several factors at work. One factor is that you are moving some of the propellant from the main charge to the travelling charge. That's the equation or the comparison that one is considering. The question is, does it do more good to put propellant from the main charge to the travelling charge than to put more propellant in the main charge? In putting it in the travelling charge, there is an obvious penalty. It increases the weight of the travelling charge, of the travelling projectile. The overall gain, however, that is hoped for, is expected to be two-fold. One is the projectile. It would seem to me that this becomes much more important for high ratios of propellant charge mass to projectile mass, since at these high ratios there is such a loss of pressure in the final stages of acceleration. The answer to the question is that I cannot offer any numbers at this time.

P.Ramette, Fr

My second question is, can you give your opinion on the use of new materials in internal ballistics related to high energy propellants?

Author's Reply

I understand the question is, what is my opinion of the practicality of liquid bi-propellant? Well, I think that the highest practical propulsion is possible today in the solid propellant field with the nitramine-type propellants, RDX and HMX. I think that HMX-type propellants are the highest, not because of energy, but because of low molecular weight, combustion products. There are other ways to get very high speeds but ways to get high speeds depend upon artificial or cumbersome ways like liquid helium or liquid hydrogen for low molecular weight. I don't know of any combustion process that is practical, that is better, much better than the nitramine propellants would allow. In the case of liquid propellant guns, there again the liquids are a possibility. I would suppose that for outer space, space defence, in principle, liquified gases are possible because they could be stored indefinitely in outer space for applications such as Star Wars and so forth. It might be possible for getting a gun based upon a low molecular weight working fluid. Of course, such a gun doesn't provide the energy. The energy has to come so it would be a two-stage gun. I don't know if that answers the question. I talked about propellants. Now, about materials of construction, I have no comment. I have nothing to say as I am not a specialist in such matters. I'm sorry.

LIQUID PROPELLANT GUN TECHNOLOGY

by
W.F.Morrison
J.D.Knapton
P.G.Baer
U.S. Army Ballistic Research Laboratory
Aberdeen Proving Ground, Maryland 21005-5066, USA

SUMMARY

Research and development efforts on liquid propellant guns have increased steadily in the United States over the past five years as a result of progress in both liquid propellant and propulsion technology. The R&D program in the United States is directed toward the use of hydroxyl ammonium nitrate (HAN) based liquid monopropellants in a regenerative liquid propellant gun. At the same time, efforts to develop liquid propellant gun systems in other NATO countries have also been increased.

HAN-based liquid monopropellants offer a number of advantages over both solid propellants and other liquid propellant formulations. The properties of these materials have been presented elsewhere[1-3], and are only briefly reviewed in this paper.

The regenerative process is based on the injection of propellant into the combustion chamber during the ballistic cycle.[4] The interior ballistic process is summarized here to provide a basis for the discussion of experimental gun firing data. A simple inline piston with multiple cylindrical injectors is used as an example in this discussion, however, the fundamental process described should not vary with injector configuration.

Regenerative investigations in the United States have focused on annular injection configurations, in which the propellant enters the chamber in the form of an annular sheet. A simple version of this configuration has been built and tested in 25mm, 30mm, and 105mm. Ballistic data from these tests are presented, along with discussions of ballistic repeatability and efficiency.

Four different computer models of the regenerative interior ballistic process have been developed in the United States. These models differ primarily in the way in which the combustion process in the chamber is handled, and the way in which the barrel flow is modeled. A comparison of these models is presented, along with parametric calculations made using one of these models.

1. LIQUID PROPELLANTS

A single class of liquid monopropellants has been the primary focus of propellant research in the United States over the past ten years[1,2]. These propellants all consist of hydroxyl ammonium nitrate (HAN), water, and an organic amine nitrate. Typical formulations for liquid gun propellants (LGPs) of this class are provided in Table 1, where TMAN is trimethyl ammonium nitrate, and TEAN is triethanol ammonium nitrate. At present, the LGPs 1845 and 1846 are the primary candidates for future fielding.

TABLE 1. Properties of Typical Liquid Monopropellants.

ORGANIC AMINE LGP	NITRATE	HAN WT %	WATER WT %	DENSITY WT %	IMPETUS (g/cc)	FLAME (J/g)	TEMP (K)
1776	TMAN	19.3	60.8	19.9	1.39	961	2600
1845	TEAN	20.0	63.2	16.8	1.46	973	2730
1846	TEAN	19.2	60.8	20.0	1.42	935	2570
Otto-II*					1.23	866	1986

* Otto-II is not a HAN-based propellant. Its formulation is 1,2 dinitroxypropane 76%, di-N-butyl sebacate 22.5%, and 2 nitrodiphenylamine 1.5%.

In addition to the traditional benefits of liquid propellants, such as efficient logistics, low cost, and high volumetric impetus, the HAN-based LGPs offer a number of improvements over propellants considered in the past, particularly in the area of safety. These materials are very difficult to ignite unless heavily confined. They do not deflagrate under ambient conditions when ignited, but rather decompose slowly in a fizz mode, releasing only a portion of their available energy. The vapor pressure of the liquid is low, and due entirely to the water component of the mixture, thus eliminating a source of both flame and toxicity hazards inherent in many other liquid propellants.

Being a concentrated nitrate salt, the liquid is moderately toxic when ingested, however, the effects are readily reversible. Additionallly, these liquids pose no corrosion hazard to skin. The HAN-based liquid propellants also appear to offer material vulnerability characteristics comparable to the LOVA propellants, plus flexibility in packaging and vehicle design which may be used to further reduce system vulnerability.

HAN-based propellant studies in the United States are focusing on two key issues; contamination of the liquid propellant, and the effects of temperature on the both propellant itself and its ballistic bevavior.

All liquids are inherently more subject to contamination than solids. Many liquid propellants or liquid propellant components have oxidizing properties, and, therefore, introduce the additional issue of material compatibility. HAN is an oxidizing liquid, and as such is incompatible with certain metals. There are two basic approaches to resolving the contamination issues in liquid propellants; eliminate the source of contamination through proper packaging and handling of the propellant, and include additives in the propellant formulation which will counteract the effects of contamination. Both approaches are being pursued in the development of the HAN-based liquid propellants. Additionally, information on material compatibility is being developed to provide engineers a selection of suitable materials for design efforts.

Military systems are required to operate over a wide range of temperatures. Conventional solid propellants exhibit a ballistic temperature coefficient, which results in the variation of maximum chamber pressure and muzzle velocity with temperature. This variation can be extreme under certain conditions or in certain gun systems, occasionally leading to catastrophic results. In the absence of experimental data, an analogous behavior is anticipated for liquid propellants. Therefore, both characterization of the liquid propellants (chemical and physical) over the temperature range of interest, and ballistic testing are underway to explore this issue, and resolve any problems which are encountered.

2. THE BASIC REGENERATIVE PROCESS

A simple regenerative liquid monopropellant gun is depicted in Figure 1. It consists of a standard gun tube attached to a chamber which contains the regenerative piston. The head of the regenerative piston divides the chamber into two sections, a combustion chamber and a propellant reservoir. The length of the reservoir, and thus the reservoir volume and maximum piston travel, are defined by a breech element through which the piston shaft extends. Cylindrical injector orifices are located in the head of the piston. These orifices are initially sealed to prevent leakage of propellant into the combustion chamber prior to ignition. An ignition train, consisting of a primer and a booster charge complete the system.

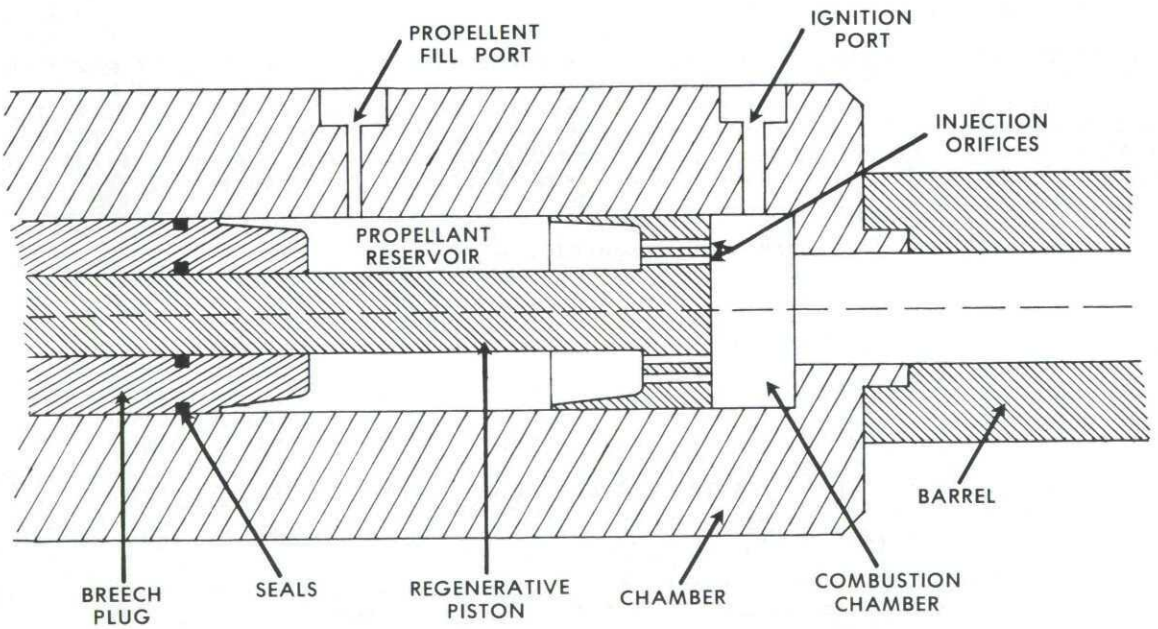

Figure 1. Schematic of a Simple Inline Regenerative Test Fixture.

A characteristic regenerative combustion chamber pressure versus time plot showing the five main phases of the interior ballistic process is presented in Figure 2. The process is initiated by the ignition train, which pressurizes the combustion chamber and forces the piston to the rear, compressing the liquid propellant in the reservoir. The area of the chamber face of the piston is greater than that of the reservoir face, providing the differential pressure required for injection of the liquid propellant.

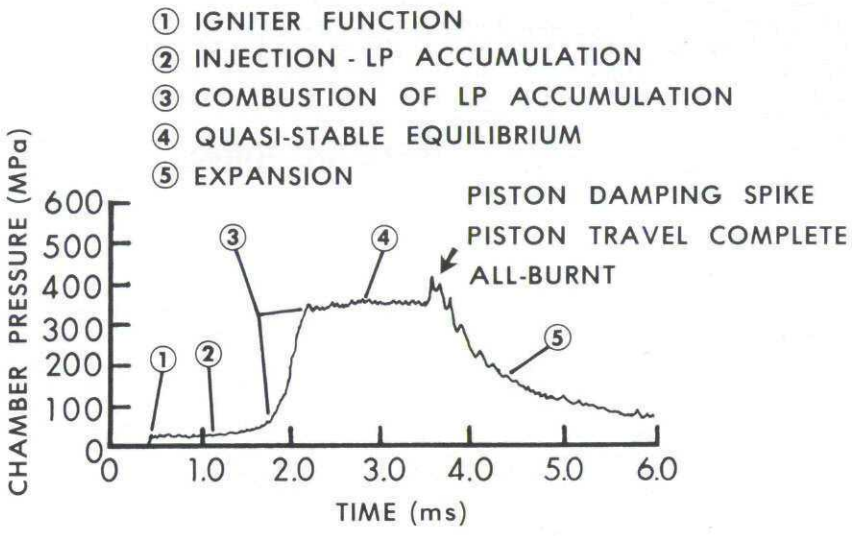

Figure 2. A Typical Regenerative Chamber Pressure vs Time Curve Showing The Five Phases of the IB Process.

The second phase is an ignition delay. During this period, the piston continues to move to the rear, injecting liquid propellant which accummulates in the combustion chamber. When the cool liquid ignites (beginning of phase three), the accummulated propellant burns rapidly bringing the chamber to operating pressure and accelerating the regenerative piston to its maximum velocity. Phase four is usually characterized by a pressure plateau. This plateau is interpreted as a quasi-stable equilibrium in which the increase of gas in the chamber (to compensate for piston motion) and the flow of gas down the barrel are balanced by the combustion of freshly injected propellant. Phase four ends at the completion of piston travel and propellant burning. The final phase is the usual expansion of the combustion gasses after all-burnt.

3. RECENT EXPERIMENTAL TEST RESULTS

In this section, we describe an advanced RLPG configuration, and present a summary of data from regenerative test firings using that configuration . Data is presented from firings using both Otto-II and HAN-based monopropellants. Only firings in regenerative fixtures utilizing Concept VI designs, shown in Figure 3, are reported. Most test firings to date utilizing this design have exhibited high frequency pressure oscillations. These oscillations are briefly discussed in this report. The Concept VI design is not practical for military application, however, advanced variants of this concept which would have practical application are currently under development. The high frequency oscillations have been reduced or eliminated in certain of these advanced concepts.

REGENERATIVE GUN CONFIGURATION

A practical mechanization of the regenerative process must meet several requirements. There must be a convenient means for projectile loading, and for achieving a rapid, ullage free propellant fill. For application in an artillery role, zoning to provide the necessary range coverage, and the ability to tailor interior ballistics (in order to launch munitions of widely varying mass and acceleration sensitivity) are required. A critical aspect of all these issues is the development of seals, with adequate lifetime and durability, for use at a number of internal locations.

The simple mechanization shown in Figure 1 proved to be an ideal test vehicle for studying the regenerative process. Modifications could be made quickly and cheaply, and the simplicity of a single moving element, together with constant propellant injection area, greatly simplified analysis of experimental data. However, this configuration is not suitable for practical applications. It is difficult to seal the injector orifices during propellant fill, and there is no means of programming the propellant injection area. The first problem makes it difficult to achieve rapid, ullage free fill. The latter problem makes it difficult to tailor the interior ballistics to accommodate different payloads.

Numerous regenerative piston configurations have been conceived to address these defects. The configuration designated Concept VI, which was utilized in the gun firings reported here, is shown schematically in Figure 3. Concept VI consists of an inline annular piston and a fixed control rod. The injection piston is a thin cylindrical shell, which is supported by a lubricant and the chamber wall during the ballistic

cycle. The injection area is defined by the opening between the foot of the regenerative piston and the contoured surface of the control rod, which prolvides a simple capability for programming injection area. This piston configuration generates an annular liquid jet. Initially, the foot of the piston contacts the control rod forming a seal which prevents leakage into the combustion chamber during the fill cycle and prepressurization of the reservoir. For all Concept VI tests reported here, the initial prepressurization of the LP was 69 MPa.

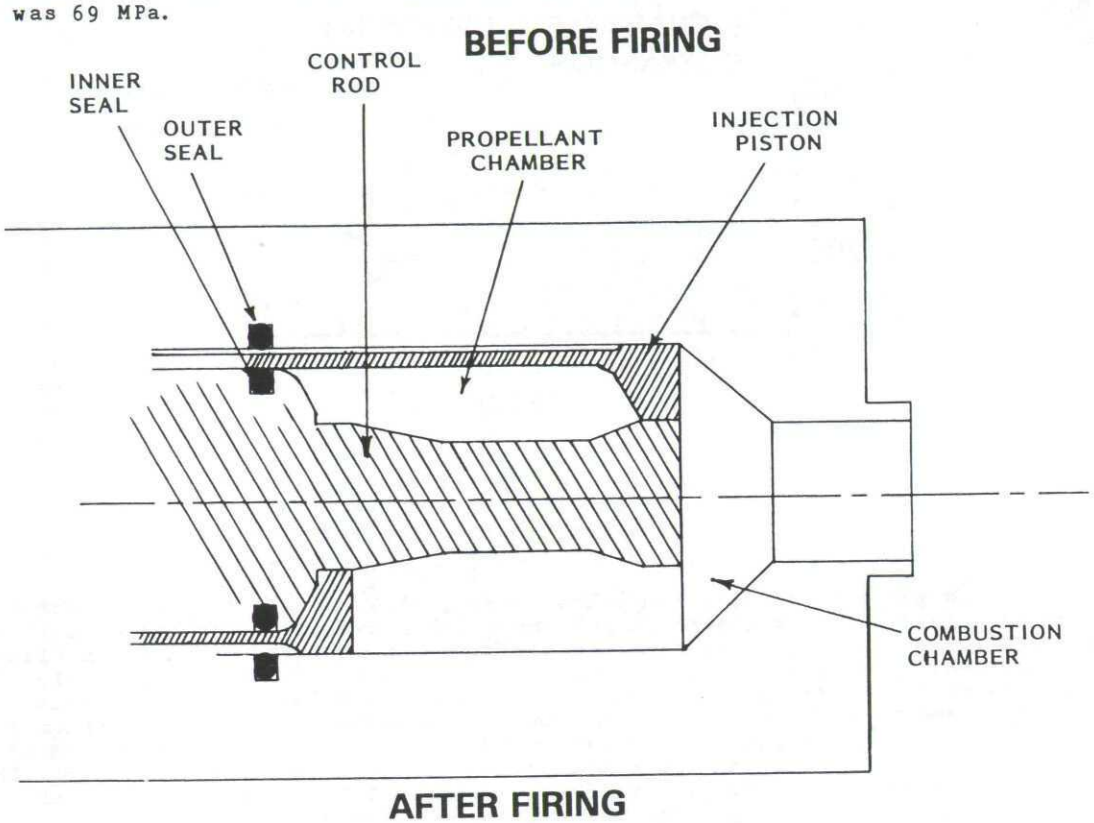

Figure 3. Concept VI, Inline Annular Piston.

The only practical feature embodied in this mechanization is the initial sealing of the injection orifice. One of the primary purposes of this particular concept was the investigation of annular sheet injection. Derivatives of Concept VI, which incorporate all necessary practical features, are currently being investigated. These advanced variants of Concept VI do not depend on contouring of the control rod to tailor injection area. Instead, the motion of the injection piston, and the control rod in variants in which both are free to move, are controlled hydraulically. This technique offers a more effective and sensitive control of the propellant injection rate.

25MM TEST RESULTS

Initial testing of Concept VI was conducted in a 25mm fixture. Chamber pressure and velocity, for an eight round reproducibility series, are summarized in Table 2. The rear and forward chamber pressure gages are located, respectively, 3.72 cm to the rear and 1.33 cm forward of the initial position of the piston face, or 5.05 cm apart. The propellant used for the tests was Otto-II. The mean charge weight was 115.7 g with a

Table 2. Summary of Reproducibility Tests for 25mm, Concept VI.

Test No.	Chamber Pressure Rear (MPa)	Chamber Pressure Forward (MPa)	Velocity (m/s)
202093912	190	157	950.3
202132204	188	166	963.7
202162833	177	161	935.4
203091315	185	159	948.2
203120125	176	161	940.6
203155953	177	154	945.4
204085344	190	162	941.8
204132842	-	-	941.8
Mean	183	160	945.9
Standard Deviation	(3.5%)	(2.4%)	(0.91%)

standard deviation of 0.29 g (0.25%), and the charge to mass ratio was 0.634. The velocity was obtained using a 15 GHz radar, and the accuracy of the data reduction technique is estimated to be no better than 0.5 - 1.0%.

In the 25mm firings, there was no evidence of oscillations below a pressure of 130-140 MPa. The maximum amplitude of the oscillations in the forward section of the chamber are about 6-12% of the maximum pressure, while the maximum amplitude of the oscillations in the rear of the chamber are about twice as large. The dominant frequency of the pressure oscillations in the chamber are in the 50 to 60 kHz range.

Additional 25mm tests were performed to investigate the effect of increasing sheet thickness. For these tests the total injection area was the same as that for the preceding reproducibility test series, however, the sheet thickness was no longer uniform. The non-uniform sheet thickness was achieved by scalloping the center bolt. The amplitude of the pressure oscillations in these tests is larger than observed in the reproducibility group. One test group was particularly interesting, and involved the firing of a projectile with twice the nominal projectile mass. During the decay of the pressure after completion of piston motion, there is an apparent excitation of the acoustical modes in the chamber, as suggested by the occurrence of the higher order harmonics. The first peak in the frequency spectrum occurs at 23.5 kHz and the approximate interval between the peaks is also about 23 kHz. The first radial mode in the chamber, assuming a uniform center bolt and a sound speed of 701 m/s, would be 23.9 kHz. The second radial mode would occur at 44.7 kHz, compared with the observed doublet at 41-44 kHz. Assuming a somewhat lower sound speed, of course, would improve the agreement. The observed frequencies occuring during the pressure decay suggests that some energy is released in the system beyond completion of the piston motion, or that the damping mechanisms in the chamber are negligible.

30MM TEST RESULTS

Test firings were conducted in a 30mm Concept VI fixture with Otto II, LGP 1845, and LGP 1846. The results of these tests are summarized in Tables 3a, 3b, and 3c. The projectile mass was nominally 287 g for these tests, all of which were fired at 2/3 the maximum propellant charge or 160 cc. The initial free volume in the combustion chamber was approximately 95 cc. The maximum pressure at three chamber locations and in the liquid reservoir is presented. The rear most gages, A90 and C30, are located 3.6 cm and 2.1 cm to the rear of the initial position of the piston face, while gage J120 is located 1.2 cm forward of the piston face. As in the 25mm firings, the data would indicate a pressure gradient between the face of the piston and the forward end of the chamber.

Table 3a. Summary of Reproducibility Tests for 30-mm, Concept VI with Otto II.

Test No.	LP	Pressure A90 (MPa)	C30 (MPa)	J120 (MPa)	LP (MPa)	Velocity (m/s)
335:14	Otto-II	174	192	164		939
336:15	Otto-II	-	-	-	-	950
342:13	Otto-II	179	180	144		930
343:12	Otto-II	168	197	179		965
Mean		174	190	162		946
Standard Deviation		(2.6%)	(3.8%)	(8.8%)		(1.6%)

In the test firings with Otto II, Table 3a, the technique for seating the projectile and the initial projectile position at the origin of rifling was varied. This variation might contribute to the poor repeatability in this test series. However, the reproducibility obtained in the LGP 1845 series, Table 3b, was about the same. In this series, the projectile was seated in nominally the same position in each firing. If the apparent outlier (Test No. 364-046) is omitted, the standard deviation in muzzle velocity becomes 0.80%. Furthermore, inspection of the data suggests that it may be divided into two distinct groups with mean velocities of 1005 m/s and 1019 m/s, for which the standard deviations are 0.05% and 0.24% respectively. Currently, there is no satisfactory explanation for this apparent grouping of data.

LGP 1846 testing is still underway, and the number of firings is limited as indicated in Table 3c. Although the statistics are not significant, there would appear to be an improvement in reproducibility.

Table 3b. Summary of Reproducibility Tests for 30-mm, Concept VI with LGP 1845.

Test No.	LP	Pressure A90 (MPa)	C30 (MPa)	J120 (MPa)	LP (MPa)	Velocity (m/s)
364-032	1845	197	190	177	-	1020
364-033	1845	181	181	167	-	1005
364-034	1845	191	190	177	-	1005
364-035	1845	194	186	182	-	1020
364-041	1845	192	189	171	227	1018
364-042	1845	195	181	182	202	1021
364-043	1845	184	177	166	-	1005
364-044	1845	-	-	-	-	1004
364-046	1845	186	178	169	-	973.5
Mean		190	184	174	215	1008
Standard Deviation		(3.0%)	(2.9%)	(3.7%)	-	(1.5%)

Table 3c. Summary of Reproducibility Tests for 30-mm, Concept VI with LGP 1846.

Test No.	LP	Pressure A90 (MPa)	C30 (MPa)	J120 (MPa)	LP (MPa)	Velocity (m/s)
364-16	1846	205	195	190	-	1023
364-17	1846	190	184	184	285	1009
364-31	1846	231	205	213	-	1011
Mean		209	195	196	-	1014
Standard Deviation		(8.1%)	(4.4%)	(6.4%)		(0.6%)

The mean velocity for the eight tests with LGP 1845 (omitting the apparent outlier) and the three tests with LGP 1846 are, respectively, 1012 m/s and 1014 m/s. This close agreement is initially surprising in view of the differences in impetus of the two propellants. The impetuses for LGP 1845 and LGP 1846 are, respectively, 972 and 936 J/g. Despite the 4% difference in impetus, the test firings yield approximately the same performance. It is significant, however, that the maximum chamber pressures for the LGP 1846 series are uniformly higher than those for the LGP 1845 series. LGP 1846 contains approximately 3% more water than LGP 1845, and closed bomb tests have shown that the decomposition rate of LGP 1846 is somewhat slower than that of LGP 1845, particularly at low pressure. Thus it may be hypothesized that during the ignition portion of the ballistic cycle, more propellant accummulates in the combustion chamber in the case of LGP 1846 (due to its lower decomposition rate), leading to a higher maximum pressure and, therefore, a slightly higher muzzle velocity despite its lower energy content.

The pressure data contains high frequency oscillations for all three propellants. The amplitude of the oscillations is larger than in the case of the 25mm reproducibility series. The dominant frequencies occur around 34-35 kHz, however, spectral analysis of this data shows a broad band of frequencies between 32 and 42 kHz. In general, there are no significant differences in these frequencies for Otto-II, LGP 1845, or LGP 1846. The frequency components in the 34-35 kHz range suggest the excitation of the second radial mode in the combustion chamber. The calculated frequency for the second radial mode is between 32.2 kHz and 42.1 kHz for sound speeds between 701 m/s and 914 m/s. However, the data does not contain frequency components corresponding to the first radial mode of the chamber. The amplitude of the oscillations was about 12% of the maximum chamber pressure in the forward section of the chamber and about 20% towards the rear of the chamber. The oscillations began when the chamber pressure reached approximately 90 MPa.

105 MM TEST RESULTS

Test results for the 105mm Concept VI firings have already been reported in References 4-6. A summary of thses results is presented in Table 4. Tests were initially conducted at 1/3 charge, about 900 cc of propellant, using a thinner than normal annular liquid sheet, i.e. a thinner injection gap. The reduced injection area was used to test the combustion efficiency of the annular liquid sheet. The results were satisfactory, and the injection area was increased for subsequent tests. A similar procedure was utilized in 5/8 charge and full charge firings. As indicated in Table 4, the projectile mass varied slightly during the test series. The last 8 full charge firings were conducted under nominally the same conditions. These tests resulted in a mean velocity

of 810.5 m/s with a standard deviation of 0.33%, which is comparable to the muzzle velocity repeatability obtained in the 105mm howitzer.

Table 4. Summary of Test Firings 105mm, Concept VI with Otto II.

Test No.	Charge	Projectile Mass (kg)	C/M	Chamber Pressure (MPa)	Muzzle Velocity (m/s)
1*	1/3	11.2	0.092	117	502.9
2*	1/3	11.2	0.092	103	499.0
3*	1/3	11.2	0.092	110	-
4	1/3	11.2	0.096	103	504.7
5*	1/3	11.2	0.096	124	517.2
6*	5/8	12.5	0.157	193	665.1
7	5/8	12.5	0.157	200	659.9
8	5/8	12.5	0.161	262	662.6
9*	5/8	12.5	0.161	269	658.4
10*	Full	12.5	0.250	221	762.6
11**	Full	12.5	0.250	172	747.7
12	Full	11.2	0.292	124	660.0
13	Full	11.6	0.278	234	808.9
14	Full	11.6	0.278	221	805.0
15	Full	11.6	0.278	255	807.7
16	Full	11.6	0.278	248	810.1
17	Full	11.6	0.278	255	814.1
18	Full	11.6	0.278	255	811.4
19	Full	11.6	0.278	248	811.0
20	Full	11.6	0.278	241	810.0

* Thin Sheet Injection
** Projectile Failed Inbore

Pressure oscillations were observed in the 105mm test data, as in the earlier, medium caliber firing data. The peak-to-peak amplitude of the oscillations at the forward end of the chamber was about 50% of mean chamber pressure, increasing towards the rear of the chamber. The oscillations began when the chamber pressure reached approximately 70 MPa. The frequencies of the oscilations observed in the combustion chamber are in the 10-50 kHz range, while the frequencies in the propellant reservoir are about twice as high. The Fourier transform of the pressure data shows a band of frequencies in the 3.5 kHz to 19.6 kHz range with evidence of some dominant frequencies between 13.8 and 15.3 kHz. Assuming a sound speed of 701 m/s, the acoustic modes of the chamber are 13.9 kHz, 14.1 kHz, 14.5 kHz and 15.2 kHz for the 2nd radial, 2nd radial-1st tangential, 2nd radial-2nd tangential, and 2nd radial-3rd tangential modes, respectively. As with the 30mm, there was no strong indication of excitation of lower chamber modes.

BALLISTIC EFFICIENCY

The Concept VI test firing results are summarized in Table 5, along with the ballistic efficiencies for the various test series. The energy of the igniter has been included in the calculation of the efficiencies, but represents only a small correction to the ballistic efficiencies, 1-3% for the 105mm and less than 1% for the 25mm and 30mm.

Table 5. Summary of Test Results 25mm, 30mm and 105mm, Concept VI.

Fixture	LP	No.of Tests	Charge Mass (kg)	C/M	Proj Travel (m)	Expansion Ratio	Velocity (m/s)	Pressure (MPa)	Ballistic Efficiency (%)
25mm	Otto II	8	0.116	0.634	2.13	7.65	946	183	21.1
30mm	Otto II	4	0.197	0.683	2.44	8.50	946	119	19.6
	LGP 1845	4	0.234	0.812	2.44	8.50	1019	195	13.9
	LGP 1846	3	0.227	0.787	2.44	8.50	1014		15.0
105mm	Otto II	3	1.04	0.092	5.18	15.90	501	110	36.1
	Otto II	2	1.09	0.096	5.18	15.90	511	114	37.6
	Otto II	2	2.00	0.157	5.18	12.80	662	196	40.4
	Otto II	2	2.04	0.161	5.18	12.80	661	266	39.4
	Otto II	2	3.17	0.250	5.18	10.40	755	196	33.8
	Otto II	8	3.27	0.278	5.18	10.40	810	245	34.9

The low ballistic efficiencies for the 25mm and 30mm test series are due primarilly to the small injection gap used with the annular piston. The small injection gap corresponds to a large web for a solid propellant, i.e. the larger the web, the smaller the solid propellant burning surface area. Thus, even for a relatively high charge mass ratios, 0.63-0.81, the propellant injection area remains relatively small, and the rate of pressure rise and the maximum pressure in the chamber are correspondingly low. In the case of the 105mm, however, the expansion ratios are greater than for the smaller calibers. The greater expansion ratio results in increased ballistic efficiencies, as

These data also illustrate one of the ballistic characteristics of the regenerative gun, variable chamber volume. In a conventional solid propellant gun, the chamber volume, and thus the expansion ratio, is fixed. This can lead to difficulties when designing artillery charges for shorter ranges, particularly for long range cannons with large chambers. In the 105mm RLPG, the initial free volume in the combustion chamber was fixed, and only the volume of the propellant reservoir changed with the charge. The ignition characteristics of the system were, therefore, independent of the charge. Also, as the charge decreased, the expansion ratio of the system increased, maintaining the ballistic efficiency of the system.

4. INTERIOR BALLISTIC SIMULATIONS

In this section we describe RLPG interior ballistic models used in the United States, and present examples of ballistic simulations using these models. In Table 6, we present a comparison of the four models currently used in RLPG simulations. Two of the models, Cushman's[7] and Bulman's[8] are used by the General Electric Co., and the other two Gough's[9] and Coffee's[10] are used at BRL. The table summarizes the treatment of various aspects of the RLPG interior ballistic process, such as events in the liquid propellant chamber, piston motion, spray phenomena, etc.

COMPARISON OF US INTERIOR BALLISTIC SIMULATIONS

As mentioned earlier, piston motion compresses the liquid propellant, injecting it through orifices into the combustion chamber as a jet. All four models assume an isothermal compressible liquid, and treat both the propellant reservoir and the combustion chamber as lumped parameter regions. The motion of the piston in all the models is governed by a balance of forces acting on the piston. The force produced by the combustion pressure acting on the piston is opposed by the force of the liquid pressure, plus a piston drag (friction) force. In the two General Electric models an additional liquid damping force is imposed on the piston in order to slow it down prior to the end of piston travel.

In the two GE models, the discharge coefficient of the piston orifice remains constant. In the two BRL models, the discharge coefficient may be either constant or vary with piston travel. Variation of discharge coefficient during the ballistic cycle has been recently suggested independently by Edelman[11] and Coffee[12] in theoretical studies of the RLPG process.

The breakup of the liquid jet into droplets and subsequent combustion of these droplets in the chamber and barrel are not well understood. It has been suggested that the accumulation of unburnt liquid droplets in the chamber and barrel has a significant influence on the ballistic cycle, and that the basic shapes of the pressure-time curves can be explained in terms of liquid accumulation.[4]

At low pressure, propellant is injected more rapidly than it is consumed, and, therefore, accumulates in the chamber. It is possible that the jet will impact the forward end of the chamber and the projectile base, enhancing breakup. Based on this scenario, substantial propellant combustion would be expected to occur near the projectile base, during early projectile motion.

However, later in the cycle, the increased chamber pressure, and piston and projectile motion would modify this picture. First, the rate of jet breakup and propellant combustion are expected to increase with increasing pressure. Second, as the piston moves toward the breech, the distance which the liquid must travel to reach the barrel entrance increases. The jet velocity also increases, but this would tend to enhance jet breakup, and, therefore, combustion. Thus, it can be argued that the portion of propellant burned in the chamber increases during the ballistic cycle, that the amount of propellant burned in the barrel decreases, and that little or no propellant combustion takes place near the base of the projectile during much of projectile travel.

Two major classes of combustion models are used. In the simpler case, it is assumed that combustion occurs instantaneously upon injection of the liquid propellant into the chamber. Only the BRL models contain the option of assuming instantaneous burning at the piston face. In the more complex case, details of the liquid jet breakup and the propellant combustion are treated. The two GE models assume that the liquid jet is atomized as it enters the chamber. The resulting droplets may either ignite and burn, or undergo further breakup before combustion occurs. Unlike the two GE models, the two BRL models assume that droplets of a fixed size are formed throughout the ballistic cycle. In the Gough model, the droplets maintain their original diameter although their number will vary as the droplets burn. In the Coffee model the droplet diameter will change as they burn, forming a distribution of droplet diameters.

TABLE 6
REGENERATIVE LIQUID PROPELLANT GUN
MODEL COMPARISON

MODEL FUNCTION	BULMAN MODEL	CUSHMAN MODEL	COFFEE MODEL	GOUGH MODEL
Liquid Chamber:	Uniform Pressure; Isothermal Compressible Eq. of State	Uniform Pressure; Isothermal Compressible Eq. of State	Uniform Pressure; Isothermal Compressible Eq. of State	Uniform Pressure; Isothermal Compressible Eq. of State
Piston:	Balance of Forces Piston Drag Liquid Damping of Motion	Balance of Forces Piston Drag Liquid Damping of Motion	Balance of Forces Piston Drag	Balance of Forces Piston Drag
Spray:	Jet Breakup Droplet Size Distribution Bernoulli Injection	Jet Breakup Droplet Size Distribution Bernoulli Injection	Droplet Size Distribution or Instant Burn Bernoulli Injection Liquid Disc.= f(Pist.Trv)	Constant Droplet Size or Instant Burn Bernoulli Injection Liquid Disc.= f(Pist.Trv)
Combustion Chamber:	Uniform Pressure, Stagnant No Heat Loss Continuity & Energy Balance Covolume Eq. of State	Uniform Pressure, Stagnant No Heat Loss Continuity & Energy Balance Covolume Eq. of State	Uniform Pressure, Stagnant No Heat Loss Continuity & Energy Balance Covolume Eq. of State	Uniform Pressure, Stagnant No Heat Loss Continuity & Energy Balance Covolume Eq. of State
Tube:	1-D, Method of Characteristics No Droplets No Heat Loss	Coupled "Spring-Mass" System No Droplets No Heat Loss	Modified Lagrange Two Phase, Homogenous Heat Loss	1-D Two Phase, Homogenous Heat Loss
Projectile:	Bore Friction Air Shock Rigid Cylinderical Body No Projectile Offset	Bore Friction Air Shock Rigid Cylinderical Body No Projectile Offset	Bore Friction Air Shock Cylinderical Projectile Projectile Offset	Bore Friction Air Shock Projectile with Optional Boom Projectile Offset
Initial Conditions:	Solid/Liquid Primer Model Initial Liquid Pressure	Solid/Liquid Primer Model Initial Liquid Pressure	Initial Gas Pressure Initial Liquid Pressure Liquid Primer Model	Initial Gas Pressure Initial Liquid Pressure

In view of the uncertainty in the initial droplet size, a rigorous treatment of droplet ignition and combustion is not warranted. Droplet combustion in both the GE and BRL models is treated by defining a linear regression rate which is proportional to the local pressure raised to a power, as in the case of solid propellant combustion.

At present, little direct information on the combustion process in a regenerative gun exists, therefore, detailed combustion models cannot be rigorously justified. At best, such models merely provide adjustable parameters in the form of a time lag for droplet formation and an initial droplet size, or droplet size distribution.

In view of the uncertainty of flow in the combustion chamber, as mentioned above, all four models assume a uniform pressure in the chamber with no flow velocity. These models also assume no heat loss to the chamber walls, since flow of gas makes the greatest contribution to heat loss.

The flow in the barrel consists of burning liquid droplets mixed with combustion gases. The two GE models assume that burning occurs in the combustion chamber only, while the two BRL models assume that burning occurs both in the chamber and in the barrel. In contrast, the solid propellant gun models assume a distribution of burning solid propellant grains between the breech end of the chamber and the base of the projectile. If the flow in the barrel can be assumed to be single phase, consisting only of combustion gases, then the pressure gradient in the barrel can be described by standard interior ballistic approximations. The alternative is the numerical solution to the one-dimensional mass and momentum conservation equations in the barrel.

The standard solid propellant gun interior ballistic approximations for the pressure gradient (Lagrange, Pidduck-Kent, etc) were originally developed with the assumption of complete propellant combustion prior to initial motion of the projectile, but have been routinely applied to gun interior ballistic problems in which solid propellant burns during most of the projectile travel. For regenerative ballistic models these approximations must be modified to account for a non-zero mass flow rate at the barrel entrance. These modified equations have been presented by Morrison et al.[13] Of the four models described above only the Coffee model uses a modified Lagrange approximation for computing the barrel pressure gradient. The other three models use various numerical approximations for solving the 1-D partial differential equations. Furthermore, the two GE models assume that there is no heat loss to the barrel, whereas the two BRL models assume convective heat loss to the barrel walls.

All four models assume that the projectile encounters frictional and air-shock forces. The two GE models assume that the base of the projectile is initially at the barrel entrance; whereas the two BRL models assume that the base of the projectile can be offset away from the barrel entrance to account for the presence of a boom attached to the projectile.

In the two GE models, a solid propellant or liquid propellant primer model is used to provide the initial pressure rise starting the regenerative ballistic process. In the Coffee model a liquid propellant primer model is used. In the Gough model, an initial gas pressure condition is used. All of the models allow for an initial pressure in the liquid.

120MM TANK GUN PARAMETRIC SIMULATIONS

The Coffee model has been used in a sensitivity analysis of a conceptual 120mm RLPG tank gun, similar to that conducted by Woodley et al,[14] using a model developed by Pagen et al.[15] In this analysis, the effect of varying selected input parameters over a ±20% range on the performance of the gun was evaluated. The input parameters which were varied were liquid volume, projectile weight, piston weight, injection area, cross-sectional area of liquid reservoir, and cross-sectional area of combustion chamber. The reference characteristics of the 120mm used in the analysis are given in Table 7.

Table 7. Characteristics of 120mm Regenerative Liquid Propellant Gun for Sensitivity Analysis.

Bore Diameter:	120 mm
Projectile Travel:	6.3 m
Projectile Weight:	7.12 kg
Piston Weight:	76.66 kg
Piston Area (Combustion Chamber):	916.3 cm^2
Piston Area (Liquid Chamber):	719.6 cm^2
Liquid Chamber Volume:	11.7 liters
Combustion Chamber Volume:	5.85 liters

The results of this analysis are presented in Table 8 and in Figures 4-6. The parameters which have the greatest effect on muzzle velocity and the two maximum pressures are the cross sectional areas of the liquid reservoir and the combustion chamber, where the changes varied from -47% to 6% in muzzle velocity and from -86% to 69% in pressure. Variations in these areas influence the balance of pressure forces

acting on the piston. Increasing the chamber area relative to the liquid area will result in a higher gas pressure force on the piston, producing a higher liquid pressure and a higher mass flow rate of the liquid into the chamber. This results in a higher chamber pressure and a higher muzzle velocity.

TABLE 8
120MM REGENERATIVE LIQUID PROPELLANT GUN
SENSITIVITY STUDY

Piston Weight		Muzzle Velocity		Max. Liq. Press.		Max. Comb Pres.	
g	%	m/s	%	MPa	%	MPa	%
61326.4	-20.0	1946.8	1.12	721.6	4.16	515.3	4.12
68992.2	-10.0	1935.3	0.52	706.9	2.04	504.9	2.02
76658.0	0.0	1925.3	0.00	692.8	0.00	494.9	0.00
84323.8	10.0	1914.2	-0.58	679.3	-1.95	485.3	-1.94
91989.6	20.0	1903.3	-1.14	666.2	-3.84	476.0	-3.82

Proj. Weight		Muzzle Velocity		Max. Liq. Press.		Max. Comb Pres.	
g	%	m/s	%	MPa	%	MPa	%
5696.0	-20.0	1985.2	3.11	622.7	-10.12	444.8	-10.12
6408.0	-10.0	1955.2	1.55	658.3	-4.98	470.2	-4.99
7120.0	0.0	1925.3	0.00	692.8	0.00	494.9	0.00
7832.0	10.0	1895.1	-1.57	726.3	4.84	518.8	4.83
8544.0	20.0	1865.8	-3.09	758.8	9.53	542.0	9.52

Liquid Volume		Muzzle Velocity		Max. Liq. Press.		Max. Comb Pres.	
cc	%	m/s	%	MPa	%	MPa	%
9360.0	-20.0	1887.8	-1.95	704.0	1.62	503.3	1.70
10530.0	-10.0	1911.9	-0.70	698.2	0.78	499.0	0.83
11700.0	0.0	1925.3	0.00	692.8	0.00	494.9	0.00
12870.0	10.0	1929.1	0.20	687.6	-0.75	490.9	-0.81
14040.0	20.0	1924.2	-0.06	682.6	-1.47	487.1	-1.58

Liquid Area		Muzzle Velocity		Max. Liq. Press.		Max. Comb Pres.	
cm^2	%	m/s	%	MPa	%	MPa	%
575.7	-20.0	1999.8	3.87	1290.9	86.33	657.4	32.83
647.6	-10.0	1996.9	3.72	972.5	40.37	594.1	20.04
719.6	0.0	1925.3	0.00	692.8	0.00	494.9	0.00
791.6	10.0	1739.0	-9.68	452.6	-34.67	370.0	-25.24
863.5	20.0	1415.8	-26.46	232.0	-66.51	214.0	-56.76

Chamber Area		Muzzle Velocity		Max. Liq. Press.		Max. Comb Pres.	
cm^2	%	m/s	%	MPa	%	MPa	%
733.0	-20.0	1021.1	-46.96	95.0	-86.29	93.2	-81.17
824.7	-10.0	1695.6	-11.93	412.7	-40.43	339.8	-31.34
916.3	0.0	1925.3	0.00	692.8	0.00	494.9	0.00
1007.9	10.0	2008.4	4.32	946.2	36.58	597.1	20.65
1099.6	20.0	2034.9	5.69	1171.4	69.08	662.0	33.76

Vent Area		Muzzle Velocity		Max. Liq. Press.		Max. Comb Pres.	
cm^2	%	m/s	%	MPa	%	MPa	%
64.8	-20.0	1789.9	-7.03	561.1	-19.01	400.0	-19.18
72.9	-10.0	1865.7	-3.10	626.1	-9.63	446.9	-9.70
81.0	0.0	1925.3	0.00	692.8	0.00	494.9	0.00
89.1	10.0	1970.6	2.35	761.2	9.87	544.2	9.96
97.2	20.0	2008.2	4.31	832.3	20.14	595.3	20.29

Variations in the vent area resulted in a -7% to 4% change in muzzle velocity and -19% to 20% change in pressure. Increasing the vent area results in a higher mass flow rate of propellant into the chamber, resulting in a higher pressure and higher muzzle velocity.

Variations in projectile weight gave changes varying from -3% to 3% in muzzle velocity and from -10% to 10% in pressures. The results are similar to those observed in solid propellant guns; decreasing projectile weight results in a higher velocity and a lowering of the pressures.

Variation in piston weight and liquid volume gave relatively small changes in velocity and pressure. Some of the changes were somewhat symmetrical around the standard; others notably liquid and combustion chamber cross sectional areas were highly asymmetrical around the standard. These results are similar to those obtained in the sensitivity analysis performed by Woodley[14] also for a 120mm RLPG tank gun.

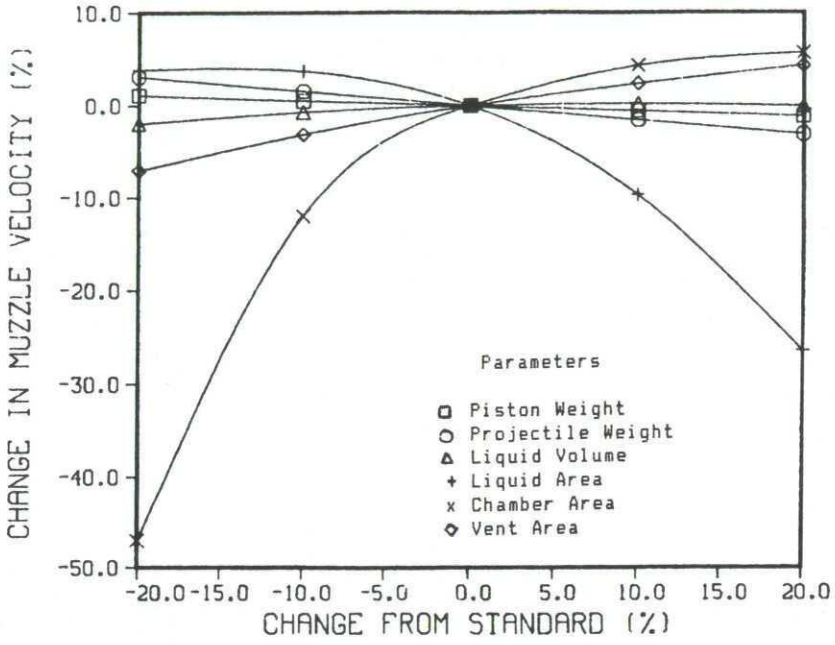

Figure 4. 120mm RLPG Sensitivity Study. Percentage Variation of Muzzle Velocity with Percentage Change in Selected Parameters.

The description of the combustion process, where and how the propellant burns, is the most significant shortcoming in current regenerative interior ballistic simulations. The effects should be most evident during the low pressure ignition phase when propellant is expected to accumulte in the combustion chamber. However, as noted, the overall shape of the pressure-time curve is also affected. Detailed experimental investigation of the jet breakup and combustion processes is required for the development of improved interior ballistic simulations.

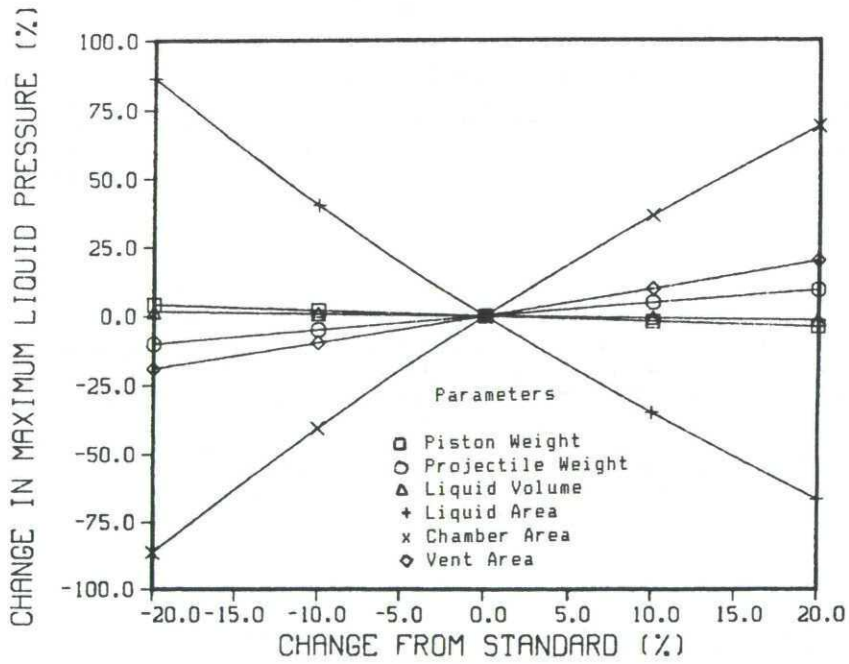

Figure 5. 120mm RLPG Sensitivity Study. Percentage Variation of Maximum Liquid Pressure with Percentage Change in Selected Parameters.

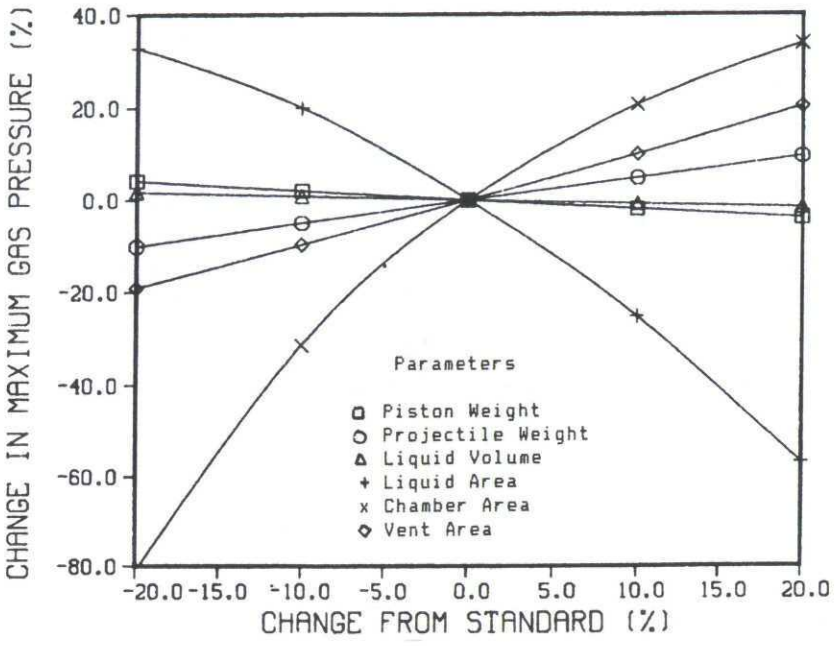

Figure 6. 120mm RLPG Sensitivity Study. Percentage Variation of Maximum Chamber Pressure with Percentage Change in Selected Parameters.

5. CONCLUSION

A family of liquid monopropellants based on hydroxyl ammonium nitrate have been developed. These propellants have undergone extensive characterization and hazards testing. The results of this testing demonstrate that HAN-based propellants offer many improvements over liquid propelants considered in the past, particularly in the area of safety, and that HAN-based propellants are suitable for military use.

Experimental firings of an advanced regenerative liquid propellant gun concept have been conducted in 25mm, 30mm, and 105mm using both a nitrate ester based liquid monopropellant, Otto II, and HAN-based liquid monopropellants, LGP 1845 and LGP 1846. Although, muzzle velocity repeatability was generally poor in the 25mm and 30mm tests, the results of the 105mm firings were as good as any obtainable with conventional solid propellant systems. Variation in tests procedures and parameters may have been responsible for the poor repeatability in the small caliber firings, and testing is now underway to resolve this issue.

Future efforts will focus on the development of practical mechanizations of the regenerative concept capable of automatic loading, automatic zoning of the propellant charge, and automatic control of the ballistic process. These issues, along with the development of durable seals and other components, are being addressed in an effort directed toward the fabrication and testing of a 155mm regenerative liquid propellant gun.

6. REFERENCES

1. E.Freedman and K.E.Travis, "Compositions, Nomenclature, Densities, and Computed Impetuses of Aqueous Liquid Gun Propellants (U)", ARBRL-MR-03076, Confidential, February 1981.

2. N.Klein, "Liquid Propellants For Use In Guns - A Review", BRL-TR-2641, February 1985.

3. W.F.Morrison, J.D.Knapton, and G.Klingenberg, "Liquid Propellants For Gun Applications", Proceedings of the Seventh International Symposium on Ballistics, April 1983.

4. W.F.Morrison, P.G.Baer, M.J.Bulman, and J.Mandzy, "The Interior Ballistics of Regenerative Liquid Propellant Guns", Proceedings of the Eighth International Symposium on Ballistics, October 1984.

5. J.Mandzy, I.Magoon, W.Morrison and J.Knapton, "Preliminary Report on Test Firings of a 105 mm Regenerative Fixture", CPIA Publication 383, Vol II, 20th JANNAF Combustion Meeting, pp.161-172, October 1983.

6. J.Mandzy, P.G.Cushman and I.Magoon, "Technical Notes on Concept VI 105-mm Evaluation", General Electric Ordnance Systems Division, Contract No.DAAK11-78-C-0054, August 1984.

7. P.Cushman, General Electric Ordnance Systems Division, Private Communication.

8. M.Bulman, General Electric Ordnance Systems Division, Private Communication.

9. T.P.Coffee, "A Lumped Parameter Code for Regenerative Liquid Propellant Guns", US Army Ballistic Research Laboratory Report, in preparation.

10. P.S.Gough, "A Model of the Interior Ballistics of Hybrid Liquid Propellant Guns", US Army Ballistic Research Laboratory Contract Report, in preparation.

11. R.Edelman, Science Applications Inc., Private Communication.

12. T.P.Coffee, U.S. Army Ballistic Research Laboratory, Private Communication

13. W.F.Morrison, M.J.Bulman, P.G.Baer, and C.F.Banz, "The Interior Ballistics of Regenerative Liquid Propellant Guns", Proceedings of the 1984, JANNAF Propulsion Meeting, February 1984.

14. C.R.Woodley, "A Theoretical Sensitivity Study of a Regenerative Liquid Propellant Gun", Royal Armament Research and Development Establishment Sevenoaks, Kent, England, 1984.

15. G.Pagen, A.Harvey, and D.C.A.Izod, "Regenerative Liquid Propellant Gun Modeling", Proceedings of the Seventh International Symposium on Ballistics, 1983.

DISCUSSION

Unidentified Speaker

I would like to know if you experienced any problems with the initial negative differential pressure with liquid propellants. Were there pressure waves between the end of the projectile and the end of the chamber?

Author's Reply

We have never observed longitudinal pressure waves between the piston face and the projectile base, indicated by a reverse pressure gradient as in a solid propellant gun. We have occasionally encountered combustion in the LP reservoir related to reverse flow in the injector during ignition. This does not lead to serious problems, and has always been corrected by hardware design modifications.

M.Dervaux, Fr

I should like to know in what position maximum rate of combustion occurs in the ballistic cycle; in what position, at what exact place, and at what time. Is it in the chamber? Is it in the barrel? Is it at the beginning of the cycle or is it towards the end of the ballistic cycle?

Author's Reply

LP accumulates in the combustion chamber during the ignition phase, and then burns rapidly during the rise to maximum pressure. However, the maximum rate of liquid consumption would probably occur at maximum pressure. This is not purely combustion related, but is heavily influenced by the jet breakup which is most efficient at maximum pressure.

B.Zeller, Fr

I have a very ordinary question to ask. Do you have any idea how much liquid propellant would cost, based on hydroxyl ammonium nitrate? I am thinking of the production of several hundred or several thousand tons a year.

Author's Reply

The US has conducted studies of the production of HAN-based liquid propellants. Being a chemical, the production of an LP would be comparable to other liquid chemicals. Standard chemical engineering equipment would be used, and the process would be completely automated, including packaging. The overall cost of the packaged LP would be on the order of $1.00 per pound in today's dollars. In comparison, the cost of solid propellants range from $6.00 to $12.00 per pound, depending on the charge.

J.M.Poussard, Fr

I wonder if you could say a few words to us about your ignition systems.

Author's Reply

We currently use a solid propellant ignition system. The solid propellant is burned in a high pressure chamber, and the combustion gases are vented into the main combustion chamber of the gun. This system would probably not be practical for a weapon.

We are working on an electrical igniter which would use a liquid propellant in the ignition train. Electrical energy would be used to ignite the liquid which would burn in a high pressure chamber and vent hot gas into the main combustion chamber, as the current igniter does, or would burn directly in the main combustion chamber.

J.S.Vigsnaes, De

In the US, liquid propellant is being studied from a technical standpoint. Have there been any tactical studies so far?

Author's Reply

Liquid propellants occupy less volume than an equivalent amount of a solid, and can be pumped from one point in a vehicle to another. This gives increased flexibility in the design of combat vehicles. Our studies indicate that the amount of ammunition (propellant plus projectiles) onboard self-propelled howitzers could be doubled by using the LP. There are also savings in handling and transportation throughout the logistics chain. Since the propellant would be pumped, only the projectile would be handled manually. This would reduce the burden on the crew, i.e., eliminate swabbing the cannon between rounds, cutting charges, etc. Autoloader design could also be simplified and a burst rate of fire of one round every 4 to 5 seconds achieved. Using automation, and the infinite zoning capability of LP, a howitzer could fire time-on-target missions, i.e., several rounds in the air together, simultaneously impacting the target. Thus, a single howitzer could have the firepower of a section, increasing combat power and the ability of service targets.

There has been interest recently in increased range for artillery in the US. Although use of an LP would not simplify the ballistic problem, an LP would greatly reduce the logistics burden of larger propelling charges.

The hydroxl ammonium nitrate LPs are formulated to be stoichiometric. This will eliminate the secondary flash and blast encountered with some solid propellant charges, reducing signature problems.

The HAN -based LPs are difficult to ignite at atmospheric pressure, and do not release energy rapidly if ignited. In vulnerability tests, they also exhibit low vulnerability characteristics. Thus, the use of HAN-based LPs will lead to increased ammunition safety and reduced vulnerability.

Finally, the liquid propellant gun will also provide benefits for direct fire weapons such as tank guns.

Performance (muzzzle velocity) can be increased by the brute force technique of increasing the propellant charge, while still increasing the onboard ammunition storage. Autoloader design is simplified, logistic resupply can be improved, and ammunition vulnerability reduced.

IGNITION, COMBUSTION, AND PHYSICAL PROPERTIES OF LIQUID PROPELLANTS AT GUN PRESSURES.

G.G.Cook and T.O.Andrews.
Royal Armament Research and Development Establishment
Fort Halstead
Sevenoaks, Kent. TN14 7BP. U.K.

SUMMARY

The Internal Ballistics of a Regenerative Injection Liquid Propellant Gun depend on the rate of injection of the liquid propellant rather than on the burning rate, owing to the small size of the droplets produced. The rate of injection is determined by the effect of the compressibility of the liquid on the motion of the piston and by its flow characteristics through the injector. The "Force Constant" of the propellant is important as it determines the combustion pressure resulting from any given flow rate.

A standard "Closed Vessel" has been modified and used with a specially developed igniter to investigate the combustion of Otto Fuel II at gun pressures. It has also been used to investigate the compressibility of inert liquid at pressures up to 600 MPa. A "Liquid Propellant Test Vessel" has been constructed for use in the investigation of the compressibility of "live" liquids and the flow of liquids at high pressures.

1 INTRODUCTION

The compressibility of the liquid propellant plays an important part in the Internal Ballistics of a Liquid Propellant Gun. In a Regenerative Injection Gun (Fig. 1) it determines the pressure rise in the liquid resulting from the motion of the piston. If the liquid is relatively more compressible at low pressures the piston will have to move further before the piston motion generates pressure in the liquid reservoir. The piston is likely to be heavy and its initial acceleration, under the pressure of the igniter, is likely to be low. There may be a significant time delay before liquid is injected into the combustion chamber.

The rate of burning of the propellant in the combustion chamber depends largely on the rate of injection and, to a lesser extent, on the size of the droplets produced. Knowledge of the linear rate of burning of the propellant is, by its self, relatively unimportant compared with the requirement for knowledge of the energy content and of the injection process.

A standard "Closed Vessel" has been modified and used in experiments to investigate the ignition and combustion of bulk "Otto Fuel II" and the compressibility of inert silicone fluid.

The experience of using this vessel has assisted in the design of a special Liquid Propellant Test Vessel for use in investigations of Liquid Propellant compressibility and injection characteristics. A "Stage 1" vessel has been constructed and preliminary tests have been made. These have included pressure proof and functioning tests using inert liquid, the ejection of inert liquid, and an investigation into the nature of the compressibility of silicone fluid and of Otto Fuel II.

2 COMPRESSIBILITY TESTS USING A MODIFIED "CV21" CLOSED VESSEL

During the early stages of the design of the Liquid Propellant Test Vessel some experiments were made using a standard "CV21" closed vessel with a modified end block. A piston was made to fit the bore of the vessel and to compress inert liquid in a cavity in the end block, the piston being driven by a solid propellant charge in the main vessel (Fig. 2). It was hoped that, as the motion of the piston could not be observed directly, liquid compressibility could be found from the frequency of oscillations in the liquid pressure (see Appendix for method of analysis) but the oscillations were too highly damped. Instead an indicator, with steel pegs set in a brass ring, was placed in the annular space round the piston. Knowing the length of the piston stem and the depth of the liquid cavity the remaining height of the indicator showed the remaining depth of the liquid at the maximum piston excursion. This method was laborious as it involved removing the piston to measure the indicator ring after each firing with only one data point each time, but 11 acceptable x/x_o values were obtained at 6 pressure levels (Fig. 3).

The curve plotted through these points is the least squares fit to the data of the function $x/x_o = ((A + B.P_o)/(A + B.P))^{1/B}$, the pressure/travel relationship which exists if the bulk modulus of the liquid increases linearly with pressure; i.e $K = A + B.P$. Fitting to these data gave a bulk modulus, for inert silicone fluid, of $K = 766 + 9.18\ P$ MPa.

The pressure/travel relationship occuring if the bulk modulus varies as a quadratic in pressure (see Appendix) was also fitted to these data but the higher order term was not statistically significant.

It was thought at the time that these data represented a true measure of the compressibility of the liquid, which it was assumed would be an adiabatic process, and they were used in a computer program to model the behaviour of the new Liquid Propellant Test Vessel in various configurations. The pressure histories observed when firing the "Stage 1" version of the new vessel are in good agreement with the predictions (Fig. 4) but when continuous records of piston motion were obtained it was seen that the agreement with the predicted motion was less good. Analysis of continuous pressure/travel data obtained with a range of peak pressures has shown that the "compressibility situation" is far more complex than was originally supposed. These results are discussed in detail in Section 5 below.

3 IGNITION TESTS USING A MODIFIED "CV21" CLOSED VESSEL

A conventional gun igniter has a filling of gunpowder which is ejected into the main charge as burning particles. If a gunpowder igniter is used to ignite a liquid propellant, either as bulk liquid or as a liquid spray, there is the possibility that the burning gunpowder will be extinguished by the liquid.

To avoid this possibility a "pyrogen" igniter was developed for use in the new Liquid Propellant Test Vessel and as a means of igniting bulk liquid for "Closed Vessel" determination of its "Force Constant" (energy content).

This igniter consists of a cap and a body into which is fitted an insert which can be replaced when its 3 mm diameter central hole becomes eroded (Fig. 5). The igniter charge consists of a 30 mm length (3.75 grams) of a 10 mm diameter 37 hole multitube triple-base gun propellant and a 0.3 gram gunpowder pellet. This is ignited by an L10 primer base, containing a conducting composition cap and fitted with a sleeve to help withstand the pressure generated. The propellant burns within the igniter body and can not be affected by the liquid in the vessel. Only the final, very small, slivers are ejected unburnt.

This igniter was used to ignite bulk "Otto Fuel II" in the modified "CV21" closed vessel. It was thought that good ignition of bulk liquid would be obtained by firing the igniter up through the liquid (Fig. 6). It was expected that the liquid would be carried up by, and mixed with, the jet of flame from the igniter. But when this was tried the liquid did not ignite.

However when the vessel was inverted, so that the liquid lay in a broader, shallower, pool in the main volume of the vessel (Fig. 7), and the igniter was fired down into the liquid, very good ignition and complete combustion were obtained. The oscillations in the pressure/time curve (Fig. 8) are thought to be due to pressure waves, originating in the rapid rise in pressure in the gas, being reflected between the ends of the vessel. It has been estimated that, for this pressure rise to have occured, the liquid must have been broken up into droplets of the order of 0.01 mm to 0.1 mm in diameter.

A mean pressure of 127 MPa. was given by 109 grams of Otto Fuel II burning in a volume of 806 ml. The igniter alone gave a pressure of 5 MPa. in this volume. Taking the volume of the liquid, 88.5 ml, as the co-volume of the gas gives a Force Constant of 0.797 MJ/Kg, with no allowance for heat loss to the vessel. If the heat-loss factor, determined for solid propellants, of 4.5% is applied the force constant of Otto Fuel II is 0.833 MJ/Kg.

This method will be used to determine the force constants of other liquid propellants when they become available, but more work is required to determine the correct heat-loss factor for use with liquid propellants.

4 THE LIQUID PROPELLANT TEST VESSEL

The planned vessel (Fig. 9) contains a Liquid Reservoir 60 mm in diameter and 60 mm long. The liquid in this reservoir can be compressed, or injected into a combustion chamber, by the action of a solid-propellant driven piston. The piston head is 120 mm in diameter giving a four-to-one pressure intensification in the liquid. The motion of the piston is shown by an indicator rod protruding through the cap closing the solid-propellant chamber.

If liquid compressibility is being observed the liquid reservoir is separated from the combustion chamber by a solid insert. Alternative inserts, with a variety of orifice shapes and sizes, can be fitted when the liquid is to be injected into the combustion chamber. The vessel, as shown in Figure 9, can be used to observe the injection characteristics of the liquid without igniting it or it can be used as a "Vented Vessel" when the liquid is ignited. The combustion chamber can be reduced in size to the first section only when it is used as a vented vessel (Fig. 10) or the vented end-closure can be replaced by a 30 mm calibre gun barrel (Fig. 11). This will not be a Regenerative Injection gun; a solid propellant charge will still be used to drive the piston and inject liquid into the combustion chamber.

The vessel has been designed to withstand pressures of 150 MPa in the solid-propellant chamber, 600 MPa in the liquid reservoir, and 400 MPa in the combustion chamber. The liquid reservoir is filled through manually-operated valves (which have been tested to 600 MPa). When liquid propellant is injected at the rate required for the vessel to be fired as a 30 mm gun the piston will need to be buffered at the end of its stroke. This will be achieved by filling the annular space round the piston with compressed gas at an initial pressure of 10 to 30 Bar. As the piston moves, and the pressure due to the solid-propellant charge falls, the pressure in the annular space will rise from its initial value to 20 to 60 MPa as the piston nears the end of its stroke, and will bring the piston to rest.

The solid-propellant chamber has a small vent (1.5 mm in diameter) in its cap. This allows the propellant gas to exhaust in a few seconds and avoids the need to approach the vessel to release the gas when it might still contain liquid propellant under pressure. This vent also results in much cleaner operation than would occur with a vent which was opened some time after firing. There is no condensed water vapour in the solid-propellant chamber and it is easy to clean out the small solid deposit which remains.

To date, the vessel has been constructed and tested up to the insert separating the liquid reservoir from the combustion chamber (Fig. 12). Liquid ejection tests have been made using an inert liquid (5 centistokes silicone fluid) and inserts with a single 2 mm hole and with four 1 mm holes. With a solid propellant charge of 20 grams of SC/Z .02 the peak liquid pressures were of the order of 160 MPa. The ejection time was 220 milliseconds (Fig. 13). The cut-off of liquid pressure at the end of the stroke is due to the buffering of the piston by a rubber "O" ring in the annular space.

There was no significant difference between the liquid ejection times with a single 2 mm hole and the times with four 1 mm holes, but they differed significantly from the times predicted by the internal ballistics model if this used the actual hole sizes. To predict the observed time the orifice diameters used in the model had to be reduced to 80 % of the actual diameters (or 64 % of the areas) which agrees with "Text Book" values for the "coefficient of contraction" for a small, sharp edged, circular orifice.

Charges of 25, 40, 55, and 70 grams of Cordite SC/Z .02 have been used to compress inert silicone fluid with rise times of 8.0, 5.7, 3.9, and 3.5 milliseconds respectively (Fig. 14). These charges gave peak liquid pressures of 224, 350, 490, and 623 MPa. , this last being the peak of oscillations about a mean pressure of 581 MPa. The frequency of these oscillations is of the right order for them to be the result of the mass of the piston acting against the spring stiffness of the liquid column. With the 70 gram charge, the highest charge used, the pressure in the solid propellant chamber was 153 MPa.

Piston travel has been recorded using an electro-optical instrument to observe the width, on the axis of the instrument, of a tapered "flag" attached to the end of the indicator rod. The pressure data are plotted against piston travel in Figure 15. Least-squares fits to these data, of the pressure/travel relationship resulting from a bulk modulus equation that is a quadratic in pressure, result in higher order coefficients that are statistically significant. It is of greater practical significance that the pressure/travel curves obtained with different charge weights are significantly different from each other.

5 OBSERVATIONS OF THE COMPRESSIBILITY OF SILICONE FLUID

When the pressure data recorded during firings of the Liquid Propellant Test Vessel were plotted against piston travel (Fig. 15) several unexpected features were observed. Firstly there were significant differences between the curves obtained with different charges and different pressure rise times. These curves all differed significantly from that obtained by fitting to the discrete points generated by the "CV21" tests (Fig. 3), the linear modulus equation for a 25 gram charge being $K = 917 + 6.53\ P$ and for a 70 gram charge $K = 1285 + 5.36\ P$. But if the maximum pressures, and the corresponding piston excursions, from the Liquid Propellant Test Vessel data were treated as individual points, the curve was closer to that obtained with the "CV21" data with a linear modulus equation of $K = 738 + 8.31\ P$ (Fig. 16).

Secondly the higher charges showed a "hysteresis" effect, the "pressure relaxation" part of the plot being displaced from the pressure rise. In some cases this obviously resulted from some leakage of liquid but in other cases it obviously did not as the curve returned to the original zero of piston position as well as of pressure. But the pressure rise curve for the lowest charge followed quite closely the pressure relaxation curve which occured after the more rapid rise given by a higher charge.

There could be some effect due to the dilation and extension of the vessel under pressure but this will only give rise to hysteresis if its frequency response is too low for it to be affected by the higher rates of pressure rise. There could also be some effect due to extension of the rod joining the piston to the measuring "flag", which would be greater for the greater piston acceleration resulting from a higher charge.

But it is thought that the effect is due, in the main, to a combination of the compression heating of the liquid and of heat transfer to the vessel. With the higher charges the compression process tends towards the adiabatic, with subsequent heat loss

to the vessel. The pressure falls, before the piston starts to return, as a result of the cooling of the liquid. The process as the piston returns is then nearer the isothermal as is the compression process with the lowest charge and a pressure rise time of 8 milliseconds. The result of the "CV2l" tests was a curve of pressure against piston travel crossing from the isothermal compressibility at low pressures to be nearer to the adiabatic at high pressures.

Tests have been made using much slower burning charges, consisting of 50, 60, and 70 grams of M31A1 multitube propellant, giving pressure rise times of 33.7, 37.0, and 40.4 milliseconds. Under these conditions the liquid was more compressible than when a fast burning charge was used, with a modulus of $K = 878 + 5.64\ P$ MPa and 20% more piston travel. These results support the adiabatic-isothermal hypothesis but it is impossible to confirm it without observations of the temperature of the liquid.

6 THE COMPRESSIBILITY OF "OTTO FUEL II"

Use of the "CV2l" to determine the compressibility of live liquid propellant was contemplated. If the bulk liquid had been inadvertantly ignited, perhaps by the heat generated by the compression of an air bubble, or by leakage of hot gas past the vent plug in the piston, the pressure produced would not have been excessive. Possibly, even, the sudden pressure drop as the lower end of the piston left the liquid cavity would have extinguished the combustion and the pressure in the main vessel would have been low.

However if the seal on the lower end of the piston should fail liquid propellant would be sprayed into the annular space. If a short time later, when a significant volume of liquid propellant had been injected into the annular space but it was still in the form of a fine spray, the seal at the upper end of the piston should fail allowing hot gas from the solid propellant charge to ignite the spray, a very high pressure would be produced.

The new Liquid Propellant Test Vessel has been designed so that if the liquid in the liquid reservoir should ignite and produce a high pressure the centre of the insert closing the liquid reservoir will fail and relieve the pressure. There is a vent to atmosphere from between the two seals fitted to the larger end of the piston, through the indicator rod, so that, in the event of seal failure, hot gas from the solid propellant charge should not reach the annular space. The annular space can also be vented to atmosphere when liquid compressibility is being measured and there is no requirement for a buffer gas pressure.

Using M31A1 propellant in this vessel, to give a slow rate of compression, the Bulk Modulus of Otto Fuel II was found to be $K = 1878 + 3.89\ P$ MPa.

When a charge of 40 grams of SC/Z .02 was used, giving a pressure rise rate of 140 MPa per millisecond, the Otto Fuel ignited. Some was partially decomposed and some remained as liquid. Whether this was due to compression ignition, or to friction, or to some other cause is not clear. There was no evidence that it was due to gas leakage from the solid propellant charge.

7 FUTURE WORK

Following further tests of the compressibility of Otto Fuel the next stage of testing will be the fast ejection of inert liquid, in 5 or 10 milliseconds, through an insert with an annular orifice, to test the buffering action on the piston of compressed gas in the annular space. It is hoped that the full vessel, which will be fired as a "Liquid Propellant Vented Vessel", will be available early in 1986 and that it will be fired as a 30 mm gun by the middle of the year. Closed Vessel firing tests and compressibility tests of other liquid propellants will be made when they become available.

8 CONCLUSION

A "pyrogen" igniter, firing down into a volume of bulk liquid propellant, breaks it up into fine droplets and gives good ignition and rapid, complete, combustion.

As the pressure/volume relationship of a liquid compressed in the Test Vessel is the same after an 8 millisecond compression to 224 MPa as it is after an 80 millisecond pressure relaxation to this pressure from 600 MPa, and both differ significantly from the result of more rapid compression, it is probable that these processes are nearly isothermal. If the heat transfer from the liquid to the vessel is largely complete in 8 milliseconds the rate of transfer must be very rapid . In a Regenerative Injection gun the initial compression of the propellant before injection may be isothermal with adiabatic compression once injection has started. The liquid will then be more compressible in the early stages and it may be necessary to take account of this in Internal Ballistic calculations.

9 ACKNOWLEDGEMENT

The Authors wish to acknowledge the assistance of Mr M A Pearce in the conduct of trials and in the recording and analysis of data.

Fig. 1

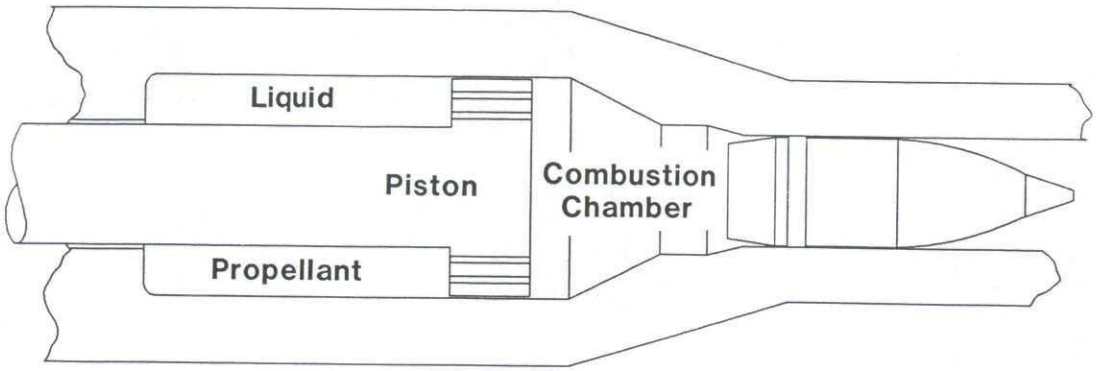

REGENERATIVE INJECTION LIQUID PROPELLANT GUN

Fig. 2

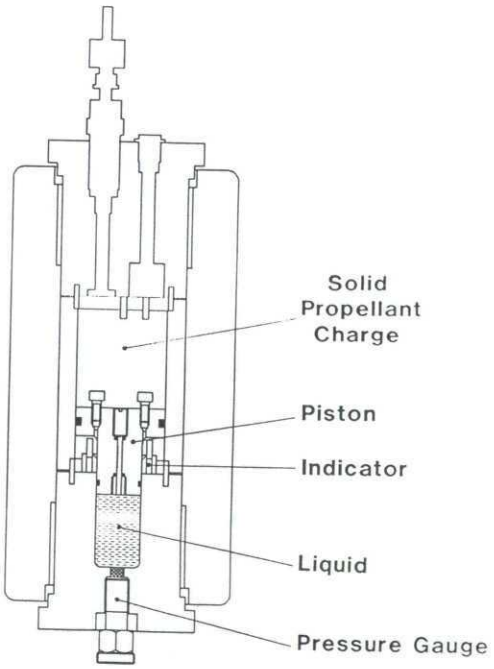

"CV21" CLOSED VESSEL MODIFIED FOR EXPERIMENTS WITH LIQUIDS

Fig. 3

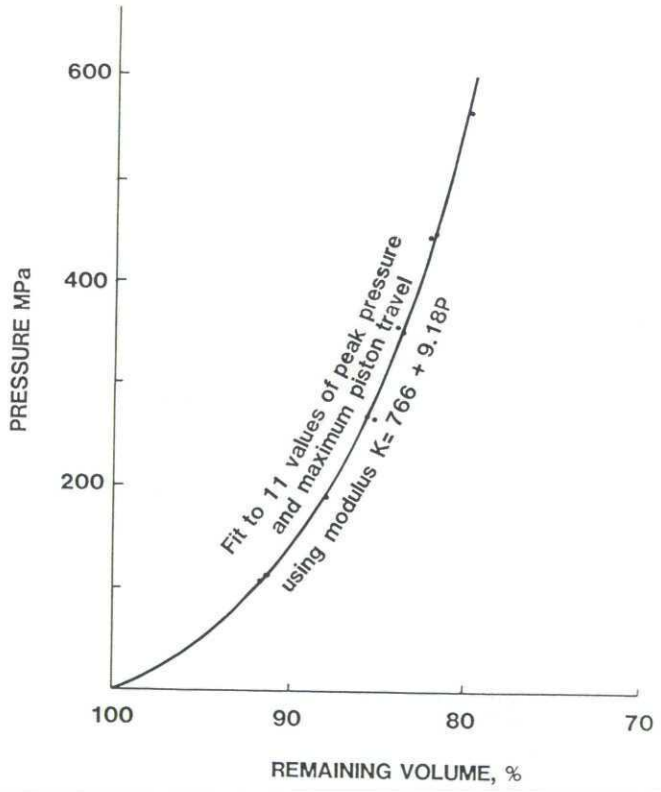

COMPRESSIBILITY OF SILICONE FLUID

Fig. 4

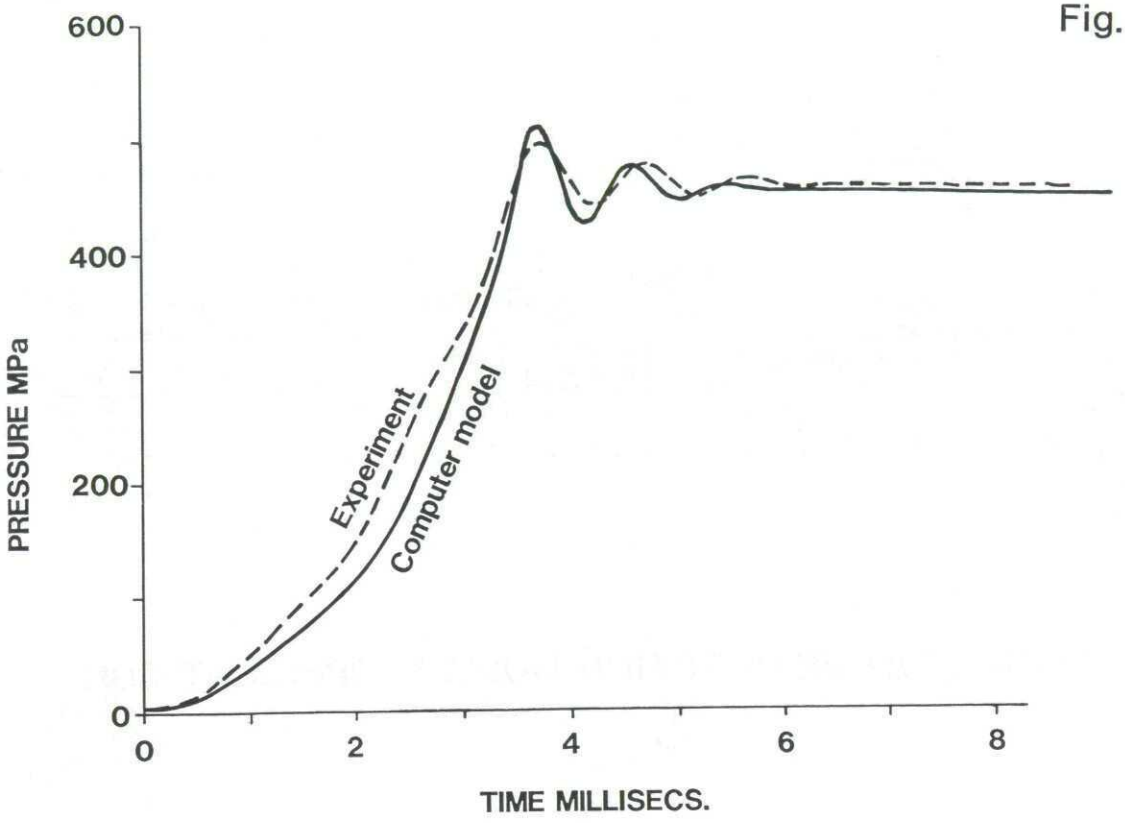

LIQUID PRESSURE, COMPRESSION OF SILICONE FLUID

Fig. 5

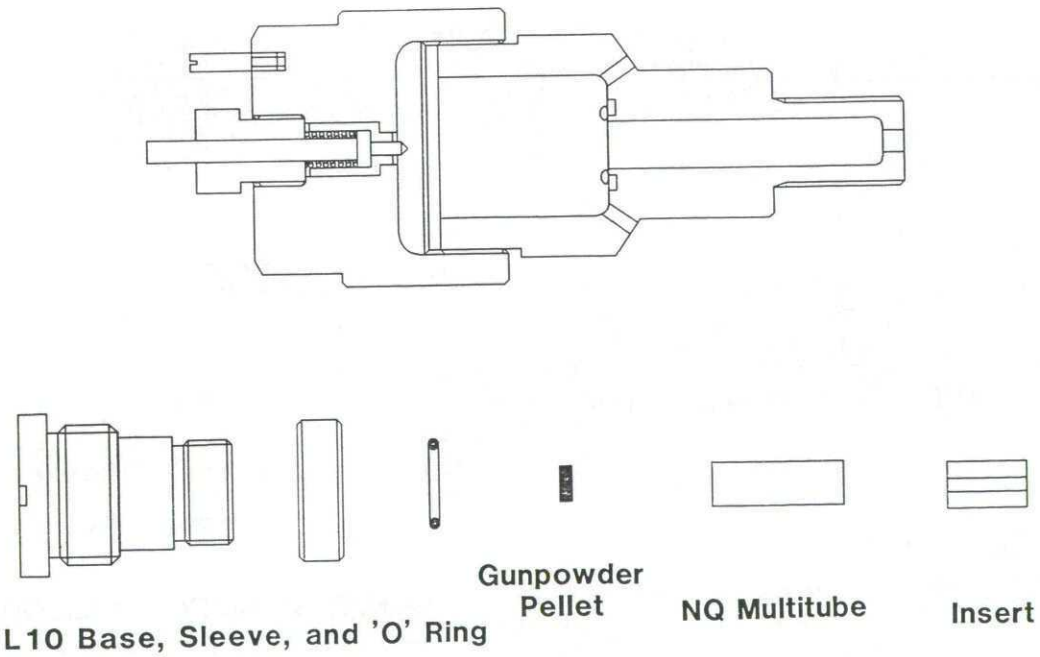

"PYROGEN" IGNITER FOR LIQUID PROPELLANT VESSEL

Fig. 6

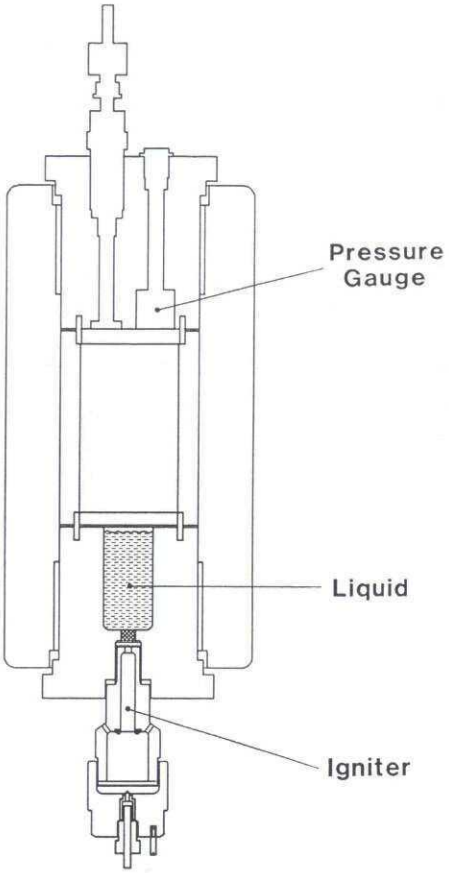

IGNITION OF BULK OTTO FUEL II
1ST ATTEMPT

Fig. 7

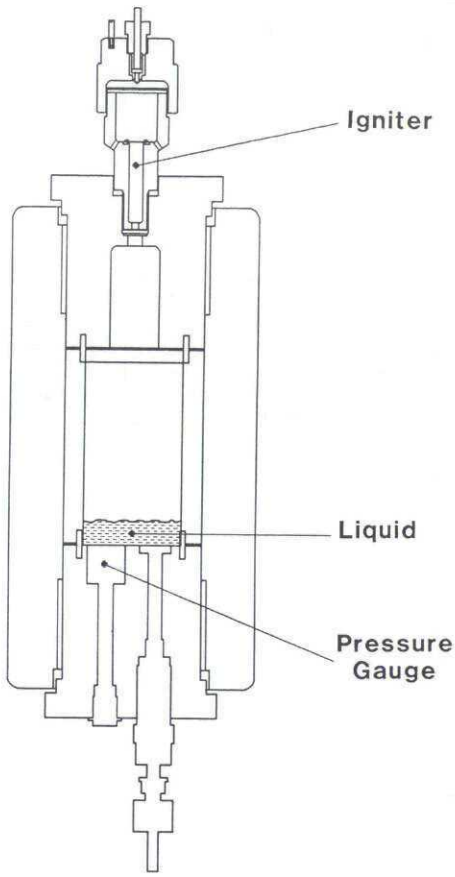

IGNITION OF BULK OTTO FUEL II
2ND ATTEMPT

Fig. 8

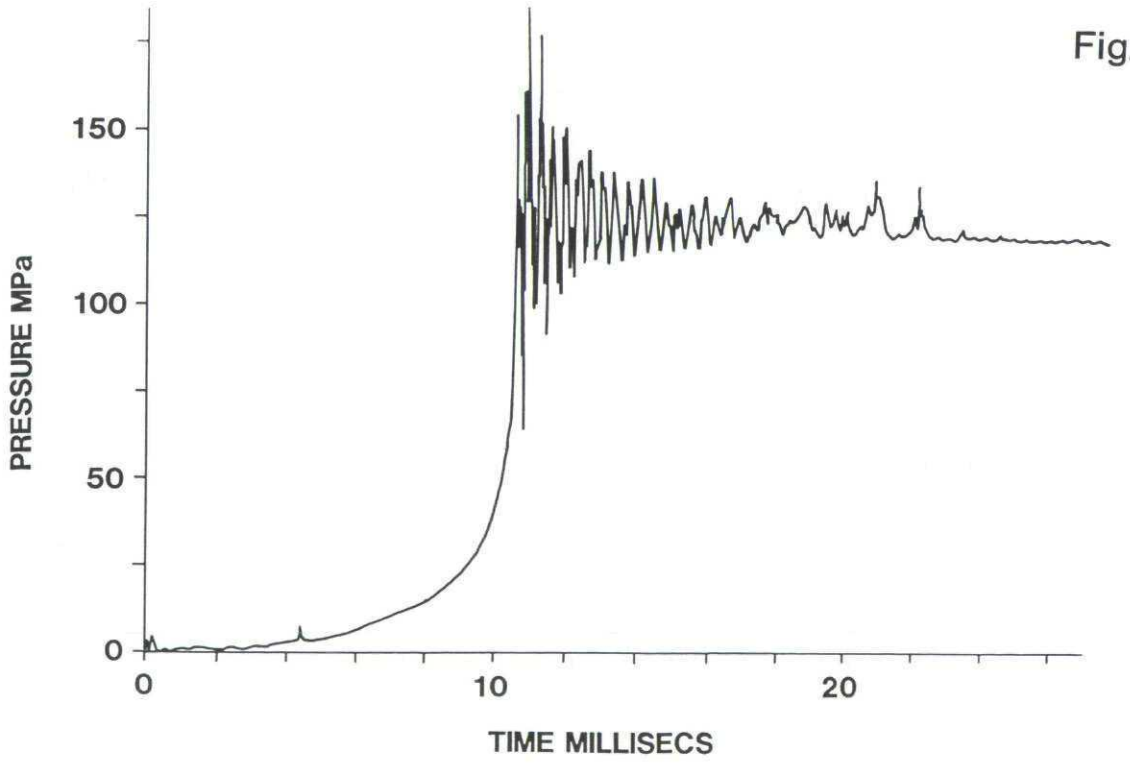

PRESSURE IN CLOSED VESSEL, OTTO FUEL II

Fig. 9

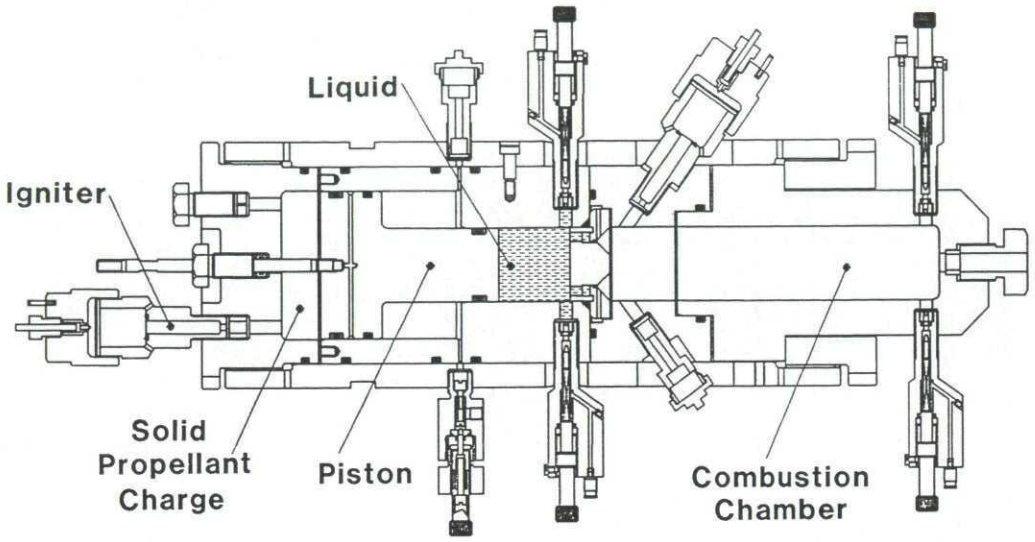

Fig. 10

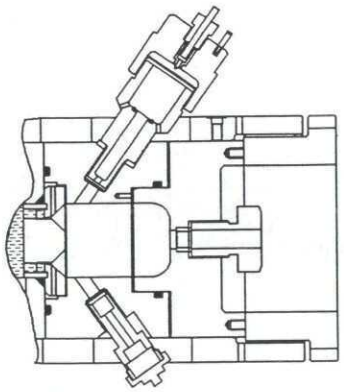

Short
Combustion
Chamber

Fig. 11

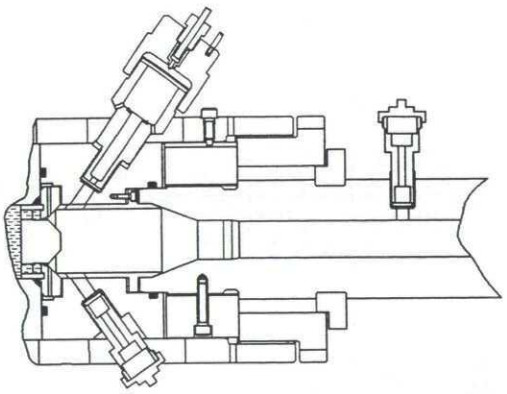

30 mm Gun Barrel

LIQUID PROPELLANT TEST VESSEL

Fig. 12

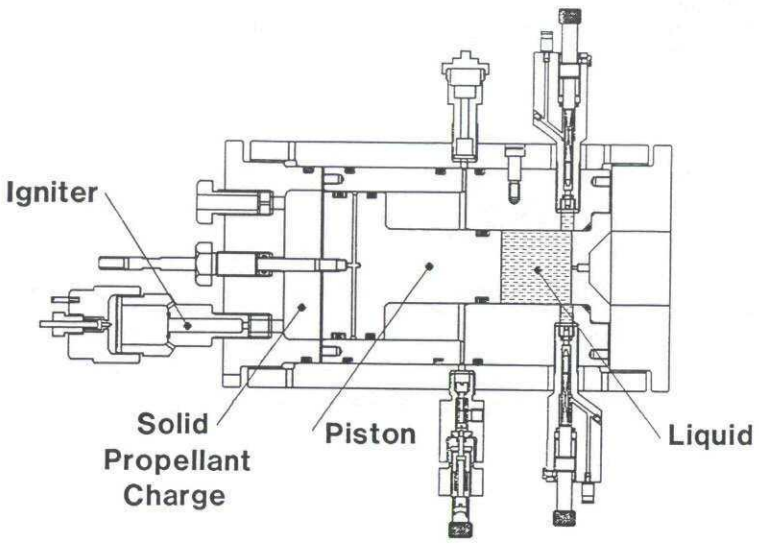

"STAGE 1" LIQUID PROPELLANT TEST VESSEL

Fig. 13

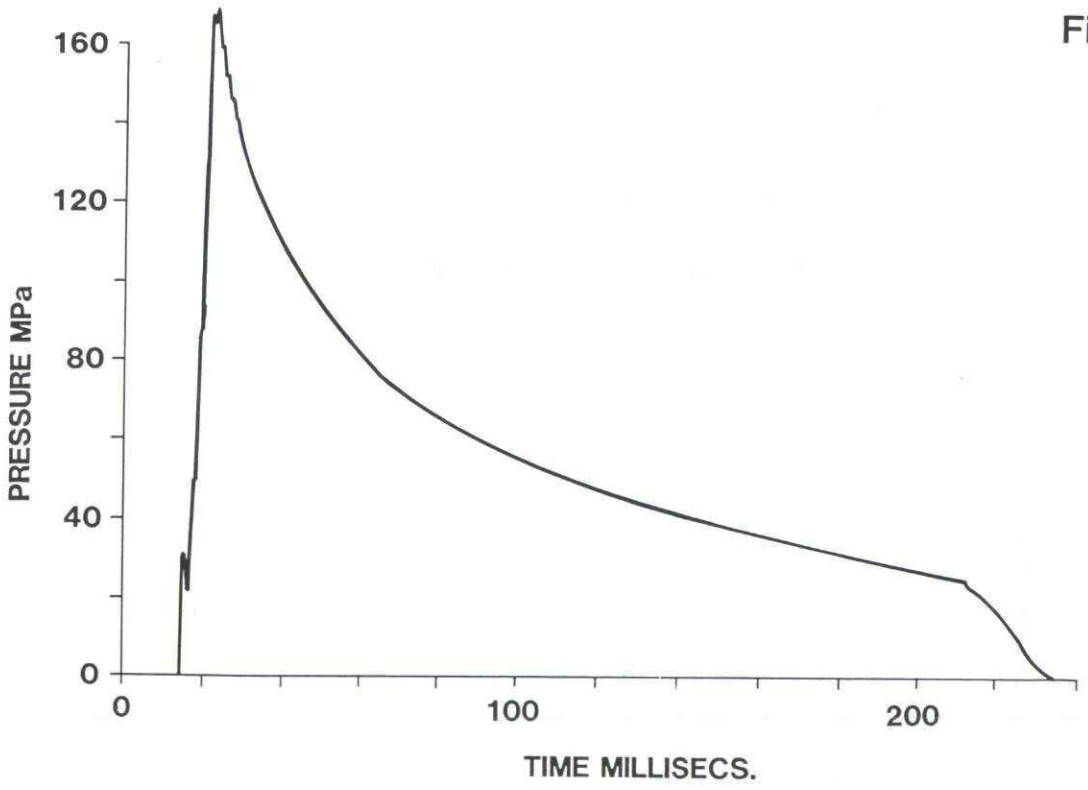

LIQUID PRESSURE, EJECTION OF SILICONE FLUID

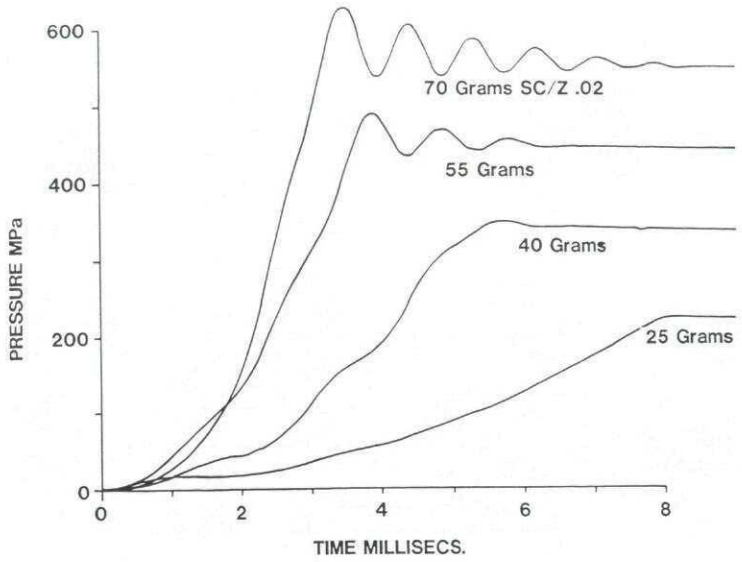

Fig. 14

LIQUID PRESSURE, COMPRESSION OF SILICONE FLUID

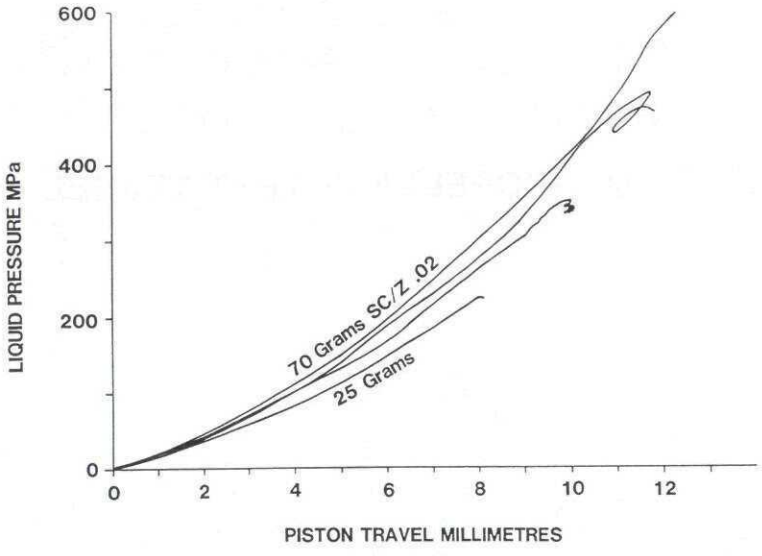

Fig. 15

COMPRESSIBILITY OF SILICONE FLUID

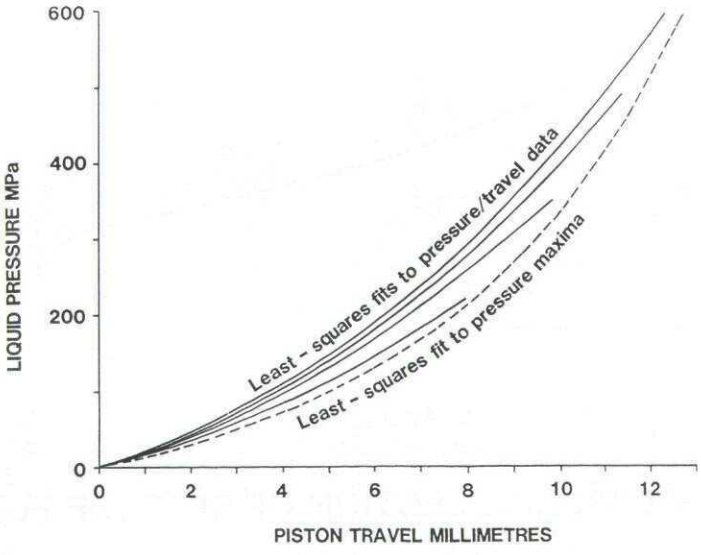

Fig. 16

COMPRESSIBILITY OF SILICONE FLUID

APPENDIX

THE ANALYSIS OF COMPRESSIBILITY DATA

The Liquid Propellant Internal Ballistics computer program currently in use at RARDE assumes that the liquid has a bulk modulus that increases linearly with absolute pressure, i.e.

$$\text{Modulus} = -V.dP/dV = A + B.P \quad . \qquad (1)$$

where V is the instantaneous volume, and dP/dV is the instantaneous rate of change of pressure with volume, at pressure P.

Integrating $V.dP/dV = -(A + B.P)$ with respect to V and P, from $V = V_o$ at $P = P_o$, gives

$$V = V_o.((A + B.P_o)/(A + B.P))^{1/B} \qquad (2)$$

The computer program takes the density of the liquid to be the reciprocal of V and uses an equation corresponding to the equation given above to determine the liquid density at pressure P from the density at P_o.

If P is Gauge Pressure, in MPa , rather than Absolute Pressure, then $P_o = 0$, and A is greater by 0.1014 B , but the equations are otherwise unaltered.

If the liquid is being compressed by a piston of known area the equivalent lengths x and x_o can be substituted for V and V_o in the above equations, with no other alterations.

A "differential corrections" procedure can be used to find a "least squares" best fit of x/x_o data as a function of P in the equation

$$x/x_o = ((A + B.P_o)/(A + B.P))^{1/B}$$

to find values for A and B. Observations of x at two or more different pressures, P (P greater than P_o), with x_o and P_o known, determine values for A and B, and so define x and dP/dx as functions of P, P_o, and x_o . It is inherent in the above equations that the product -V.dP/dV, or -x.dP/dx, increases linearly with pressure.

If the liquid is compressed by a piston driven by a solid propellant charge it can be expected to oscillate at the end of its stroke with a frequency determined by the mass of the piston and the stiffness of the spring represented by the liquid column. If the Bulk Modulus of the liquid is

$$K = A + B.P \quad (= -x.dP/dx)$$

then the linear stiffness of the liquid column (-a.dP/dx) is K.a/x where a is the piston area and x the equivalent length of the liquid column.

If the mass of the piston is M and the frequency of oscillation is f,

Then $$f = \sqrt{K.a/M.x}\ /2\pi \quad (\text{neglecting the mass of the liquid}) \qquad (3)$$

and $$K = A + B.P = M.x.(2\pi f)^2/a \quad . \qquad (4)$$

As x can be expressed in terms of x_o, A, B, and P, observations of frequency, at two or more pressures, can be used to find A and B without measurement of x. Or if x is measured, as well as frequency, values for A and B at a particular pressure can be determined from a single experiment. But if K is not linear with P the values of A and B determined by this method for the maximum pressure may not agree with the values obtainable from the whole of the x/P relationship recorded at the same time.

Bridgman, in The Physics of High Pressures, Chap. 5, proposed using different compressibility laws for pressures above and below 50 MPa. Above 50 MPa he proposed an equation of the form

$$V = V_o.(D - E.\text{Ln}(P)) \quad \text{where P is gauge pressure.} \qquad (5)$$

This equation implies a Zero bulk modulus at P = 0 and $V = V_o$. He suggested that below 50 MPa the compressibility should be represented by a quadratic, i.e.

$$V = V_o.(1 + F.P + G.P^2) \quad . \qquad (6)$$

In practice it would be awkward to use such a scheme with the need to fit different curves to different sections of the compressibility data, while ensuring continuity at the change-over point, and to switch from one equation to the other during the running of an internal ballistics computer program.

If experimental data show that a bulk modulus increasing linearly with pressure is not an adequate representation then using equations derived from

$$\text{Modulus} = A + B.P + C.P^2 \quad , \qquad (7)$$

where P is "gauge pressure", should be considered.

This has the advantage, over equations of the "Bridgman" type, in the Liquid Propellant Internal Ballistics Program, of giving a single relationship between x/x_o and P for the full pressure range, and only a single relationship to consider when obtaining coefficients by fitting to experimental data.

The x/P relationship obtained by integration of

$$x.dP/dx = -(A + B.P + C.P^2) \qquad (8)$$

is more complex than that considered before, and depends on the relative magnitudes of B^2 and $4A.C$. If $B^2 = 4A.C$, the equation for the modulus reduces to

$$\text{Modulus} = C(B/2C + P)^2 \qquad (9)$$

$$\text{and} \quad x = x_o.\exp(2(1/(B + 2C.P) - 1/B)) \quad . \qquad (10)$$

If $B^2 > 4A.C$ and if $S = \sqrt{B^2 - 4A.C}$

$$x = x_o.((2A + B.P - S.P)/(2A + B.P + S.P))^{1/S} \qquad (11)$$

If $B^2 < 4A.C$ and if $S = \sqrt{4A.C - B^2}$

$$x = x_o.\exp(2(\tan^{-1}(B/S) - \tan^{-1}((B + 2C.P)/S))/S) \qquad (12)$$

To make a "differential corrections" least squares fit of x/x_o and P data to these equations requires that the equations be differentiable with respect to each of A, B, and C . This is possible, by fitting $\text{Ln}(x/x_o)$ in all cases, the last two equations (11 & 12) giving the same partial differentials.

DISCUSSION

M.Summerfield, US

This is a comment, although I would be interested in learning the position of Dr Cook or Dr Andrews on this point.

Liquid monopropellants are not in use in the liquid propellant rocket field; bi-propellants are used instead in applications where liquids are more appropriate than solids. As for solid propellants, homogeneous type solids (e.g., nitrocellulose-base) are not used for manned applications, like the Space Shuttle. In both cases, there is a good reason: the sensitivity of such homogeneous propellants, liquid or solid, seems to be too great.

In the US, in the 1940s and early 1950s, there was a long and (for the time) quite expensive development effort centred on the possible use of liquid nitromethane as a monopropellant. After many years of experimentation, the effort was abandoned. There were too many unexplained explosions, even though the liquid is deemed safe enough to ship on railroads and trucks in tanks as an industrial product. There was a similar effort in Germany during World War II. Their liquid monopropellant was named Myrol, and it consisted of a mixture (a true solution) of methyl alcohol and methyl nitrate. They developed a rocket fighter for it, but abandoned the project when the sensitivity proved too great. We know also that nitrocellulose-base propellants show a much greater sensitivity to impact or shock-induced explosion, and also a lower initiation temperature, than the well-known heterogeneous propellants based on ammonium perchlorate.

In the case of the liquid monopropellants intended for LP gun application, there have been several unexplained (surprising) initiations and explosions, for which we have no explanation within the knowledge we have at present. Therefore, if we wish to retain the mechanical simplicity of a monopropellant, but reduce markedly the hazard, we might consider a heterogeneous type liquid monopropellant analogous to the heterogeneous solid propellants. There would be a large variety of composition possibilities. For example, the liquid monopropellant designated as 1845 (see the earlier Paper 2 by Morrison, et al) consists of a mixture of HAN, a somewhat oxidizing salt dissolved in water, with a water-soluble fuel. If an insoluble finely-ground fuel were used instead, the suspension or mixture could be called a heterogeneous monopropellant. There are other possibilities that can occur to the chemist. The requirement of mutual solubility of the two reactive components in a small percentage of an acceptable solvent had restricted the possibilities at first; that requirement can thus be dropped. There would, however, be some severe limitations, thermochemical balance on the one hand and thixotropy on the other. But still, the payoff would surely be a sharply reduced sensitivity, inasmuch as the degree of molecular contact is far less for the case of a heterogeneous propellant than for a homogeneous one.

The comment is, therefore, that it would be worthwhile for the NATO countries not to duplicate the efforts of the US but to try some different routes. It is not clear that the present LP gun development in the US will prove acceptable to the ultimate user. It was the ultimate user who refused the nitromethane rocket motor; it may well happen in this case. We cannot be sure, so other approaches should be tried.

P.Ramette, Fr

On Figure 14, you show a maximum liquid pressure of 623 MPa from a test. Is that the maximum value of liquid pressure that you have obtained during your test? That's part of my question. On the other hand, do you plan to have a test at higher pressure by modifying, if need be, your closed vessel?

Author's Reply

This is the maximum pressure that we have used in our experiments and we have no plans in the immediate future to raise this figure. The value of 600 MPa is the maximum safe liquid working pressure of our liquid propellant test vessel. However, in the longer term we would like to go to higher liquid pressures.

N.Rhodes, UK

Would it be worthwhile to incorporate a more conventional equation of state in your model? For example, consider those used in explosion containment models in which equations are solved simultaneously for volume and energy.

Author's Reply

This is one of the possible approaches that we have in mind. One can look at the rapid compression of the liquid propellant from the viewpoint of thermodynamics rather than conventional fluid mechanics.

W.F.Morrison, US

We have also made estimates of the temperature rise in LPs when rapidly compressed. Our estimates are on the order of 10 to 15 deg C, compared to the estimated temperature rise of 40 deg C quoted for your silicone fluid. How did you make your estimate?

Author's Reply

The temperature rise was estimated from the compression work, assuming a simple adiabatic process. We would expect that the water-based propellants (i.e., the HAN-type materials) would have a significantly lower temperature rise due to the fact that they are less compressible that the inert fluids which we have tested. The temperature rise for Otto Fuel II, because of its bulk modulus, will lie between the values for the silicone fluid and the HAN-based propellant.

MECHANICAL BEHAVIOUR OF PROPELLANT GRAINS UNDER HEAVY DYNAMIC LOAD

Gerd Zimmermann

Fraunhofer-Institut für Kurzzeitdynamik, Ernst-Mach-Institut
Abteilung für Ballistik (EMI-AFB), Hauptstrasse 18, D-7858 Weil am Rhein

SUMMARY

Special test devices have been constructed to simulate the dynamic forces on gun propellant grains during shots at ambient and low temperatures (-40 °C). With these devices the dynamic stress at failure, the fragmentation type (pasty, brittle) and other correlated physical characteristics of several propellant types were measured. Conclusions are drawn for the propellant behaviour under real gun conditions.

1. INTRODUCTION

In the FRG, at the beginning of the eighties some incidents with ammunition charged with granular propellants led to more intensive studies of the interior ballistics of guns using this kind of ammunition. For this reason, a working group under the leadership of the Federal Office for Armament Technology and Procurement (BWB), WM IV 6 (Mr. Leber), was set up comprising the Proving Ground E 91 at Meppen, several research institutes and companies. The working group deals especially with the generation of pressure waves due to bad igniter functions, and their consequences [1]. One of these consequences is the heavy dynamic loading of the propellant grains, in particular near the projectile base. Therefore, during the last years, in different countries a large number of studies in this domain have been carried out. It is not the intention of this paper to give a general overview of all this work, but to present the work done by the Ernst-Mach-Institut (Fraunhofer-Institut für Kurzzeitdynamik) within the frame of the working group cited above, and to outline the ideas on which it is founded.

2. MEASUREMENT OF THE LOAD ON PROPELLANT GRAINS IN GUNS

The first of the principal elements of studies of the load effect on propellant grains should be an estimation of this load under real gun conditions. For this purpose, we developed two instruments. The one on the basis of a piezoelectric foil should allow us to measure the sum of the forces on the projectile base (for a flat projectile base at least) during the ignition process.

The principle of this measurement is shown in Figure 1. In fact, we measure the sum of these forces divided by the gauge surface area, and we call this quotient "grain pressure", superposed by the gas pressure, if present. The sum of grain pressure and gas pressure is called "total pressure". The grain pressure can be determined by subtracting the gas pressure from the total pressure. But frequently, in the beginning of propellant ignition, the gas pressure near the projectile base is negligible, and the gauge then measures directly the grain pressure. Typical gauges installed in a projectile are shown in Figure 2.

Figure 3 depicts some results of total pressure measurements, together with gas pressure measurements for a small caliber ammunition. Figure 4 shows similar curves for a 105 mm tank gun test ammunition: Figure 4a for a normal shot fired with a 105 mm simulator at E 91 Meppen, FRG, and Figure 4b for a shot with a manipulated igniter for unilateral ignition.

From such tests for a given ammunition normal and worst case grain pressure-time curves can be deduced. Since the measurement method is rather new, the available data base is relatively small. Most of our tests have been carried out in simulators, i.e., combustion chambers of the same interior dimensions as that of real guns, but with a very short barrel. Besides that, for small caliber some shots have been made with real guns, and for large caliber some shots with the simulator of the E 91 which is, in fact, a real gun with shortened barrel. Most of the tests were made at ambient temperature, but experiments at temperatures as low as -40 °C are under way. The following values have been measured for ambient temperature:

Small calibers:	Grain pressure: up to and greater than 100 MPa for small grains Rate: 200 GPa/s
Large calibers (normal):	Grain pressure: 20 MPa Rate: 60 GPa/s
Large calibers (manipulated igniter):	Grain pressure: 60 MPa Rate: 250 GPa/s

The following factors decrease the grain pressure: lower loading density, bigger grains, shorter combustion chambers, lower igniter gas velocity, lower igniter gas pressure (of course, correct ignition must be guaranteed), higher grain stiffness.

The latter factor which, in general, should lead to comparably smaller grain pressures or lower temperatures, will be discussed again later on, because of the problems created by brittleness of the grains.

Unfortunately, the grain pressure measurements do not give immediately the stress on the grains. For that purpose, the contacting surfaces between the grains and between the grains and the projectile base should be known. The contacting surfaces between grains and projectile base before the shot can be estimated by putting a column of grains on a glass plate and looking through it. Like this, we estimated the sum of the contacting surfaces between a M30 propellant charge and the projectile base to be 1/10 of the base surface. So the mean stress should be about ten times higher than the grain pressure. During the shot when the grain pressure rises, the grains are deformed and the contacting surface increases. Cleve and coworkers of the E 91 Meppen attempted to look at the grains during the ignition phase by using a glass projectile. Until now, the projectiles have broken before the grain pressure maximum was reached. But, as far as we know, these experiments are continuing.

The second method to measure the load on propellant grains consists in equipping hollow cylindrical grains made of steel with strain gauges and put them on the projectile base (Figure 5). The disadvantage of this method is the fact that the grain can only be calibrated for coaxial charges (on the top of the cylinder), but the forces exerted on the grain within the propellant bed are rarely purely coaxial. That is why good measurements of this kind are rare. One of them is presented in Figure 6. There, the measured stress on the grain is compared to the grain pressure measured in the same shot. Until the destruction of the steel grain, the stress on the grain follows quite well the grain pressure, multiplied by eleven. In that experiment, the grain pressure was rather small, and this is perhaps one of the reasons why the measurement with the steel grain gave good results.

3. SINGLE GRAIN TESTS, SETUP

Logically, the next step after the measurement of the grain pressure would be to put granular propellant inside a cylinder, load it with similar forces as measured under real gun conditions, and look what happens. But the phenomena occurring in these experiments can be more easily understood if the behaviour of single grains is known before.

Therefore, a test device was developed which allows us to measure dynamic stress-strain curves of single grains and to see the grain break-up and the fragmentation patterns afterwards (Figure 7). The device mainly consists of a propellant driven piston and an anvil, between which a propellant grain (or multiple grains) can be placed.

The piston displacement is measured in two ways: by an optical tracker (low resolution, long displacement) and an inductive system (high resolution, e.g., 0.1 mm). The anvil contains a gauge allowing the measurement of the force transmitted and, for well-defined contacting surfaces, the determination of the stress for single grain tests or of grain pressure for multiple grain tests. The fragmentation process can be filmed by a high speed camera. A cooling chamber has been built to carry out tests from ambient temperature to -40 °C.

Before the tests, the piston can be held by a shear pin at a given distance from the grain in such a way that it hits the grain with a certain impact velocity. But until now, this feature has not yet been used. The problems we investigate arise with ammunition with very high propellant loading density, not allowing long free flight paths for the grains. Therefore, we put the piston on the grain before the test begins, so that the stress rate on the grain does not rise abruptly as it would at impact.

On cylindrical grains both longitudinal and lateral loading tests were carried out. The piston normally was not allowed to compress the grains completely, because there was a self-ignition limit where the compressed material deflagrated, causing at least the loss of the force gauge. For this reason, a slotted steel ring surrounded the grain under test (e.g., with an inner diameter of 30 mm for a grain with a diameter of 8 mm) intercepting the piston at a given height. Stopping the piston at different heights furthermore provided a means to study the break-up process of the grains in detail without the use of the high speed camera.

4. TEST RESULTS WITH SINGLE GRAINS

Ambient Temperature Longitudinal Compression

At ambient temperature (about 20 °C) the behaviour of most of the tested propellant grains under load is plastic or even pasty. The elastic domain is very small. Figure 8 shows typical phases of compression in longitudinal direction. The grain bulges like a cask, increasing its diameter especially in the middle. The strain at fracture can be as high as 50 %, and fracture happens by overstrain on the outer surface. The fragments do not separate, and the compressed grain looks like an asterisk.

There is a limit of compressibility, where the inner mechanical confinement prevents a lateral flow. At this limit, the stress-strain curve steeply rises and the risk of self-ignition becomes imminent. A typical stress-strain curve is shown in Figure 9, together with a stress-time curve.

Indeed, there is a problem. In principle, the stresses should be calculated with the aid of the actual cross-sectional area. But this area depends on the location of the cross-section and varies with time. For our basic investigations this complicated calculation is not yet necessary, but for later applications the cross-sectional area variation during the test should be taken into account. In all stress curves presented here, the stress has been calculated by dividing the (measured) force by the initial cross-sectional area of the grains.

Not all propellants show the same behaviour. The triple-base propellant KN 5470 of the M30 type at ambient temperature does not only show longitudinal cracks on the outer surface, but lateral cracks too, and the coherence between the fragments is smaller, Figure 10. This is indicated too by the stress-strain curves in Figure 11, which after fracture drop down to a minimum which is lower than that of most of the other propellants. The fracture is not as plastic as with the other propellants, though at that temperature far from being brittle.

-40 °C, Longitudinal Compression

At -40 °C most of the propellants tested became more or less brittle. This is indicated by the fragment patterns as well as by the stress-strain curves. Figure 12 shows fragments of a M30 propellant together with its stress-strain curves, Figure 13 the same for a JA2 propellant, and Figure 14 for the propellant Q 5560 which maintained a large degree of plasticity down to that temperature.

In general, the increasing brittleness at low temperatures is accompanied by a higher stress at fracture, which at -40 °C is frequently two or three times that at ambient temperature. (Remember that for the calculation of the stress, the original contacting surface was always used.) See Figure 15.

Figure 16 shows the fragmentation process for the M30 propellant at -40 °C. The propellant grains were graphited and black. During the test, the surface breaks up and the nearly white interior material appears. The clouds which can be seen are composed of very fine material in dust form.

-40 °C, Lateral Compression

In lateral compression, the stress distribution over the grain is very inhomogeneous. Therefore, the stress-strain curves differ considerably from those measured with longitudinal compression. First fracture happens at a relatively low compression level (1/10 of that at longitudinal compression). But the first fragments created are relatively large so that successive cracking of fragments occurs during the movement of the piston towards the anvil (Figure 17). In this figure, the signal of a photodiode was recorded too, indicating the approximate time of self-ignition. After self-ignition, the grain very quickly burns away, allowing the piston to move forward again until it hits the anvil.

5. MULTIPLE GRAIN TESTS

As noted before, multiple grain tests can give results which are very similar to that of real firings, and they are the link between real shots and single grain tests. The measurement setup is very similar to that of the single grain tests, but the head of the piston is modified as shown in Figure 18. The force gauge can be used to determine the corresponding "grain pressure", and by selection of different types of propellant, piston weight and height of the intercepting ring a large variation of the "grain pressure" functions versus time is possible.

At ambient temperature, nearly all propellant charges can be compressed without breaking, so much, that only small slots remain between some of the grains. The form of the grains changes to fill up the available space, see Figure 19.

At low temperatures, nearly all the propellants become more stiff, as said before, and therefore the compression of a charge, e.g., at -40 °C is much more difficult. It is done by repacking the grains in a more dense way or by breaking some grains rather than by adaptation of the outer grain shape to the available empty space.

Figure 19 gives the results of a multiple grain test with a JA2 propellant. The charge had a diameter of 30 mm and the same height. It contained 31.7 g of the JA2 propellant. In a cross-sectional area about 8 grains could be found. The piston was intercepted after 10 mm. Figure 19b shows a longitudinal cut of half of the charge after compression, Figure 19c a transverse cut of the other half of the charge at about half the charge height (Figure 19a). The force versus compression measured on the anvil is depicted in Figure 19d. It shows a first main maximum at a piston displacement of 8.2 mm. The time from force 0 to this displacement was 450 µs. An analysis of this and preceeding experiments gives the following results: Up to a piston displacement of 8.2 mm, the charge compression was mainly done by grain repacking. Then, at about 24 kN the first grains cracked, giving a short relaxation. Due to the continuing load, the charge was compressed furthermore until a new blocking occurred, but now the compression was interrupted by external piston interception. At this moment, nearly all of the grains were severely damaged, a large number of them totally destroyed. The fragments filled the space between less damaged grains nearly completely, and the majority of them was very

small comprising a certain amount of propellant material in dust form. It is significant, that the cracking process begins abruptly on a large scale after the force has reached a certain level. This level corresponds in our experiments approximately to the fracture level for a single grain side-on test (24 kN: 8 grains = 3 kN/grain). The force of fracture for a longitudinal test was in the order of 15 kN for a single grain. A look at Figure 19a and 19b allows the supposition, that the grains which were originally mainly randomly distributed, attempted to align themselves perpendicular to the main force direction, so that they were loaded side-on. The original distribution was insofar not random, as the grains on the projectile base as well as on the anvil always tend to be parallel to the surface they touch.

6. SELF-IGNITION

We do not consider self-ignition of propellant grains to be the reason of breech-blow accidents. The forces and compressions necessary are too high. Self-ignition effects could be important for propellant handling and especially in mechanical properties tests. At ambient temperature, it occurred frequently in our tests when during compression the propellant grains were compressed to small pellets, the mechanical self-confinement of which hindering further reduction. At low temperatures, with increasing embrittlement the self-ignition happened earlier; perhaps the mechanical self-confinement level is reached earlier, but this has not been studied in detail. An M30 propellant grain of 12 mm length at ambient temperature had to be reduced to about 1 mm to ignite, at -40 °C to 3 mm. After self-ignition, the grains burned away within some 10 µs. A shock wave has not been measured, so that presumably the grain did not detonate, but deflagrate. The force necessary to induce self-ignition was about three times that necessary for grain break-up.

The problem of self-ignition is more critical for multiple grain tests, when the granular charge is confined by a housing (e.g., a steel ring). Given the relatively high loading density of the test charges, a relatively small compression leads to a consolidated block of propellant material. In a multiple grain test with JA2 propellant, similar to that described above, self-ignition occurred after a piston displacement of 13.5 mm, i.e., a compression of 45 %, at unknown force level, causing considerable damage. The charge density at that moment was 1.45 g/cm^3, corresponding to the density of the propellant material. In quasistatic loading, self-ignition never occurred.

7. CONCLUSIONS

The experimental methods presented should help us to foresee possible risks of overpressure due to mechanical grain destruction during the ignition phase for a given charge/igniter assembly. For that purpose, the results of worst-case experiments with "grain pressure" measurements have to be compared to those of stress-strain measurements in mechanical single and multiple grain tests. In this way, the security margin between the maximum grain pressure and the stress at fracture could be determined as well as possible fragment patterns after break-up of the grains.

Up to now, this procedure has not been carried out consequently, and the data base available is relatively small and some aspects like the influence of the duration of the mechanical forces on the fragment patterns have not yet been sufficiently investigated. But we hope to improve our methods in future to get a reliable aid for the selection of charge assemblies.

In this presentation, a lot has been said concerning the embrittlement and break-up of propellants. In this respect, a comment is necessary. Most of the existing propellants (though not all of them) show brittle fracture at -40 °C, if a certain stress level is exceeded. This does not mean that these propellants necessarily are unsafe. It means only, that the charge must be assembled in such a way, that the break-up stress level cannot be reached, even under unfavourable conditions. Rules, which help to satisfy the safety conditions, are

- low charge density,
- uniform ignition over the length of the combustion chamber,
- soft ignition (no sharp and high pressure rises, low igniter gas velocity),
- high permeability of the propellant bed for the igniter gases (big grains).

Following these rules, safe charges can be made even for propellants with a high degree of brittleness at low temperatures. In this context, "safe" means safe against the effects of grain break-up due to excessive mechanical loads during the shot. Certainly, we should not forget that this is only one aspect of the safety of ammunition.

REFERENCES

[1] G. Zimmermann, "Investigations of Gas Pressure Waves and Intergranular Stress Waves in Large Caliber Guns Using Granular Propellants", AGARD Conference No. 367, Lisse, The Netherlands, 1984

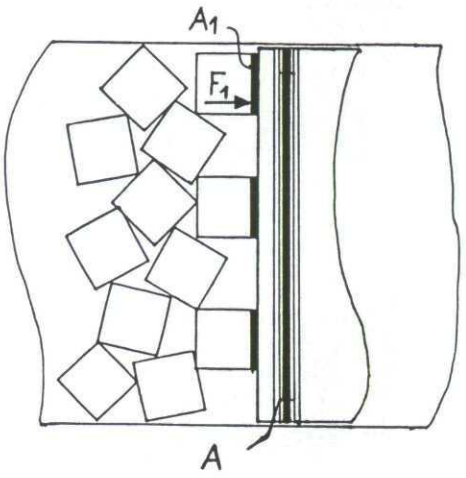

MEAN MECHANICAL STRESS ON THE CONTACTING SURFACES BETWEEN GRAINS AND PROJECTILE BASE

$$P_{nm} = \frac{1}{n} \cdot \Sigma \frac{F_i}{A_i} \approx \frac{\Sigma F_i}{\Sigma A_i}$$

for $A_k \approx A_i$

GRAIN PRESSURE (MEASURABLE)

$$P_y = \frac{\Sigma F_i}{A}$$

EVALUATION P_{nm}:

$$P_{nm} \approx P_g \cdot \frac{A}{\Sigma A_i}$$

FIG. 1: EXPLICATION OF THE EXPRESSION "GRAIN PRESSURE"

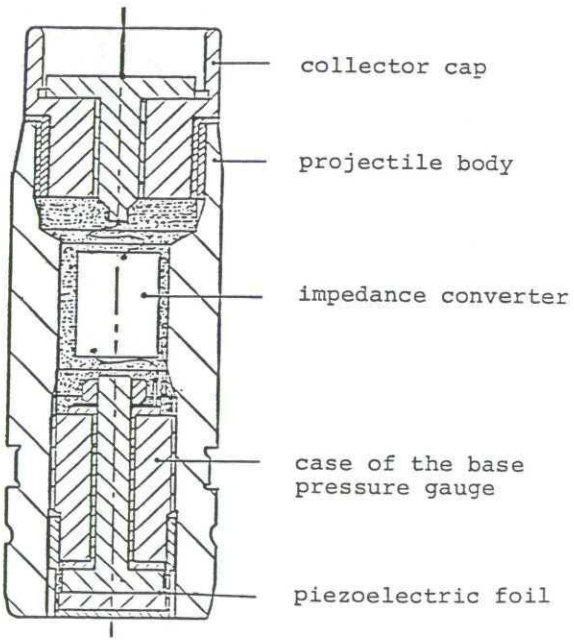

Fig. 2a: 25 mm projectile with piezoelectric foil sensor

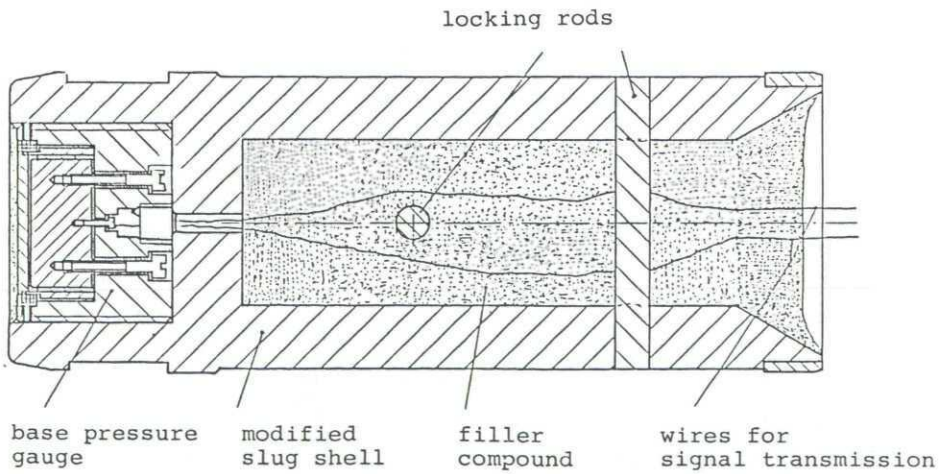

FIG. 2B: 105 MM PROJECTILE WITH PIEZOELECTRIC FOIL SENSOR

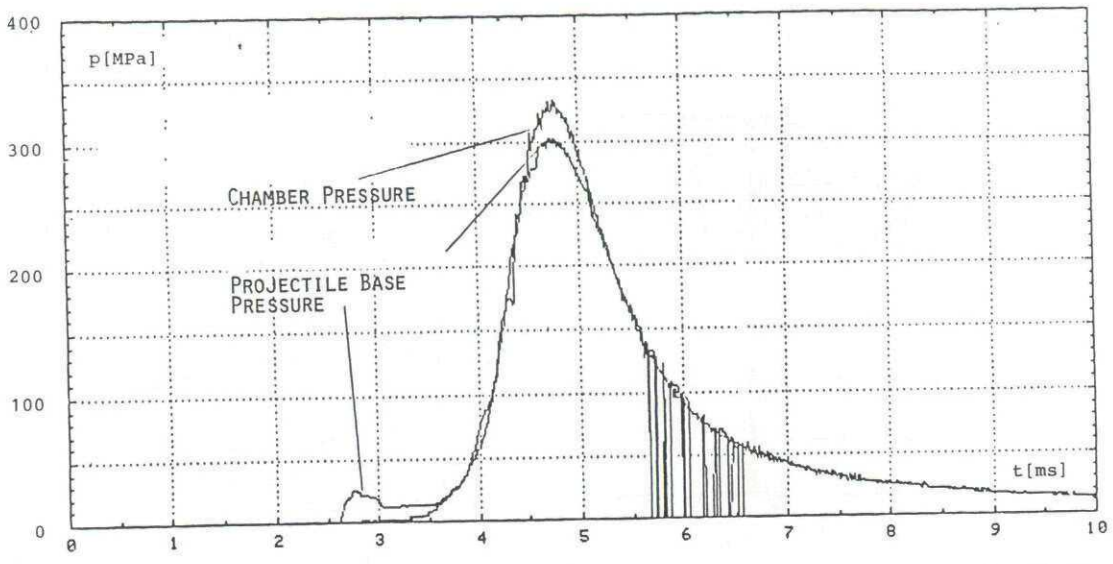

Fig. 3: Chamber pressure and projectile base pressure vs. time, cal. 20 mm

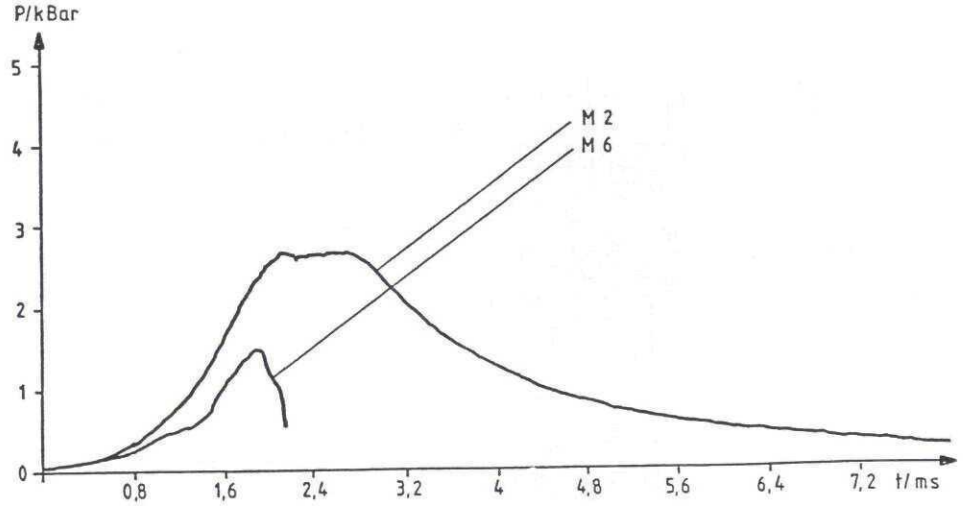

Fig. 4a: Pressure vs. time for original ammunition, ambient temperature, cal. 105 mm, shortened barrel

M 2: Gas pressure at a distance of 5 cm from projectile base

M 6: Total base pressure

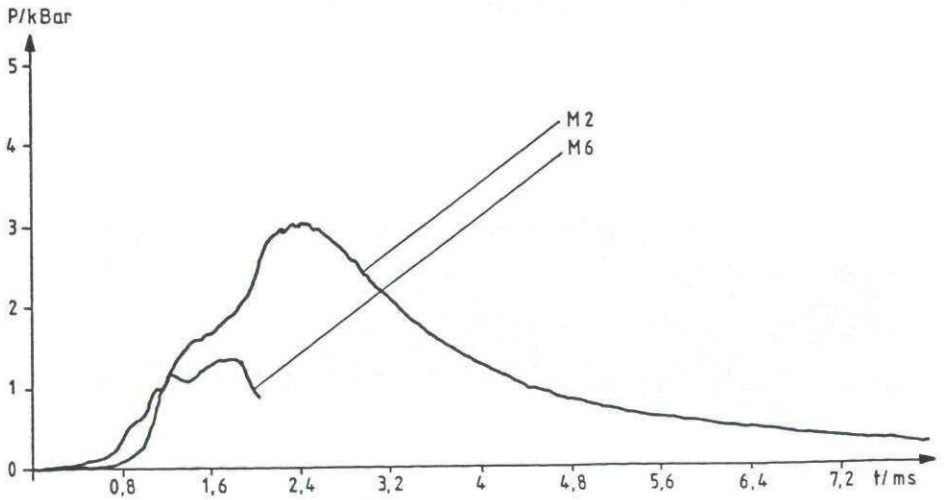

Fig. 4b: Pressure vs. time for original ammunition, ambient temperature, cal. 105 mm, shortened barrel, igniter manipulated for almost unilateral ignition near the breech

M 2: Gas pressure at a distance of 5 cm from projectile base

M 6: Total base pressure

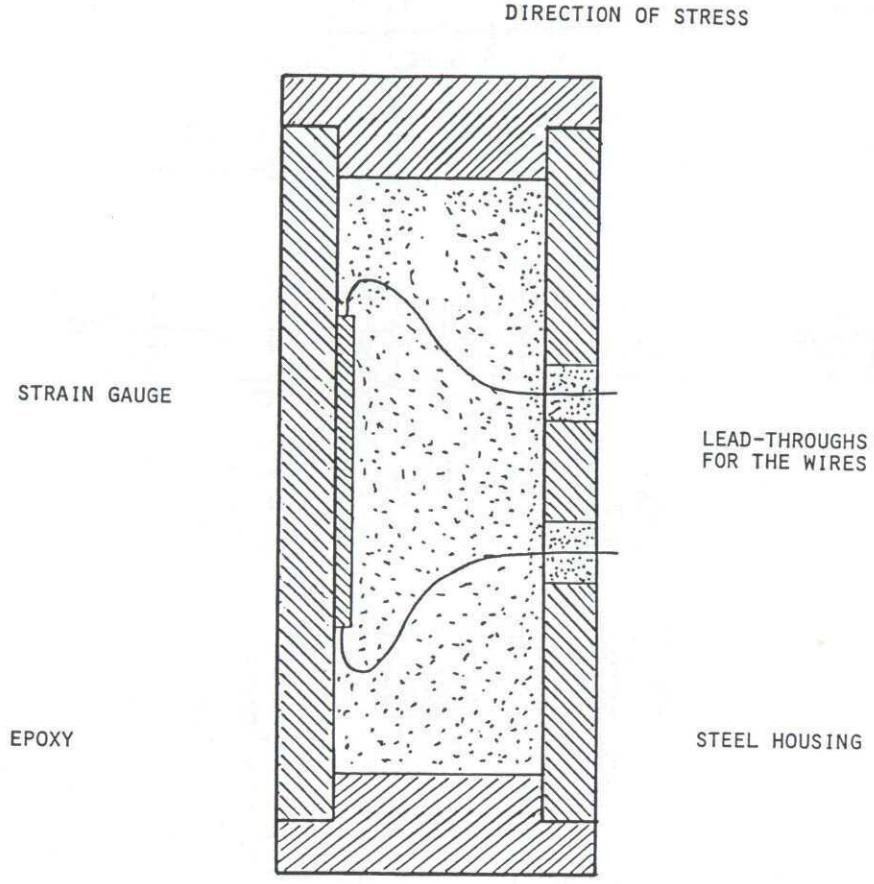

Fig. 5: Cylindric gauge for stress measurements simulating a powder grain

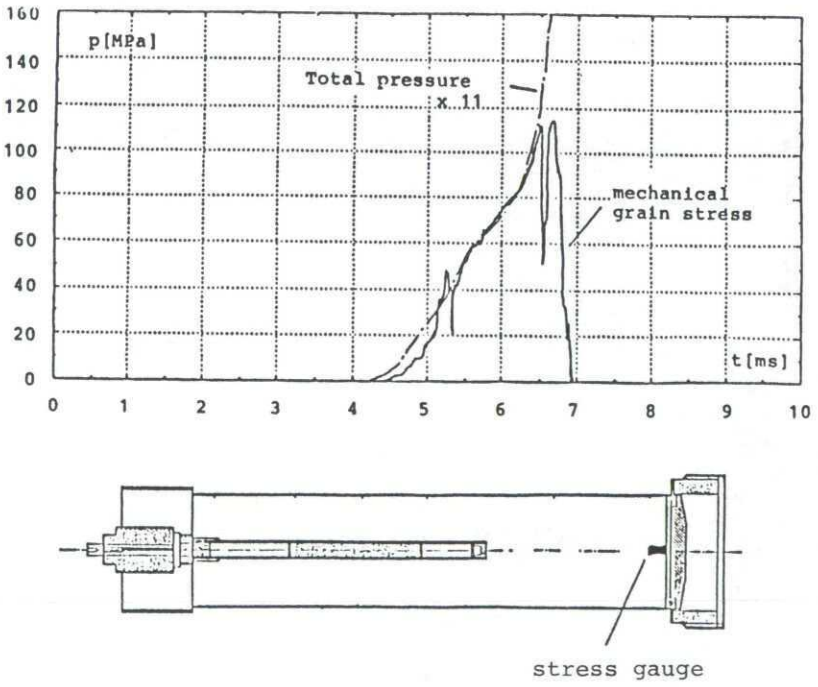

Fig. 6: Mechanical grain stress and total pressure on the shear disc, multiplied by 11, versus time

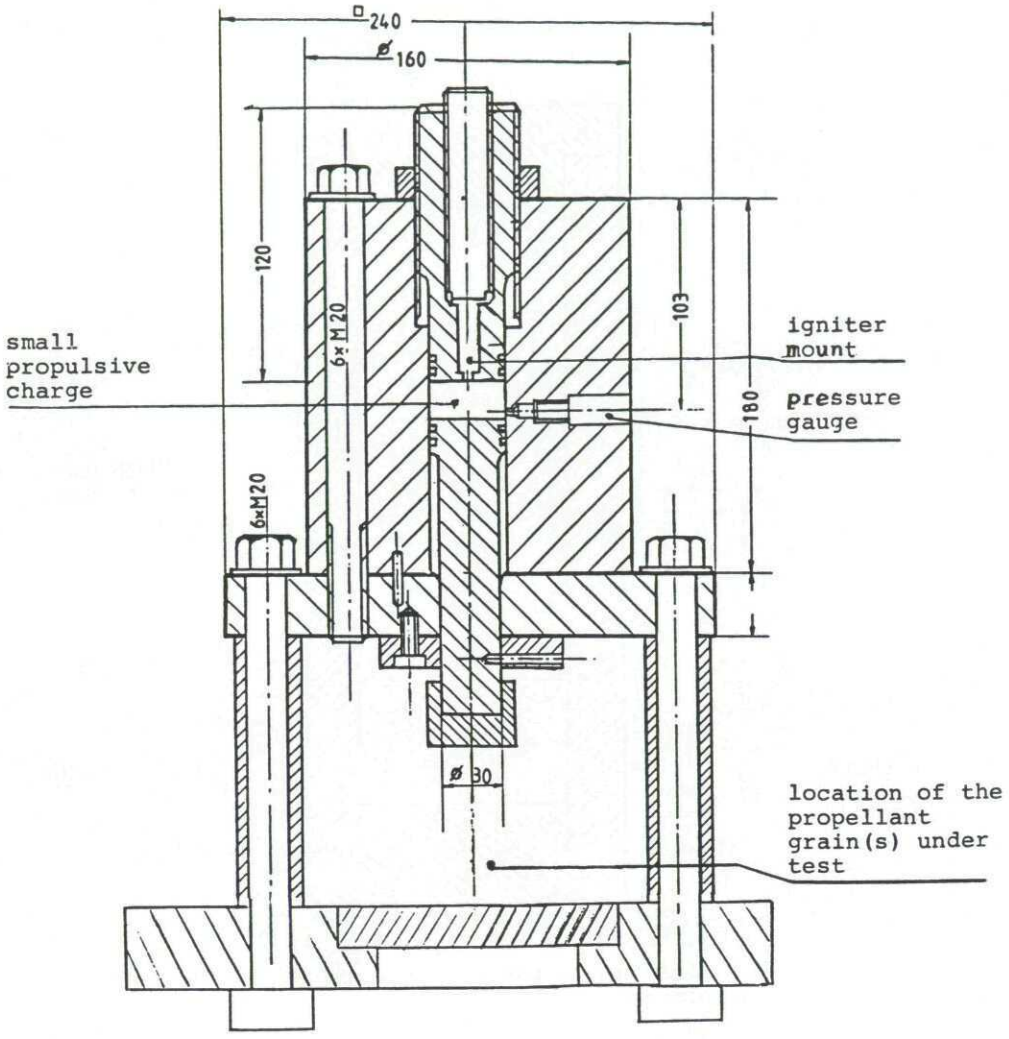

Fig. 7: Test device for the mechanical behaviour of propellant grains under heavy mechanical load, EMI-AFB

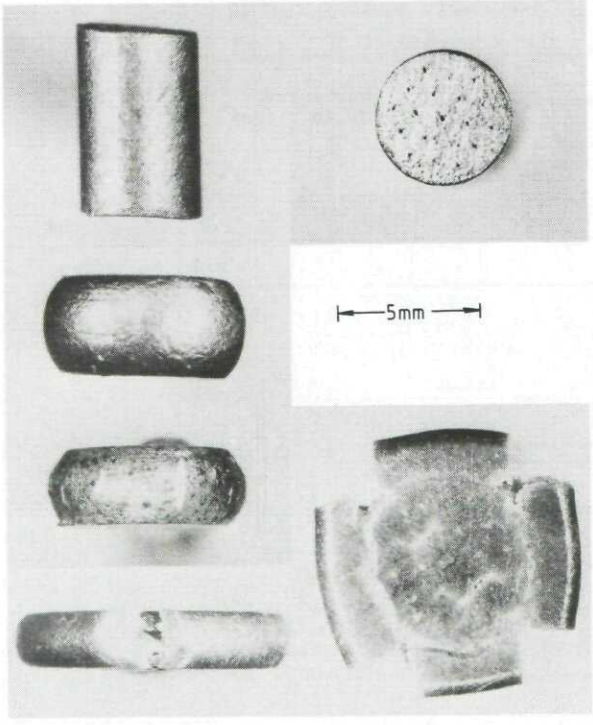

Fig. 8:
Typical fragmentation process of a gun propellant at a temperature of 20 °C

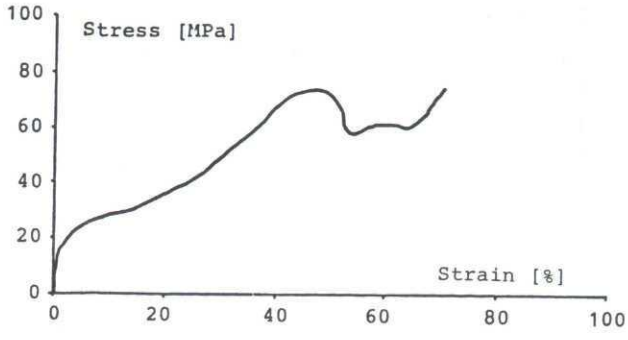

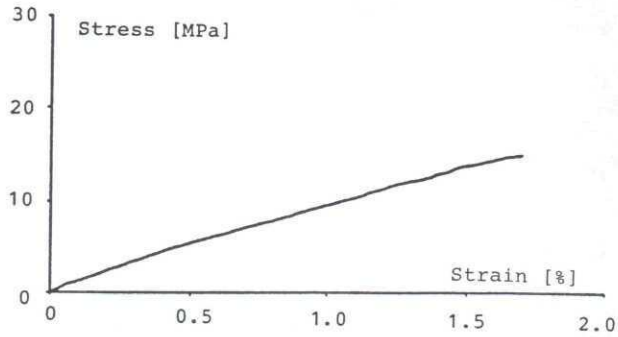

a) Stress vs. strain, low resolution b) Stress vs. strain, high resolution

Fig. 9: Results of a test with the EMI-AFB Tester of Mechanical Grain Properties, longitudinal load
Temperature: 20 °C; Propellant (JA2) L 5460 NC 1002/78

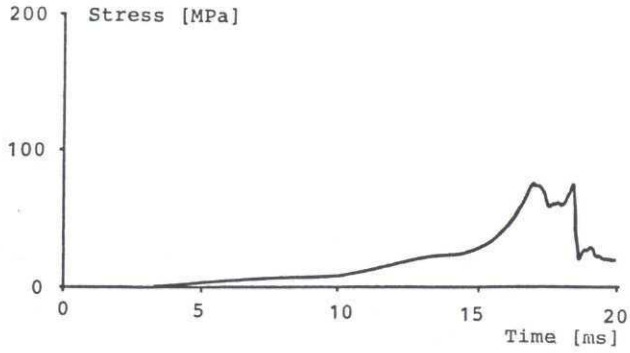

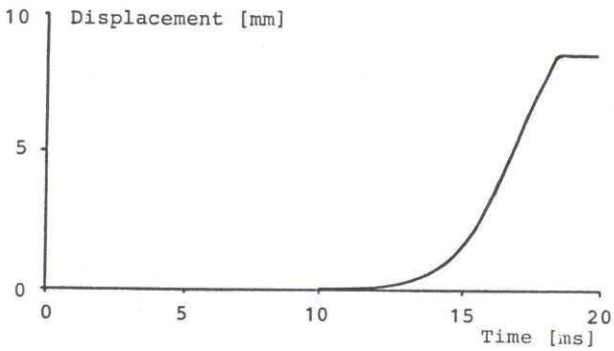

c) Stress vs. time d) Piston displacement vs. time

Fig. 9: Results of a test with the EMI-AFB Tester of Mechanical Grain Properties, longitudinal load
Temperature: 20 °C, Propellant (JA2) L 5460 NC 1002/78

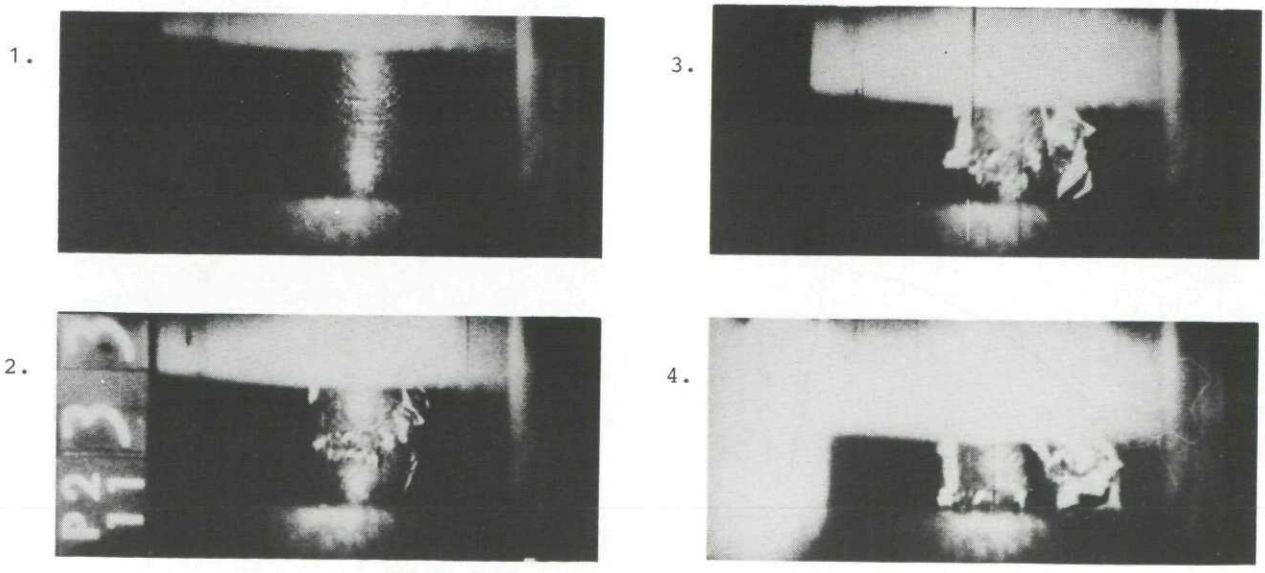

Fig. 10: Phases of fragmentation of a single grain under dynamic load at 20 °C
Time distance of the photos: 150 µs

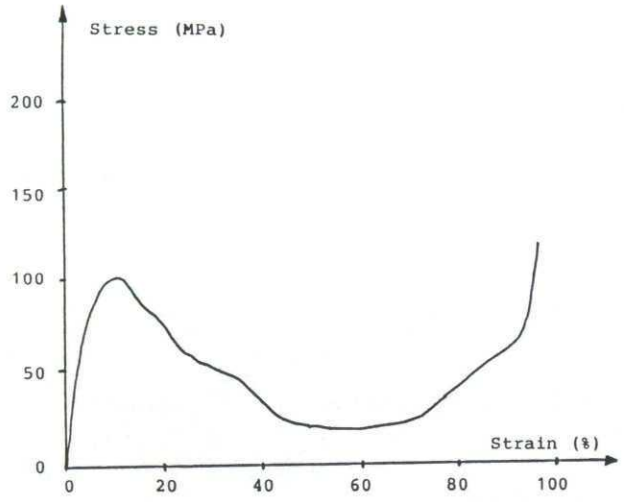

Fig. 11: Stress versus time for an M30 propellant, longitudinal load, temperature 20 °C

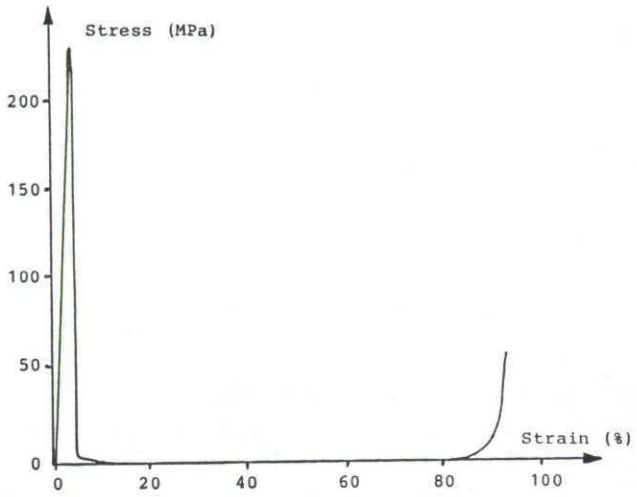

Fig. 12a: Stress versus time for an M30 propellant, longitudinal load, temperature -40 °C

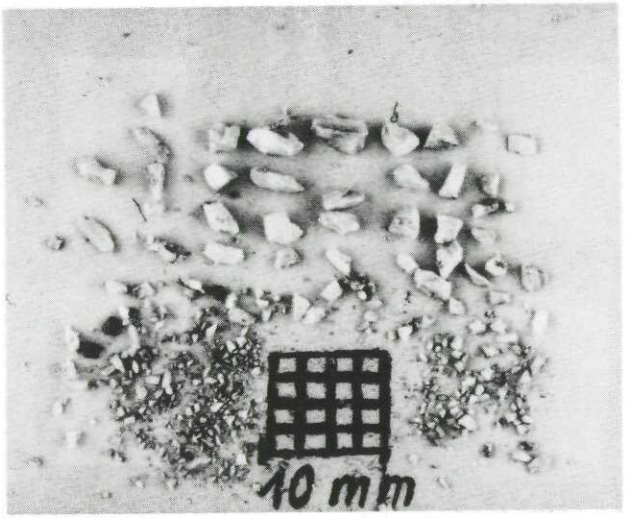

Fig. 12b:

Recovered fragments of an M30 propellant after a test at -40 °C (longitudinal load). Fragments in dust form were not recovered.

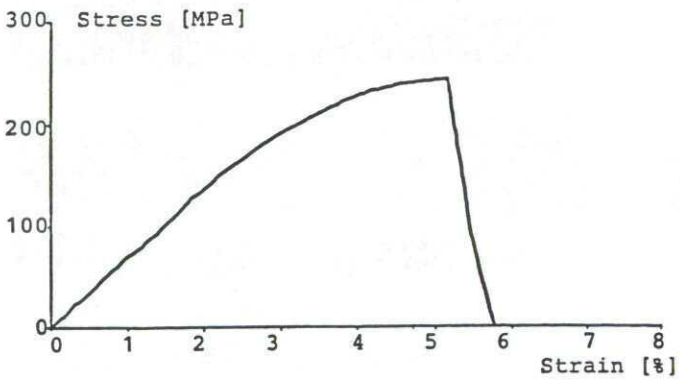

Fig. 13a: Stress versus strain for a JA2 propellant, longitudinal load, temperature -40 °C

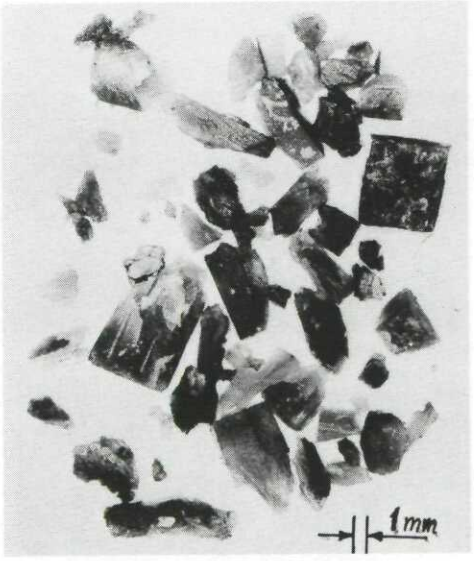

Fig. 13b:

Recovered fragments of a JA2 propellant after a test at -40 °C (longitudinal load)
Fragments in dust form were not recovered

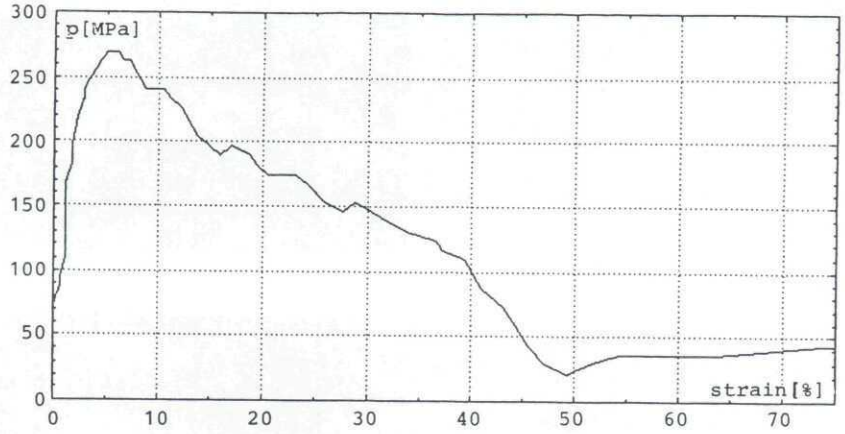

Fig. 14a: Stress versus strain for the propellant Q 5560, longitudinal load, temperature -40 °C

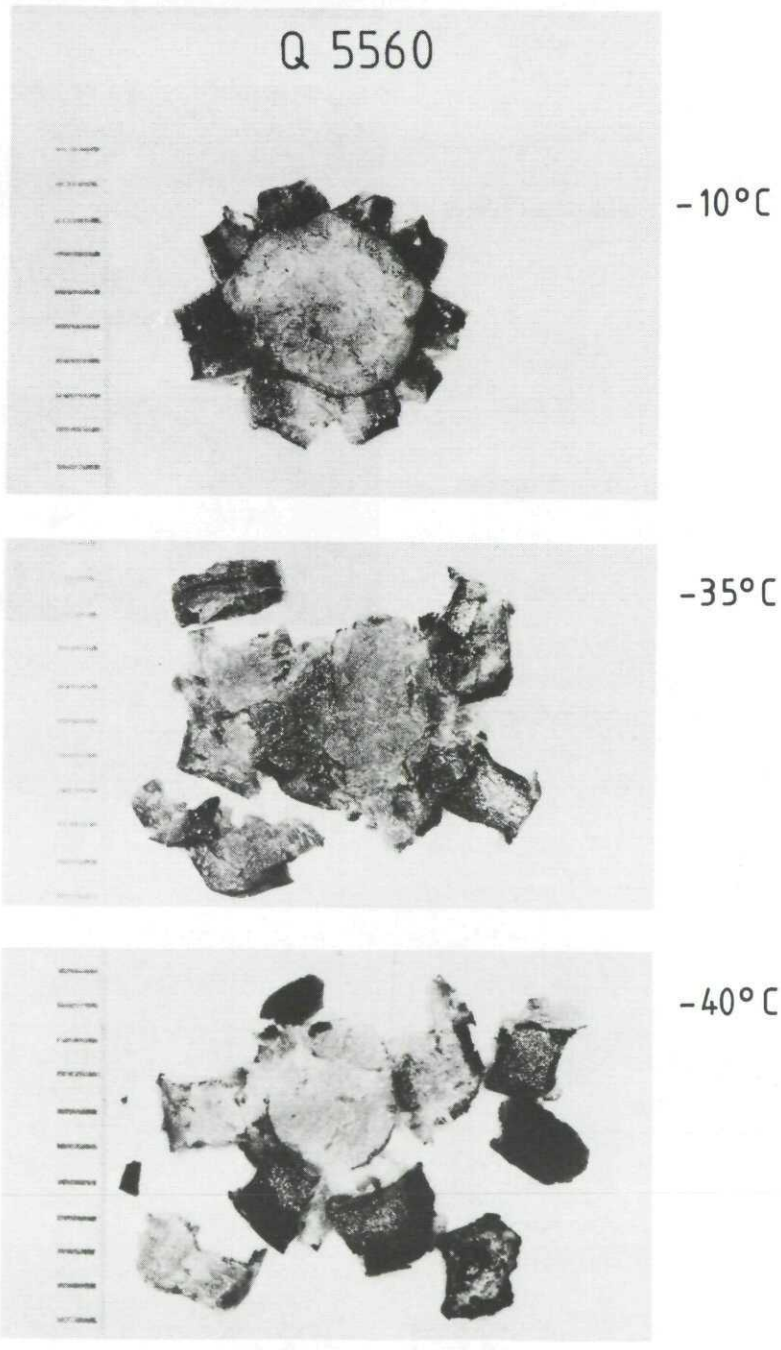

Fig. 14b: Fragmentation pattern of the propellant Q 5560 at different temperatures

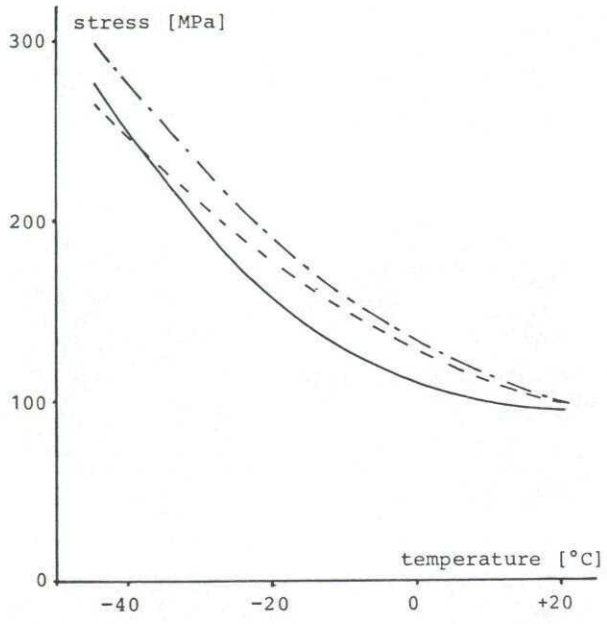

Fig. 15: Stress at failure for three different propellants

——— JA2 (mean value of different lots)
----- M 30
-.-.- Q 5560

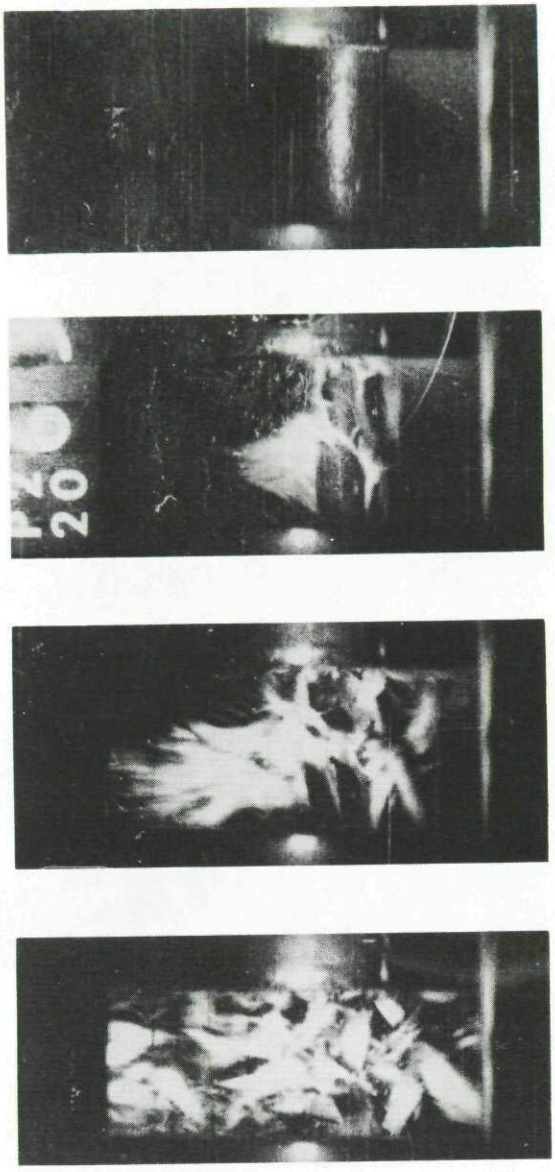

Fig. 16: Phases of fragmentation of a single grain under dynamic load at -40 °C. Time distande of the photos: 150 µs

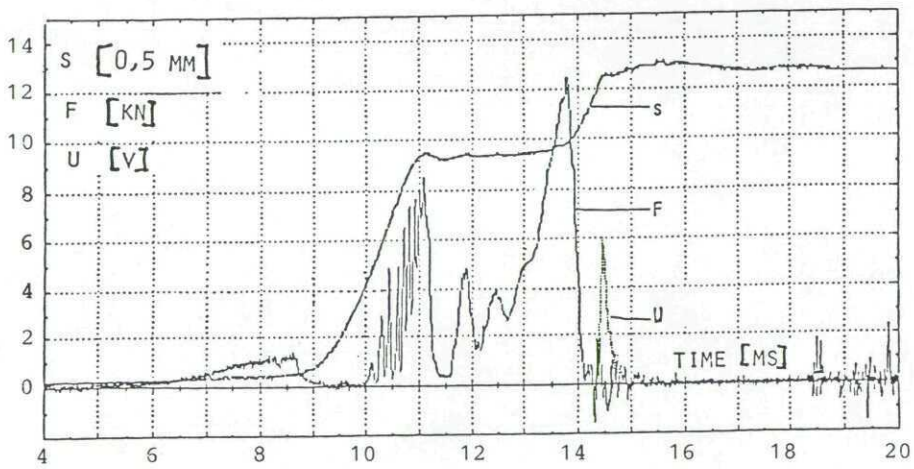

Fig. 17: a) Force F,
b) Piston displacement S,
c) Signal of the photodiode U

versus time t

Propellant: N 5470-33, temperature -45 °C, Side-on mode (force applied on the cylinder side)

Piston velocity up to the grain fracture: 0 - 3 m/s
Force rate up to the grain fracture: 0 - 0.4 kN/s

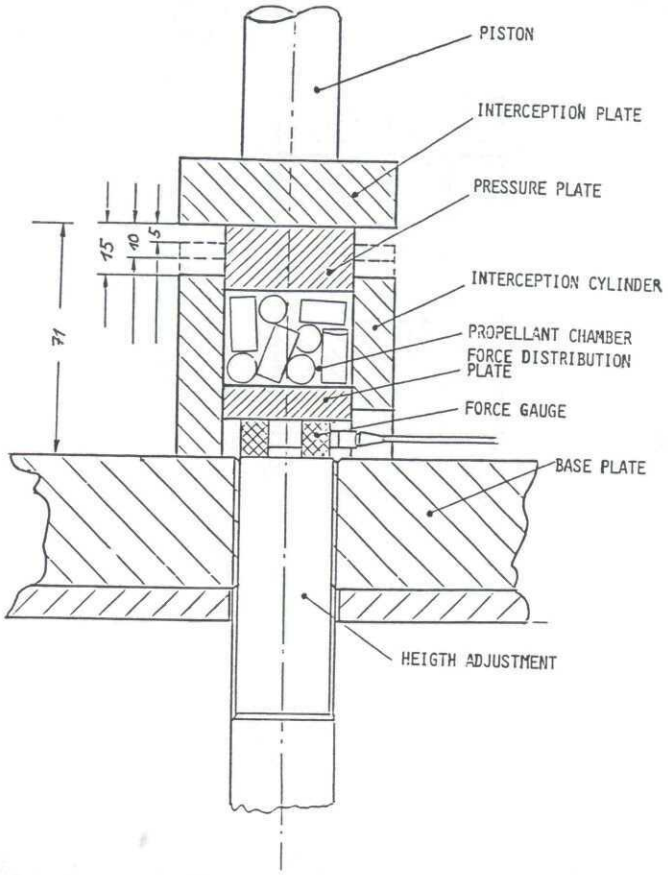

Fig. 18: Adaptor for multiple propellant grain tests

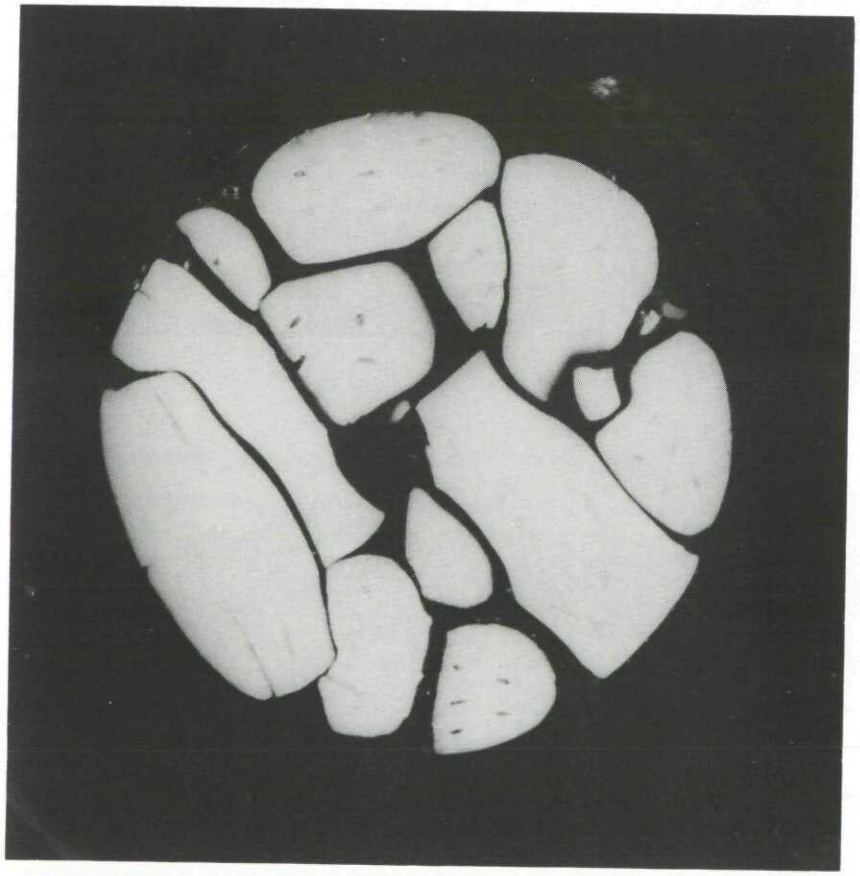

Fig. 19: Transversal cut of a M30 propellant charge after quasistatic compression at ambient temperature. The form of the originally cylindrical grains changes to fill up the available space.

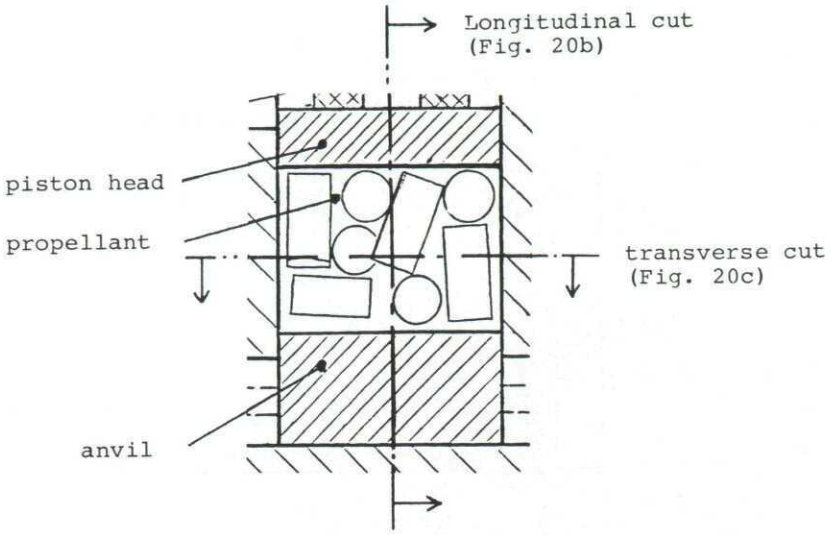

Fig. 20a: Cuts of a JA2 propellant bed after compression at -40 °C.
Only one half of the cut is presented in Figures 20b and 20c

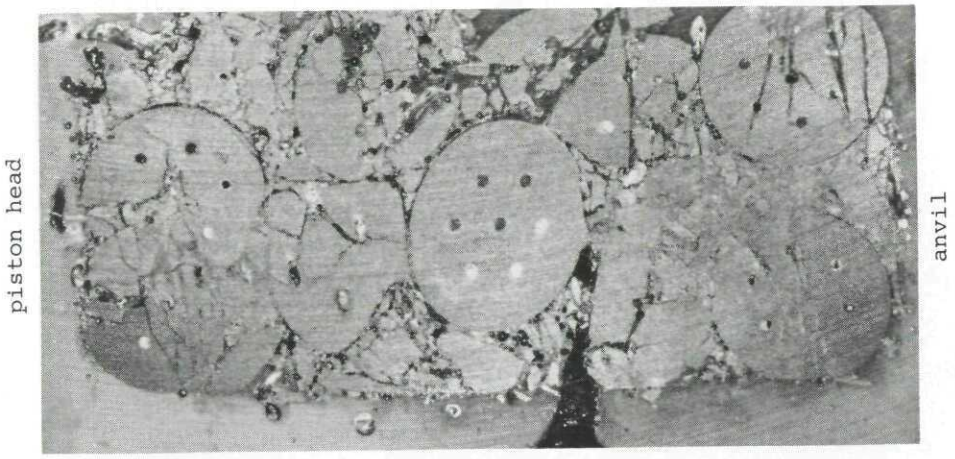

Fig. 20b: Longitudinal half-cut of the propellant bed

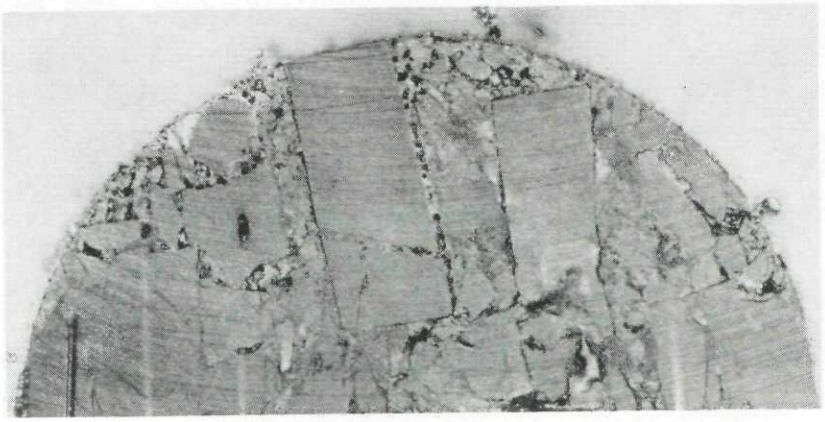

Fig. 20c: Transversal half-cut of the propellant bed

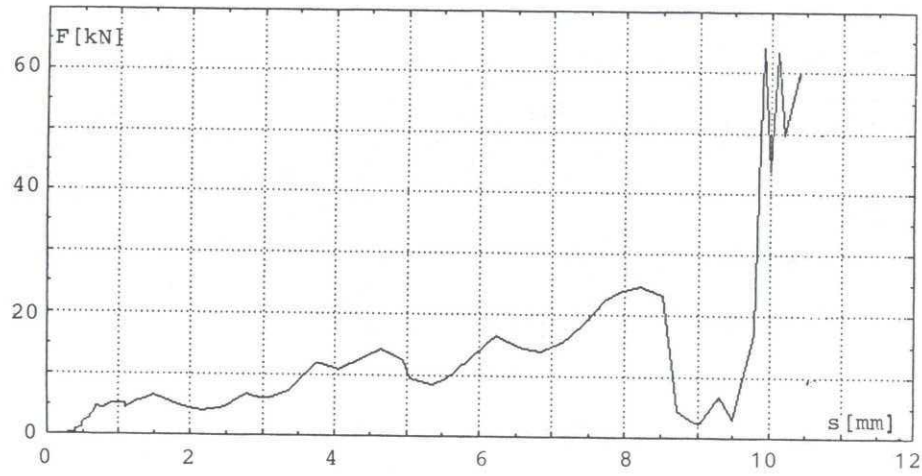

Fig. 20d: Force versus piston displacement (compression), JA2 propellant charge, -40 °C

FIELD ARTILLERY GUN PERFORMANCES

RELATED TO TRIPLE-BASE POWDER QUALITY

by

B. D'Andrea, M. Petrucci, M. Di Lorenzo

SNIA BPD S.p.A. 12, Corso Garibaldi - Colleferro (Rome)

ITALY

ABSTRACT

In order to achieve the best results in the 155 - 39 mm field artillery gun, several parameters affecting the triple-base powder quality have been investigated. Mainly Nitro-cellulose molecular weights (M.W.) and molecular weight distributions (M.W.D.), determined by means of gel-permeation chromatography (G.P.C.) related to the powder rheological properties are reported. In addition theoretical interior ballistic evaluations, tailored on powders manufactured with different nitrocellulose samples, based on computer program calculation, are compared with the firing test results.

INTRODUCTION

During the production of powders for calibers up to 155 mm and in particular for combustion-chambers with elevated diameter-length ratio, several problems arise in the respect of the specification limits. To solve such problems several parameters have been investigated and mainly technological process parameters and nitro-cellulose characteristics.

To optimize the before said parameters, different analyses were conducted and in particular:

- microscopic examination of the powder;
- gel-permeation - high performance liquid chromatography;
- closed vessel tests;
- internal ballistic evaluation by means of computer aided simulation.

During the study several powder samples were fired in the gun; four of the most significant are discussed.

EXPERIMENTAL PHASE

Before analyzing in details the various attempts to reduce the defects of the powder (bubbles, cracks, porous area) which are responsible of a low powder density and high pressure in the gun, expecially at low temperature, the powder composition, geometry and specification limits are summarized. In addition the general technological process is outlined.

Composition and chemical requirements

Nitrocellulose (N_2 = 13.15%)	20.80%
Nitroglycerine	20.60%
Picrite	55.00%
Stabilizer	3.60%
Flame retardant (added)	2.00%
Total volatiles	0.18%
density (gr/cc)	$\geq$ 1.665
heat test (at +65.5°C)	$\geq$ 10 min

Geometry

Shape	cylindrical slotted tube
Outer diameter	7.5 mm
Inner diameter	1.5 mm
Length	730 mm

Ballistic requirements

Nominal charge weight	12.250 kg
Muzzle velocity	827 m/s
Mean deviation	$\leq$ 2,5 m/s
Average pressure at +21°C (bar)	3'250 $\leq \overline{P} \leq$ 3'450
Average pressure at -31°C (bar)	$\overline{P} \leq$ 3'050
Average pressure at +51°C (bar)	$\overline{P} \leq$ 3'850

Technological process

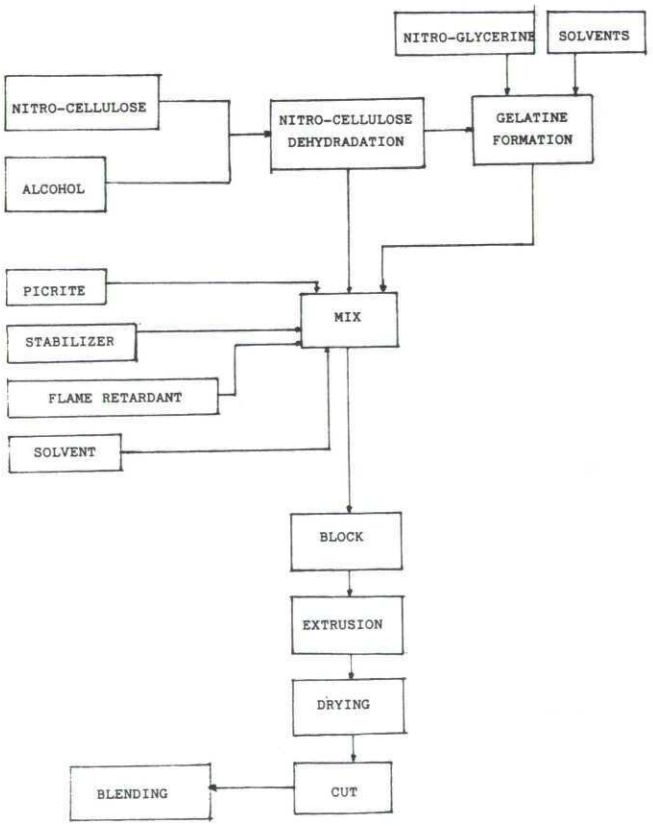

As said in the introduction, before analyzing the Nitro-cellulose characteristics affecting the rheology and powder properties, it was necessary to optimize several process parameters and mainly:

- water content in dehydrated N-cellulose;
- ingredients sequence addition to the mix;
- mixing time and temperature;
- propellant storage before blocking operation;
- time and pressure values during blocking operation;
- stick powder extrusion-rate;
- drying operation.

From the analysis, density in particular, of several small powder samples, it was possible to investigate the process parameters behaviour before starting to investigate the influence of the Nitrocellulose on the process rheology and powder performances. In order to achieve the maximum powder density the results of this parameters process optimization exhibited the following indications:

- water content of the dehydrated N-cellulose lower as possible;
- increase in mixing time;
- mixing temperature below 40°C;
- to avoid cold and solvent evaporation before blocking and extrusion;
- higher pressure and longer pressure application time during blocking;
- slow extrusion rate;
- slow drying operation;

The characteristics of the Nitrocellulose used for this activity are following summarized:

	LOW NITROGEN CONTENT	HIGH NITROGEN CONTENT	BLENDED
Nitrogen content (%)	12.59	13.42	13.14
Viscosity (cps)	4.43	5.43	5.10
Fineness (cc)	68	68	68
Eth. Alc. Solubility (%)	99.2	4.5	37.0
ratio (%)	33.74	66.26	-

At the end of the optimization of the process parameters the first powder sample to be fired in the gun was manufactured. The following table summarizes the laboratory control results and the firing test results compared with the specification requirements.

TABLE 1

	1st SAMPLE - C1 -	SPEC. REQUIR.
N-cellulose	20.90 %	in spec.
N-glycerine	21.50 %	" "
Picrite	54.20 %	" "
Stabilizer	3.40 %	" "
Flame retardant (added)	2.00 %	" "
Total volatiles	0.18 %	" "
Heat test at 65.5°C	21 min	$\geqslant$ 10 min
Density	1.665 gr/cm^3	$>$ 1,665
Calorific value	894 cal/gr	-
Inner diameter	1.25 mm	$\sim$ 1.50
Outer diameter	7.30 mm	$\sim$ 7.50
Length	725 mm	in spec.
Charge weight	12.050 kg	" "
Average pressure (+21°C)	3'550 bar	$3'250 \leqslant \overline{P} \leqslant 3'450$
Average pressure (-31.5°C)	3'450 bar	$\overline{P} \leqslant 3'050$
Average pressure (+51.5°C)	3'800 bar	$\overline{P} \leqslant 3'850$
Mean deviation	2.1 m/s	max 2.5 m/s

As the results show, although laboratory data were in specification limits not the same was for the firing acceptance test in the gun.

In order to high light hypothetical defects and evaluate theoretically internal ballistic performances of the powder, the following additional laboratory controls were performed:

- Nitrocellulose mean molecular weights determination;
- microscopic examination of the powder;
- interrupted combustion;
- internal ballistic evaluation.

Further powder samples, manufactured with Nitrocelluloses having different characteristics, were fully investigated and the results of the laboratory controls were compared with the first powder sample fired in the gun.

SAMPLES CHARACTERIZATION

Several Nitro-cellulose samples were selected and fully characterized. That is, for every sample, these main parameters were determined:

- Nitrogen content, expressed as nitrogen percentage;
- Viscosity value in cps, by means of Hoppler viscosimeter;
- Fineness value in ml;
- Solubility degree, related to alcohol-ether solution.

Moreover, weight and number average molecular weights ($\overline{M}_W$, $\overline{M}_N$) and molecular weights distribution (M.W.D.) were determined by means of Gel Permeation Chromatography, in order to achieve a univocal Nitro-cellulose characterization.

GEL PERMEATION CHROMATOGRAPHY APPARATUS AND REAGENTS

The GPC analysis has been performed by means of

- Series 3B Perkin-Elmer Liquid Chromatograph
- LC 100 P.E. Thermostatic oven
- Sigma 15 P.E. Integrator
- 3600 Data Station P.E. Computer
- Waters ultrastyragel columns - 10^6, 10^5, 10^4, 10^3
- L.C. P.E. variable wave length detector
- GPC 5 P.E. software
- Millipore Millex 0.2 μ filters
- Merck Tetrahydrofurane, HPLC grade.

Calibration

The calibration of the cromatographic columns set has been done plotting retention times of 15 monodisperse polystyrene standards, with molecular weight range from $8 \cdot 10^2$ up to $8 \cdot 10^6$, versus corresponding weight average molecular weights. The calibration curve has been calculated by means of least squares linear fit and it is reported in fig. [1] .

Samples preparation

100 grams of nitrocellulose have been dried in an oven at +50°C for 16 hours. Small amounts have been taken up to a weight of 1.0000 $\pm$ 0.0001 g. This amount has been dissolved in THF in order to have 1% solution and the solution has been left overnight. A part of the solution has been diluted to 0.2 % and filtered before injection.

Operating conditions

- Flow rate	1 ml/min
- Sample concentration	0.2 % (weight-volume ratio)
- Columns temperature	+35°C $\pm$1°C
- Detector wave length	220 mm
- Injection volume	50 μl

GPC results

In fig. 2 is reported a typical diagram obtained by the GPC analysis indicating the meaning values and their sense.

Finally the results of the Nitrocellulose samples used to manufacture the further powder samples, to be fired in the gun, are illustrated (fig. 3 and fig. 4).

To manufacture the powder samples, starting from the Nitrocelluloses characterized before, some adjustments of the process parameters were required and in particular the solvent amount during the mixing and its composition.

Related to the different N-celluloses following are pointed out the final results of the solvent optimization.

N-CELLULOSE	TOTAL SOLVENT	ALCOHOL-ACETONE RATIO
A	18.5 %	30/70
B	19.5 %	30/70
C	19.5 %	35/65
D	20.0 %	40/60

In order to exhibit cracks, bubbles and porous area in the powder and to evaluate its performances, the samples manufactured were fully analyzed.

Following are summarized the results of chemical analysis, microscopic examinations (fig. 5), closed vessel test and interrupted combustions (fig. 6). At least is described the internal ballistic evaluation based on computer program calculation and the firing test results.

TABLE 2

Chemical analysis results

	C1	C2	C3	C4
N-cellulose	20.90	20.75	21.16	20.60
N-glycerine	21.50	21.00	21.00	21.00
Picrite	54.20	54.70	54.34	54.90
Stabilizer	3.40	3.55	3.50	3.50
Flame retardant (added)	2.00	1.89	1.90	1.89
Total volatiles	0.18	0.14	0.16	0.16
Heat test at 65°C	21 min	22 min	21 min	21 min
Density	1.665	1.665	1.668	1.670
Calorific value	894	893	897	898
N-Cellulose type	A	B	C	D

TABLE 3

Closed vessel test results

VIVACITY AT +21°C

	C1	C2	C3	C4
10 % P.M.	7.521	7.466	7.592	7.671
20 % P.M.	6.413	6.186	6.448	6.554
30 % P.M.	5.716	5.614	5.872	5.819
40 % P.M.	5.203	5.169	5.437	5.340
50 % P.M.	4.845	4.820	4.940	4.903
60 % P.M.	4.612	4.589	4.679	4.665
70 % P.M.	4.343	4.349	4.333	4.387
80 % P.M.	3.956	4.028	3.879	4.044
90 % P.M.	3.404	3.660	3.385	3.661
P. MAX kg/cm^2	2.450	2.440	2.455	2.448

INTERNAL BALLISTIC EVALUATION

Closed bomb interior ballistic code

Starting from the data of vivacity by the closed bomb often, and expecially at low temperature, powders considered similar from a ballistic point of view give different results when fired in the gun.

Following is described an analysis method which data are in agreement with the firing test results. The aim of the method was to locate the burnt fraction powder at which the first burning-rate anomalies, as propellant grains cracking, occur. Referring to the theories of the internal ballistic of the guns, are considered powders of good quality those in which the anomalies during the burning occur after the 60%. In addition, at the same level of burnt fraction, are considered to be better the powders with slower burning-rate.

Summary of assumptions

- Heat losses to the walls of the bomb are negligible;
- All exposed burning surfaces recede at a uniform rate, implying that all propellant grains shrink symmetrically, thus neglecting any erosive augmentation in the perforations.

The burning-rate data, computed from the pressure-time curves by the closed bomb experiments, were fitted to equation

$$v_c = \beta p^{\alpha} + \text{const.} \qquad \text{over } 500 \div 1800 \text{ kg/cm}^2$$

The combustion products may be described using the equation of state

$$p = \frac{\lambda \cdot z \cdot c}{v_b - \eta c z - (1 - z)\frac{c}{\varsigma}}$$

v_b = chamber volume
c = initial weight of the powder
ς = powder density
η = powder covolume
λ = specific force constant
z = powder burnt fraction at the time "t".

Input data

Size and configuration of propellant-grains
powder density
powder covolume
chamber volume
initial weight of the powder
specific force constant
pressure vs. time curve from closed bomb experiments.

Output data

Burning-rate curve vs. pressure
powder burnt fraction vs. pressure
equation of burning rate

Starting from the equation

$$\text{vivacity} = \frac{1}{p} \cdot \frac{1}{p_{max}} \cdot \frac{dp}{dt}$$

the curve of vivacity was calculated.
All the curves were plotted vs. pressure.

Analysis of the results

The anomalies during combustion are evident when large per cent differences between point by point burning-rate and analytical burning-rate occur.

At that value it is possible to locate the powder burnt fraction at which the before said phenomena occur.

TABLE 4

Firing test results

	C1	C2	C3	C4
Charge weight	12.050	12.380	12.350	12.350
Average pressure at +21°C	3'550	3'500	3'500	3'380
Average pressure at -31°C	3'450	3'150	3'080	2'900
Average pressure at +51°C	3'800	3'800	3'780	3'780
Mean deviation	2.1	2.2	2.1	2.1

CONCLUSIONS

The main difficulties to achieve the ballistic performances of the ammunition for the field-artillery gun 155-39 mm have been met to obtain a powder without inner defects as bubbles, cracks and porous area. These defects give rise to anomalies during the combustion which cannot be pointed out by the usual laboratory controls (density, closed vessel test and chemical analysis). The elimination and control of such defects have been possible both keeping under examination every manufacturing phase and checking the influence of the single parameters affecting the quality of the powder. After having defined the manufacturing process, the influence of the Nitro-cellulose characteristics affecting the performances of the powder have been investigated by means of G.P.C. analysis. The best results have been obtained using a Nitrocellulose (blend of high and low nitrogen content) with high polidispersity, high $\overline{M}_W$ and high $\overline{M}_N$. Naturally such conclusions have to be considered not in absolute but only in comparison to the other samples characterized by the same apparatus. In order to check the ballistic performances of the powders before the firing test a computer program calculation based on laboratory data (chemical, dimensional and closed vessel test results) has been optimized.

Looking at the results is evident that for the powder under examination, the usual laboratory controls were not able to foresee the firing test results. Otherwise the additional experimental data show that when anomalies occur in the burning-rate before reaching the 65 % of the burnt fraction of the powder, the defects inside the powder compromise the ballistic acceptance of the same.

FIGURE 1
CALIBRATION CURVE

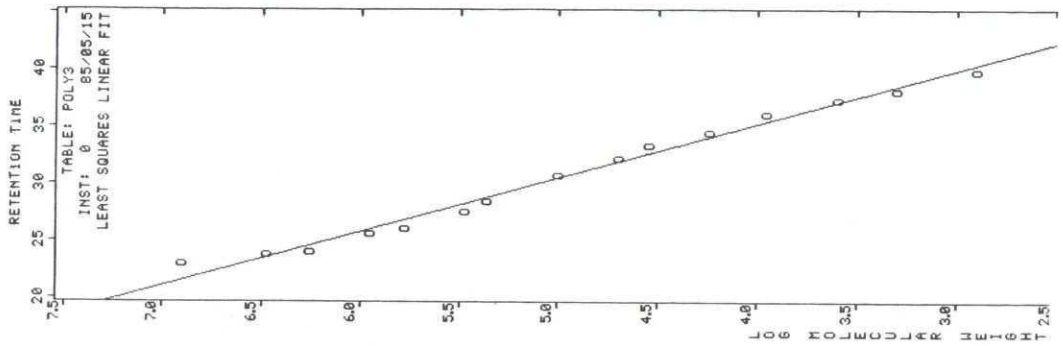

FITTED TABLE: POLY3
INST: 0 85/05/15

MERGED REPORTS:
MARK-HOUWINK CONSTANTS
SAMPLE: K = 1.000 a = 0.0000
STANDARDS: K = 1.000 a = 0.0000

TIME	MOL. WT.	UNIV. MOL. WT.
22.920	8.0000E+06	8.0000E+06
23.720	3.0000E+06	3.0000E+06
23.950	1.8000E+06	1.8000E+06
25.610	9.0000E+05	9.0000E+05
25.970	6.0000E+05	6.0000E+05
27.460	3.0000E+05	3.0000E+05
28.370	2.3300E+05	2.3300E+05
30.710	1.0000E+05	10.0000E+04
32.200	5.0000E+04	5.0000E+04
33.260	3.5000E+04	3.5000E+04
34.400	1.7500E+04	1.7500E+04
36.000	9.0000E+03	9.0000E+03
37.220	4.0000E+03	4.0000E+03
38.110	2.0000E+03	2.0000E+03
39.740	8.0000E+02	8.0000E+02

FIT STATISTICS FOR TABLE: POLY3

INST: 0 85/05/15
15 DATA POINTS

Log(M) = C0 - C1 * T

C0 = 11.46420 C1 = 0.21213

STANDARD ERROR OF ESTIMATE = 0.13875

CORRELATION COEFFICIENT = - 0.993859

FIGURE 2
TYPICAL G.P.C. DIAGRAM

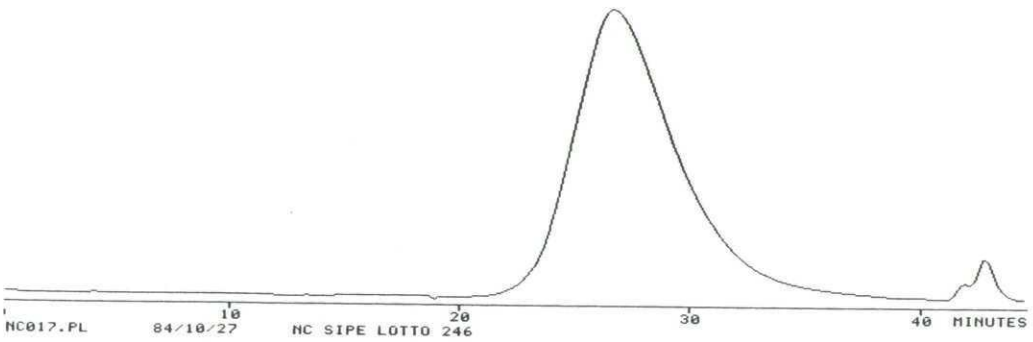

GPCS DATA REPORT FROM DISK
REPORTED AT: 08:51 ON 85/05/15

CHROMATOGRAM: NC017.PL INSTRUMENT: 3
NC SIPE LOTTO 246
ACQUIRED: 84/10/27 CALCULATED: 84/10/30

CALIBRATION TABLE: POLY3.CT

BASE POINTS: 15.796 AND 41.016 MINUTES
SUMMATIONS FROM 17.986 TO 40.684 MINUTES
12.00 SECONDS PER DATA POINT

WEIGHT AVERAGE MW = 519,168

NUMBER AVERAGE MW = 192,227

POLYDISPERSITY = 2.701

Z AVERAGE MW = 1.52700E+06

161.25 MV

FIGURE 3
GEL PERMEATION CHROMATOGRAPHY RESULTS

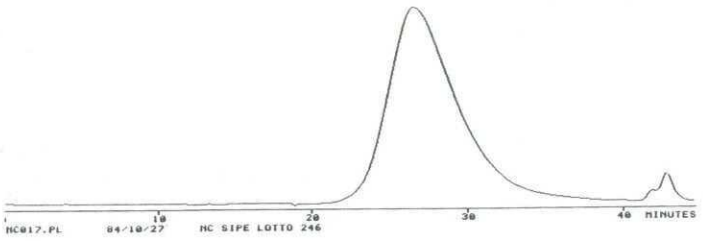

GPC5 DATA REPORT FROM DISK
REPORTED AT: 08:51 ON 85/05/15

CHROMATOGRAM: NC017.PL
NC SIPE LOTTO 246
ACQUIRED: 84/10/27
INSTRUMENT: 3
CALCULATED: 84/10/30

CALIBRATION TABLE: POLY3.CT

BASE POINTS: 15.796 AND 41.016 MINUTES
SUMMATIONS FROM 17.986 TO 40.684 MINUTES
12.00 SECONDS PER DATA POINT

WEIGHT AVERAGE MW	=	519,169
NUMBER AVERAGE MW	=	192,227
POLYDISPERSITY	=	2.701
Z AVERAGE MW	=	1.52700E+06

161.25 MV

A1

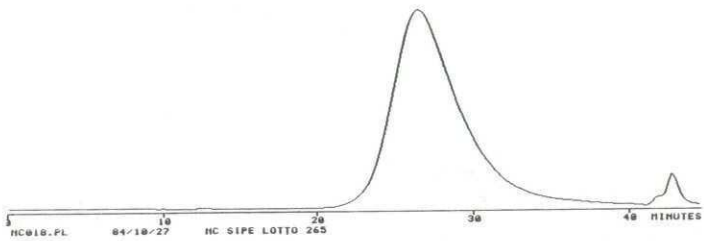

GPC5 DATA REPORT FROM DISK
REPORTED AT: 09:36 ON 85/05/15

CHROMATOGRAM: NC018.PL
NC SIPE LOTTO 265
ACQUIRED: 84/10/27
INSTRUMENT: 3
CALCULATED: 84/10/30

CALIBRATION TABLE: POLY3.CT

BASE POINTS: 15.796 AND 41.016 MINUTES
SUMMATIONS FROM 17.986 TO 40.684 MINUTES
12.00 SECONDS PER DATA POINT

WEIGHT AVERAGE MW	=	580,797
NUMBER AVERAGE MW	=	174,781
POLYDISPERSITY	=	3.323
Z AVERAGE MW	=	2.29950E+06

152.49 MV

A2

SAMPLE A = A1:A2 = 31:69

A1[N_2 = 12.56%, ν = 4.48 cps, fineness = 65 ml]

A2[N_2 = 13.43%, ν = 5.12 cps, fineness = 68 ml]

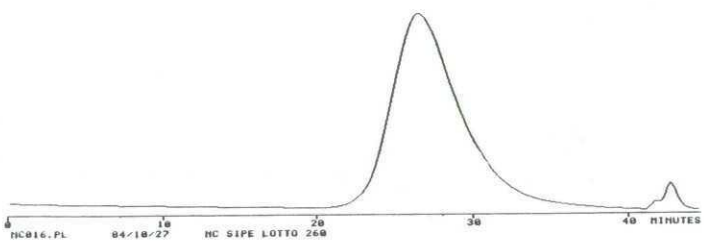

GPC5 DATA REPORT FROM DISK
REPORTED AT: 08:54 ON 85/05/15

CHROMATOGRAM: NC016.PL
NC SIPE LOTTO 260
ACQUIRED: 84/10/27
INSTRUMENT: 3
CALCULATED: 84/10/30

CALIBRATION TABLE: POLY3.CT

BASE POINTS: 15.796 AND 41.016 MINUTES
SUMMATIONS FROM 17.986 TO 40.684 MINUTES
12.00 SECONDS PER DATA POINT

WEIGHT AVERAGE MW	=	565,600
NUMBER AVERAGE MW	=	201,516
POLYDISPERSITY	=	2.807
Z AVERAGE MW	=	1.98577E+06

167.11 MV

B1

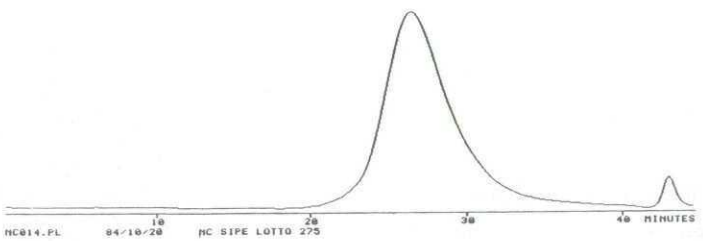

GPC5 DATA REPORT FROM DISK
REPORTED AT: 09:39 ON 85/05/15

CHROMATOGRAM: NC014.PL
NC SIPE LOTTO 275
ACQUIRED: 84/10/28
INSTRUMENT: 3
CALCULATED: 84/10/22

CALIBRATION TABLE: POLY3.CT

BASE POINTS: 14.469 AND 41.945 MINUTES
SUMMATIONS FROM 17.322 TO 41.680 MINUTES
12.00 SECONDS PER DATA POINT

WEIGHT AVERAGE MW	=	757,646
NUMBER AVERAGE MW	=	219,963
POLYDISPERSITY	=	3.444
Z AVERAGE MW	=	4.82384E+06

149.85 MV

B2

SAMPLE B = B1:B2 = 33:67

B1[N_2 = 12.59%, ν = 4.62 cps, fineness = 68 ml]

B2[N_2 = 13.42%, ν = 6.90 cps, fineness = 68 ml]

FIGURE 4
GEL PERMEATION CHROMATOGRAPHY RESULTS

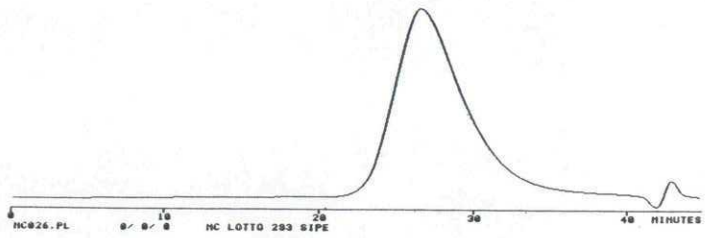

GPC5 DATA REPORT FROM DISK
REPORTED AT: 08:57 ON 85/05/15

CHROMATOGRAM: NC026.PL INSTRUMENT: 3
NC LOTTO 293 SIPE
ACQUIRED: 84/11/19 CALCULATED: 84/11/19

CALIBRATION TABLE: POLY3.CT

BASE POINTS: 19.867 AND 39.200 MINUTES
SUMMATIONS FROM 20.733 TO 38.733 MINUTES
12.00 SECONDS PER DATA POINT

WEIGHT AVERAGE MW	=	576,624
NUMBER AVERAGE MW	=	137,117
POLYDISPERSITY	=	4.205
Z AVERAGE MW	=	3.18500E+06

167.97 MV

C1

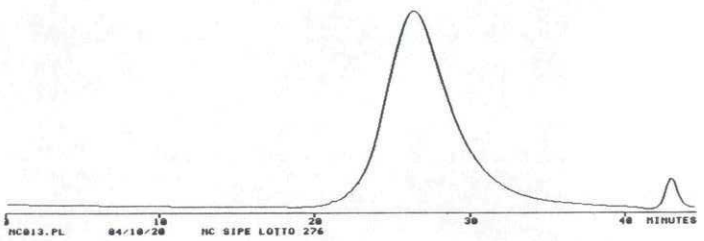

GPC5 DATA REPORT FROM DISK
REPORTED AT: 09:42 ON 85/05/15

CHROMATOGRAM: NC013.PL INSTRUMENT: 3
NC SIPE LOTTO 276
ACQUIRED: 84/10/20 CALCULATED: 84/10/22

CALIBRATION TABLE: POLY3.CT

BASE POINTS: 15.796 AND 41.746 MINUTES
SUMMATIONS FROM 17.986 TO 41.414 MINUTES
12.00 SECONDS PER DATA POINT

WEIGHT AVERAGE MW	=	1.11562E+06
NUMBER AVERAGE MW	=	113,345
POLYDISPERSITY	=	9.843
Z AVERAGE MW	=	1.08941E+07

150.39 MV

C2

SAMPLE C = C1:C2 = 30:70

C1[N_2 = 12.61%, ν = 4.24 cps, fineness = 74 ml]

C2[N_2 = 13.41%, ν = 8.96 cps, fineness = 76 ml]

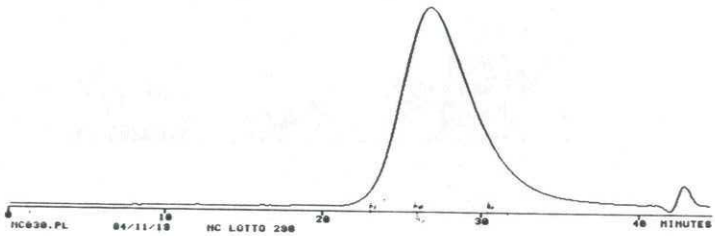

GPC5 DATA REPORT FROM DISK
REPORTED AT: 09:01 ON 85/05/15

CHROMATOGRAM: NC030.PL INSTRUMENT: 3
NC LOTTO 298
ACQUIRED: 84/11/19 CALCULATED: 84/11/21

CALIBRATION TABLE: POLY3.CT

BASE POINTS: 20.176 AND 39.954 MINUTES
SUMMATIONS FROM 20.641 TO 39.224 MINUTES
12.00 SECONDS PER DATA POINT

WEIGHT AVERAGE MW	=	565,908
NUMBER AVERAGE MW	=	125,463
POLYDISPERSITY	=	4.511
Z AVERAGE MW	=	3.02361E+06

136.81 MV

D1

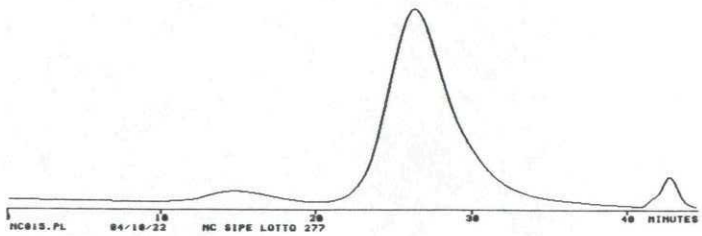

GPC5 DATA REPORT FROM DISK
REPORTED AT: 09:44 ON 85/05/15

CHROMATOGRAM: NC015.PL INSTRUMENT: 3
NC SIPE LOTTO 277
ACQUIRED: 84/10/22 CALCULATED: 84/10/22

CALIBRATION TABLE: POLY3.CT

BASE POINTS: 19.712 AND 41.016 MINUTES
SUMMATIONS FROM 19.977 TO 40.618 MINUTES
12.00 SECONDS PER DATA POINT

WEIGHT AVERAGE MW	=	713,709
NUMBER AVERAGE MW	=	258,664
POLYDISPERSITY	=	2.825
Z AVERAGE MW	=	3.72624E+06

152.41 MV

D2

SAMPLE D = D1:D2 = 35:65

D1[N_2 = 12.63%, ν = 4.09 cps, fineness = 73 ml]

D2[N_2 = 13.44%, ν = 9.21 cps, fineness = 76 ml]

FIGURE 5
MICROSCOPIC EXAMINATION

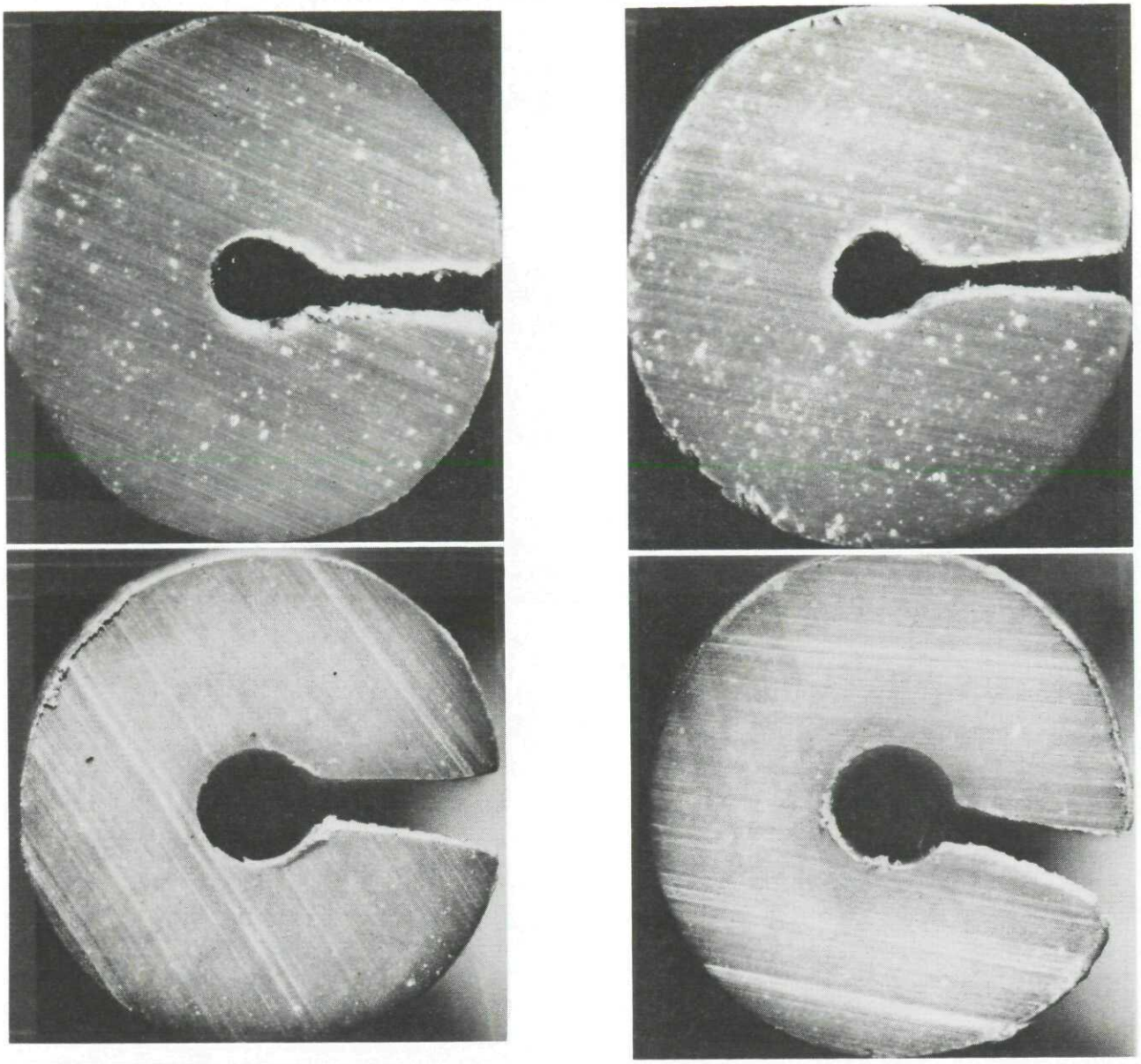

30 x ENLARGEMENT

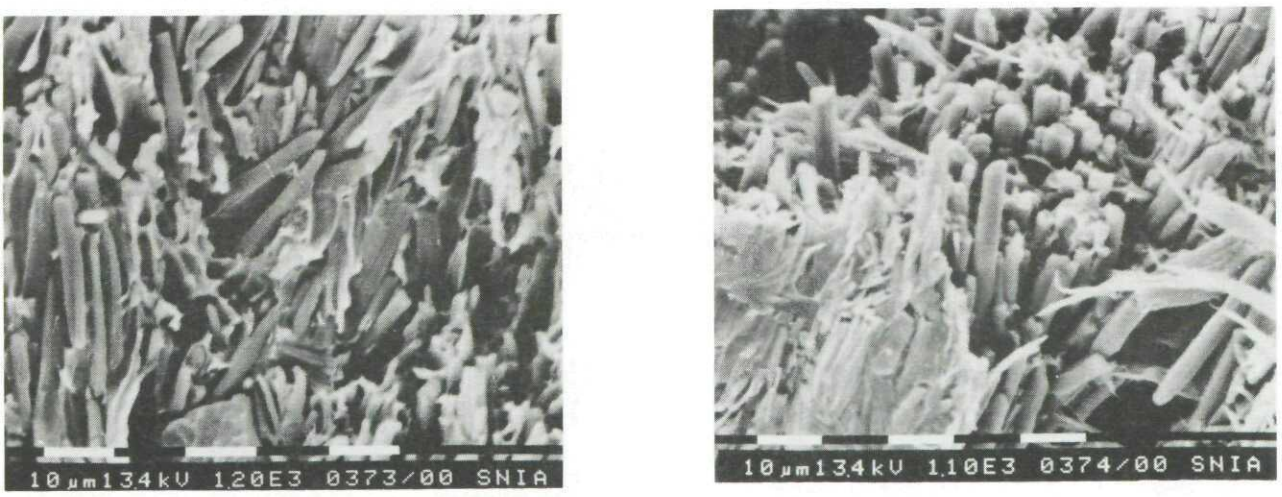

SCANNING ELECTRONIC MICROSCOPIC EXAMINATION

FIGURE 6

INTERRUPTED COMBUSTION RESULTS

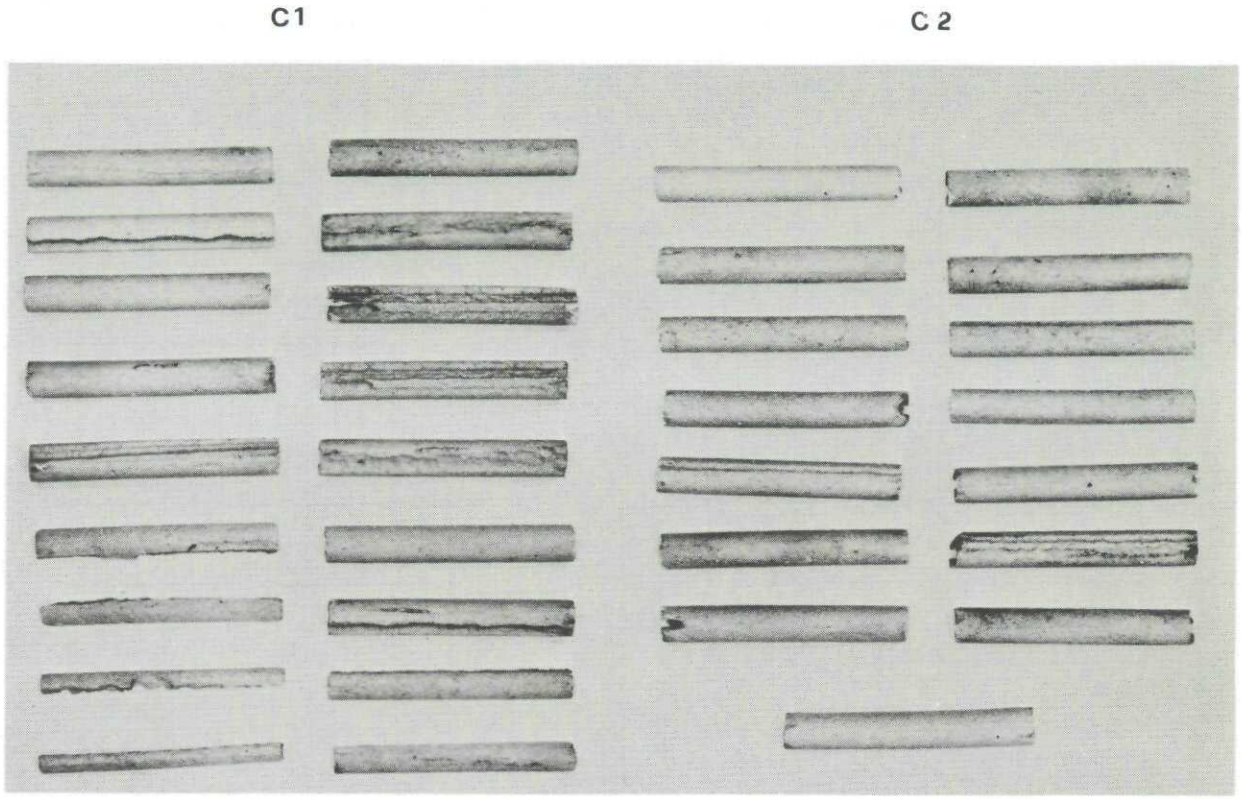

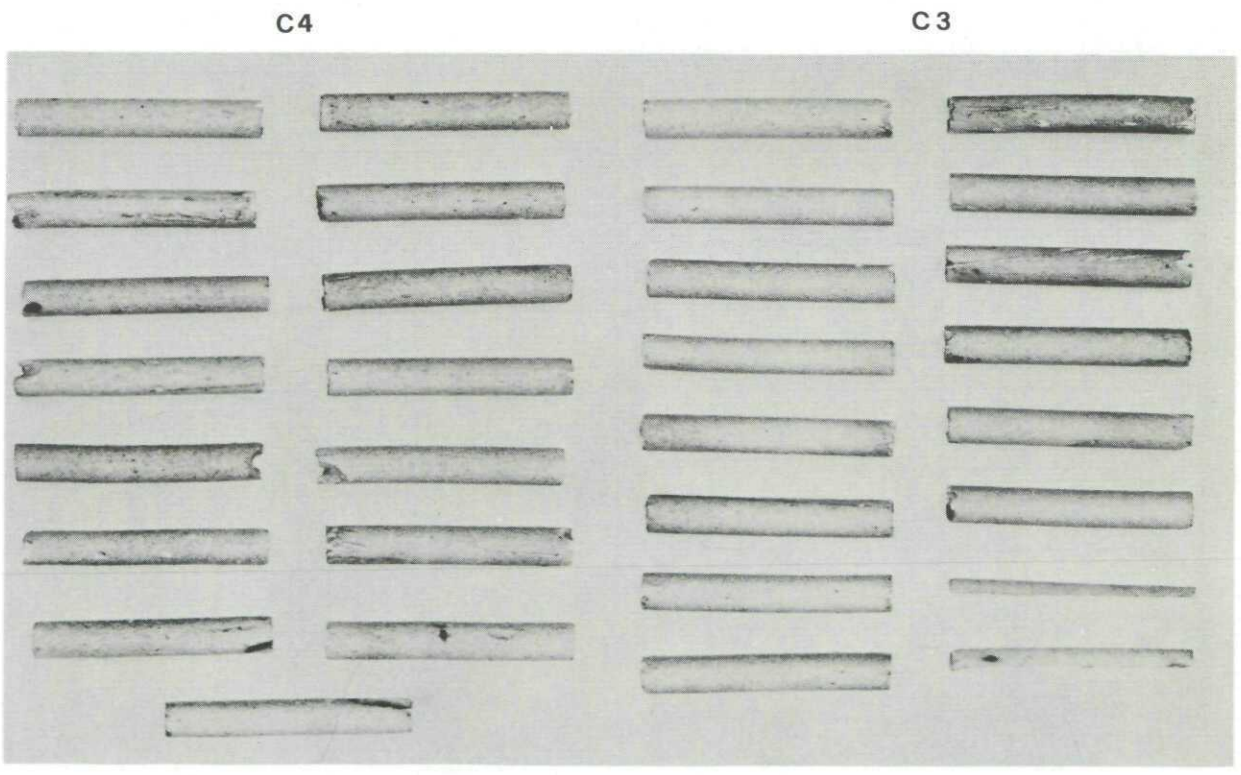

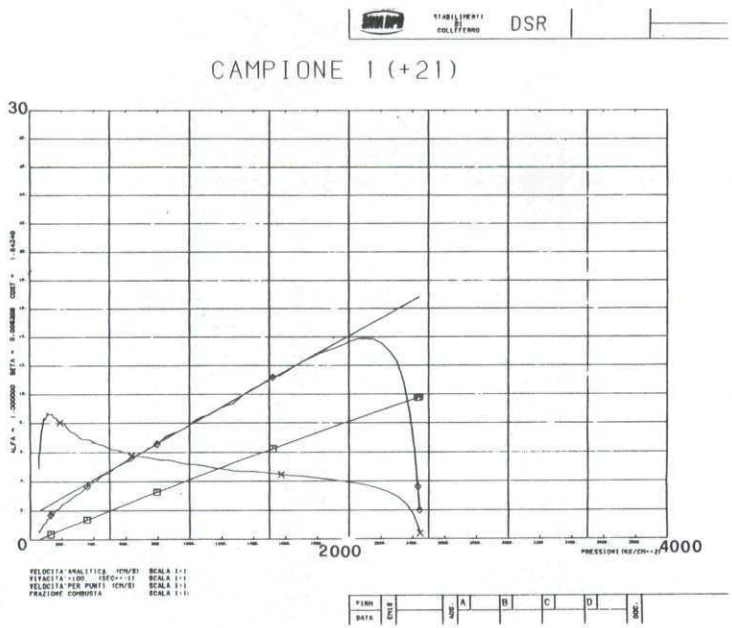

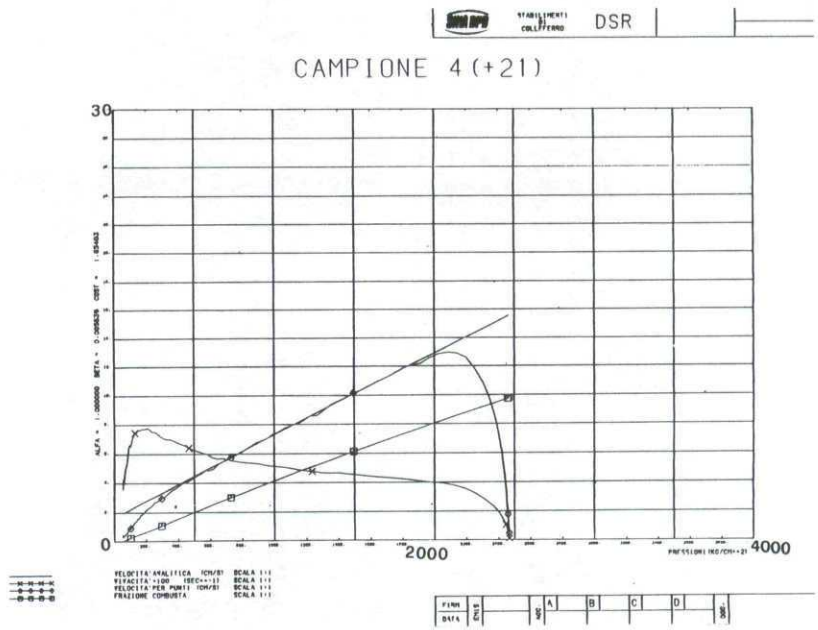

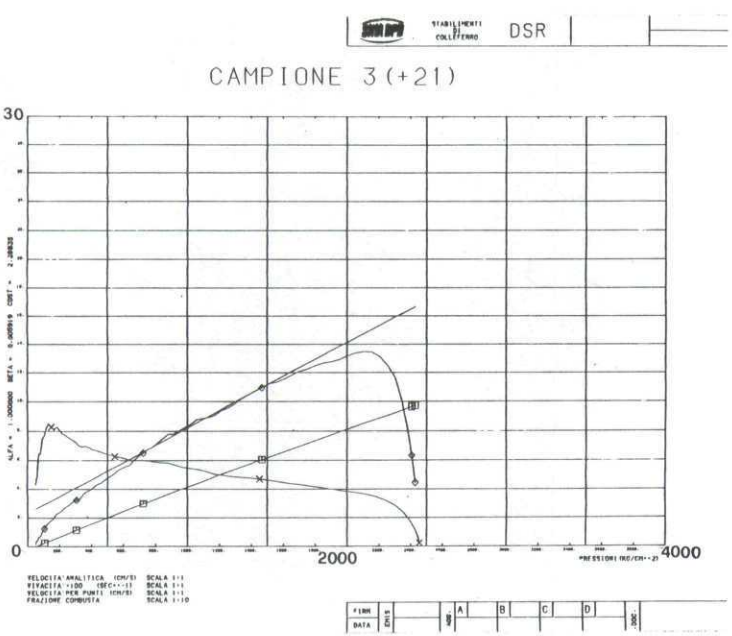

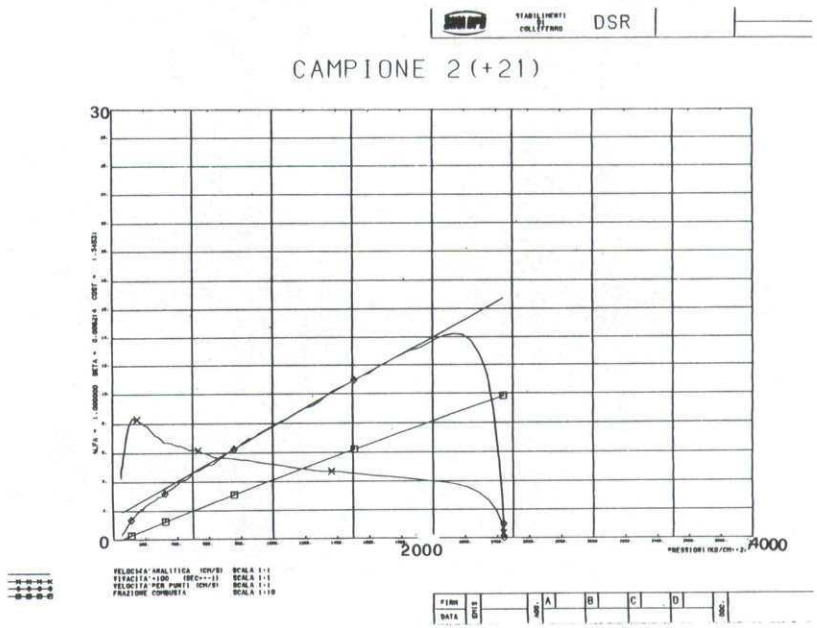

FIGURE 7
INTERIOR BALLISTIC EVALUATION RESULTS
AT +21°C

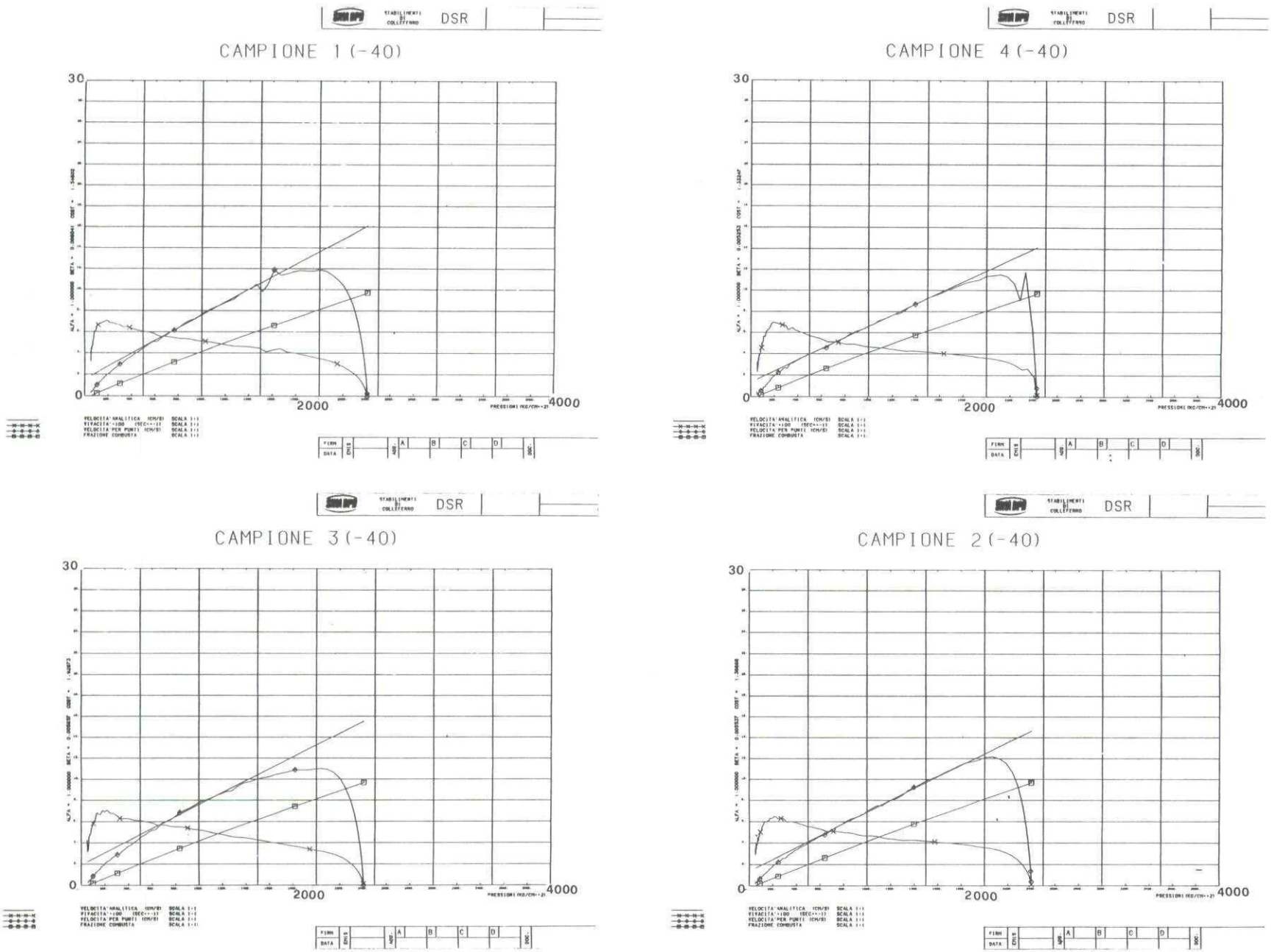

FIGURE 8
INTERIOR BALLISTIC EVALUATION RESULTS
AT -40°C

PRESSURE WAVE - GUN BARREL INTERACTIONS

A. B. Crowley and W. P. C. King

School of Management and Mathematics,
Royal Military College of Science,
Shrivenham, Swindon, Wilts SN6 8LA, UK.

Abstract

A theoretical study of the interaction of pressure waves generated during the internal ballistics cycle with the vibrations of a tank barrel, and the possible effects on accuracy, is described. The investigation is based on codes simulating the complete internal ballistics cycle, including the venting of gases after shot exit, and the longitudinal and flexural vibration modes of the barrel, both of which have been developed at RMCS. The putative effects of pressure waves on both accuracy and structural integrity are discussed for a number of different charge and barrel configurations.

Introduction

In this paper a theoretical investigation is carried out into the effects of internal ballistic phenomena, such as pressure waves, on the vibrations of medium and large calibre weapons. Such vibrations are potentially damaging to the structure of the weapon, as well as being a significant source of inaccuracy of fire due to the barrel motion and gun jump. There is therefore a requirement to model the barrel motion during the firing sequence to enhance our understanding of the sources of vibration, and improve the accuracy of the weapon.

It has been assumed in most previous work on gun barrel vibrations that the internal ballistic effects, which are the driving force for the entire motion of the barrel, may be modelled sufficiently accurately by a pressure force acting at the breech, and the shot-barrel interaction forces acting at the current shot position. The breech pressure, usually obtained by computation using a lumped parameter model, is taken to be acting on the bore area (= breech face area - normal component of forcing cone area) to provide a rearward acceleration force. In a lumped parameter code, the pressure is either assumed to be uniform along the chamber, or to be a prescribed function of space, decreasing monotonically towards shot base. However, during the ignition and flamespread phase of the internal ballistics cycle pressure waves are inevitably set up, unless simultaneous ignition of the entire propellant charge is achieved. Therefore the forward pressure on the forcing cone may well exceed the pressure at the breech for part of the cycle, and the reflection of pressure waves at shot base and breech face superimposes a higher frequency component on the basic exciting force as computed by a lumped parameter code.

In the research outlined here we examine the effects on the gun barrel vibrations, in particular the longitudinal acceleration at the breech and the muzzle motion, of including a more realistic representation of the pressure forces. We consider, therefore, the breech pressure acting on the full chamber cross-sectional area to produce a rearward pressure force, counteracted by a forward force exerted at the forcing cone by the pressure there acting on the chamber area minus the bore area. We show that the incorporation of this leads to significant changes in the behaviour of the muzzle at shot exit, with corresponding effects on accuracy.

The results shown here are based on computations performed using two internal ballistics codes, HMSOV3 a lumped parameter code based on the equations derived in [1], and ABC1 a code which models the quasi-one-dimensional flow of gas and propellant particles in the volume between breech and shot-base. The gun barrel vibrations were calculated using an in-house program. All of these codes have been developed over the past few years at RMCS, Shrivenham.

In the next section the models on which these codes are based are described briefly. In the following sections results are shown for two different weapon systems, and for different charges in each weapon. It should be stated here that while the parameters used are representative of real guns, they do not describe any particular weapon system. The first weapon considered is a 100mm calibre gun, while the second is of larger calibre (125mm) and heavier, being more characteristic of a modern tank weapon. The paper concludes with a discussion of the results obtained, which demonstrate our contention that pressure waves have a significant effect on the barrel motion and cannot with impunity be ignored.

The Internal Ballistics and Gun Vibration Models

Two different types of internal ballistics model have been used in this paper, and as will be shown later, the choice made influences the barrel vibrations obtained even in the absence of pressure waves. The first model HMSOV3 is a lumped parameter code, in which it is assumed that the behaviour of the burning propellant, and the gases produced is adequately described in terms of the average properties of the gases. That is, any spatial variations along the length of the gun chamber are neglected in the calculation of the

rate of burning of the propellant, and in the energy balance equation. However, it is assumed that the gas velocity increases linearly from breech to shot base, and consequently there is a quadratic pressure distribution which decreases monotonically towards the shot base. A model such as this provides reasonably accurate predictions of peak pressure and muzzle velocity in systems for which such assumptions are justified. The equations are integrated numerically using a fourth-order Runge-Kutta scheme.

In order to investigate the ignition and flamespread a gas dynamics model is required. If radial variations of the variables may be neglected, the equations are those of quasi-one-dimensional flow of a mixture of gas and solid propellant particles, in which the change in cross-sectional area of the gun tube from chamber to barrel is incorporated. It is assumed that the field variables represent average values over a region large compared with the scale of heterogeneity of the mixture. This allows each phase to be treated as a continuum, the two phases occupying disjoint and complementary regions in space. The equations are

Conservation of mass

Gas

$$\frac{\partial}{\partial t}(\rho_1 A_1) + \frac{\partial}{\partial x}(\rho_1 A_1 u_1) = m_p + \dot{m}$$

Propellant

$$\frac{\partial}{\partial t}(\rho_2 A_2) + \frac{\partial}{\partial x}(\rho_2 A_2 u_2) = -\dot{m}$$

Conservation of momentum

Gas

$$\frac{\partial}{\partial t}(\rho_1 A_1 u_1) + \frac{\partial}{\partial x}(\rho_2 A_2 u_2^2) = \dot{m} u_2 + \text{Drag} - A_1 \frac{\partial p}{\partial x}$$

Propellant

$$\frac{\partial}{\partial t}(\rho_2 A_2 u_2) + \frac{\partial}{\partial x}(\rho_2 A_2 u_2^2) = -\dot{m} u_2 + \text{Drag} - A_2 \frac{\partial p}{\partial x}$$

Conservation of energy

Gas

$$\frac{\partial}{\partial t}(\rho_1 A_1 (e_1 + \tfrac{1}{2}u_1^2) + \frac{\partial}{\partial x}(\rho_1 A_1 u_1 (e_1 + \tfrac{1}{2}u_1^2) + A_1 u_1 p) = -p \frac{\partial}{\partial x}(A_2 u_2)$$

$$+ m_p e_p + \dot{m}(e_2 + \tfrac{1}{2}u_2^2) - u_2(\text{Drag})$$

Conservation of particles

$$\frac{\partial}{\partial t}(N_2) + \frac{\partial}{\partial x}(N_2 u_2) = 0$$

where ρ, A, u, e denote density, cross-sectional area, velocity and internal energy of each phase, and subscripts 1,2 indicate gas, solid properties respectively. It is assumed that the pressure, p, is the same for each phase, and that heating of the bulk of the solid is insignificant. N_2 denotes the number density of propellant particles, $\dot{m}$ the rate of mass transfer to the gas phase by burning, and m_p the rate of injection of mass from the primer. In addition constitutive laws are needed to describe the burning of the propellant, and the form of the interphase drag. A surface temperature ignition criterion is used, assuming that the temperature of the surface of the propellant may be approximated by the local gas temperature. These equations constitute a model with the same general features as those outlined in [2].

In the current version of the ABC code, the equations are reformulated in a moving coordinate system chosen so that the computational domain is $0 < X < 1$, and are solved using a forward-backward MacCormack finite difference scheme. The results obtained with this scheme are felt to be better than those obtained using the earlier version (outlined in [2]) which employed a Lax-Wendroff integration scheme.

The model for the analysis of the gun barrel vibrations, is based on the Euler-Bernoulli theory for the vibration of thin beams, in which it is assumed that the bending moment is proportional to curvature. The effects of attached masses at both breech and muzzle (ie muzzle reference system) with centres of gravity off the bore axis are incorporated. The cradle bearings are modelled as elastic supports of finite length, and rotation of the rigid cradle is considered. A fuller description of the model may be found in [3].

Results for a 100mm Calibre Weapon

Two different charges were considered in this weapon, with a range of igniter performances being considered in the gas dynamics calculations. The first charge consisted of 6.3 Kg of multitubular propellant, with a force constant of 1.18 MJ/Kg, with a shot of mass 7 Kg, and the second of 6.7 Kg of the same propellant, with the same shot. Using the lumped parameter model these give peak pressures of 494 MPa and 594 MPa respectively, and the

corresponding muzzle velocities are 1379 m/s and 1439 m/s. These charge masses were chosen to give, in the first instance, a peak pressure typical of a high-velocity weapon, and in the second case, approximately the peak pressure quoted as the target for the next generation of weapons.

The internal ballistics for each charge using the gas dynamics model was also calculated. In the case of the larger charge three different igniters were considered. The energy release from the igniters was kept constant, but the time for which they vented, and the length of the propellant bed over which the venting took place was varied. This resulted in different pressure wave behaviour. In the first case the igniter was assumed to vent uniformly over virtually the total length of the propellant bed, to give simultaneous ignition of all the propellant, and a pressure-time history free of pressure waves. In the second case the igniter vented over the first third of the propellant bed. This gave rise to what might be termed 'normal' pressure waves, in which the first negative minimum in the graph of pressure difference (breech - shot base) (Δp) versus time was at -32MPa (see fig. 5b). The third case considered was a rapid venting of the igniter gases over the first 8 cm of the propellant. This led to 'catastrophic' pressure waves, with Δp being -134MPa. The pressure histories calculated were then used as input to the barrel vibration program, and the results compared.

The first comparison made was to investigate the effect on the barrel vibrations of increasing the charge mass when using the lumped parameter code. It was found that the shape of the graph of breech longitudinal acceleration against time was virtually unaltered, but the amplitude of the oscillations was increased by about 30%. The period of these oscillations corresponds to the time taken for a disturbance to be propagated from breech to muzzle and return.

In figs. 1 and 2 the pressure history at the breech face and at shot base are shown as calculated from, respectively, the lumped parameter code HMSOV3 and the gas dynamics code ABC. Here the igniter was assumed to vent uniformly over the propellant bed, to simulate the lumped parameter model as closely as possible. However, one important difference is seen. In the gas dynamics model with distributed ignition the shot base pressure remains less than the breech pressure, and hence the local burning rate is lower at shot base than at the breech, resulting in the propellant being burnt out at the breech earlier than at shot base. As shown in fig. 3, this leads to a very rapid change in the pressure difference between breech and shot base near propellant all-burnt, with a similar effect on the pressure difference between the breech and forcing cone.

The breech longitudinal acceleration history for each of these pressure histories is shown in fig. 4, together with that for the pressure history with pressure waves shown in fig. 5. In the results from the ABC code without pressure waves, there is evidence of a higher frequency mode superimposed on the fundamental frequency seen in the results from HMSOV3 input. As the magnitude of the pressure waves is increased, by considering the case when the igniter vents over the first third of the propellant bed, (see fig. 5), so further oscillations are seen. Graphs of the vertical muzzle deflection against time are shown in fig. 6, and again the superposition of the higher frequency mode on the basic curve resulting from the HMSOV3 input is clearly seen.

Fig. 7a shows the pressure-time history for the case of 'catastrophic' pressure waves outlined above, obtained when the igniter vents rapidly close to the breech. In fig. 7b the corresponding breech longitudinal acceleration is plotted against time, (note the change of scale). Again the same shape of curve is obtained, although the amplitude of the vibrations is much greater.

Results for 125 mm Calibre Weapon

This weapon, with a large breech mass and a muzzle reference system, is intended to simulate a tank gun. In this weapon the charge considered was 9.2 kg of NQ propellant, in the form of slotted stick of ballistic size 0.14 cm, firing a projectile of mass 10 kg. The peak pressure as calculated by HMSOV3 was 554MPa, and the muzzle velocity was 1489 m/s. With the gas dynamics model the effect of changing the length of the charge (ie of having or not having ullage near shot base) was considered. With stick propellant the drag between the gas and solid propellant is much decreased compared to the situation for granular propellant, because the gas flow path is far less tortuous. Hence the incidence of pressure waves due to slowness of flamespread is much reduced. However, the presence or absence of ullage near shot base has a considerable effect on the early part of the history of pressure difference between breech and shot base, as shown in fig. 8.

Here with this heavier weapon the breech accelerations are much reduced, but again there is evidence of higher frequency oscillations in the vibrations resulting from the pressure input from the ABC code, as shown in fig. 9. In this case, with a longer barrel, and a muzzle reference system providing an off-axis load at the muzzle, the muzzle deflections are somewhat larger than for the lighter weapon discussed above.

Remarks and Discussion

Some general remarks can be made concerning the results of the calculations described here. We first consider the internal ballistics aspects. It was found for the first weapon that the peak pressure was highest when the lumped parameter code HMSOV3 was used, and that the magnitude of the peak pressure decreased steadily as the amplitude of the pressure waves increased. The calculated muzzle velocity was lower when HMSOV3 was used

(1446 m/s) than when the gas dynamics code ABC was used (1480 - 1500 m/s). From comparison of the graphs of shot base pressure against time, it is clear that less work is done on the shot by the pressure forces when it is assumed a priori that there is a quadratic drop in pressure from breech to shot base. The travelling pressure waves have little effect on the muzzle velocity achieved, although there was significant variation in the peak pressure calculated.

We turn next to the barrel vibrations and their effect on the accuracy of the weapon. Table 1 shows the conditions at the muzzle at the time of shot exit as calculated for the larger charge in the first weapon. The first line is the results from HMSOV3, and the following lines are results from ABC in order of ascending pressure wave magnitude.

Table 1.

Code	Δp	Muzzle transverse velocity	Muzzle deflection	Muzzle slope	Muzzle jump
	MPa	m/s	mm	mr	mr
HMSOV3	-	0.08	0.071	0.331	0.386
ABC	-0.37	0.111	0.072	0.352	0.426
ABC	-31.6	0.215	0.042	0.224	0.370
ABC	-60.6	0.264	-0.011	-0.005	0.174
ABC	-134.0	0.234	-0.125	-0.481	-0.325

From these results it is clear that the pressure waves introduced during the flamespread phase of the internal ballistic cycle can have a significant effect on the accuracy of the weapon. A change in gun jump of similar magnitude (0.6 mr) was found from the calculations for the larger calibre weapon, although the pressure waves were weaker. This is thought to be due to the difference in shape of the pressure-time curves as calculated by the two models.

The maximum tensile stress at the breech corresponding to the maximum rearward acceleration was calculated, and was found to be approximately 40MPa in excess of the peak pressure for the usual cases, increasing to 70MPa for the case of 'catastrophic' pressure waves. In all cases calculated with the gas dynamics code the maximum rearward acceleration of the breech is increased, and there is evidence of higher frequency modes superimposed on the vibrations. The first higher frequency seen, in the absence of travelling pressure waves is due to the rapid change in the pressure difference between breech and forcing cone near propellant all-burnt. The other frequencies are excited by the pressure waves. It is probable that the presence of these higher frequency modes of vibration would have an adverse effect on the fatigue life of the weapon system.

In conclusion, we have shown that the use of a gas dynamics internal ballistics model to calculate the pressure forces on the gun leads to significant changes in the pattern of barrel vibrations. In particular, the muzzle jump may be completely reversed. It is therefore important that gas dynamics effects are considered in future work on gun dynamics.

Acknowledgements

The authors wish to acknowledge the support of the Royal Armament Research and Development Establishment during the course of this work. In addition one author (WPCK) acknowledges their financial support.

References

1. F R W Hunt (Ed), Internal Ballistics, London, HMSO, 1951.

2. AGARD report, Fluid Dynamics Aspects of Internal Ballistics, AGARD-AR-172, 1982.

3. W P C King, A Mathematical Model for Gun Dynamics with Particular Reference to the L11A5, RMCS report 82002, 1982.

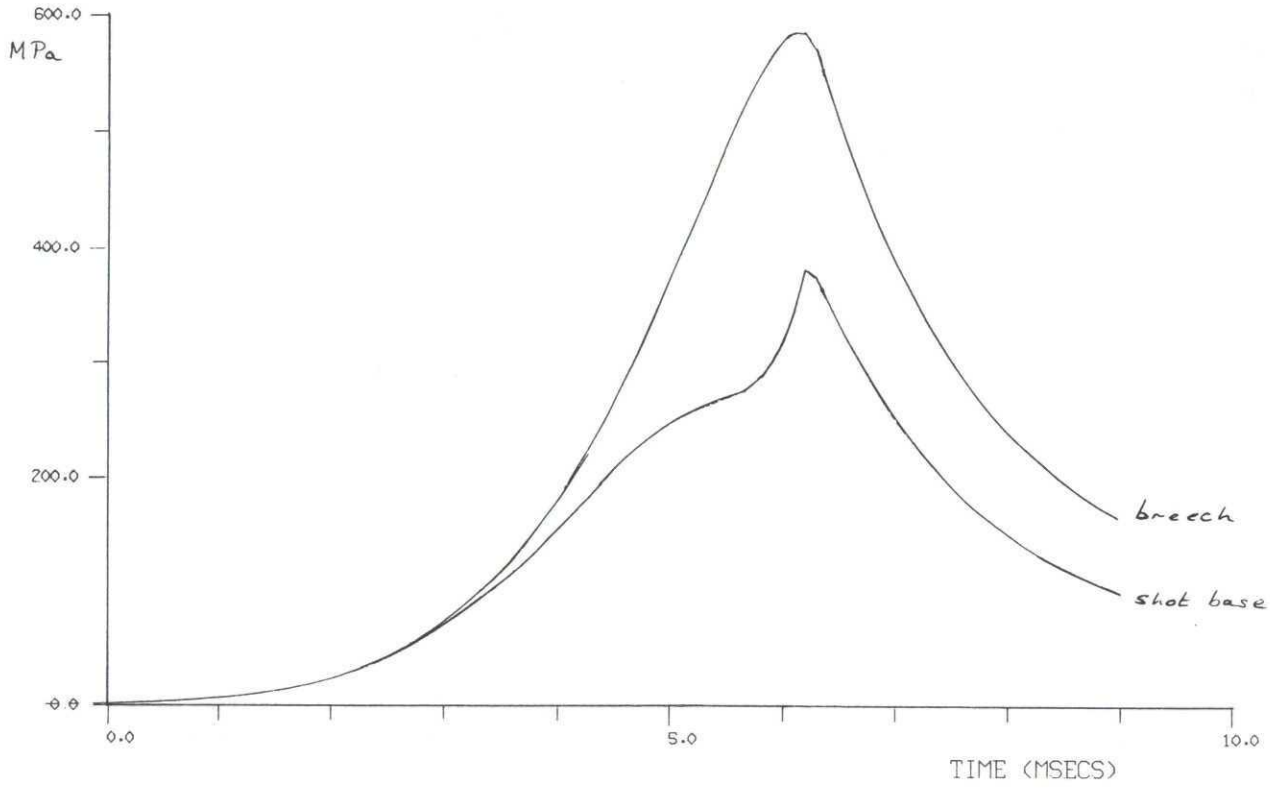

Fig 1. Pressure history for 100 mm calibre weapon using HMSOV3.

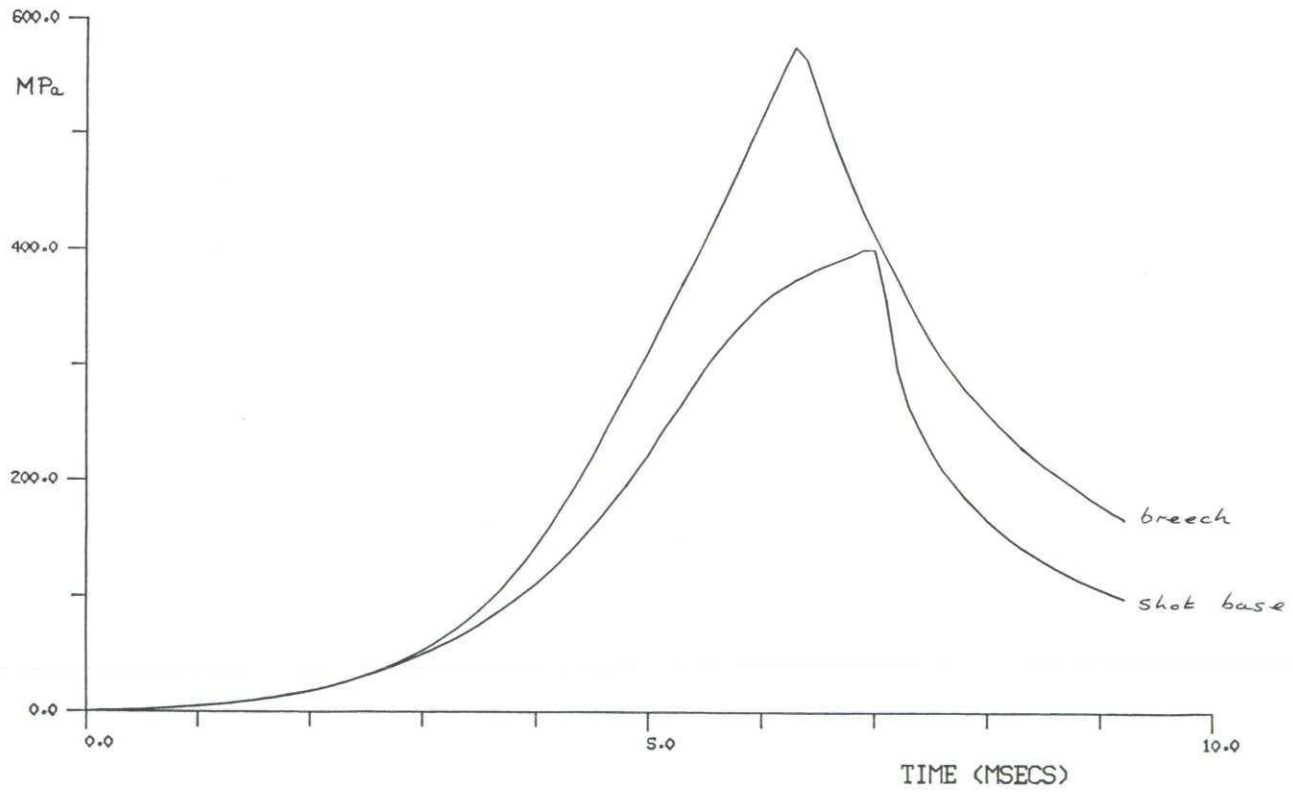

Fig 2. Pressure history for 100 mm calibre weapon using ABC (uniform venting).

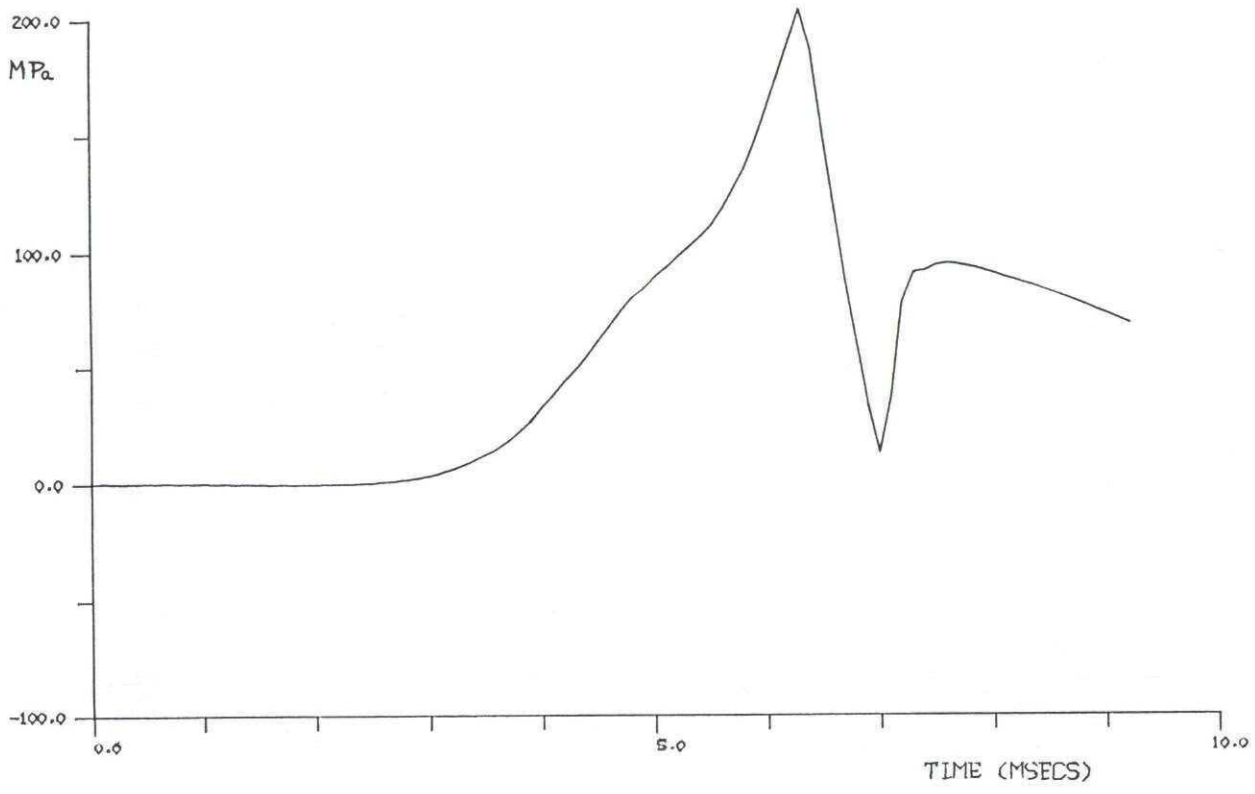

Fig 3. Pressure difference (breech - shot base) for 100 mm weapon using ABC.

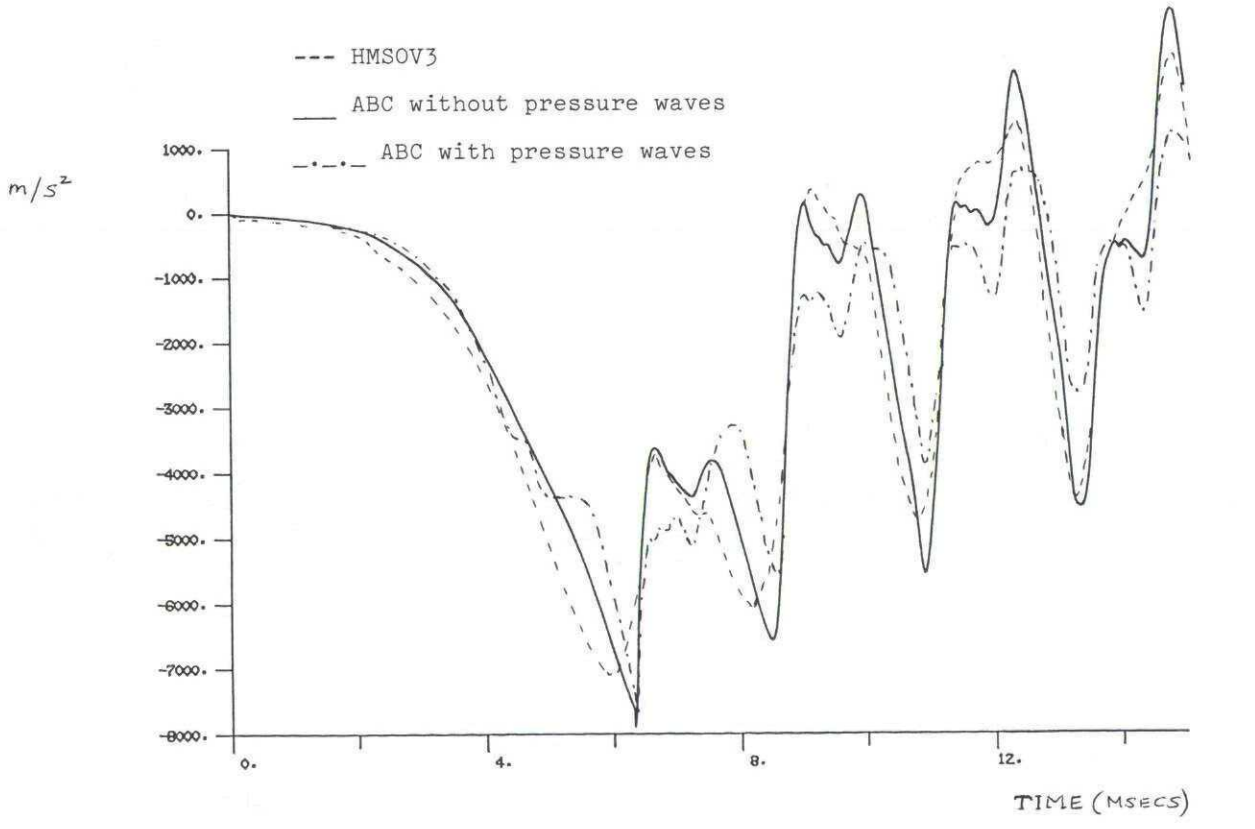

Fig 4. Breech longitudinal acceleration histories for corresponding to pressure histories in Figs 1, 2, 5.

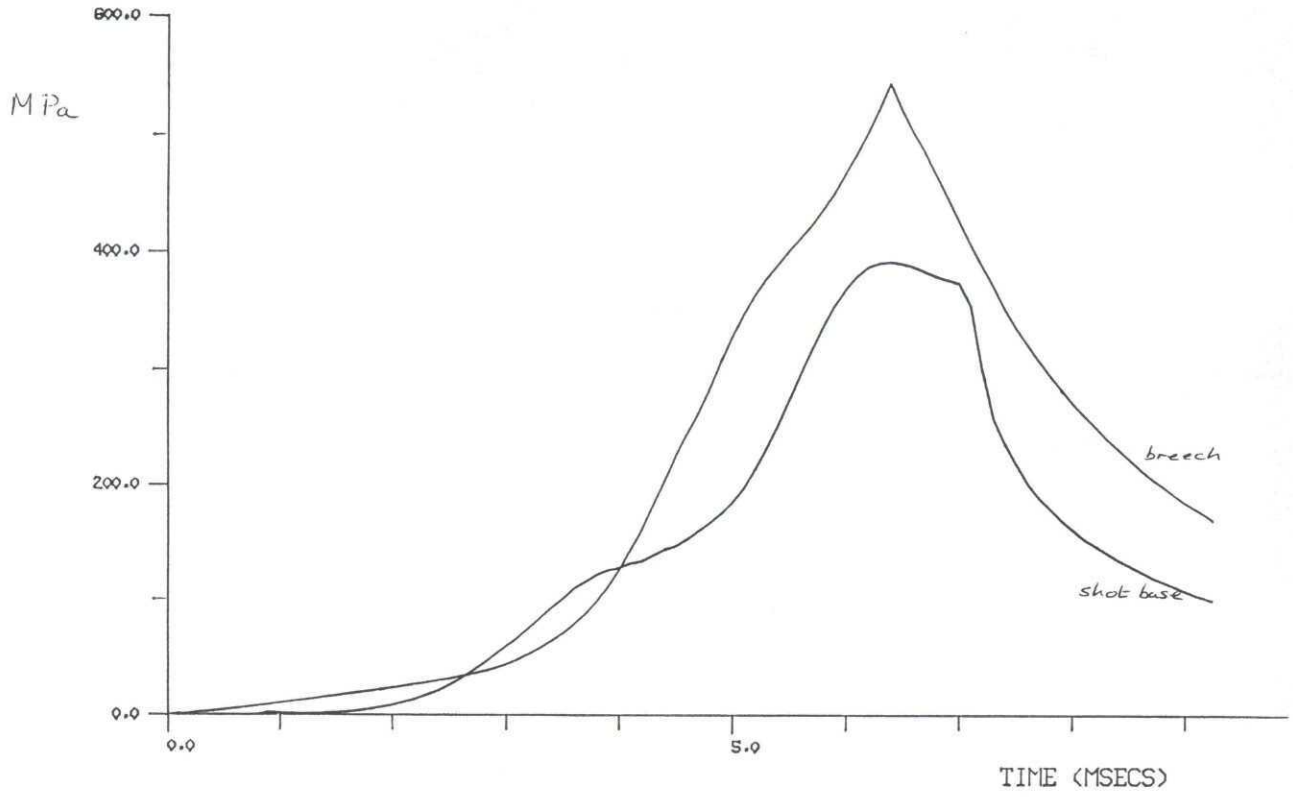

Fig 5a. Pressure history for 100 mm calibre weapon using ABC (venting over first third of propellant bed)

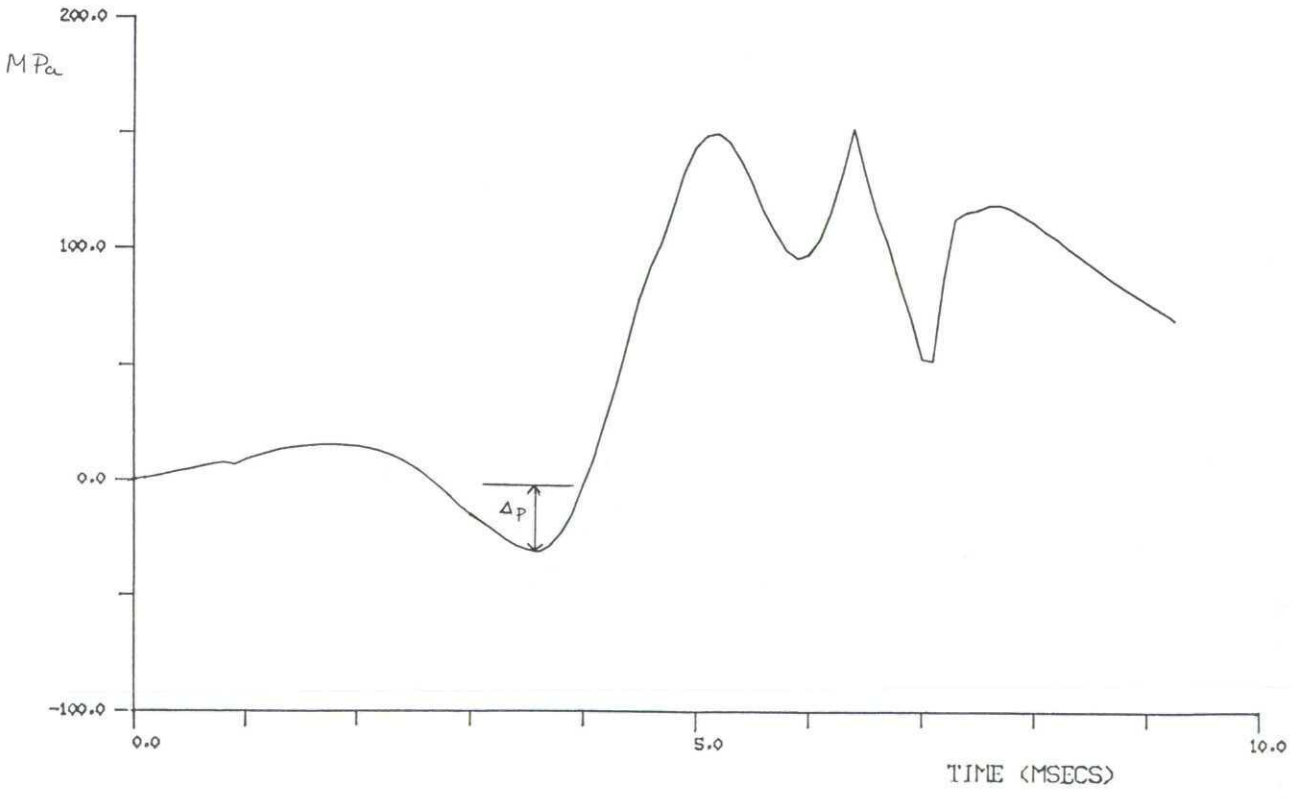

Fig 5b. Pressure difference (breech - shot base) for this case.

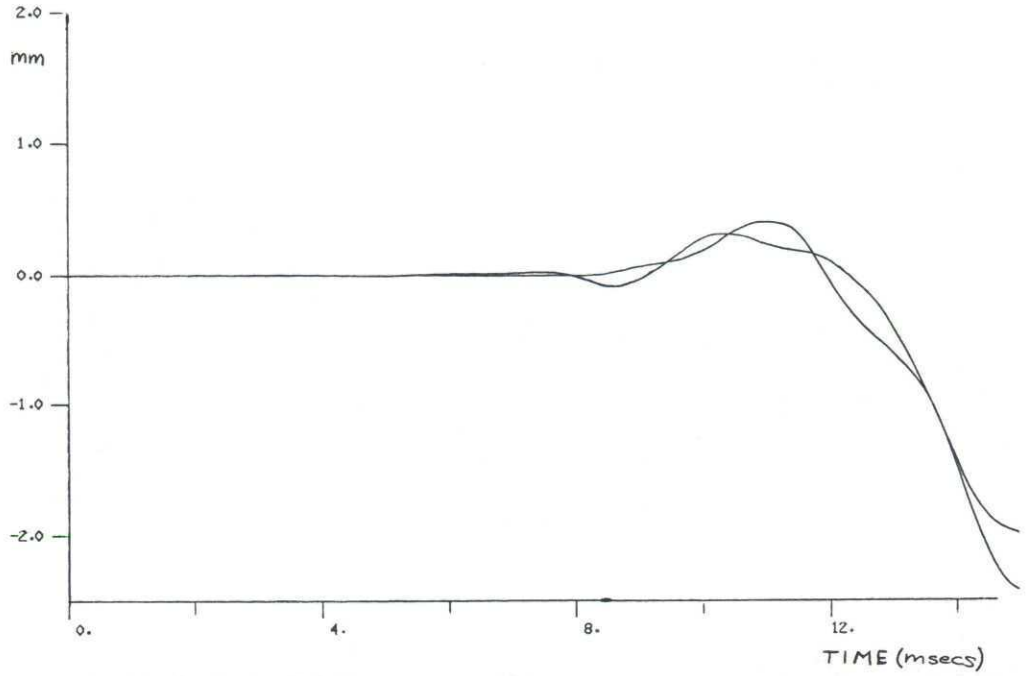

Fig 6. Vertical muzzle deflection v. time using HMSOV3 and ABC with pressure waves.

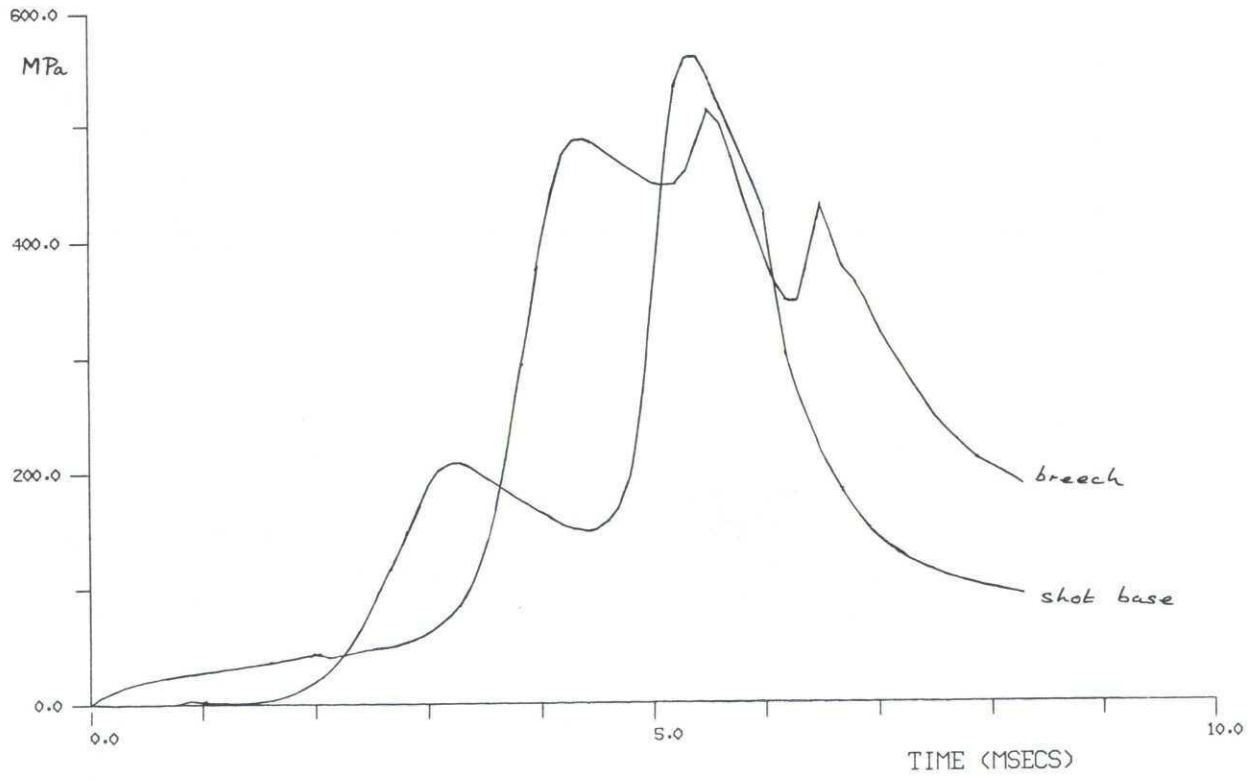

Fig 7a. Pressure history for strong pressure waves using ABC.

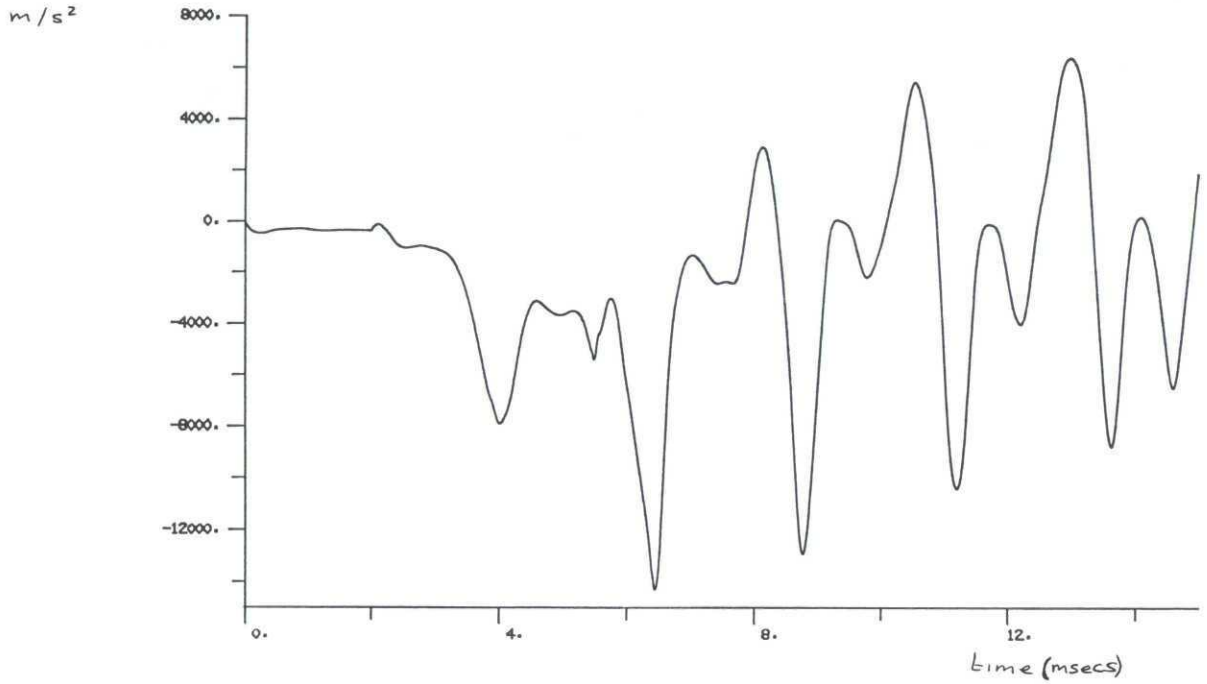

Fig 7b. Corresponding breech longitudinal acceleration.

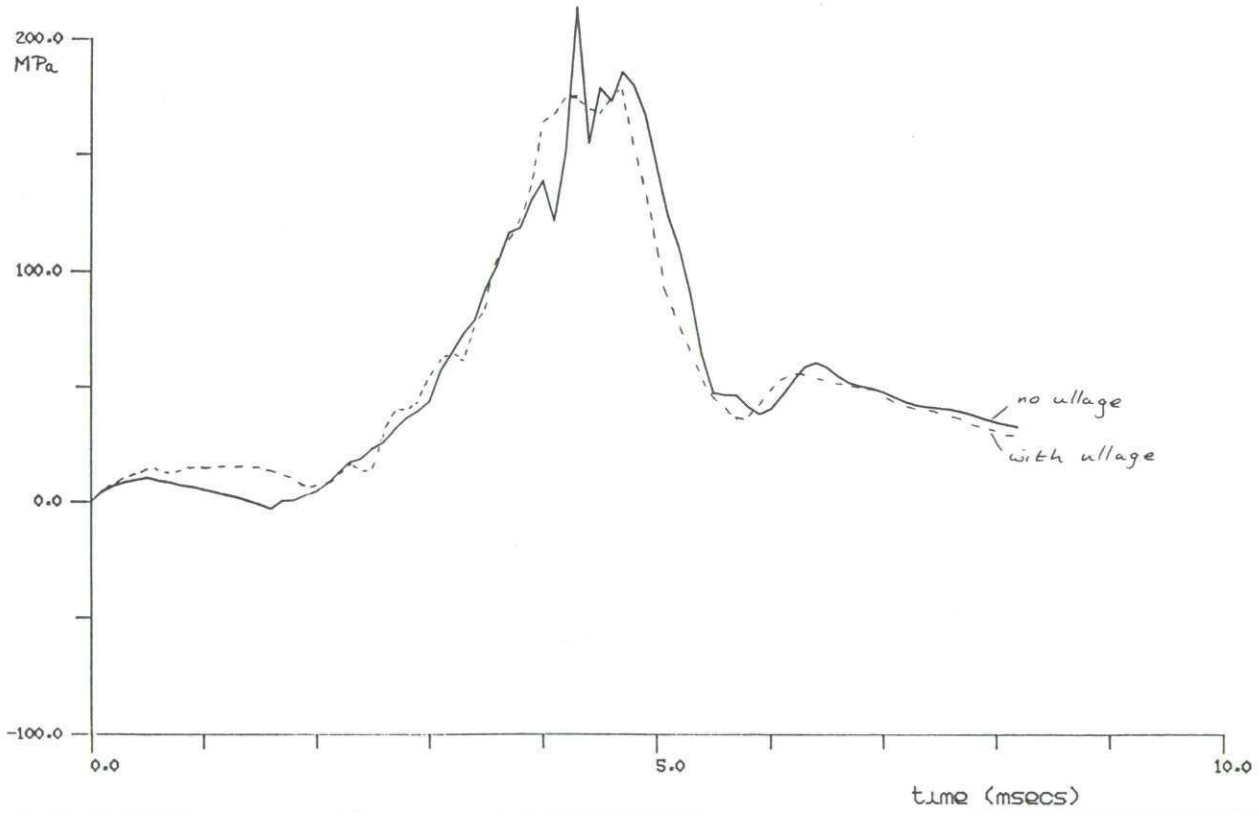

Fig 8. Breech pressure histories for 125 mm calibre weapon with and without ullage at shot base.

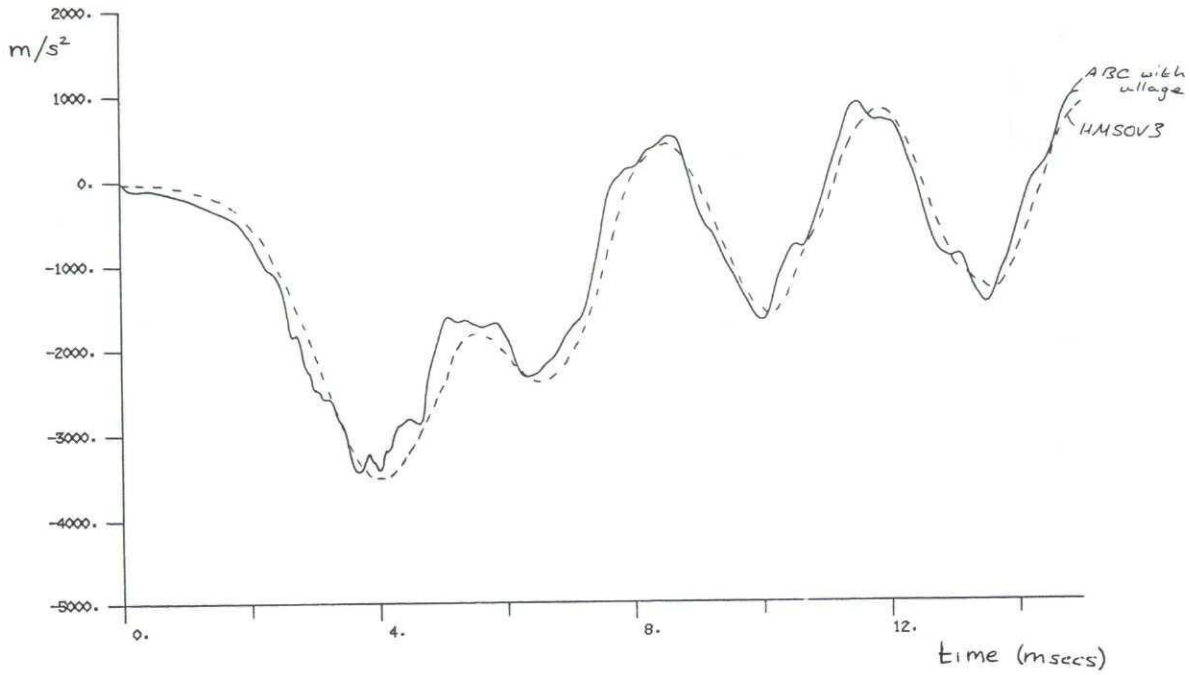

Fig 9. Breech longitudinal acceleration history for 125 mm calibre weapon using HMSOV3 and ABC with ullage.

DISCUSSION

P.Ramette, Fr

Do you intend to extend your model of pressure waves to 2-D configurations, taking into account radial effects?

Author's Reply

Yes, it is our intention to extend the modelling to two space dimensions in due course.

J.M.Frankle, US

Since the breech pressure and the base pressure are related by a constant involving C/W in most lumped parameter codes, how come the two pressure — time curves in your Figure 1 aren't scaled versions of each other?

Author's Reply

We use the relation:

$$P_{breech} = P_{shot} + C/2A \, d/dt\{z * v + (1-z)\hat{v}\}$$

where: v = projectile velocity
$\hat{v}$ = propellant velocity at shot base
C = charge mass
A = cross-sectional area
z = fraction burned

to calculate the breech or shot base pressure once average chamber pressure is known. This reduces after all burnt to the form you describe, but is far from constant in the earlier stages.

N.Rhodes, UK

The muzzle jump must be an easy parameter to measure. Do you have any comparisons with data; is there any experimental information which indicates a sensitivity of the direction of muzzle jump to the presence of pressure waves?

Author's Reply

The studies described here are for hypothetical weapon systems. We do intend to compare our results with experimental data in the near future.

Lt Col.Spasa, It

I want to know if it has been established which is the critical value in differential pressure between the shot base and breech end that can be used to judge a good propellant for tank gun ammunition.

Author's Reply

There is certainly evidence for many granular propellants that there are pressure waves set up within the chamber. As this was not for a real weapon system, I'm sorry I cannot tell you that these exactly match.

BORE TEMPERATURE AND HEAT FLUX IN A 40 mm GUN BARREL

by

B Lawton

Senior Lecturer
RMCS (Cranfield)
SMMCE
Shrivenham, Swindon
Wilts SN6 8LA
England

SUMMARY

A method of measuring the bore surface temperature fluctuation in a 40 mm gun is decribed. Fast response, 1μs, eroding type, surface thermocouples are used and a feature is that they can tolerate up to 3 mm wear and pressures up to 2000 bar. The bore temperature is measured at three positions along the barrel and the pressure is measured at the breech. All three signals are captured using digital oscilloscopes and are transferred to a digital computer through an IEEE interface. The signals are processed to give instantaneous heat flux, shot velocity, shot travel and total heat transfer. Gas leakage past the shot is found to be significant. A simple theory is proposed for calculating the maximum bore temperatures and the total heat transfer and this theory is confirmed by measurements on fourteen different rounds made up using three propellants and various charge masses and grain formulations.

LIST OF SYMBOLS

a	= bore radius; constant	m
A	= constant	
b	= outer radius of barrel; constant	m
c	= constant	
c_i	= $\delta r/(2(a + i\delta r))$	
c_m	= muzzle velocity	m/s
c_v	= specific heat of gun steel	J/kg K
d	= bore of gun = 2a	m
h	= surface heat transfer coefficient	W/m^2 K
H	= heat transfer	J/m^2
H	= total heat transfer	J/m^2
i	= node number	
k	= thermal conductivity of gun steel	W/mK
k_g	= thermal conductivity of propellant gas	W/mK
K	= thermal diffusivity of gun steel = $k/(\rho C_v)$	m^2/s
m	= charge mass	kg
p	= $K\delta t/\delta r^2$; Laplace transform constant	
Pr	= Prandtl number	
q	= heat flux	W/m^2
q_o	= surface heat flux	W/m^2
r	= radius; $\sqrt{p/K}$	m
R_T	= thermal property ratio = $\frac{k}{k_g}\sqrt{\frac{c_m d}{K}}$	
Re	= Reynolds number = $mC_m/(d^2\mu)$	
t	= time	s
t_o	= time constant	s
T	= temperature of barrel	K
T_o	= surface temperature	K
T_i	= temperature at node 'i'	K
T_i'	= temperature at 'i' δt seconds later	K
T_f	= propellant flame temperature	K
T_g	= gas temperature	K
T_{max}	= maximum bore surface temperature	K
$\tilde{T}$	= Laplace transform of T	
u	= t/t_o	
u'	= t'/t_o	
x	= distance from surface	m

α = constant
β = constant
δ = constant
δx = distance between nodes m
δt = time increment s
μ = viscosity of gas Ns/m^3
ρ = density of gun steel kg/m^2
τ = non-dimensional time = $(h/k)^2$ Kt

INTRODUCTION

An accurate knowledge of bore temperature and heat transfer is important to gun designers for several reasons. If the gun bore is hotter than about 180 deg C and combustible cartridge cases are used then there is a real danger of case ignition. Even metal cartridge cases can ignite the propellant if they are left in a hot barrel for sufficient time. However, if the round is fired immediately after loading, much higher barrel temperatures can be tolerated. On automatic weapons, barrel temperatures up to 500 deg C or 600 dec C are possible before the strength of the barrel is seriously impaired. These considerations limit the rate of fire and the number of rounds that can be fired.

An equally important consideration is the maximum temperature of the bore surface when a gun fires. This may be as high as 1200 deg C and is of fundamental importance in relation to barrel wear. As early as 1947 Thornhill quantified this relationship and proposed that wear per round is a linear function of the maximum bore temperature, reference (1). At that time it was not possible to measure the maximum bore temperature and so Thornhill used calculated values, reference (2). A thermal theory of gun erosion was suggested by Bannister, reference (3) and also by several other workers. Brosseau and Ward, reference (4), demonstrated a relationship between wear and total heat transfer by direct measurement using sub-surface thermocouples positioned about 0.5 mm from the bore. Their results confirmed that quite small reductions in heat transfer, say 10%, increased the barrel life three or four times. The most general relationship between wear, heat transfer and propellant chemistry is that proposed by Lawton, reference (5).

This paper, therefore, has three main objectives. Firstly, to describe a method of measuring bore surface temperatures and heat flows. Secondly, to present typical results and thirdly, to show that these results can be calculated by means of a very simple theory. This theory is in two parts. Firstly, an equation is derived that relates the maximum bore temperature to the main variables such as: charge mass, propellant flame temperature, gun bore and the usual thermal properties. Secondly, an equation is derived relating the total heat transfer per round to the maximum bore temperature. The first equation is important in relation to barrel wear and the second equation is important in relation to the rate of fire and self-ignition of propellant on the hot barrel.

EXPERIMENTAL METHOD

One of the main problems in measuring the bore temperature when a gun fires is that, in order to have a fast response, the hot junction must be very small; of the order of 2 µm. Such small thermocouple junctions can be made but may not last very long on the surface of a gun tube where erosion can be expected to vary from 1µm to 200 µm per round.

Figure 1 shows how a sinusoidal surface temperature fluctuation is attenuated as it travels into the metal. A frequency of 10 Hz reduces in amplitude from 1 at the surface to about 0.2 1 mm below the surface. Higher frequencies attenuate even faster. A 5 kHz frequency scarcely penetrates 0.1 mm into the surface. In order for a thermocouple to respond to frequencies as high as 5 kHz without losing more than 8% of the amplitude it is necessary for the thermocouple hot junction to be not more than 2µm from the surface. The problem is to make a thermocouple with a hot junction 2µm deep that can tolerate wear rates as high as 200 µm per round. Surprisingly such thermocouples do exist and are available commercially, figure 2.

Fast response, eroding thermocouples are available from a number of manufacturers; the one shown in figure 2 is manufactured by the Swedish firm of ASEA. A Ni-Al centre pin is separated from an outer annular tube by a 2µm dialectric. The whole is mounted inside a 4.5 mm diameter tapered steel tube. The hot junction is formed at the butt-end by abra ding the end to transfer or smear a thin film of metal across the 2 µm dialectric. This gives a hot junction 2 µm wide and about 2 µm deep. As the surface wears the hot junction continuously re-forms and up to 3 mm of wear can be tolerated. Figure 2 also shows the method used to install the thermocouple into a barrel. This method was chosen because it allows the thermocouple to be removed for inspection and cleaning. It was also necessary to shape the thermocouple to conform with the contours of the rifled barrel. The thickness of the 'wear spacer' may be adjusted to align the thermocouple surface exactly with that of the barrel. The thermal properties of this thermocouple are not too different from those of the gun steel:

for the thermocouple $k = 24$ W/mK $K = 7.3 \times 10^{-6}$ m^2/s

for the gun steel $k = 35$ W/mk $K = 9 \times 10^{-6}$ m^2/s.

The general arrangement of the instrumentation is shown in figure 3. Three surface thermocouples are fitted to the barrel of a 40 mm, 70 calibre gun, formerly a Bofors gun. This gun may be arranged to fire in the conventional mode or as a recoilless or partially gun. In the tests reported here the gun fired in conventional mode. The ammunition

fired is 40/70 break-up shot. The three thermocouples, A, B and C, are situated 25, 125 and 1025 mm respectively, from the commencement of rifling. The thermocouple signals are amplified with a gain of 20 and frequency response from dc to 200 kHz. The amplified signals are captured on two digital oscilloscopes arranged to trigger at the same instant. The breech pressure is measured by a Kistler piezo-electric transducer and charge amplifier. The pressure signal is used to trigger the oscilloscopes. After capture the signals may be stored on the oscilloscope's floppy disc or may be transferred through an IEEE interface to a digital computer.

SIGNAL PROCESSING

The pressure-time curve is readily integrated and scaled within the computer to give the shot velocity. A further integration gives the shot position. For numerical integration Simpson's rule is used with a step length of 20 μs per point. Processing of the observed temperature-time curves to give heat flux and total heat transfer is a little more involved. The heat conduction equation can be written as:

$$\frac{\partial^2 T}{\partial r^2} + \frac{1}{r}\frac{\partial T}{\partial r} = \frac{1}{K}\frac{\partial T}{\partial t} \qquad (1)$$

Essentially, the right hand side is known, at the surface, and this allows the left hand side to be computed to yield the radial temperature distribution in the barrel at any instant. An explicit finite-difference scheme is used to reduce equation (1) to:

$$T_i' = (1 - 2p)T_i + p(1 + C_i)T_{i+1} + p(1 - C_i)T_{i-1} \qquad (2)$$

where $p = K\delta t/\delta r^2 < 0.5$ for stability
and $C_i = \delta r/(2(a + i\delta r))$.

From the initial values of T_i and the measured surface temperature, T_o, it is easy to compute the subsequent temperature at any sub-surface node, T_i'. The number of nodes required is not excessive because the temperature penetrates only a short distance into the surface. For instance, if δt = 20 μs and p = 0.25 then the node spacing is 27 μm and 100 nodes penetrates 2.7 mm beneath the surface. This is adequate because the temperature at a point 2.7 μm below the surface does not begin to rise until 50 ms after firing.

From equation (2) it is possible to compute the radial temperature distribution at any instant in time. Two useful quantities may be determined from such data. Firstly, the data can be integrated to give the total heat transferred into the barrel:

$$H = \frac{\rho C_v}{a}\int_a^b Trdr \ J/m^2 \qquad (3)$$

Simpson's rule is used for numerical integration. Secondly, the temperature gradient at the bore surface may be determined. When multiplied by the thermal conductivity of the thermocouple this yields the instantaneous surface heat flux. For numerical differentiation a fourth order finite difference equation is used, namely:

$$q_o = k\,\frac{T_4 - 5T_3 + 10T_2 - 11T_1 + 5T_0}{2\delta r}\ W/m^2 \qquad (4)$$

RESULTS

Figure 4 shows a complete set of results for a single round. The upper graph shows the observed breech pressure , the shot velocity and travel which are calculated from the breech pressure. In this case the maximum pressure is only 1200 bar and muzzle velocity is about 600 m/s. The middle graph shows the surface temperature rise at the three thermocouples, A, B and C. As can be expected, thermocouple A is the first to show a temperature rise followed in due course by thermocouples B and C. At thermocouple A the maximum temperature rise is about 690 deg C, at thermocouple B it is about 675 deg C and at thermocouple C it is 400 deg C. In other tests the temperature at thermocouple B sometimes exceeds that at thermocouple A. The typical form of the temperature-time curve is a very rapid rise to the maximum temperature followed by a much slower fall. The maximum temperature rise is usually at thermocouple A and occurs a little after the instant of maximum pressure. In figure 4 the maximum temperature at A occurs 0.6 ms after maximum pressure; at B it occurs 1.2 ms after maximum pressure and at C it occurs 3.6 ms after maximum pressure. Shot exit is 5.0 ms after maximum pressure. It is noticeable that there is a significant change in the slope of the temperature-time curves at the instant of shot exit.

The total heat transfer, lower graph of figure 4, is calculated from the observed temperature-time curves using equations (2) and (3). Heat transfer is initially very rapid but it reduces as the gas pressure falls. Most heat transfer occurs before shot exit but a significant amount also occurs after shot exit. At the instant of maximum temperature about 45% of heat transfer has occurred at thermocouple A. The remaining 55% of heat is transferred into a cooling surface. This is because heat conduction away from the surface exceeds the convective heat transfer to the surface and so the surface temperature falls.

An interesting feature of these results is that gas leakage between the shot and the barrel causes a very considerable temperature rise. In theory, the bore temperature should start to rise at the moment the rear edge of the shot uncovers the thermocouple thus exposing it to the hot propellant gas. Observations made on about 40 different rounds show that in all cases the temperature begins to rise before the shot clears the thermocouple. This is observed at all three thermocouple locations but is most marked at thermocouple A and least significant at thermocouple C. This temperature rise may be caused by friction as the shot passes over the thermocouple but the more likely reason is that it is caused by hot propellant gas escaping past the shot.

The magnitude of heat transfer caused by gas leakage is demonstrated in figure 5. The rear face of the shot is 0.124 m from thermocouple A when first loaded. Thus, when the shot has moved 0.124 m the thermocouple should be exposed to the hot propellant gas and the temperature should start to rise. Examination of figure 5 shows that when the shot has moved 0.124 m the temperature at thermocouple A is already 680 deg C and 0.11 MJ/m^2 of heat has been transferred. This is about 75% of the temperature rise and 18% of the total heat transfer. The implication here is that an improved design of driving band may reduce heat transfer and thereby reduce barrel erosion.

At this point it is convenient to compare the observed results with theory. The easiest way of predicting barrel temperature is to modify an existing internal ballistics computer programme to calculate the variation of heat transfer coefficient and gas temperature with time. The equations described in Appendix II of reference (6) are suitable. Knowing the heat transfer coefficients and the gas temperature a finite-difference equation, such as that shown in equation (2), may be used to compute the barrel temperature. Some additional equations to allow for gas leakage are required. This has been done for all the rounds fired in the 40/70 gun but the results are not presented in this paper. Instead, some simpler correlations between maximum bore temperature, total heat transfer, charge mass, flame temperature, bore, and the usual thermal properties of the propellant and gun steel, are presented. Such a relationship, described in Appendix A, takes the form:

$$\frac{T_f - \beta T_i}{T_{max} - T_i} = \beta + \delta R_T / Re^b \qquad (5)$$

The value of b is taken to be 0.86 after reference (6) and the equation is made to fit the observed results by choosing suitable values of β and δ. If the value of β is taken to be 1.8 then the quantities $(T_f - 1.8T_i)/(T_{max} - T_i)$ and $R_T/Re^{0.86}$ can be calculated for each of the fourteen rounds fired and the results plotted as in figure 6. The method of least squares is used to give the best straight line through the results. This gives $\beta = 1.8$ and $\delta = 288$ and a goodness of fit, r^2, of 0.886. This solution is correct because the assumed value of β and the computed value are the same. If this were not so then the calculation must be repeated using a better value for β. Thus the observed maximum bore temperature is represented by:

$$\frac{T_f - 1.8T_i}{T_{max} - T_i} = 1.8 + 288\ R_T/Re^{0.86} \pm 4\% \qquad (6)$$

where

$$R_T = \frac{k}{k_g}\sqrt{\frac{C_m d}{K}} \quad \text{and} \quad Re = \frac{mC_m}{\mu d^2}$$

A better indication of the validity of equation (6) is shown in figure 7 where the observed temperature is compared directly with the temperature computed by equation (6). The observed temperatures vary from 900 K to 1200 K and all results lie within $\pm$ 50 deg C of the calculated temperature.

An interesting aspect of equation (6) is revealed when the following substitutions, representing typical values, are made:

$$k = 35\ W/mK; \quad K = 9 \times 10^{-6}\ m^2/s; \quad C_m = 900\ m/s$$
$$k_g = 0.09375\ W/mK; \quad \mu = 50 \times 10^{-6}\ Ns/m^2 \qquad (7)$$

Thus

$$\frac{T_f - 1.8T_i}{T_{max} - T_i} = 1.8 + 616\ \frac{d^{2.22}}{m^{0.86}} \qquad (8)$$

This can be compared with a much used equation, originally derived by Thornhill, references (1), (2) and (6) which, in SI units, takes the form:

$$\frac{T_f - T_i}{T_{max} - T_i} = 1.7 + 670\ \frac{d^{2.22}}{m^{0.86}} \qquad (9)$$

Equations (8) and (9) are not identical but are similar and give similar results if the initial barrel temperature, T_i, is low. However, as T_i increases equation (9) becomes inaccurate. Nevertheless equations (8) and (9) are sufficiently similar for it to be

concluded that equation (6) is the most general form of Thornhill's equation. However, equation (6) has several advantages over Thornhill's equation, namely:

(1) its theoretical base is clear
(2) it is valid in any consistent units
(3) no variables are missing
(4) the constants are chosen to fit observed data and are therefore more reliable
(5) the equation remains valid for hot barrels ($T_i > 20^{\circ}C$).

If the equation describing heat flow into a surface is known then it is possible to solve the heat diffusion equation and hence derive a relationship between the maximum bore temperature and the total heat transfer. The lower graph in figure 4 suggests that the heat flow into the barrel might be represented by:

$$H = H_{\infty}(1 - \exp(-t/t_o)) \tag{10}$$

where H_{∞} and t_o are appropriate constants. In Appendix B it is shown that, given equation (10), the surface temperature is:

$$\frac{(T_o - T_i)k}{H_{\infty}} \sqrt{\frac{\pi t_o}{K}} = 2\sqrt{u}\ \exp(-u) \left\{1 + \frac{u}{3} + \frac{u^2}{5\times 2!} + \frac{u^3}{7\times 3!} + \ldots\right\} \tag{11}$$

where $u = t/t_o$.

The series converges rapidly. Equations (10) and (11) are plotted in figure 8. The maximum surface temperature occurs when $t/t_o = 0.85$ and has a value defined by:

$$\frac{(T_{max} - T_i)k}{H} \sqrt{\frac{\pi t_o}{K}} = 1.082 \tag{12}$$

This maximum occurs when 73% of the heat has been transferred.

Equation (11) gives a very reasonable representation of the observed temperature time curves if the values of H_{∞} and T_{max} are substituted into equation (12) to give the value of t_o. This is confirmed in figure 9 which shows typical results for thermocouples A, B and C plotted in non-dimensional form.

It was found that the value of the time constant varied from round to round. The relationship between total heat transfer, maximum bore temperature and the time constant is given by equation (12) and is plotted in figure 10 for time constants in the range 1 ms < t_o < 10 ms. The observed temperature rise and heat transfer for each of the fourteen rounds is also plotted on figure 10. As can be seen, the time constants varied from 2 ms to 4 ms. Thornhill, reference (1), suggests that his time constant be taken as the time to shot exit which he took to be $t_o = d/10$. Thus for the 40 mm gun the time constant should be 4 ms for all rounds. Attempts have been made to correlate the time constant with muzzle velocity and bore but such correlations are very poor. The best correlation is obtained when the time constant is taken to be equal to the time for the gas pressure to rise from 5% to 95% of its maximum value. The correlation is shown in the lower graph of figure 10. This time constant is valid only at thermocouple A. The time constants at thermocouples B and C were shorter than at thermocouple A.

By combining equations (6) and (12) an equation for calculating the total heat transfer per round is obtained:

$$H_{\infty} = \frac{k(T_{max} - T_i)}{1.082} \sqrt{\frac{\pi t_o}{K}}$$

$$H_{\infty} = \frac{k(T_f - 1.8T_i)}{1.082\ (1.8 + 288\ R_T/Re^{0.86})} \sqrt{\frac{\pi t_o}{K}} \tag{13}$$

Substituting the values set out in equation (7) and Thornhill's definition of the time constant, $t_o = d/10$, gives

$$H_{\infty} = \frac{6044(T_f - 1.8T_i)\ \sqrt{d}}{1.8 + 616\ d^{2.22}/m^{0.86}} \tag{14}$$

This can be compared with Thornhill's equation which, in SI units, takes the form:

$$H_{\infty} = \frac{3270(T_F - T_I)\ \sqrt{d}}{1.7 + 670\ d^{2.22}/m^{0.86}} \tag{15}$$

Equation (13) is clearly the most general form of Thornhill's equation and it has the advantages of being non-dimensional, having all the relevant variables, having constants chosen to fit experimental results and remaining accurate at high barrel temperature ($T_i > 20^{\circ}C$). Equation (14) has no general validity at all and is derived simply for the

purposes of comparison.

An interesting aspect of equation (13) is that it has a reasonable 'radiation' temperature. It has long been known that as the initial barrel temperature, T_i, rises, the heat transfer reduces. The radiation temperature is the imaginary barrel temperature at which the heat transfer reduces to zero. The radiation temperature is known to be much less than the propellant flame temperature and is often assumed to be about 1000 deg C. From equation (14) the radiation temperature is $T_f/1.8$, which is of the right order.

CONCLUSIONS

Thermocouples A and B near the commencement of rifling always gave similar results. The temperature rise varied from 600 deg C to 950 deg C and the total heat varied from 0.5 MJ/m^2 to 0.8 MJ/m^2. Gas leakage between the shot and the barrel proved to be significant and produced about 70% of the temperature rise and 15% to 25% of the total heat transfer. Improved gas sealing by the driving band should reduce barrel temperature and thereby increase barrel life. The maximum temperature occurs just after the period of gas leakage and, at thermocouple A, just after the instant of maximum pressure. At thermocouple C, situated about half way along the barrel, the heat transfer is about 65% of the heat transfer at thermocouple A and the temperature is correspondingly lower.

The maximum bore temperature at thermocouple A is well represented by equation (6). The 14 rounds fired all gave temperatures within $\pm 50^{o}$C of the temperature predicted by equation (6). The total heat transfer per round is well described by equation (13) if the time constant, t_o, is taken to be the time for gas pressure to rise from 5% to 95% of its maximum value. The bore surface temperature variation with time is well represented by equation (11). The 'radiation' temperature appears to be $T_f/1.8$.

REFERENCES

(1) Thornhill, C K, 'An analyis of gun erosion', ARD Report No 38/47, 1947.
(2) Hicks, E P and Thornhill, C K, 'Gun erosion and barrel cooling in automatic fire', ARD Report 23/97, 1947.
(3) Bannister, E L, 'Thermal theory of erosion of guns by propellant gases', BRL Tech Note 1740, Sept 1970.
(4) Brosseau, T L and Ward, J R, 'Reduction of heat transfer to gun barrels by wear-reducing additives', Trans ASME, paper 76-HT-K, Nov 1975, pp 610-614.
(5) Lawton, B 'Thermal and chemical effects on gun barrel wear', 8th International Symp on Ballistics, Orlando, Flo, Oct 23-25, 1984 pp II-27 to II-35.
(6) 'Internal Ballistics', HMSO, London, 1951.
(7) Carslaw, H S and Jaeger, J C, 'Conduction of Heat in Solids', OUP, 1947.

ACKNOWLEDGEMENTS

This work was done under the terms of a contract from GR2 Branch, RARDE, Fort Halstead, England and the author wishes to thank Mr P Fuller, Dr D Izod and Dr G Cook for their helpful advice and assistance. At RMCS Mr P Mumford and Mr K Elmore have been invaluable.

APPENDIX A: MAXIMUM BORE TEMPERATURE

The bore temperature rises very quickly to its maximum value and therefore, during this short period, the propellant gas temperature and surface heat transfer coefficient may be assumed to be constant. Under these circumstances the surface temperature is given in reference (7) as:

$$\frac{T - T_i}{T_g - T_i} = 1 - \exp \tau \operatorname{erfc} \sqrt{\tau} \qquad (A1)$$

where $\tau = (h/k)^2 Kt$.

This well known result can be approximated by:

$$\frac{T_g - T_i}{T - T_i} = 1 + 1/\sqrt{1.5\tau} \qquad (A2)$$

Now the heat transfer coefficient may be calculated from Reynold's and Prandtl's numbers.

$$h = \frac{a\, k_g}{d} Re^b\, Pr^c \qquad (A3)$$

where $Re = mC_m/(d^2\mu)$.

The time taken to reach maximum temperature is taken to be

$$t = \alpha d/C_m \qquad (A4)$$

and the mean gas temperature is related to the propellant flame temperature by

$$T_g = T_f/\beta \tag{A5}$$

Putting A3, A4 and A5 into A2 gives the required result:

$$\frac{T_f - \beta T_i}{T_{max} - T_i} = \beta + \delta R_T/Re^b \tag{A6}$$

where β and δ are constants

R_T = thermal property ratio = $\frac{k}{k_g}\sqrt{\frac{dC_m}{K}}$

and Re = Reynold's number = $mC_m/(d^2\mu)$.

From experimental results $\beta = 1.8$ and $\delta = 288$.

APPENDIX B: BORE TEMPERATURE AND HEAT TRANSFER

The heat diffusion equation for a semi-infinite solid with a surface at x = 0 is

$$\frac{\partial T}{\partial t} = \frac{1}{K}\frac{\partial^2 T}{\partial x^2}$$

Taking the Laplace transform yields the ordinary differential equation:

$$\frac{d^2\tilde{T}}{dx^2} - r^2\tilde{T} = \frac{T(0)}{K}$$

where $r = \sqrt{\frac{P}{K}}$

If the initial temperature is T(0) = 0 then the solution is

$$\tilde{T} = A \exp(-rx) + B \exp(rx)$$

Now T = 0 at x = ∞ for all t and thus B = 0

$$\therefore \quad \tilde{T} = A \exp(-rx) \tag{B1}$$

If the heat flow into the surface is

$$H = H_\infty(1 - \exp(-t/t_o)) \tag{B2}$$

then Fourier's equation for heat conduction gives

$$q_o = -k\left(\frac{\partial T}{\partial x}\right)_{x=0} = \frac{H_\infty}{t_o}\exp-\left(\frac{t}{t_o}\right)$$

which transforms to

$$\left(\frac{d\tilde{T}}{dx}\right)_{x=0} = \frac{-H_\infty}{kt_o}\left(\frac{1}{p + 1/t_o}\right) \tag{B3}$$

Differentiating (B1) and substituting into (B3) gives

$$A = \frac{H_\infty}{kt_o r}\left(\frac{1}{p + 1/t_o}\right)$$

and (B1) becomes

$$\tilde{T} = \frac{H_\infty}{kt_o}\left(\frac{1}{p + 1/t_o}\right)\left(\frac{e^{-rx}}{r}\right) \tag{B4}$$

The inverse transform of (B4) is found by using the convolution theorem.

$$T = \int_0^t \frac{H_\infty}{kt_o}\exp\left(\frac{t' - t}{t_o}\right)\sqrt{\frac{K}{\pi t'}}\exp\left(\frac{-x^2}{4Kt}\right)dt' \tag{B5}$$

This can be integrated numerically to give the barrel temperature at any position from the surface and at any time. A useful solution can be obtained for the surface temperature by putting x = 0 and writing (B5) in non-dimensional form:

$$\frac{T_o k}{H}\sqrt{\frac{\pi t_o}{K}} = \exp(-u)\int_0^u \frac{1}{\sqrt{u'}}\exp(u')\,du' \tag{B6}$$

where $u = t/t_o$ and $u' = t'/t_o$.

Replacing exp (u') by its power series and integrating gives

$$\frac{T_o k}{H_\infty}\sqrt{\frac{\pi t_o}{K}} = 2\sqrt{u}\exp(-u)\left\{1 + \frac{u}{3} + \frac{u^2}{5\times 2!} + \frac{u^3}{7\times 3!} + \frac{u^4}{9\times 4!} + \ldots\right\} \qquad (B7)$$

This equation has a maximum value of 1.082 when u = 0.85 and thus the total heat transfer is given by

$$H_\infty = k\sqrt{\frac{\pi t_o}{K}}\,\frac{(T_{max} - T_i)}{1.082} = \frac{(T_{max} - T_i)\sqrt{\pi k \rho c_v t_o}}{1.082} \qquad (B8)$$

Experiments show that the time constant, t_o, should be taken as the time for the gas pressure to rise from 5% to 95% of its maximum value.

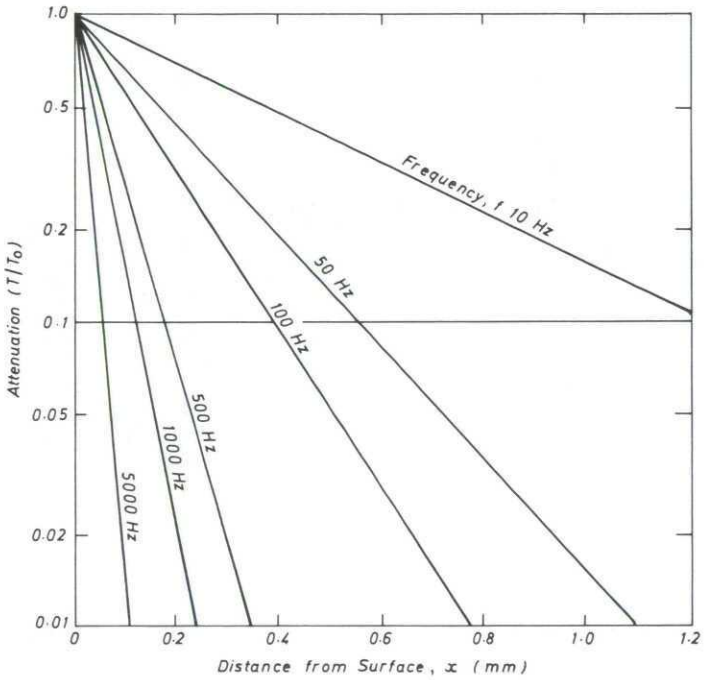

$T = T_0 \sin(2\pi ft)$ at $x = 0$

$T/T_0 = \exp(-x\sqrt{\pi f/K})$; $K = 8.9 \times 10^{-6}\ m^2/s$ (Steel)

Figure 1 ATTENUATION OF A SURFACE HARMONIC TEMPERATURE (T_0)

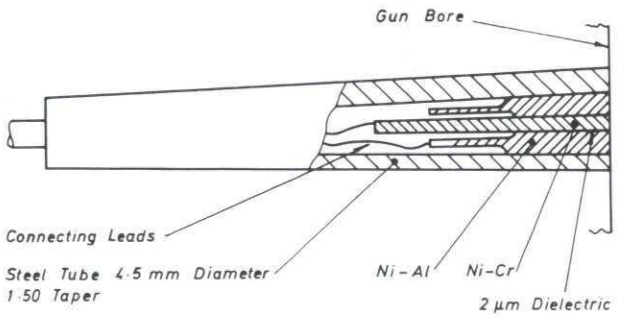

Rise Time (10–90%) = 1 µs

Maximum Temperature = 600°C (continuous); 1500°C (Flash)

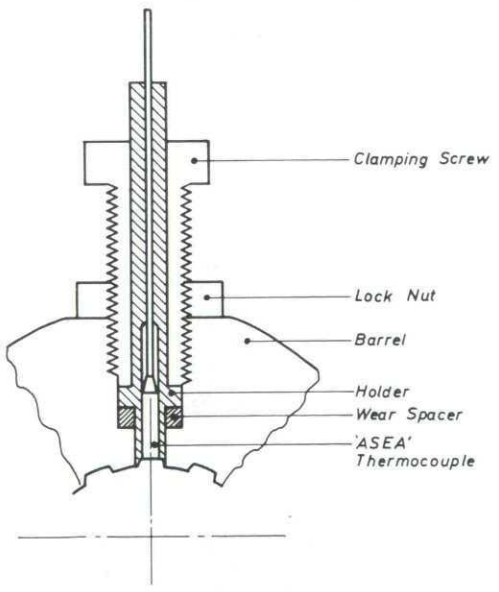

Figure 2 'ASEA' THERMOCOUPLE AND METHOD OF FITTING IN GUN BARREL

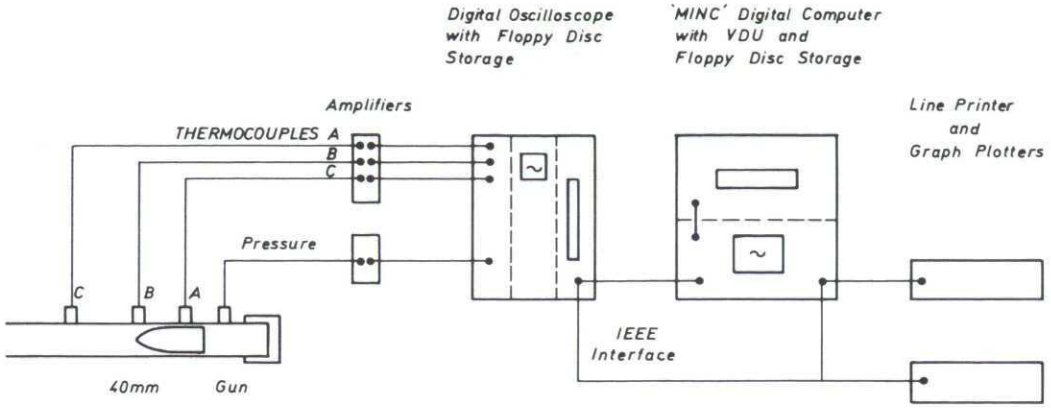

Thermocouple A = 25 mm from commencement of rifling
Thermocouple B = 145 mm from commencement of rifling
Thermocouple C = 1025 mm from commencement of rifling
Barrel length = 2500 mm approx

Figure 3 DATA COLLECTION AND PROCESSING

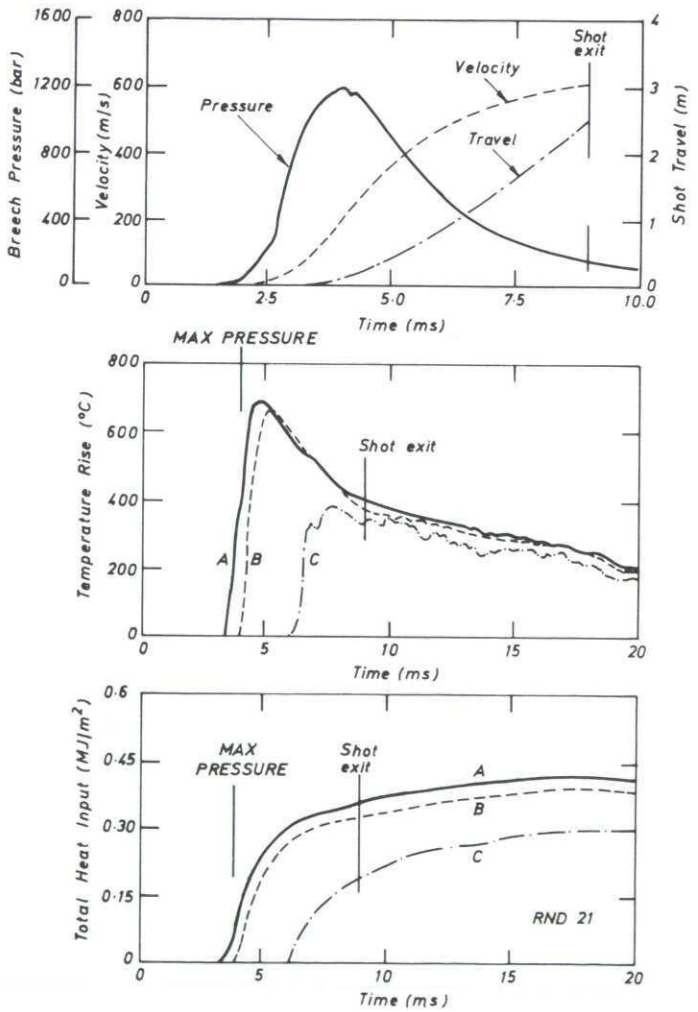

Thermocouple A 2·5 cm from C of R
Thermocouple B 12·5 cm from C of R
Thermocouple C 102·5 cm from C of R

Figure 4 TYPICAL SET OF EXPERIMENTAL RESULTS

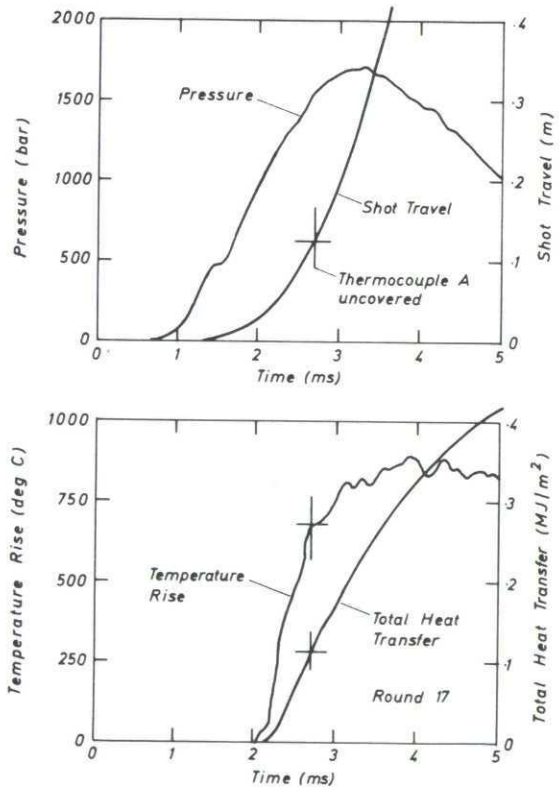

Total Heat Tranfer = 0·61 MJ/m²
Maximum Temperature Rise, TC/A = 880°C
Temperature Rise during gas leakage = 680°C (77%)
Heat Transfer during gas leakage = 0·11 MJ/m² (18%)

Figure 5 SHOWING TEMPERATURE RISE AND HEAT TRANSFER CAUSED BY GAS LEAKAGE PAST THE SHOT

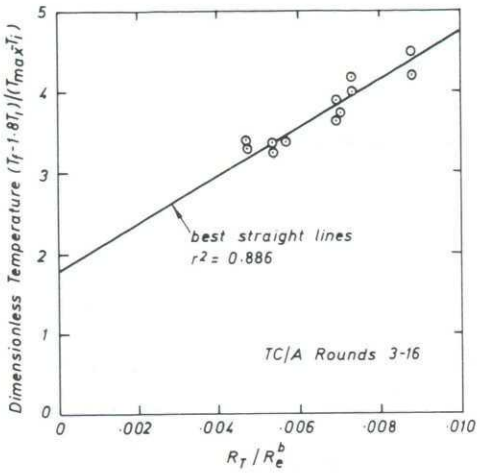

$$\frac{T_f - 1.8\,T_i}{T_{max} - T_i} = 1.8 + 288\ R_T / R_e^{0.86} \pm 4\%$$

$T_i = 293K$ $k = 24\ W/mK$ $K = 7.3 \times 10^{-6}\ m^2/s$

$kg = .09375\ W/mK$ $Cp = 1500\ J/kg\ K$ $Pr = 0.8$

$\mu = 50 \times 10^{-6}\ kg/ms$ $b = 0.86$ $d = 0.04\ m$

Figure 6 BEST STRAIGHT LINE (LEAST SQUARES) FOR OBSERVED BORE TEMPERATURE RISE AT TC/A ROUNDS 3-16 40/70 GUN

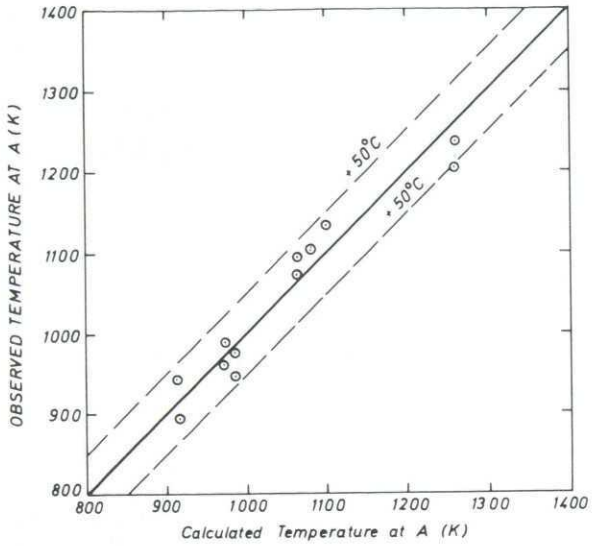

$$T_A = 293 + \frac{T_f - 527}{1.8 + 4.3/(m^{.86} C_m^{.36})}$$

Figure 7 COMPARISON OF OBSERVED AND CALCULATED TEMPERATURE AT THERMOCOUPLE A ROUNDS 3-16 40/70 GUN

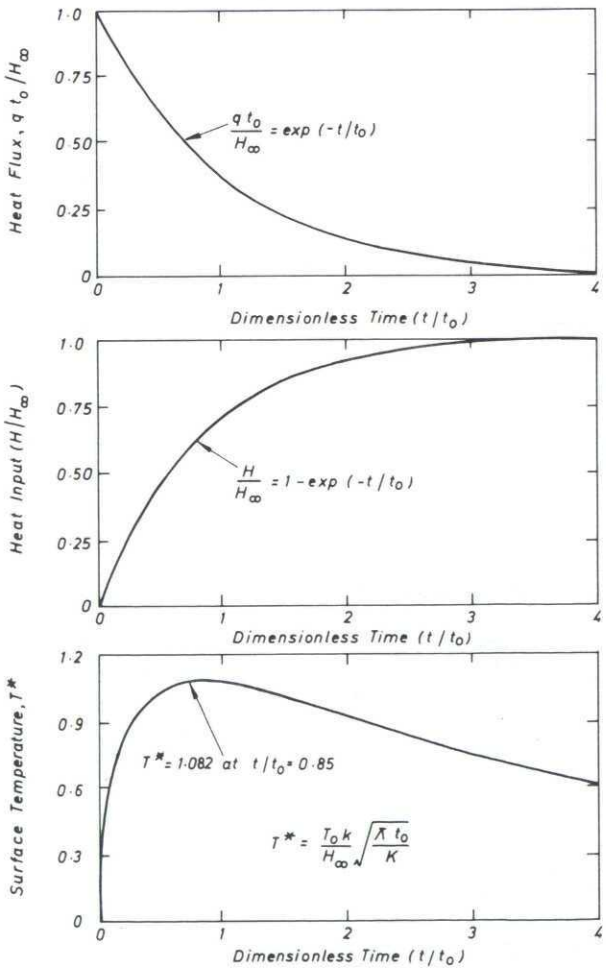

Figure 8 HEAT FLUX, TOTAL HEAT INPUT AND SURFACE TEMPERATURE VARIATION WITH TIME

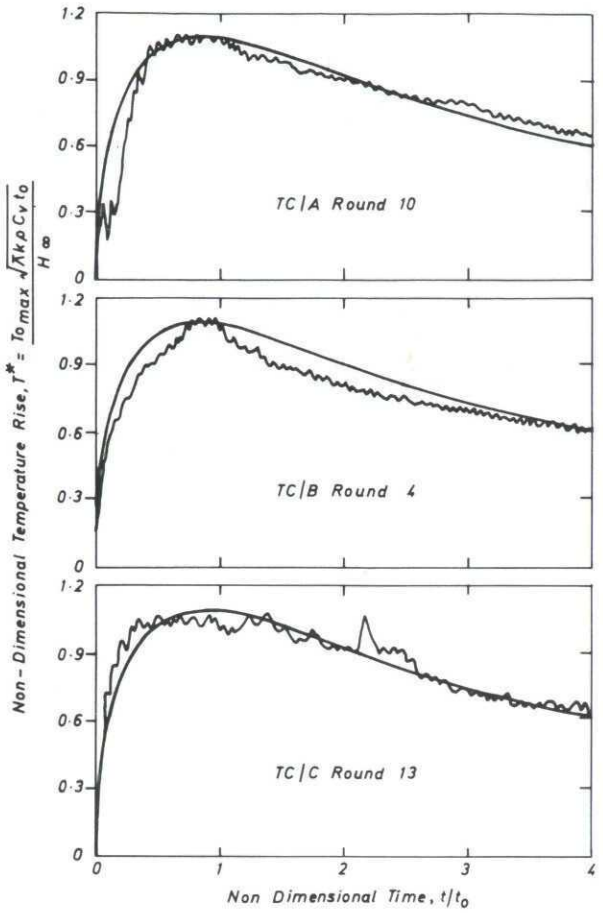

Figure 9 COMPARISON OF OBSERVED AND THEORETICAL BORE SURFACE TEMPERATURE, AT THERMOCOUPLES A, B & C 40/70 GUN

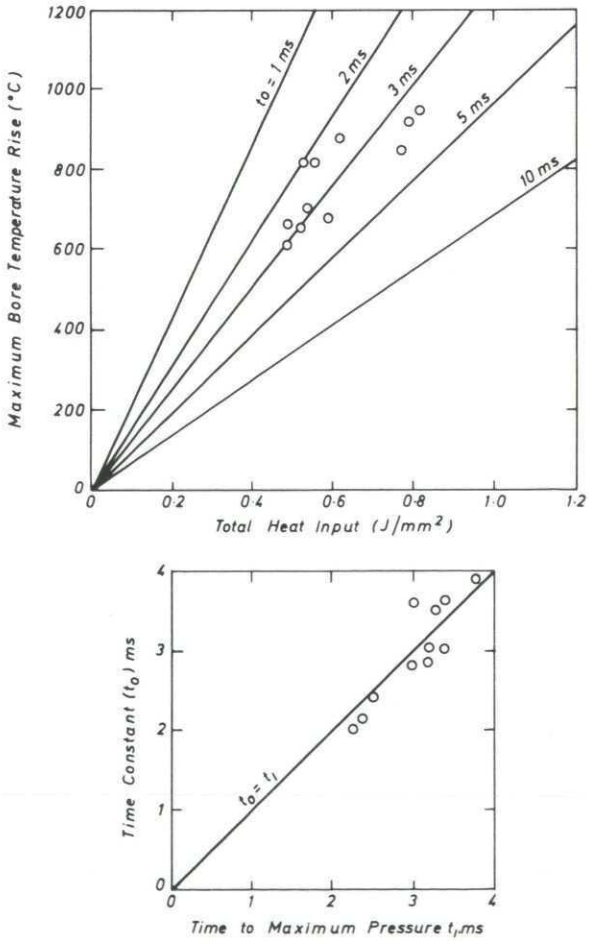

Figure 10 DETERMINATION AND CORRELATION OF TIME CONSTANT t_o TC/A ROUNDS 3-16 40/70 GUN

DISCUSSION

P.Ramette, Fr

What are the different propellants that you have used and have you noticed any differences in the theory/experiment comparison connected to the propellant itself?

Author's Reply

In the tests reported here, I used three different propellants, namely: AX, SC, and WM10. Details of SC and WM10 can be found in Reference 6 of my paper. AX has a flame temperature of 3584 K, WM10 is 3220 K, and SC is 3106 K.

The properties important for maximum bore temperature are the adiabatic flame temperature and the usual transport properties of the gas (U, Cp, Kg, Pr). The latter have a slight effect only. The flame temperature is the important property and in these and subsequent tests, I have not noticed any significant deviation from Equation (6) that could be attributed to the propellant itself.

LOW VULNERABILITY AMMUNITION/PROPELLANT TECHNOLOGY

by

J.J.Rocchio
Ballistic Research Laboratory
ARRADCOM
Aberdeen Proving Ground
MD 21005
USA

The text of this paper was not available at the time of printing.

DISCUSSION

B.Zeller, Fr

Have you studied the influence of replacing a metallic case by a combustible case on the vulnerability of a tank munition with respect to the various threats you have described?

Author's Reply

Yes, the effect is somewhat complex. Wtih respect to spall, the combustible case can be ignited by low velocity spall which would not penetrate a metal case. At higher velocities, there is no difference versus metal cases as it is the propellant which is initiated. With respect to a shaped charge jet, the combustible case ruptures at a lower pressure so the violence of reaction is lower than with a metal case. However, when placed in a metal storage tube, as in a tank, this difference disappears.

B.Zeller, Fr

Can you tell us something about the LOVA concept which you just described and the liquid propellant weapons concepts? I mean, will these two concepts be in competition or will they supplement each other? Could you give us an idea of the interaction between the two types of concepts?

Author's Reply

BRL tests have shown the HAN-based monopropellants to have low vulnerability characteristics. Thus, LP gun systems may present another way to reduce weapon system vulnerability. The fielding of LP weapons systems is still 5 to 10 years away. In this interval and beyond, there will be a large fleet of conventional gun systems which will require LOVA propellants.

P.Ramette, Fr

You've said that you were studying reactions to hypervelocity impact. Could you tell us the hypervelocity envelope which is of interest in these studies? Could you give us some values and figures?

Author's Reply

For hypervelocity impact, we are talking about velocities of the residual shaped charge jet which are on the order of 4 to 8 km/s.

P.Ramette, Fr

You study LOVA propellants which are mainly based on RDX. You said that you studied the RDX base compared to the HMX base for economic reasons. Have you done a technical and economic study enabling you to reach that conclusion, which explains your choice since HMX has more energy?

Author's Reply

Yes. Economically, RDX is produced in 10 times the quantity that HMX is produced in and HMX costs five times as much as RDX. Energetically, RDX and HMX are essentially equivalent. RDX computes to give a slightly higher energy than HMX (about 2—4 per cent). The higher density of HMX (4 per cent) is not important at gun loading densities. From a sensitivity standpoint, RDX has a lower thermal ignition threshold and a slightly greater shock sensitivity; however, these differences are small and can be overcome with modifications of the formulation.

P.Ramette, Fr

Could you give us an idea of the production price of the LOVA propellant that you studied?

Author's Reply

Cost estimates at this time are about $10 per pound. Continuous production processing would reduce this to about $6 per pound.

ON THE THERMAL BEHAVIOUR OF THE BARREL DURING THE INTERIOR BALLISTIC CYCLE OF PROPELLANT GUNS

W.J. Kolkert, M. Waas and H.G. The
Prins Maurits Laboratory, Defense Research Organization TNO
P.O. Box 45, 2280 AA Rijswijk,
The Netherlands

Thermal stress-cycling during firing constitutes a major mechanism for erosion, wear and fatigue in gun barrels and cannon tubes.

In order to predict spatial and temporal temperature distributions at the inner envelope of and through the barrel and in the gasdynamic flow accompanying the interior ballistic cycle, a two-dimensional, quasi two-phase flow (turbulent, viscous and compressible) model, was developed. A one-dimensional model treating radial heat conduction in the barrel was coupled to this flow-model. Input parameters for these models were calculated with a one-dimensional, two-phase flow, burning routine, describing propellant deflagration.

Besides a description of these models, results of a prediction for amongst others heat-loss, projectile-travel and pressure, temperature and flow velocity distributions in the gasdynamic flow and temperature-time histories in the barrel wall are given for the interior ballistic cycle of a caliber .50in gun.

Although predicted results for heat-flow into and through the barrel and predicted temperature-time histories in the barrel cannot be compared with experimental results in a reliable way at this very moment, predicted results for pressure-time distributions and projectile-travel fit the experimental results in a promising way.

SYMBOLS

A	=	cross sectional area		$[m^2]$
A_d	=	van Driest damping constant,	26.	[-]
a	=	Hunts' constant,	12.4	[-]
b	=	covolume		$[m^3/kg]$
C_p	=	heat capacity at constant pressure		[J/kg.K]
C_v	=	heat capacity at constant volume		[J/kg.K]
C_1	=	$\alpha(T).dt/dr$ = constant in equation (3)	1.8	[m]
C_{1k}	=	Sutherland constant for the thermal conductivity; equation (19),	$0.25\ 10^{-2}$	$[kg.m/s^3K^{3/2}]$
$C_{1\mu}$	=	Sutherland constant for the viscosity; equation (18),	$0.145\ 10^{-5}$	$[kg/m.s.K^{1/2}]$
C_{2k}	=	Sutherland constant for the thermal conductivity; equation (19),	194.444	[K]
$C_{2\mu}$	=	Sutherland constant for the viscosity; equation (18),	110.333	[K]
D	=	web size		[m]
E	=	total specific energy		[J/kg]
e	=	specific internal energy		[J/kg]
F	=	force constant		[J/kg]
f	=	unburnt web fraction		[-]
H	=	specific enthalpie		[J/kg]
K	=	ratio of propellant and gas velocity		[-]
k	=	thermal conductivity		$[kg.m/s^3K]$
l	=	mixing length		[m]
M	=	$dr^2/\alpha(T).dt$		[-]
m	=	mass		[kg]
n	=	Hunts' constant,	11.3	[-]
p	=	pressure		[Pa]
Pr_t	=	Prandlt number,	0.9	[-]

q	=	heat-flux	$[J/m^2.s]$	$\alpha(T)$	=	$k(T)/\rho_b C_p(T)$ thermal diffusivity	$[m^2/s]$
Ri	=	inbore radius	$[m]$	α	=	burning exponent	$[-]$
r	=	radial coordinate	$[m]$	β	=	burning coefficient	$[m/s.Pa]$
Re_x	=	Reynolds number defined at a certain distance from the breech	$[-]$	γ	=	C_p/C_v = heat capacity ratio	$[-]$
s	=	propellant motion factor	$[-]$	δ	=	boundary-layer thickness	$[m]$
T	=	temperature	$[K]$	ε	=	kinematic eddy viscosity ($\varepsilon = \mu'/\rho$)	$[m^2/s]$
t	=	time	$[s]$	Θ	=	shape factor	$[-]$
u	=	axial-velocity component	$[m/s]$	κ	=	von Karman constant, 0.41	$[-]$
V	=	volume	$[m^3]$	λ	=	boundary-layer constant 0.09	$[-]$
v	=	radial-velocity component	$[m/s]$	μ	=	dynamic viscosity	$[kg/m.s]$
$W(t)$	=	Hunts' asymptotic function: ref [9]	$[-]$	ρ	=	density	$[kg/m^3]$
x	=	axial coordinate	$[m]$	σ	=	propellant mass fraction	$[-]$
y	=	vertical coordinate	$[m]$	τ	=	shear stress	$[Pa]$
Z	=	burnt charge fraction	$[-]$	$\|\|$	=	absolute value	

SUPERSCRIPTS

$\bar{}$	mean value
$'$	turbulent

SUBSCRIPTS

a	adiabatic	ch	chamber	j	time index
b	barrel	g	gas	w	wall
c	propellant	i	radial index	0	initial

1. INTRODUCTION

Present days' development of super-charges and the introduction of nitramine propellants focus extra attention to the long-existing problem of barrel erosion, wear and fatigue.

Both from the point of view of life cycle time and safety-during-use, the problem of wear of gun barrels and cannon tubes asks for a detailed study, which is now going on for several years. From these studies it appears that evidently both mechanical and thermal stress cycling of the barrel during firing are the major mechanisms leading to both limited life time and accidental failure of the barrel. Material properties of the barrel on one hand and ballistic properties of the charge and projectile to be launched on the other, give rise to a certain extent of barrel wear and fatigue.

Thermal stress-cycling of the barrel during firing intuitively seems to be the dominant mechanism as it leads to high temperature gradients of short duration at the inner surface of the barrel, already exhibiting some deformation by projectile friction. It gives rise to phase-changes, local melting and recrystallisation of barrel alloys while especially carbon and nitrogen radicals are exchanged at this surface during the interior ballistic cycle, where a reactive gasdynamic flow is moving rapidly along it. Apart from a possible relocation of molten material of the barrel, minor amounts can be transferred in the flow, while recrystallization leads to a mechanically stressed situation in the barrel near its inner surface. Combined with the imposed stress during firing, cracks may grow more rapidly inwards into the barrel, possibly leading to a catastrophic situation during subsequent firings.

To analyze and quantify parameters governing these processes, a modelling effort was started. In order to predict the temperature-time history of the barrel during firing and to obtain a reliable estimate of the temperature behaviour of the inner surface of the barrel, a heat conduction model for the barrel material was adapted and tested by reverse analysis with experimental data. Convective heat transfer towards the barrel and interface-boundary conditions were described with a two-dimensional, quasi two-phase, compressible and viscous flow, including turbulent and laminar boundary-layers near the inner surface of the barrel. The necessary input parameters for the reactive, gasdynamic flow were derived from a one-dimensional burning routine describing deflagration of the propellant charge. Modelling of ignitor phenomenae are not yet included.

All three models mentioned are described in this paper and results for a simulation with the overall model -IBPML2D- of the firing cycle of a caliber .50in. gun are presented. Besides familiar results for projectile travel, pressure-, pressure difference-and temperature-time behaviour in an axial direction during the interior ballistic cycle, axial flow velocity-time and temperature-time behaviour in radial direction, including that in the barrel, are presented. Heat-flux and temperature-time profiles at the inner surface of the barrel are given too.

An experimental set-up, designed for interior ballistic study in general and for thermal stress cycling study in particular is described in short and experimental results obtained thusfar are given and compared with predicted ones.

2. MODELLING OF THE REACTIVE, GASDYNAMIC FLOW.

To quantify heat-loss to the surroundings during the interior ballistic cycle in an explicit way, the underlying physical phenomenae should be appreciated and described. Important phenomenae are :

1. Heat transfer towards the barrel by forced convection in the more-dimensional, two-phase flow during combustion and projectile travel. This process is strongly influenced by the formation of a boundary -layer near the barrel wall,

2. Radiation from the burning propellant and hot deflagration products,
3. Conduction of heat through the gas to the barrel wall,
4. Dissipation of heat in the barrel and
5. Heat transfer from the barrel to the surroundings.

The contribution of radiation to heat transfer is very small compared to that of forced-convection, so it will be neglected. As the study reported in this article considers only processes during the interior ballistic cycle itself, heat-loss to the surroundings is not taken into account. Heat generated by projectile-barrel friction during launch, is neglected too.

To describe the process of heat-loss, the reactive, gasdynamic-flow and the conduction of heat through the steel wall of the barrel have to be modelled. A model for the reactive gasdynamic-flow must include a detailed description of boundary-layer build-up.

Mandatory is an approach where the coupled two-dimensional partial differential equations for conservation of mass, momentum and energy are solved over the entire in-bore area.
The gasdynamic-flow is thought to be built-up out of two regions :

1. the mainstream, which consists of a two-phase (burning propellant and burned gaseous products) inviscid flow, described here with a one-dimensional scheme. The values of parameters of the mainstream impose boundary conditions on
2. the boundary-layer flow which is described by a one-phase (gas), viscous and compressible flow described here with a two-dimensional scheme.

Figure-1 shows the multiple grid system for calculating the inviscid mainstream, viscous interacting flows and the dissipation of heat in the barrel wall.

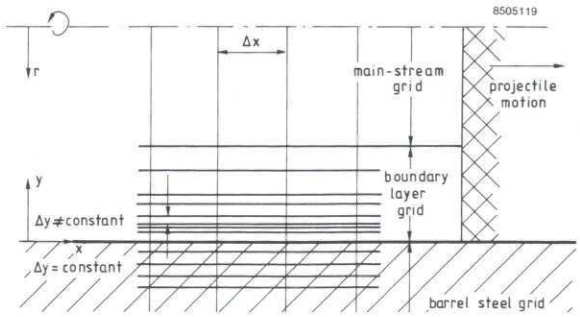

Figure-1 Grid matrix for the calculation of flow parameters in a barrel

On account of the main objective of the study reported here, the heat-conduction model will be described first. Subsequently, the governing equations and scheme for the numerical solution of mainstream and boundary-layer flows are given.

The quality of the overall model is demonstrated by simulating the interior ballistic cycle of a caliber .50 in. gun firing and comparing results with experiments.

2.1 The heat-conduction model

In order to calculate the heat-loss during the interior ballistic cycle, the time-dependent, inner-surface temperature of the barrel has to be predicted. This implies modelling of heat conduction through the barrel wall.
During the interior ballistic cycle the radial temperature gradient ($\partial T/\partial r$) is orders of magnitude larger than that in axial direction. Therefore, the heat-conduction process can be described with a one-dimensional representation of Fouriers-law in cylindrical coordinates:

$$\frac{\partial T}{\partial t} = \alpha(T)\left[\frac{\partial^2 T}{\partial r^2} + \frac{1}{r}\frac{\partial T}{\partial r}\right] \qquad (1)$$

This equation can be used for all internal points of the barrel i.e. points which have conductive input and output. The thermal diffusivity ($\alpha(T)$) in equation (1) is defined as

$$\alpha(T) = k(T)/\rho_b C_p(T)$$

As shown in the above notation, thermal conductivety (k), specific heat (C_p), and so, by definition the thermal diffusivity $\alpha(T)$ of the metal are assumed to be dependent on temperature, whereas the steel density (ρ_b) is considered to be a constant. Equation (1) is solved numerically. The approach used here follows that of Heiney [1]. Linearisation and rearranging equation (1) gives :

$$\frac{T_{i,j+1} - T_{i,j}}{\Delta t} = \frac{\alpha(T_{i,j})}{\Delta r}\left[\frac{T_{i+1,j} - 2T_{i,j} + T_{i-1,j}}{\Delta r} + \frac{T_{i+1,j} - T_{i-i,j}}{2r_i}\right] \qquad (2)$$

Rearranging and substituting $M = (\Delta r)^2/\alpha(T).\Delta t$ and $C_1 = \alpha(T).\Delta t/\Delta r$ leads to :

$$T_{i,j+1} = \frac{T_{i+1,j} + (M-2)\,T_{i,j} + T_{i-1,j}}{M} + \frac{C_1}{2r}\left(T_{i+1,j} - T_{i-1,j}\right) \qquad (3)$$

Now the temperature at radial position i at time j+1 can be calculated knowing the temperature at this and adjacent positions at time j. To avoid instability, however, the value of M must be equal to or greater than 2. In order to calculate the entire distribution, the temperature at all grid positions and the wall temperature at time j = 0. have to be known, while addition and/or subtraction of heat (convective heat -input and a conductive out-flow of heat at the inner surface of the barrel) has to be accounted for. With a heat-flux at the inner surface defined by :

$$q_{w,j} = -k(T_{i,j}) \left.\frac{\Delta T}{\Delta r}\right|_{r = R_i} \qquad (4)$$

equation (3) can be rearranged to give :

$$T_{1,j+1} = T_{1,j} + \frac{\Delta t.\ \alpha(T_{i,j})}{\Delta r}\left[\frac{T_{2,j} - T_{1,j}}{\Delta r} + \frac{q_{w,j}}{k(T_{1,j})} + \frac{T_{2,j} - T_{1,j}}{2r}\right] \qquad (5)$$

Knowing the heat-flux into the wall of the barrel and the temperature of grid 1 and 2 at time j, the temperature at time j+1 can be calculated with equation (5). Then, heat-flow through the barrel can be predicted with equation (3).

To validate the heat-conduction model described above, the measured temperature distribution in a 20 mm pressure barrel, reported by BRL [2] was used. With equation (3) and starting from the temperature profile measured at a position closest to the inner surface of the barrel, the temperature distribution at different measuring positions is simulated.
The temperature dependencies of heat conductivity and specific heat and the density of barrel steel (SAE 4340) used in the simulation have been taken from ref. [3] and are :

$$C_p(T) = 472.6 - 0.00123\ T + .0003\ T^2 \quad [J/kg.K]$$
$$k(T) = 40.59 + 0.0172\ T - .0000285\ T^2 \quad [kg.m/s^3.K]$$

From Figure-2 it can be deduced that this approach is able to simulate measured data at other radial positions sufficiently accurate.

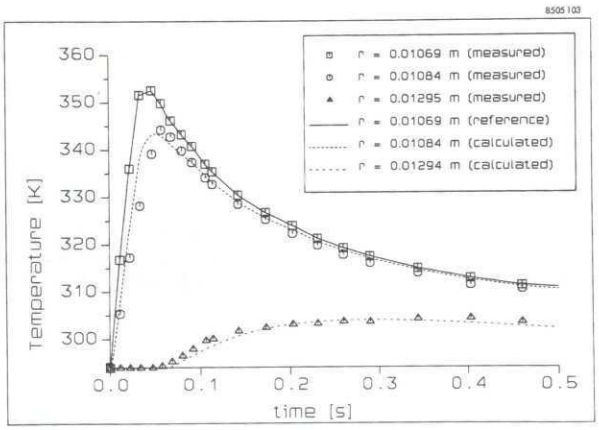

Figure-2 Simulation of 20 mm barrel temperature measurements, given in [2].

2.2 Modelling of the mainstream region of the in-bore flow

The gasdynamic model for the mainstream region of the in-bore flow is based on the one-dimensional equations for conservation of mass, momentum and energy. The flow consists of a mixture of burning propellant particles and gas (deflagration products), assumed to behave as two-phase fluid with density ρ. The two phases are coupled by the cross-sectional area constraint and by transfer of mass, momentum and energy between them. Assuming the gas phase to be nonviscous and the solid propellant to be incompressible the generalized continuity equations can be written in the form :

$$\frac{\partial U}{\partial t} + \frac{\partial F}{\partial x} + I = 0 \qquad (6)$$

where :

$$U = \begin{bmatrix} \rho \\ \rho\sigma \\ \dfrac{\rho\sigma}{1-Z} \\ \rho u_g \left\{1. - (1-K)\sigma\right\} \\ \rho E \end{bmatrix}, F = \begin{bmatrix} \rho u_g \left\{1 - (1-K)\sigma\right\} \\ \rho\sigma\, u_g K \\ \dfrac{\rho\sigma\, u_g K}{1-Z} \\ \rho u_g^2 \left\{1 - (1-K^2)\sigma\right\} \\ \rho u_g \left\{ E + \dfrac{P}{\rho} - \sigma(1-K)\left(\dfrac{K^2 u_g^2}{2} + \Delta H + \dfrac{P}{\rho_c}\right)\right\} \end{bmatrix} \quad \text{and}$$

$$I = \begin{bmatrix} \rho u_g \left\{1 - (1-K)\sigma\right\} \dfrac{\partial \ln A}{\partial x} \\ \rho\sigma u_g K \dfrac{\partial \ln A}{\partial x} + \rho\sigma \dfrac{\partial f}{\partial t} \\ \dfrac{\rho\sigma}{1-Z}\, u_g K \dfrac{\partial \ln A}{\partial x} \\ \rho u_g^2 \left\{1 - (1-K^2)\sigma\right\} \dfrac{\partial \ln A}{\partial x} + \dfrac{\partial P}{\partial x} \\ \rho u_g \left\{ E + \dfrac{P}{\rho} - (1-K)\sigma\left(\dfrac{K^2 u_g^2}{2} + \Delta H + \dfrac{P}{\rho_c}\right)\right\} \dfrac{\partial \ln A}{\partial x} \end{bmatrix}$$

with the total specific energy of the mixture E, defined as :

$$E = (1-\sigma)\left(e_g + \frac{u_g^2}{2}\right) + \sigma\left(\Delta H + \frac{K^2 u_g^2}{2}\right) \qquad (7)$$

The pressure P is related to the internal energy and density of the gas by a van der Waals like equation of state (Noble-Abel equation) :

$$P = \frac{(\gamma - 1) e_g}{\left(\frac{1}{\rho_g} - b\right)} \qquad (8)$$

Written in mean-flow variables, equation (8) becomes :

$$P = \frac{(\gamma - 1)\left\{ E - \sigma\left(\Delta H + \frac{K^2 u_g^2}{2}\right) - \frac{u_g^2}{2}(1-\sigma)\right\}}{\left\{\frac{1}{\rho} - \frac{\sigma}{\rho_c} - b\,(1-\sigma)\right\}} \qquad (9)$$

For the single-perforated propellant grains used in the experiments, the linear burning rate and form-function are respectively given by :

$$\frac{\partial f}{\partial t} = -\frac{\beta P^{\alpha}}{D} \quad (10) \quad \text{and} \quad Z = (1-f)(1-\Theta f) \qquad (11)$$

The value of the ratio between propellant and gas velocity is modelled according to Murphy et.al [4], which is based on the experimental fact (Hornemann [5]) that burning propellant particles have a greater tendency to move towards the flame front :

$$K = Z^s \qquad (12)$$

Here s is a constant determining the mobility of the propellant particles in the flow and is set to 1.

For the numerical solution of the dynamic problem described by the equations above, the Lax-Wendroff method was chosen. This time-splitted scheme is solved with the Flux-Corrected-Transport algorithm which gives very good results when steep gradients (for instance pressure waves) occur. Boris [6] has developed a computer code based on this algorithm which is able to solve the one-dimensional generalized continuity equations in the form shown.

Modelling of propellant burning is performed in a straightforward way ignoring the phenomenon occuring during ignition. This implies that the beginning of the interior ballistic cycle cannot be predicted accurately. This problem can be handled by starting the calculation at a pressure (P_{start}) and time where igniter-effects have become minor. The propellant burnt, for reaching this pressure can be calculated using Resals equation :

$$Z = \frac{P_{start}}{m_{c,0}} \frac{\left(V_{ch} - \frac{m_{c,0}}{\rho_c}\right)}{\left\{F + P_{start}\left(b - \frac{1}{\rho_c}\right)\right\}} \qquad (13)$$

Assuming constant density and zero gas velocity in the chamber, the starting values for E and σ can be calculated.

It should be noted that heat-loss is not included in the equations described. Heat-loss will be accounted for indirectly through adjusting the local, total energy contents after boundary-layer calculations are performed.

2.3 Modelling of the turbulent boundary-layer flow

In the region near the inner surface of the barrel, the assumption that the dynamics of the gas flow are one-dimensional and non-viscous are no longer valid. Here the viscous terms are indeed significant and axial (x) gradients are mostly not larger than radial (r) gradients. Intensive research (Bartlett et. al. [7], Dahm et. al. [8] and Schols [15]) has shown that the turbulent boundary-layer thickness in the in-bore flow is orders of magnitude smaller than the caliber of the barrel. This indicates that the surface of the barrel wall can be modelled as a flat plate. (Figure-3 shows the momentum and thermal boundary-layer build-up on a cooled flat plate).

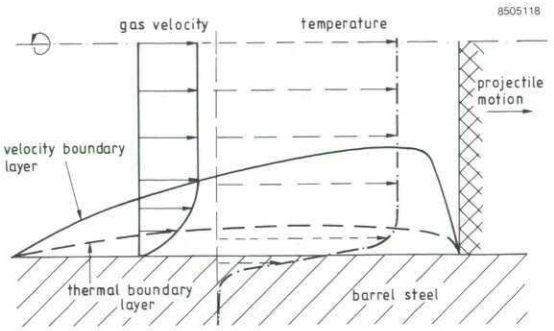

Figure-3 Momentum and thermal boundary-layer behind the projectile in a barrel.

Assuming the gas flow over the flat plate to be turbulent, viscous and compressible, the two-dimensional time-averaged continuity equations (ignoring the mixed derivative terms and diffusion in axial direction) can be written in the form :

$$\frac{\partial U}{\partial t} + \frac{\partial F}{\partial x} + \frac{\partial G}{\partial y} = 0 \qquad (14)$$

where

$$U = \begin{bmatrix} \bar{\rho} \\ \overline{\rho u} \\ \overline{\rho v} \\ \overline{\rho E} \end{bmatrix}, \quad F = \begin{bmatrix} \overline{\rho u} \\ \overline{\rho u^2} + \bar{P} \\ \overline{\rho uv} \\ (\overline{\rho E} + \bar{P})\bar{u} \end{bmatrix}, \quad G = \begin{bmatrix} \overline{\rho v} \\ \overline{\rho uv} + \bar{\rho}\,\overline{u'v'} - \mu \frac{\partial \bar{u}}{\partial y} \\ \overline{\rho v^2} + \bar{P} - (\mu + \mu')\frac{\partial \bar{v}}{\partial y} \\ (\overline{\rho E} + \bar{P})\bar{v} - \frac{\lambda}{C_v}\frac{\partial \bar{e}}{\partial y} + \bar{\rho}\,\overline{v'H'} - \mu\,\bar{u}\frac{\partial \bar{u}}{\partial y} - (\mu + \mu')\bar{v}\frac{\partial \bar{v}}{\partial y} \end{bmatrix}.$$

With the total specific energy of the gas defined as eq. (15) and the specific enthalpy as eq. (16)

$$\bar{E} = \bar{e} + \frac{\bar{u}^2 + \bar{v}^2}{2} \qquad (15) \qquad \bar{H} = \bar{e} + \frac{\bar{P}}{\bar{\rho}} \qquad (16)$$

Again, like in the system of equations describing the mainstream region of the in-bore flow, the pressure is related to the specific internal energy and (gas) density by eq. (17).
For the temperature dependance of the thermal conductivity (k_g) and the dynamic viscosity (μ) of the gas the analytic relations of Sutherland as expressed by eqs. (18) and (19), are used.

$$\bar{P} = \frac{(\gamma - 1)e_g}{(\frac{1}{\rho_g} - b)} \qquad (17), \qquad \mu = \frac{C_{1\mu}\, T_g^{3/2}}{C_{2\mu} + T_g} \qquad (18), \qquad k_g = \frac{C_{1k}\, T_g^{3/2}}{C_{2k} + T_g} \qquad (19)$$

To solve the system of boundary-layer equations listed above some additional assumptions are necessary, as computer-memory constraints in relation to fineness of the computational mesh are limiting the resolution of all significant eddy-length scales in the highly turbulent flow. The smaller turbulence effects have to be accounted for, by for instance adding to the viscosity coefficient a turbulence term expressing the Reynold stress and turbulent convection, leading to mean-stream properties:

$$\mu' = \rho.\varepsilon \qquad (20) \qquad \bar{\rho}\,\overline{u'v'} = -\rho.\varepsilon\,\frac{\partial u}{\partial y} \qquad (21) \qquad \bar{\rho}\,\overline{v'H'} = -\frac{\varepsilon.\rho}{Pr_t}\frac{\partial H}{\partial y} \qquad (22)$$

where ε denotes the kinematic eddy viscosity and Pr_t is the turbulent Prandlt number. The eddy viscosity can be determined by solving either algebraic relations in terms of mean-flow variables or additional differencial-flow equations. Here, a simpler approach of using an algebraic relation where the eddy viscosity is given by :

$$\varepsilon = l^2 \left| \frac{\partial u}{\partial y} \right| \qquad (23)$$

is chosen.

The mixing length (l) is supposed to be proportional to the distance of the wall (y) and, for a smooth wall, can be specified according to van Driest as :

$$l = \kappa\, y \left[1 - \exp\left[- y \frac{\sqrt{\tau_w \rho_g}}{A_d \cdot \mu} \right] \right], \quad 0 \leq y \leq \frac{\lambda\delta}{\kappa} \quad (24) \text{ and } l = \lambda\delta \quad , \quad \frac{\lambda\delta}{\kappa} < y \quad (25)$$

For the calculations reported in this paper the von Karman constant(κ), van Driest constant (A_d) and the constant λ are set to 0.41, 26. and 0.09 respectively. The shear stress τ_w at the wall can be calculated from mainstream values assuming that the radial density gradient is small (i.e. the Boussinesq approximation is valid) :

$$\tau_w = \frac{Ri}{2} \left[\frac{\partial(\rho u)}{\partial t} + \frac{\partial(\rho u^2)}{\partial x} + \frac{\partial P}{\partial x} \right] \quad (26)$$

Finally, in order to obtain a closed-system of equations the boundary-layer thickness, dependent on time and axial position, has to be determined.
In most literature the momentum thickness of the boundary layer is defined as the value of y where the axial velocity has reached a value of 0.995 times the mainstream value and this can be determined from calculated axial-velocity profiles in radial direction at different axial locations at time t. However, due to the relative courseness of the computational grid, this leads to discontinuities in momentum thickness, eddy viscosity and axial velocity at time t+dt. Therefore an expression given by Hunt [9] will be used to calculate the momentum thickness :

$$\delta(x,t) = \frac{x \; W(t)^{\left(\frac{n+1}{n+3}\right)}}{a^{\frac{2n}{n+3}} \; Re_x^{\frac{2}{n+3}}} \quad (27)$$

This equation was derived using the boundary-layer momentum integral for turbulent flow along a flat plate and a generalized form of the Blasius Power law. The values of the constants a and n are set to 12.4 and 11.3 respectively.

Simple models as shown above cannot be expected to predict accurately all details of the turbulent motion. However, they have proven to be adequate for a variety of flows and warrant further study on that basis. Several investigators (Cebeci et. al. [10], Lin et. al. [11], Christoph et. al. [12]) have recently reported special modifications of the turbulence model used in this paper to account for wall -roughness as present in barrels with riffling.

The numerical solution of the equations representing the turbulent, viscous and compressible flow was developed by MacCormack. The method consists of splitting the governing equations into an hyperbolic (inviscid) and a parabolic (viscous) part. Then, the appropriate numerical procedures for the specific parts are used and the separate solutions are combined to give the overall results. The overall mathematical scheme, applied to the equations used here, is given in detail in [13].

2.4 Overall modelling and results

In order to predict the heat-loss and inner surface temperature-time distribution during the interior ballistic cycle, the models for the processes discussed, have to be coupled. The physical interacting sequence (instantaneously in reality) between the different processes has to be modelled and problems related to the fact that the different numerical solution methods have different stability criteria, have to be overcome.

First, parameters classifing the mainstream region of the in-bore flow at time j+1 are calculated without considering the boundary-layer. Second, values of the mainstream region at time j+0.5 impose boundary conditions on the boundary-layer flow during the entire periode of time from j to j+1. Simultaneous with the boundary-layer calculations, the heat-flux, inner surface temperature and the penetration of heat into the barrel are predicted. Knowing the values of the parameters of the boundary -layer flow at time j+1 the mainstream region is adjusted for transport of mass, momentum and energy towards or from the boundary-layer.

In Figure-4, the axial pressure distribution in the mainstream region of the in-bore flow between breech and projectile-base is shown as a function of time.
Calculations are started at a pressure (Shot-start pressure: 80 MPa, shot-start motion t=0.001 s) determined from ten, caliber .50in. firings. The relative steep gradient around a distance of 0.0735 m from the breech agrees with ducting at the transition from chamber to tube. Other parameters classifying barrel, projectile and propellant are given in chapter 3.
In Figure-5 the temperature distribution in the mainstream is given.

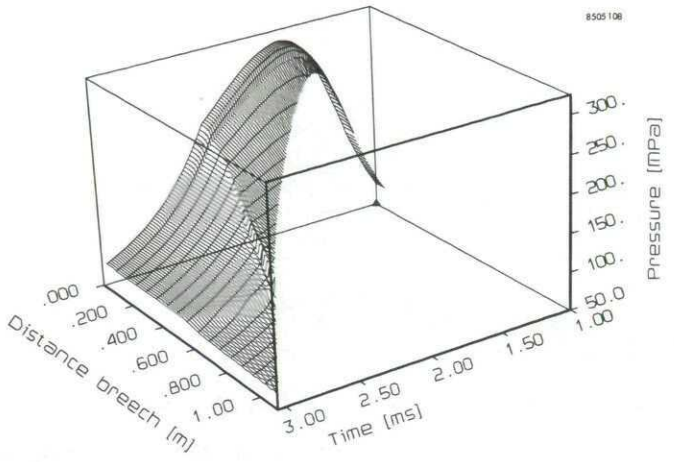

Figure-4 Calculated pressure gradient in the non-viscous mainstream as a function of the distance from the breech and the time during the interior ballistic cycle.

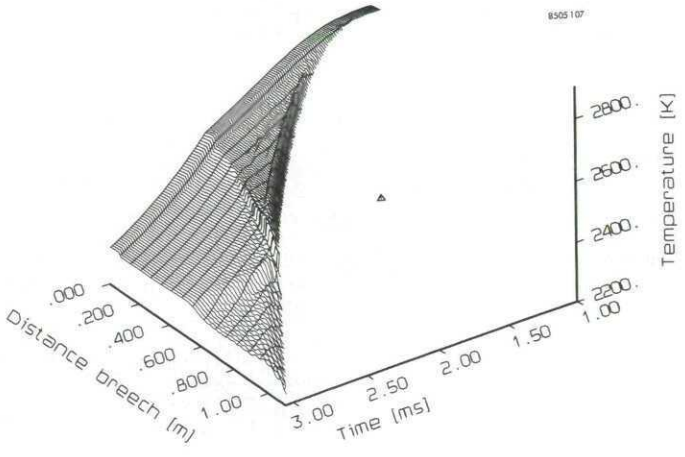

Figure-5 Calculated gas temperature distribution in the non-viscous mainstream as a function of the distance from the breech and the time during the interior ballistic cycle.

The axial-velocity component and pressure gradient across the turbulent boundary-layer at two axial locations are given as a function of time in Figure-6a and 6b. It can be seen that the pressure is remarkably constant throughout the boundary-layer, whereas the axial-velocity component varies greatly with radial position. The momentum boundary-layer thickness varies between 0.00 mm and 1.0mm during the interior ballistic cycle of the caliber .50 in. barrel.

Temperature distributions in both boundary-layer and barrel steel for the same axial positions as above are shown in Figure-6c. As heat-conduction is very slow compared to the other processes occurring during the interior ballistic cycle, the penetration-depth at the end of the interior ballistic cycle is only 0.05 mm At this moment, calculations cannot be performed beyond this cycle as isentropic expansion of the in-bore flow after muzzle-clearance has to be modelled yet.

Figure-6a Calculated axial velocity gradient in the viscous, turbulent boundary-layer as a function of radial position and time at two axial positions. (left Figure: 106 mm from breech, right Figure : 574 mm from breech).

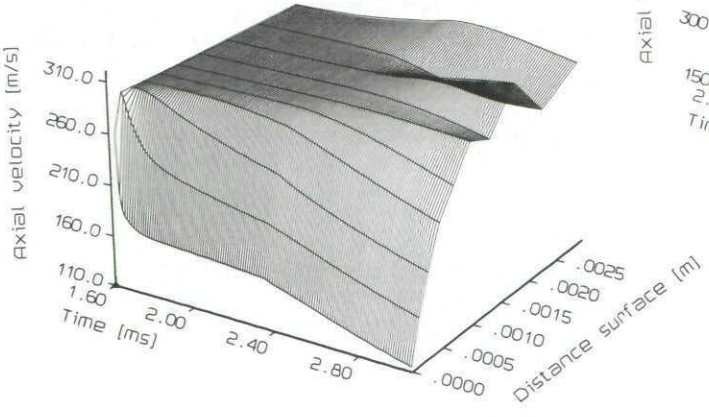

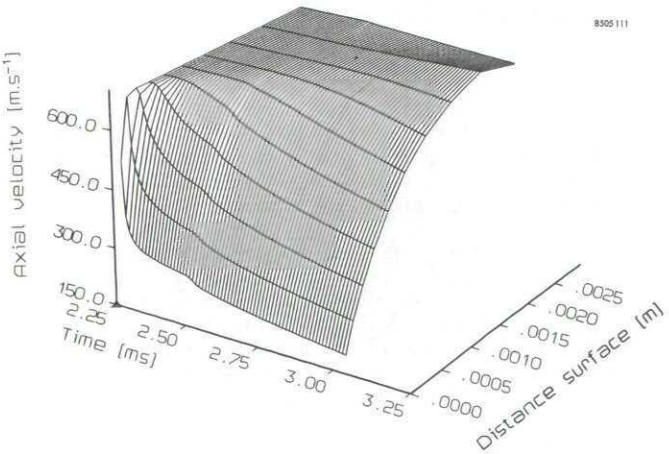

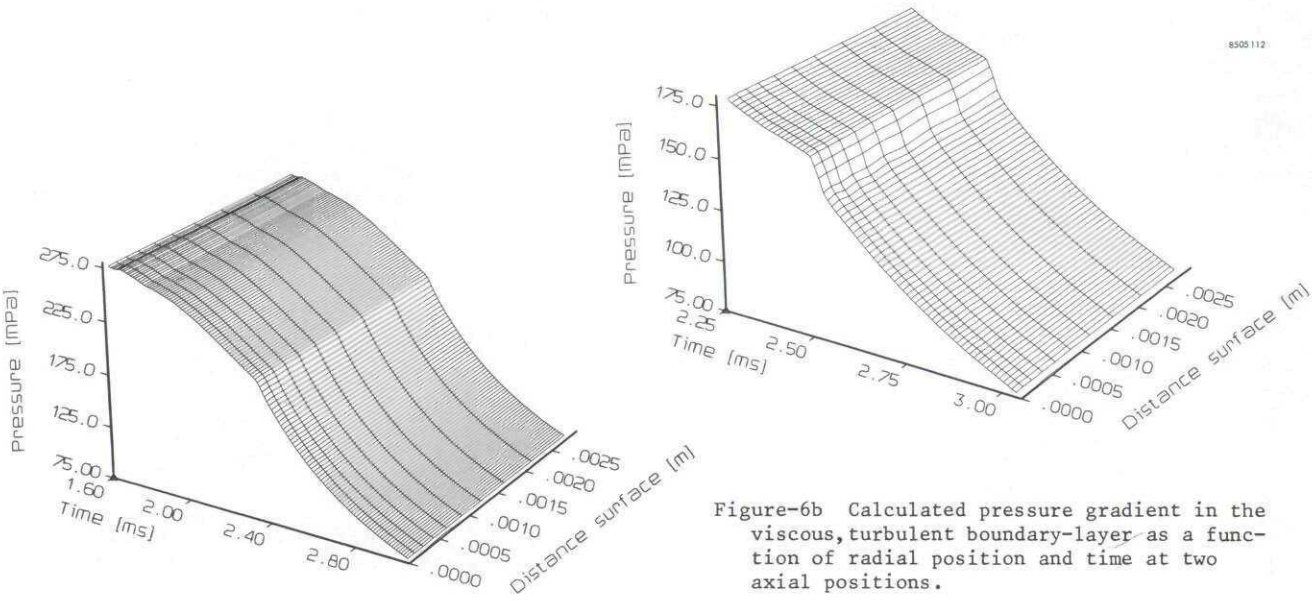

Figure-6b Calculated pressure gradient in the viscous, turbulent boundary-layer as a function of radial position and time at two axial positions.

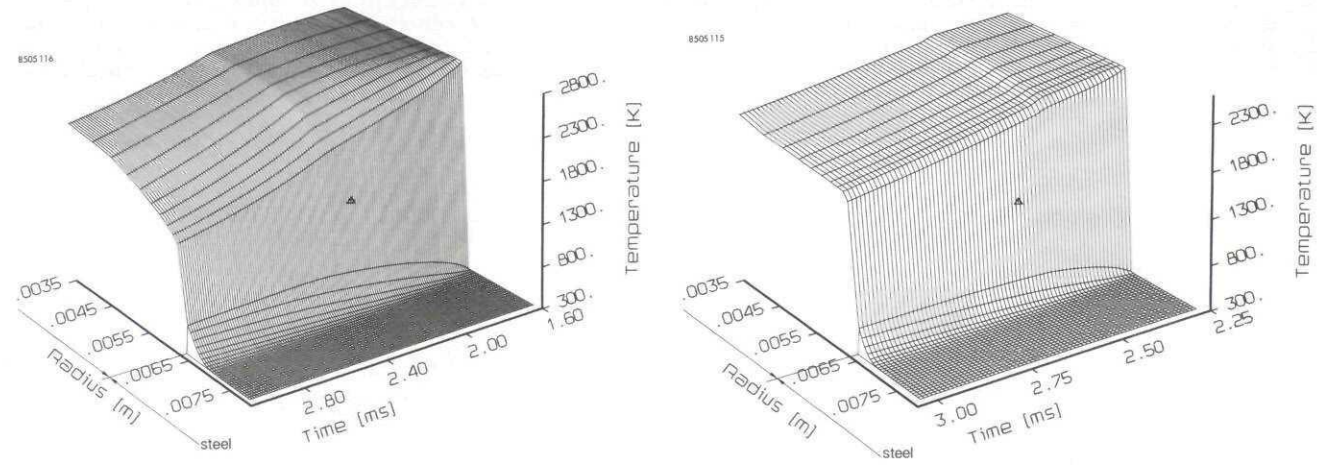

Figure-6c Calculated temperature distribution in the viscous, turbulent boundary-layer and barrel as a function of radial position and time at two axial positions.

Figure-7 shows the inner-surface temperature of the barrel as a function of time. The temperature at all axial locations stays well below the melting temperature for a single firing.

When a particular position in the barrel is passed by the projectile, heat-flow into the barrel starts instantaneously (Figure-8), resulting from the assumption in the overall model that large vortices behind the projectile reduce the boundary-layer thickness to a minimum (Figure-3). Then, boundary-layer build-up starts and heat-flux decays to lower values. The effects of increasing mainstream axial velocity and boundary-layer thickness further down-streams, result in a maximum of the heat-flux at an axial location x=0.167 m. Because of the difference in "passing" time of the different axial locations, this maximum does not coincide with the maximum in barrel wall temperature (x = 0.100 m, Figure-7)

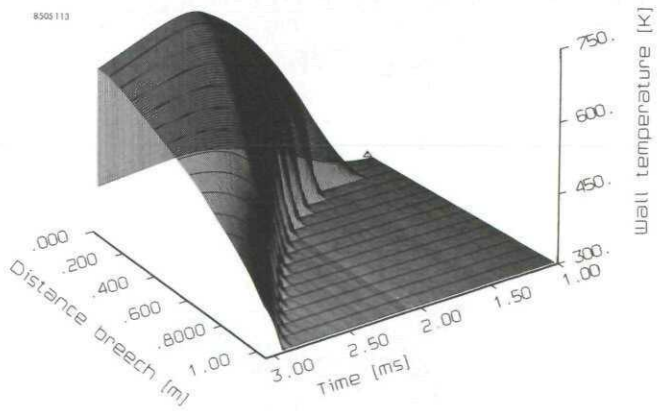

Figure-7 Calculated temperature of the inner-surface of the barrel as a function of the distance from the breech and time during the interior ballistic cycle.

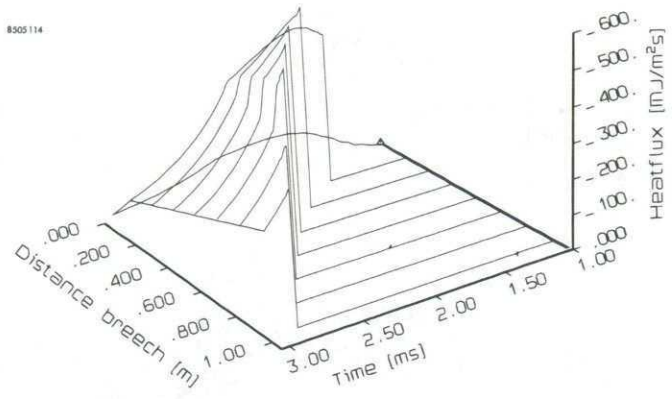

Figure-8 Calculated heat-flux at the inner surface of the barrel as a function of the distance from the breech and time during the interior ballistic cycle.

3. DESIGN OF THE EXPERIMENTAL SET UP

To validate the simulation model developed, amongst others, an experimental set-up was designed. Hereto a caliber .50in. (Browning MzHB) barrel was instrumented. A short description of this set-up is given.

A number of transducers are inserted in the barrel to measure interior ballistic parameters. An important parameter to fix, is the starting time, t=zero, of the ballistic cycle. The start of the ballistic cycle is defined as that point in time, where major burning of the ignitor begins. This point is determined within 1μs with an optical fiber placed in the ignitor cup. This signal also provides a mark on the time -basis of all measuring devices involved.
Interior ballistic parameters measured in this set-up are pressure in the combustion chamber, projectile velocity and the temperature history of the barrel. The location of the different sensors involved is depicted schematically in Figure-9.

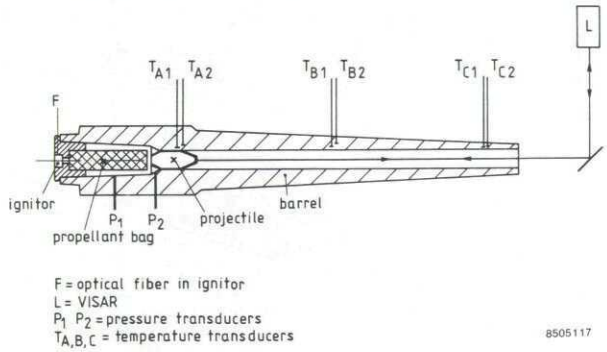

Figure-9 Schematics of the instrumented caliber .50 in. barrel.

Pressure is measured at two axial positions in the combustion chamber, one in the middle (40 mm from the breech) and the other at the end of the combustion chamber, just behind the tail of the projectile (80.mm from the breech).
The velocity of the projectile is measured continuously with the Velocity Interferometer System for Any Reflecting Surface (VISAR). To this end, the projectile is provided with a blunt nose, covered with reflecting material. To prevent gas-leakage during projectile-travel, a teflon obturator is placed behind it.

The temperature behaviour of the steel barrel is measured at six places, three in axial direction and at each axial position there are two thermocouples placed at different radial position. These thermocouples are made out of single constantan wires, diffusion-welded to the barrel at the wanted position according to [2].
All signals were recorded on a tape recorder (SE 7000) digitized (5μs sample time) and processed on a VAX 11/750 afterwards. An extensive description of the experimental set-up is given in [14]. The most important physical properties of the barrel, projectile and propellant used are given below.
Burning characteristics of the propellant were determined in-house with closed-vessel experiments.

BARREL, PROJECTILE AND PROPELLANT PROPERTIES

BARREL :

Caliber	0.0127	[m]
Length	1.036	[m]
Volume combustion chamber	$0.1955*10^{-4}$	[m^3]
Steel density	7750.	[kg/m^3]
Initial wall temperature	284.	[K]

PROJECTILE :

Weight	.0497	[kg]

IGNITOR : standard

PROPELLANT : (Single base, single perforated grains packed in a paper bag)

Force constant	1.129	[MJ/kg]
Adiabatic flame temperature	2887.	[K]
Heat capacity ratio	1.215	[-]
Web size	.00053	[m]
Shape factor	.2454	[-]
Specific mass	1600.	[kg/m^3]
Charge mass	.015	[kg]
Burning exponent	1.086	[-]
Burning Coefficient	$.2463*10^{-9}$	[m/s/Pa]
Co-volume	.00053	[m^3/kg]
Propellant motion factor (s)	1.0	[-]

3.1 Preliminary results

Reproducible results from ten firings were used for further analyses. The measured pressure-time profiles at two axial positions in the combustion chamber are shown in Figure 10a. The maximum pressure appeared to be 310MPa, while the shot-start pressure and time were about 80 MPa and 0.001s respectively. Standard deviation is 3% and 10% respectively.
The mid-chamber pressure transducer gives the complete pressure gradient in the middle of the combustion chamber. The second transducer has a delay time, caused by the initial locking-effect of the teflon obturator behind the projectile. After clearing, pressure jumps to 90-100 MPa.

The pressure distribution as predicted with the overall model described in the previous chapter is shown in Figure-10b. The pressure differences calculated from both the measured and calculated distributions are given in Figure-10c. Although the shape of both pressure difference-time profiles are almost the same, their values differ somewhat. Probably, this is caused by the simple one-dimensional burning routine used in the overall model.

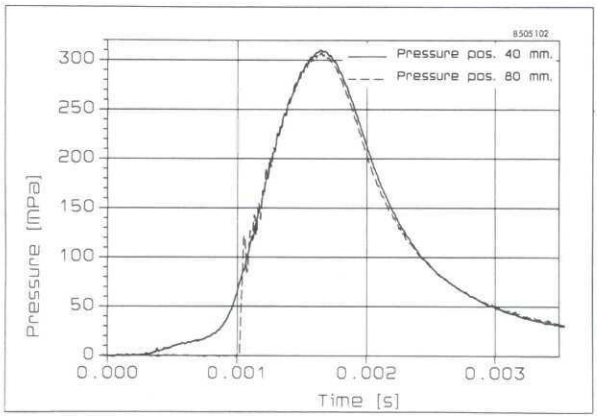

Figure-10a Measured pressure-time profile at a position of 40mm and 80mm from the breech.

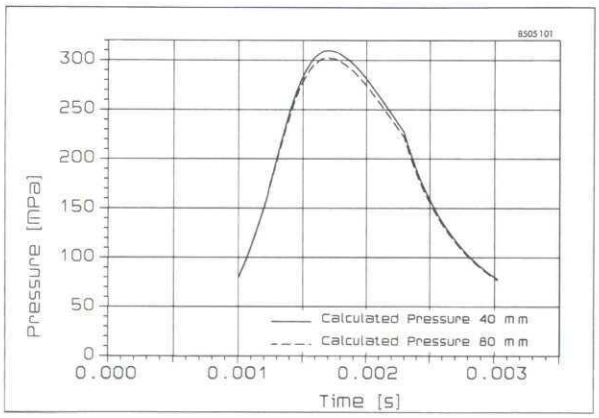

Figure 10b Calculated pressure-time profile at a position of 40mm and 80mm from the breech.

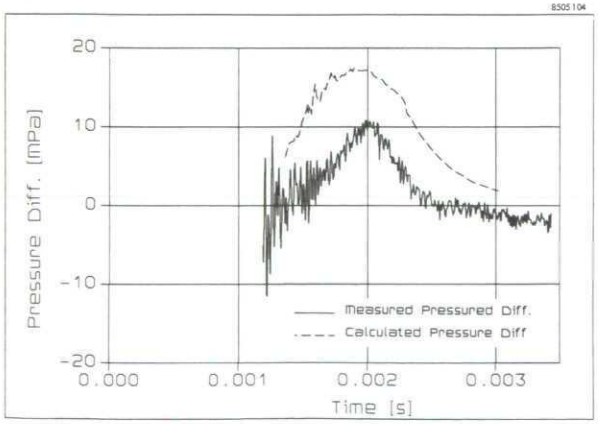

Figure 10c Measured and calculated pressure difference-time profiles.

Comparing the measured projectile velocity-time history during travel down the bore (Figure-11) with calculated values, shows a reasonable agreement. The measured muzzle-velocity is 845 m/s while the calculated one amounts 900 m/s.
Figure-12 depicts the measured temperature-time profiles at the beginning of the forging cone in the barrel, at radial positions of 1.00mm and 2.04mm from the inner surface of the barrel.

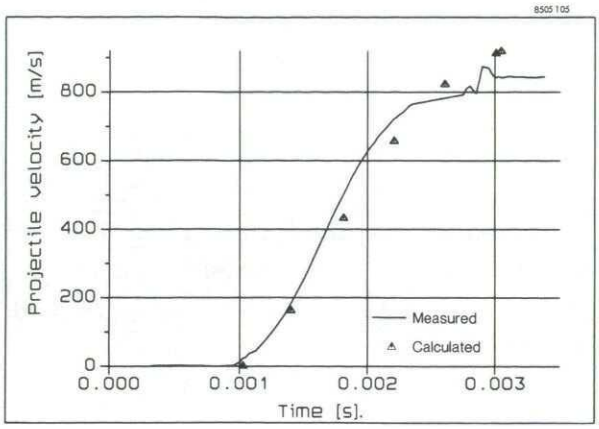

Figure-11 Measured and calculated projectile velocity-time behaviour in the barrel.

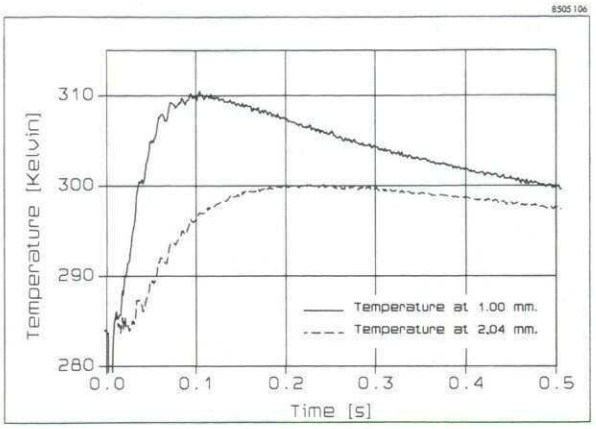

Figure-12 Measured temperature-time history in the barrel at a position 106mm from the breech and at radial positions of 1.00 and 2.04mm from the inner surface.

At this moment an accurate comparison of the measured temperature-time profiles at different locations in the barrel with calculated ones is not possible, as the model developed is not yet able to predict the temperature behaviour of the barrel beyond the time-interval of the interior ballistic cycle.

4. CONCLUSIONS

As thermal stress-cycling during firing of a propellant gun constitutes a major mechanism in erosion, wear and fatigue, an approach to study heat transfer during the interior ballistic cycle is presented. Both modelling and experiments were used to this end.

Heat transfer by conduction in the barrel material and by forced convection in the in-bore flow is described here with a one-dimensional Fourier-law and a two-dimensional, quasi two-phase viscous, compressible and turbulent model, respectively. Input parameters were calculated with a one-dimensional, two-phase burning routine, describing propellant deflagration.

From reverse analysis of experimental temperature-time profiles, obtained near the inner surface of a barrel, it appears that the heat conduction model is able to simulate measured profiles at positions further outwards in the barrel accurately.

Although description of the in-bore gasdynamic flow during projectile launch incorporates important aspects as more dimensionality and viscous, compressible and fluid-flow behaviour, both turbulency and the two-phase flow aspect are treated in an approximative way. By virtue of the numerical solution-algorithm used, steep gradients caused by e.g. pressure waves can be handled adequately.

As the burning routine does not include modelling of ignition phenomenae and flame-spreading by virtue of its one-dimensional character, one cannot expect that simulation of the interior ballistic cycle of a propellant gun with the coupled models mentioned above (IBPML2D), gives an accurate description of each aspect. However, comparing experimental results obtained from firings with an instrumented caliber .50 in. gun with results from the overall model (IBPML2D) gives encouraging agreement for maximum pressure, pressure difference-time behaviour, muzzle velocity and projectile travel. The new application of VISAR for continous measurement of projectile-motion in a single stage propellant gun appears to be succesfull.

The overall model does not yet include a description of the gasdynamic, in-bore flow after muzzle -clearance. This means that the temperature-time behaviour of the barrel over a period of time longer than the interior ballistic cycle cannot be predicted. So, a reliable comparison between predicted and measured temperature-time profiles in the wall of the barrel and a final validation of the overall model, cannot be made at this time.

Preliminary experimental results show however that for time-intervals smaller than the interior ballistic cycle, the temperature-time history at different axial and radial positions in the barrel wall can be predicted confidently.

Future work will be done in the areas of ignition and flame-spread modelling together with improving the experimental set-up for propellant burning and barrel-temperature studies.

5. REFERENCES

1. Heiney, O.K., "Ballistics Applied to Rapid-Fire Guns"
in "Interior ballistics of Guns", editors: Krier H; Summerfield M., AIAA (1979).

2. Brosseau, T.L., "An experimental method for accurately determining the temperature distribution and the heat transferred in gun barrels", ARBRL-TR-1740 (1974).

3. Versteegen, P.L. and Varcolik, F.D., "Heat Transfer studies in gun barrels"
ARBRL-CR-00393 (1979).

4. Murphy, J.R.B., Badhwar, L.K. and Lavoie, G.A., "Interior Ballistics Calculation System for Light Gas Guns and Conventional Guns",
in "The Fluid Dynamic Aspects of Ballistics", AGARD Conference Proceedings No. 10 (1966).

5. Hornemann, U., "Investigation of propellant combustion in X-ray transparent Gun Tubes"
Proceedings Fourth International Symposium on Ballistics, Monteray, Canada (1978).

6. Boris, J.P., "Flux-Correted Transport Modules for solving generalized continuity equations"
NRL Memorandum Report 3237 (1976).

7. Bartlett, E.P., Anderson, L.W. and Kendall, R.M., "Time-Dependent Boundary Layers with Application to Gun Barrel Heat Transfer"
Proceedings Heat Transfer and Fluid Mechanics Institute, Standford University (1972).

8. Dahm, T.J. and Anderson, L.W., "Propellant Gas Convective Heat Transfer in Gun Barrels"
Report SWERR-TR-72-43, (1972), Research Directorate Weapons Laboratory at Rock Island, U.S. Army Weapon Command.

9. Hunt, F.R.W., et al., "Internal Ballistics",
Published by His Majesty's Stationery Office, London (1951)

10. Cebeci, T. and Chang, K.C., "Calculation of Incompressible Rough-Wall Boundary-Layer Flows"
AIAA Journal 16, (1978), 730-735

11. Lin, T.C. and Bywater, R.J., "Turbulence Models for High-Speed, Rough-Wall Boundary Layers"
AIAA Journal 20, (1982), 325-333.

12. Christoph, G.H. and Pletcher, R.H., "Prediction of Rough-Wall Skin Friction and Heat Transfer"
AIAA Journal 21, (1983), 509-515.

13. MacCormack, R.W., "An Efficient Explicit-Implicit-Characteristic Method for Solving the Compressible Navier-Stokes Equations"
SIAM-AMS Proceedings 11, (1978), 130-154.

14. The, H.G., Kolkert, W.J. and Dexel, J., "Design of an instrument single-stage propellant gun"
Proceeding Aero Ballistic Range Association, 36th meeting 1985, San Antonio, TX, USA (1985)

15. Schols J.L.J., "Calculation of convective heat-loss during the interior ballistic cycle" (in Dutch)
PML 1981-5, Prins Maurits Laboratory TNO, Rijswijk, The Netherlands.

Acknowledgement

The authors acknowledge mr. J. Dexel for his experimental efforts and analysis of the numerous data.

DISCUSSION

P.Ramette, Fr

Do you intend to extend your model in order to take into account what is happening after muzzle exit?

Author's Reply

Yes, in a short time.

INTERIOR BALLISTICS OF SMALL ARMS : PARTICULAR PROBLEMS

Part one

HEAT TRANSFER AND COOK-OFF PHENOMENON IN A SMALL CALIBER WEAPON

R. MEŸSMANS, Professor ir.
Head of the Department of Applied Chemistry
Royal Military Academy
Brussels - BELGIUM

SUMMARY

The purpose of this communication is to introduce the research in "heat transfer and cook-off phenomenon in a small caliber weapon" performed in the Department of Applied Chemistry at the Royal Military Academy Brussels, Belgium in co-operation with Fabrique Nationale (FN) Herstal, Belgium.

The present work summarises the first results obtained since beginning 1983. Induction periods and critical temperature, measured during salvo-firings in a small caliber weapon (FNC - 5.56 ammunition) are compared with the values theoretically predicted by means of a mathematical model, describing as correct as possible what happens in the combustion chamber. The determination of some physico-chemical parameters, to be used in the mathematical model, is discussed.

LIST OF SYMBOLS

B	: linear heating rate
c	: heat capacity
E	: activation energy
h	: thickness of propellant layer (ball powder)
h_{ref}	: thickness of reference material
K	: thermal diffusivity
k	: thermal conductivity
k_{ref}	: thermal conductivity of reference material
L	: length
Q	: heat of decomposition
R	: universal gas constant
r	: radius
T	: temperature
$T_0, T_1, T_2 \ldots$	: temperature indicated by the thermocouples 0, 1, 2 ...
T_c	: critical temperature
T_e	: temperature of an external heat source
T_m	: temperature corresponding to maximum heat release
t	: time
t_i	: induction time
z	: frequency factor
δ	: FRANK-KAMENETSKII parameter
ε	: mass release
ρ	: density
τ	: period

1. INTRODUCTION

Cook-off or thermal explosion is defined as an unintended function of the propellant of a cartridge. It results from heat transfer between an overheated barrel or combustion chamber and the propellant and appears even at unexpected low temperatures (150 - 170 °C).

To prevent cook-off it is necessary to know the highest temperature T_c, the critical temperature, to which a propellant can be exposed without thermal explosion. This temperature is a function of the physico-chemical properties of the propellant (activation energy, heat of decomposition, thermal conductivity, weight ...). Exposed to a temperature $T>T_c$ cook-off will occur after a time t_i, the induction time.

2. EXPERIMENTAL EQUIPMENT

A small caliber weapon (FNC - 5.56 ammunition) is mounted on a solid vibration-free frame and supplied with a series of thin thermocouples on the barrel surface and also in the wall of the barrel and the combustion chamber up to 1 mm from the inner surface of the weapon (Fig. 1). With these thermocouples connected to a micro-computer it is possible (Fig. 2):

- to measure the temperature in the different measuring points as a function of time;
- to control the firing of the ammunition and to count the number of shots;
- to measure the time difference between the introduction of a cartridge and the moment of thermal explosion.

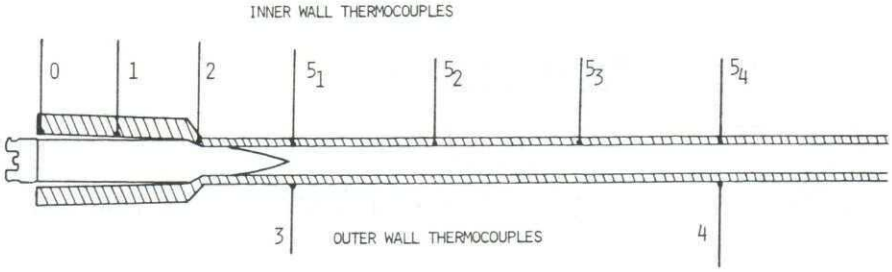

Fig. 1 : Thermocouple distribution on the weapon

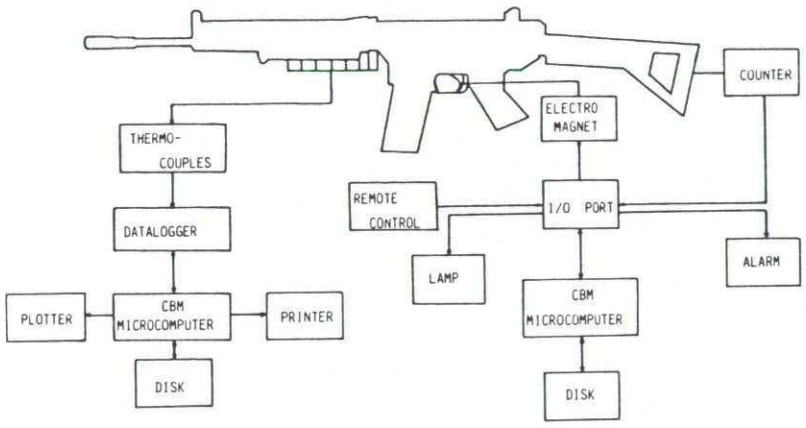

Fig. 2 : Schematic representation of the experimental equipment

3. EXPERIMENTS

3.1. Maximum temperature and its distribution in the weapon

Interested in the knowledge of maximum temperature and temperature distribution in the weapon, various experiments were carried out.

Since the weapon only fires cartridges contained in loaders (30-cartridge loaders) the experiments were made by firing one loader after another in automatic firing (∿2.5 s/loader) or computer-controlled firing (0.5 s, 1.0 s or 2.0 s of interval between each percussion).

Typical temperature evolution graphs are shown in Fig. 3 (a), 3 (b) and 3 (c):

Fig. 3 (a): 10 loaders - automatic firing;
3 (b): 10 loaders - 0.5 s time interval between each percussion;
3 (c): 30 loaders - automatic firing; this experiment was set up to determine the maximum temperature that could be reached in the weapon.

(These graphs represent the combustion chamber temperatures (T_0, T_1 and T_2) and only one inner barrel wall temperature viz. the maximum one: max T_5).

Results:

- the maximum temperature in the weapon can exceed 700 °C in a point at about 15 cm in front of the combustion chamber. This hottest point regresses in the direction of the combustion chamber by automatic firing;
- the combustion chamber is characterised by an important temperature gradient; where the neck of the cartridge-case pinches in the centering pole of the barrel the temperature can go up to 300 °C, whilst the height of the cartridge-bottom never exceeds 170 °C during firing.

It is important to know the time and space distribution of the temperature in the combustion chamber; it is to be used in the mathematical model, simulating what happens in the cartridge and serving to predict the induction time corresponding to a given external temperature distribution.

- immediately after the firing is stopped, all temperatures in the weapon decrease very quickly, except in the coldest region of the combustion chamber; here the temperature first increases about 30 °C by a heat flow coming from the overheated barrel (the combustion chamber is closed by the breech-block during this period of temperature drop).

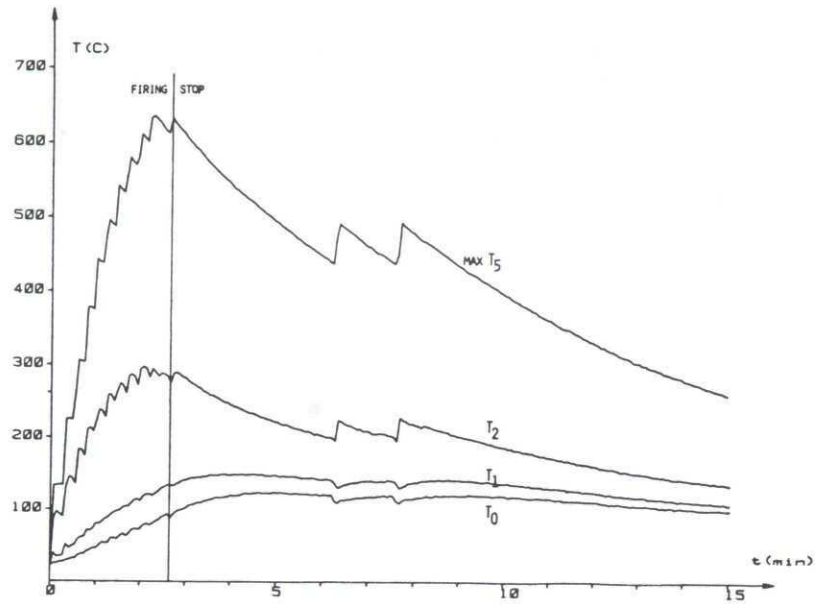

Fig. 3 (a)
T-evolution in the weapon
10 loaders-automatic firing

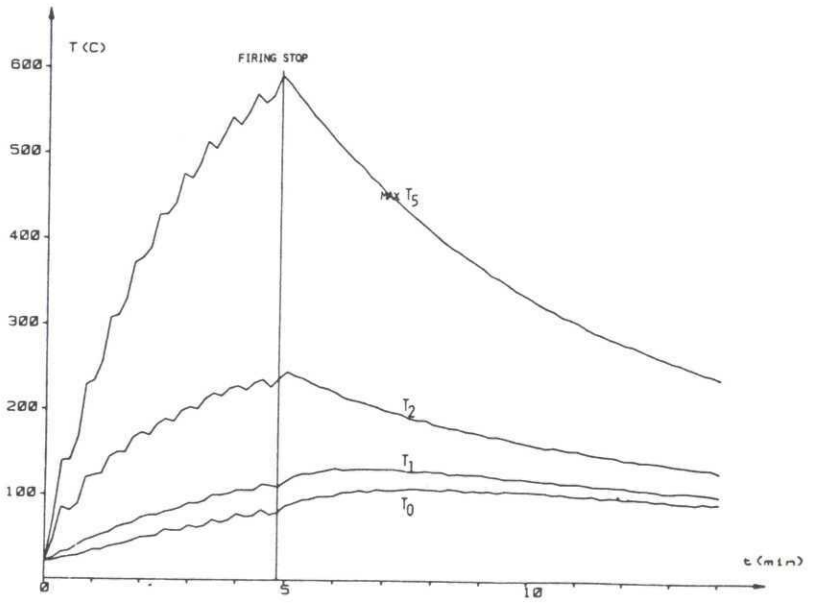

Fig. 3 (b)
T-evolution in the weapon
10 loaders-computer-controlled: 0.5 s

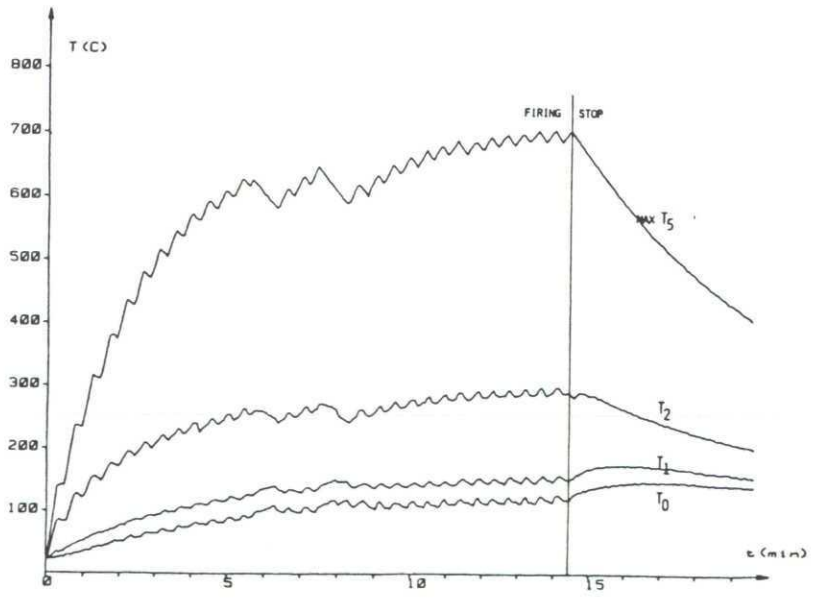

Fig. 3 (c)
T-evolution in the weapon
30 loaders-automatic firing

3.2. Induction time and critical temperature

A second series of experiments was carried out to determine the induction time of a cartridge propellant, remaining in the overheated combustion chamber until cook-off happens.

Therefore the weapon is warmed up by a series of salvo-firings to bring the temperature T_2 (Fig. 1: thermocouple 2) of the combustion chamber as high as 300 °C. Once the desired temperature is reached a loader containing real cartridges but without percussion-cap is mounted on the weapon and a first cartridge is manually loaded in the combustion chamber. The cook-off, happening after a certain induction period, takes care of the loading of a second cartridge without percussion-cap; its cook-off feeds a third cartridge and so on. Thus it is possible to determine the induction time as a function of the decreasing temperature in the combustion chamber.

The graph $t_i = f(T_2$ at the moment of cartridge loading) shows the results of such experiments (Fig. 4).

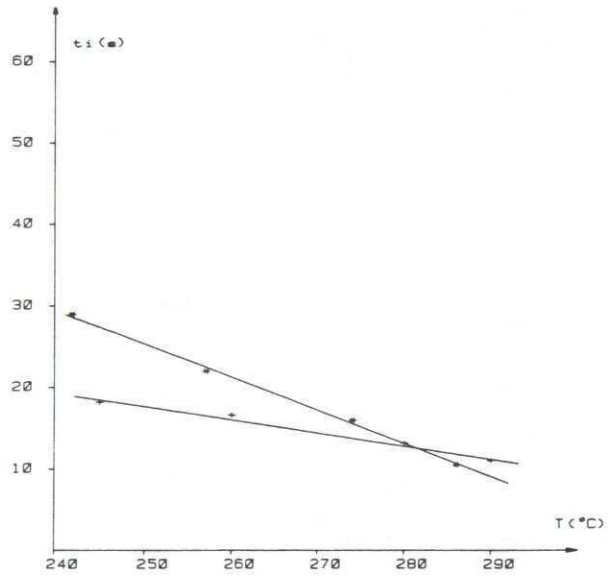

Fig. 4 : $t_i = f(T_2)$
(weapon overheated by salvo-firing)

Comments:

- there is an important dispersion between the results for different experiments; in spite of apparently the same experimental conditions, there may be a difference in:
  - the temperature distribution in the combustion chamber at the moment of loading the cartridge;
  - the contact between the cartridge and the inner wall of the combustion chamber; the cartridge neck and shoulder are always properly pinched in the centering pole of the barrel, but the air gap between cartridge and inner wall of the combustion chamber can vary from experiment to experiment;
- a cook-off was never observed at temperatures T_2 less than 220 °C;
- cartridges without percussion-cap were used to study only the behaviour of the propellant. The primer mixture used in these caps is characterised by the following $t_i = f(T_e)$; (Table 1). T_e is the homogenous and constant temperature of a cylindrical aluminium block, provided with a central hole in which the primer mixture is laid to determine t_i. Its critical temperature is situated between 160 °C and 170 °C. Note that in the weapon a percussion-cap in contact with the colder breech-block never reaches its critical temperature; also consider the temperature T_o of thermocouple O in Fig. 3 (a),(b) or (c).
- some of these experiments terminated in an unexpected incident. At a temperature T_2 of about 220-230 °C the cartridge-case was broken to pieces by the cook-off and only the back part of the cartridge-case was ejected by the ejector. A next cartridge was automatically loaded but without locking the combustion chamber by the breech-block. When the next cook-off happened, metal parts of the cartridge-case were projected all around; at the same time the weapon was deteriorated. A dangerous incident! An explanation for this abnormal damage of a cartridge-case is probably to be found by using the mathematical model (see § 4.3: comments).

Table 1

$t_i = f(T_e)$ primer mixture

T_e (°C)	t_i (s)
270	2.8
250	5.0
220	6.0
190	9.2
180	14.0
170	23.0
160	no ignition

3.3. Heat transfer to the cartridge-case

In order to determine the heat registered by the cartridge-case during firing, a special calorimeter was arranged to pick up the cartridge-cases at the moment of their ejection.

The results, reported in the next tables, are expressed in Joule/case as a function of:

- the number of cartridge-cases picked up in the calorimeter to calculate a mean value (Table 2);
- the firing sequence (automatic or 0.5 s, 1.0 s and 2.0 s of interval computer-controlled) and the number of the loader fired. Here the mean values are calculated with respect to 30 cartridge-cases picked up in the calorimeter (Table 3).

Table 2

Heat registered, in Joule/cartridge-case

round n°	15 cases	25 cases	30 cases
1	178.2	193.7	194.5
2	179.9	194.6	193.6
3	180.3	193.9	195.8
4	177.4	195.1	195.1
5	181.2	194.1	194.1
mean value	179.4	194.3	194.6

Table 3

Heat registered, in Joule/cartridge-case

(mean value with respect to 30 cartridges = loader capacity)

firing sequence / number of loader	automatic	0.5 s	1.0 s	2.0 s
first	196.2	196.6	205.0	215.5
second	211.7	220.9	226.0	230.1
third	217.6	230.1	233.0	242.7
fourth	225.9	240.9	240.6	251.0

Comments:

- because of a constant temperature rise in the weapon during the firing and the existence of an important temperature gradient in the combustion chamber, it is impossible to distinguish the heat absorbed by the cartridge-case due to on one hand the deflagration of the propellant and on the other hand to the heat flow from the overheated barrel and combustion chamber. Nevertheless this heat represents only 3.3 à 4.2 % of the real potential of the propellant. This real potential (heat released during an isothermal deflagration at constant volume; water vapour) is about 5.92 kJ/cartridge charge.
- with a heat capacity of 0.38 J/°C.g and a mean weight of 6.8 g/case, the mean temperature rise of a cartridge-case above the ambient temperature (22 °C) varies from about 75 °C (first cartridge fired) to 100 °C (last cartridge fired).

4. MATHEMATICAL SIMULATION OF THE COOK-OFF PHENOMENON

In order to predict critical temperature and induction times by theoretical calculations, a mathematical model has been developped at FN/R&D Herstal, Belgium. The model describes as exactly as possible what happens in the weapon, taking into account the geometry of the combustion chamber and of the cartridge, as well as the air gap, the metal the cartridge-case and the bullet are made of and also the physico-chemical characteristics of the propellant used.

The well-known transient heat conduction equation for a reactive solid, obeying zero-order kinetics is solved by using the finite element spatial description method.

$$\rho.c.\frac{\partial T}{\partial t} = k.\nabla^2 T + \rho.Q.z.\exp(-E/RT)$$

The computation is carried out by the software SAMCEF on VAX 750 (DEC). SAMCEF = Système d'Analyse des Milieux Continus par les Eléments Finis, developped by the L.T.A.S. (Laboratoire des Techniques Aérospatiales, Université de Liège, Belgium). This method is described in ref.[1].

4.1. Experiments in a weapon heated by an external heat source

As the real existing boundary conditions of the weapon are complicated (viz. the time depending temperature gradient in the combustion chamber) it is quite difficult to produce them in a mathematical model, so we performed a new series of experiments. Now the combustion chamber of the weapon was heated uniformally at a fixed temperature by an external heat source. The combustion chamber is provided with a series of thermocouples as indicated in Fig. 1.

Cartridges, with and without percussion-cap, were loaded and subjected to a constant boundary temperature in order to measure the induction time corresponding to a given temperature.

The loading of a cold (at ambient temperature) cartridge lowers the temperature of the combustion chamber with a few degrees; ΔT up to 5 °C, depending on the applied external

temperature as well as on the location of the thermocouple. The highest temperature lowering is observed where there is a close metal-metal contact between centering pole and the cartridge-case. The original temperature is restored quickly, but not fast enough when the induction times are short, this means at high external temperatures.

The results of experiments on two propellants (Ball Powder Lot n° 1 and Lot n° 2) are summarised in Table 4 and on Fig. 5: $t_i = f(T_2)$.

Table 4 : $t_i = f(T_2)$

(each result is the mean value of at least 10 experiments)

T_2 (°C)			t_i (s)
at cartr. loading	ΔT	at explosion	
Ball Powder Lot n° 1			
151,6	2,4	151,6	793,4
156,7	2,7	156,7	305,9
162,4	3	161,9	215,2
165,1	3,2	164,6	180,1
167,9	3	167,4	136
171,3	3,4	170,6	138
174,3	4	172,6	117,5
178,8	4,2	177,1	92,2
184	3,7	182	75,9
188,5	4	186	59,8
Ball Powder Lot n° 2			
151,6	2,9	151,6	771,6
156,3	3,2	155,5	322
162,2	3,9	161,5	215,8
164,7	3,6	164,2	175,9
164,9	3,7	164,4	161,1
168,9	3,5	167,4	132,4
175,1	2,5	173,3	112
181,5	3,7	179,8	85,7
183,5	3,7	181,8	67,3
190,5	4,2	188	56,9
194	5	190,3	48,5

In each of these experiments the breech-block was at ambient temperature (22 °C).

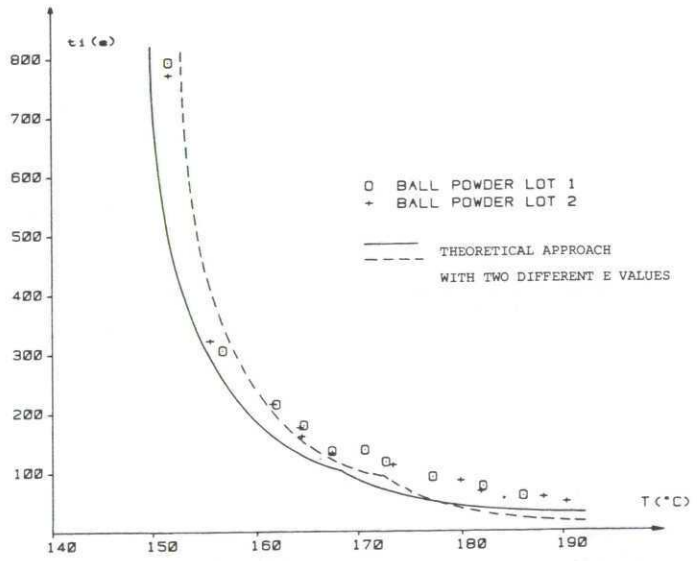

Fig. 5: $t_i = f(T_2)$
(constant boundary temperature)

The experimental critical temperature for this propellant is about 148 °C.

At temperatures between T_c and about 170 °C the cartridge-case is often torn in pieces (also note the end of §3.2.).

When the temperature exceeds 200 °C the cook-off phenomenon is caused by the thermal explosion of the primer mixture.

4.2. Physico-chemical parameters of the propellant

The use of the mathematical model requires the knowledge of a series of physico-chemical parameters of the propellant.

a. Activation energy: E

A lot of methods for the estimation of this kinetic parameter are available; most of

them are based on thermal analysis (DSC: differential scanning calorimetry), and each is characterised by its own limitations.

The methods described in ref.[2, 3, 4, 5 and 6] were used, but there is certainly no correlation between the observed results. The mean values vary from 150 kJ/mol to 300 kJ/mol with relative deviations as high as 30 %.

Inspired by the theory of ZINN & MADER [7], as KENT & RAT [8] did, the activation energy was determined based on the "Arrhenius Lines", deduced from the experimental $t_i = f(T)$ (see § 4.1) and the relation:

$$\ln(t_i) = \frac{E}{R.T} + \text{constant}$$

Whilst the measured induction time t_i consists of the warming-up time of the cartridge-case (from ambient temperature to T) as well as the real induction time, only those experiments, having a warming-up time << real induction time, can be taken into account. Limiting the calculation of the Arrhenius Line on the temperatures 150 °C < T < 164 °C, or t_i > 160 s, the value of E is about 171 kJ/mol Ball Powder Lot n° 1 and 168 kJ/mol Ball Powder Lot n° 2 (Fig.6: Arrhenius Lines).

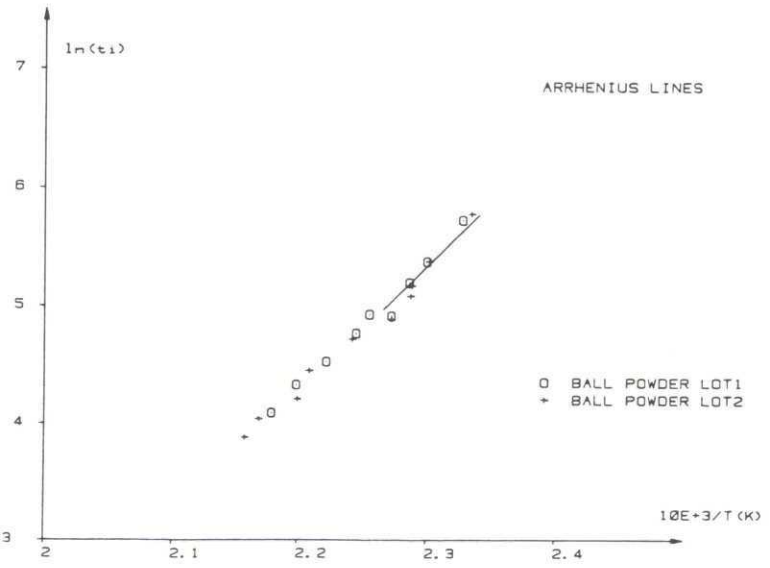

Fig.6:
Arrhenius Lines

b. Frequency factor: z

In ref. [4] ROGERS preconizes a formula, valid for a first-order reaction and based on a thermal analysis experiment (DSC):

$$z = B.E.\exp(E/(R.T_m))/(R.T_m^2)$$

with B = 2/6 K/S, T_m = 476 K and E = 170 kJ/mol the frequency factor equals 1.39×10^{16} s^{-1}.

An alternative formula is proposed in ref.[9]:

$$z = \frac{1}{t_o} \int_o^{\varepsilon} \frac{1}{(1-\varepsilon)^n} \exp\left(\frac{E}{R.T_e}\right) d\varepsilon$$

Where "ε" is the mass release (in %) after a heating time "t_o" at a temperature "T_e"; for ε<<1, this formula becomes:

$$z = \frac{1}{t_o} .\varepsilon.\exp\left(\frac{E}{R.T_e}\right)$$

without knowing the order of the reaction.

Thermogravimetric analysis provides the necessary data:
with T_e = 428 K, t_o = 18000 s, E = 170 kJ/mol and ε = 45 % the value of z is 1.35×10^{17} s^{-1}.

c. Density:

Its determination by a classical laboratory experiment gives a mean value of 1063 kg/m³ (σ_{rel} = 0.08 %) at ambient temperature. Note that the density depends on the piling up of the grains; the mentioned value corresponds with a piling up obtained after a 3-time shaking during 30 s.

d. Heat capacity: c

The exploitation of thermal analysis experiments (DSC) produces the following expression of the heat capacity as a function of temperature between 70 °C and 110 °C; the reliability diminishes above 110 °C due to the increasing chemical decomposition of the propellant.

$$c = 3.98\ T\ (°C) + 1.13 \times 10^3\ (J/kg.K)$$

e. Heat of decomposition of the propellant: Q

The use of DSC is classic in the determination of this parameter; nevertheless the heating rate is to be limited in order to realise a thermal decomposition rather than a deflagration. With a maximum of 20 °C/min the heat of decomposition of the propellant is 2.28×10^3 kJ/kg (σ_{rel} = 2,2 %).

f. Thermal conductivity: k

Two methods have been used for the determination of this parameter.

i) Relative method:

The thermal conductivity is established in an experiment using a reference material with approximately the same thermal conductivity as the propellant. The experimental equipment is represented in Fig.7.

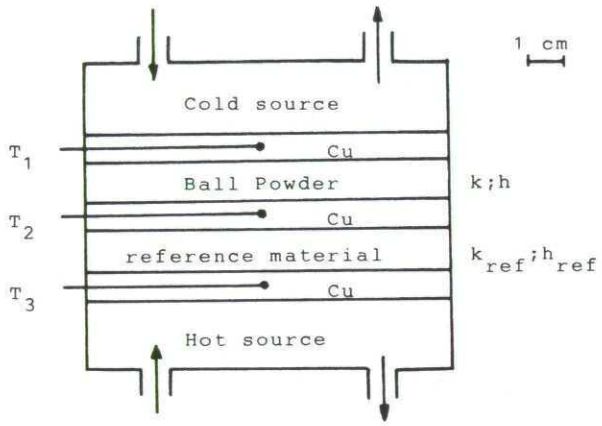

Fig.7:
Thermal conductivity - Relative method

At stationary regime the heat flow passing through the propellant layer equals the heat flow through the reference material; then:

$$k = k_{ref} \frac{T_3 - T_2}{T_2 - T_1} \cdot \frac{h}{h_{ref}}$$

In these experiments the difference ($T_3 - T_1$) is about 10 °C, with T_3 from ambient temperature to 65 °C.

The obtained value for "k" varies from 0.126 to 0.143 W/m.K with important standard deviations of about 10 %, probably due to the difficulty of reproducible filling of the corresponding space with the propellant.

ii) Heat wave method:

This method is based on an experiment developped in the Department of Physics, Royale Militaire, Bruxelles, where it is used in the study of heat conduction in metals. A hollow rod of lenght "L" filled with the propellant is submitted at one end to a square wave T(t) with a period τ by means of a hot and a cold heat source. The heat conduction in the propellant is governed by the relation:

$$K \frac{\partial^2 T}{\partial x^2} - \frac{\partial T}{\partial t} = 0$$

"K" is the thermal diffusivity of the material.
The study of this relation shows that in x=0 every harmonic function of the temperature leads to a dimmed heat wave travelling through the propellant. The square wave can be analysed into its harmonics by using Fourier series. The heat wave produced by the square wave is the sum of the heat waves produced by each harmonic. The measurement of the amplitude evolution of the resulting heat wave in a point with abscis x allows the calculus of K:

$$K = \frac{\pi . x}{\tau . \ln(T_{max} - T_{min})}$$

This experiment is very delicate and characterised by an important spread of the results. A mean value of K is 7.73×10^{-8} m²/s.
The relation:

$$k = K . \rho . c$$

produces the thermal conductivity, for example at 100 °C, k = 0.126 W/m.k.

g. Critical temperature: T_c

The critical temperature can be estimated by the next relation, solution of the Frank-Kamenetskii equation for cylindrical geometry, ref. [10].

$$T_c = \frac{E}{R} \ln\left(\frac{\rho . r^2 . z . Q . E}{\delta . T_c . k . R}\right)$$

with $\delta = 2.00 + 3.37(\frac{r}{L})^2$

r and L are respectively the radius and the length of the cylinder. This relation is to be solved by the iterative method of Newton-Raphson.

A parameter study of this relation shows at the value of T_c the very important influence of the activation energy, the frequency factor and the thermal conductivity of the propellant.

4.3. The mathematical model

From the preceding paragraphs it becomes evident that it is extremely difficult to obtain the necessary data to be introduced in the mathematical model. The value of the activation energy and of the frequency factor depends on the used experimental method as well as on the way of analysing the experimental results. Likewise it is impossible to determine the propellant density and heat capacity in the circumstances of the cook-off experiments. How to determine the thermal conductivity of the propellant at temperatures $T > T_c$?

Nevertheless a set of values was selected for the different physico-chemical parameters and introduced in the mathematical model. A parameter study and a refinement of the model were necessary to correlate - as good as possible at this moment - the theoretical induction time versus temperature curve with the experimental one.

A theoretical $t_i = f(T)$ is represented as a solid line on Fig.5.

Comments:

- the general slope of the theoretical curve is in accordance with the experimental results;
- the selected value for the activation energy has a great influence on the position of the theoretical curve. The dotted line on Fig.5. represents $t_i = f(T)$ with another but greater value for E;
- the value of E needed for good accordance seems to be greater than expected a priori;
- the slope of the theoretical curve shows a kink in the vicinity of 170 °C. The finite elements method for resolution of the mathematical model reveals a transition of the propellant ignition point from the middle of the propellant charge to the bottom of the bullet and further on to the neck of the cartridge-case when the increasing boundary temperature exceeds 170 °C. Fig.8.

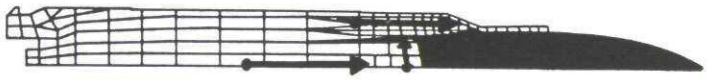

Fig. 8 : Transition of ignition point

This could be an explanation of the incidents occuring in the foregoing experiments and related in § 3.2 and § 4.1. At higher boundary temperatures a deflagration front starts at the neck of the cartridge-case and travels across the propellant charge. At boundary temperatures <170 °C a deflagration front starts in the middle of the charge in both directions, one to the bullet another to the bottom of the case. Could reflected waves produce an overpressure causing the case rupture? Was there a deflagration to detonation transition (DDT)? Up to now a satisfying answer has not been found.

- altough the mathematical model is not perfect, it forecasts the behaviour of the ammunition in respect with cook-off phenomenon when changing some parameters like dimensions, type of propellant, caliber...

5. CONCLUSION

At this moment a quite reliable mathematical model is at our disposal. It is to be refined in the prospect of a behaviour study of small caliber weapons characterised by other geometry and by using new generation propellants and ammunition.

We have acquired a lot of experience in the determination of the physico-chemical parameters of the propellant. Yet a new experimental equipment has been developped to ensure a better control of the experimental circumstances described by a simpler mathematical model. We are convinced that it must be possible to acquire more acceptable values for the physico-chemical parameters by using this equipment.

REFERENCES

[1] Brauwers, M. and Devos; P. "Modèlisation mathématique du phénomène cook-off,"in Proceedings of the " Symposium Armement et Balistique" Ecole Royale Militaire, Bruxelles, Belgique, 19 - 22 juin 1984.

[2] Kissinger, H.E., "Variation of peak temperature with heating rate in differential thermal analysis," J. Res. Nat. Bur. Stand. Vol 57, 4, (1956).

[3] Rogers, R.N. and Morris, E.D., "On estimating activation energy with a differential scanning calorimeter," Analyt. Chem., Vol 38, 3, pg 412, (1966)

[4] Rogers, R.N. and Morris, E.D., "Estimation of pre-exponential factor from thermal decomposition curve of an unweighed sample," Analyt. Chem. Vol 39, 8, pg 1025, (1967).

[5] Rogers, R.N., "A comparision of thermochemical methods for the determination of kinetic constants,", ICT-Jahrestagung, pg 41 - 56, (1971).
[6] Duswalt, A.A., "The practice of obtaining kinetic data by differential scanning calorimetry," Thermoch. Acta 8, pg 57 - 68, (1974).
[7] Zinn, J. and Mader, C.L., "Thermal initiation of explosives," J. Appl. Phys., Vol 31, 2, pg 323 - 328, (1960).
[8] Kent, R. and Rat, M., " Explosion thermique (cook-off) des propergols solides," Propellants, Explos. Pyrotech., 7, pg 129 - 136, (1982).
[9] Chapman, A.J., "Heat transfer," 3 rd Edition, MacMillan Publ. Co, Inc, N.Y. (1974).
[10] Frank-Kamenetskii, D.A., "Diffusion and Heat Transfer in Chemical Kinetics,", translated from the Russian edition by Thon, H., Princeton University Press, (1955).

ACKNOWLEDGEMENTS

The author wishes to thank his collaborators of the Department of Applied Chemistry, Ecole Royale Militaire, Brussels, for the developing of so many experimental equipments and for the lot of work they did in analysing the results of hundreds of experiments.

Fabrique Nationale, Herstal, Belgium, has helped us in this work with an important logistic support.

INTERNAL BALLISTICS OF SMALL ARMS : PARTICULAR PROBLEMS

Part two

THERMODYNAMIC MODEL - POWDER PARAMETERS - INITIATION

E. CELENS, Professor ir
Head of the Department of Armament and Ballistics
Royal Military Academy
Brussels - Belgium

INTRODUCTION.

- As part of its teaching function, the Weapons and Ballistics Department of the Royal Military Academy conducts research in various branches of armament in general and in external, internal and terminal ballistics in particular.
- The Department laboratory has specialized ballistics metrology equipment available for experimental studies.
- Specific progress in each field is based essentially upon the results of final course works by officer students in the Polytechnic Division ; this work can be completed only in part by the permanent staff of the Department mainly because of the wide (and entirely justified) variety of studies in progress.

  During the last five years the studies in external and terminal ballistics have been emphasized. Nevertheless two final course works were dealing with the applicability of the thermodynamic model in small caliber weapons and two other ones were dealing with appropriate computer algorithms for optimal exploitation of closed vessel trials. Finally for a better understanding of the initiation phase, the working of primary high explosive compounds was studied by visualising the ignition phenomenon in a transparent chamber.
- This paper summarizes the results obtained in these studies : only the most interesting results or findings which we believe will be helpful in similar applications are mentioned.

1. The thermodynamic model in small caliber weapons.

The thermodynamic model approaching the phenomenon characterizing the motion imparted to a projectile inside a gun tube by deflagration of a propellant is given during the combustion phase by the following basic equations (after all burnt z = 1)

- Equation of motion $$d\left(\frac{1}{2}\mu v^2\right) = pdc \qquad (1)$$
- Equation of combustion $$dz = A \cdot \varphi(Z) \cdot p^{\alpha} \cdot dt \qquad (2)$$
- Energetic equation $$\frac{1}{2}\mu v^2 = \frac{f \cdot \overline{\omega} \cdot Z}{n-1} - \frac{p(C - \eta_Z \cdot \overline{\omega})}{n-1} \qquad (3)$$

where $$\eta_Z = \eta \cdot Z + (1 - Z)\frac{1}{e} \qquad (4)$$

$$dc = \sigma \cdot v \cdot dt \qquad (5)$$

$\mu = (1 + i)m$: fictive mass of the projectile.

Note that i reflects the work done against frictional resistance including the rotational energy due to rifling. The order of magnitude of i often cited in the litterature is 0,07.

v : velocity of the projectile at instant t

p : mean value suitably averaged over the pressure gradient at t.
Notice that in equation (1) p actually represents base pressure.

c : volume behind the projectile at moment t

Z : specific fraction of burnt propellant at moment t

$A = \beta \cdot \frac{S_o}{V_o}$: absolute vivacity of the propellant $\left[\frac{1}{\text{bar} \cdot S}\right]$

where β : chemical characteristic of the propellant used in the combustion law (Vieille, Charbonnier, Muraour)

$\frac{S_o}{V_o}$: mechanical characteristic of the propellant denoted fragmentation index

S_o : initial emission surface of propellant

V_o : initial volume of propellant

$\varphi(Z)$: form function of the propellant grains at instant t

α : pressure coefficient used in the vieille combustion law

f : "force constant" of the propellant $\left[\frac{N.m}{kg}\right]$

$\overline{\omega}$: total mass of propellant

n : polytropic expansion coefficient-order of magnitude : 1,25

η : covolume per unit mass of gass $\left[\frac{cm^3}{g}\right]$

ρ : specific mass of the propellant

S : cross sectional area of the bore

2. Experimental equipment.

The weapon used, caliber 7.62 mm, is composed of a manometric block and an interchangeable barrel BMCI (foto 1). The block possesses a NATO-standardized-chamber. The block and the barrel are provided with several pressure-measuring channels. One uses Kistler pressure gauges type 6203 with charge amplifiers Kistler type 5007. A 4 channel mikroprocessor controlled "sample and hold" circuit TR SE 2550 is used. If more than 4 signals have to be registered simultaneously a two channel HP frequency analyser is available. Via an interface bus the data are transmitted from the Transient Recorder to a deskcomputer HP 9825B, which is control-unit between the Transient Recorder and the XY-Plotter HP9826 . The moment the bullet is leaving the barrel is registered by an optical muzzle flush detector type BAL 607. With the aid of conventional optical screens the velocity of the bullet outside the barrel can be measured at several distances.

3. Choice of the initial values of the variables p, c, v, Z and t.

These initial values depend on the choice of the moment we decide the equations (1) to (3) are applicable.

– a. One plausible approach supposes that the pressure wave produced by the percussion cap is powerful enough to push the bullet out of the cartridge and to put it in motion over a distance of about 3mm at the end of which the cylindric part of the bullet comes in contact with the rifled part of the barrel. The always present short "plateau-effect" at the beginning of the pressure curves (see later registrations) can be explained as a temporary pressure equilibrium between the limited energy amount generated by the primary high explosive compounds of the percussion cap on one hand and the volume increase caused by the initial motion of the bullet without great resistance on the other ; the real combustion of the propellant itself only starts at the beginning of the engraving process.

Consequently this choice implies following initial values :

p_d = 350 kgf/cm^2 corresponding to the pressure of the plateau effect

C_d = 3,050 (cartridge volume) + $\frac{\pi}{4}$ x (0,775)^2 x 0,3 = 3,2 cm^3

v_d = 0

Z_d = 0

– b. An other approach, more plausible with the generally formulated definition of the pressure p_d and the fictive mass μ supposes the initial moment corresponding to that position of the bullet at which the cylindric part of the bullet jacket is completely engraved i.e. in fact a travelling distance of 8,5 mm after cartridge exit. Special attention has been paid to the experimental determination of this so called departure pressure p_d. Therefore very reduced charges of propellant have been used and the exact moment of complete engraving of the cylindric part of the bullet corresponds to the beginning of the motion of a very light stick placed carefully in the gun tube. This initial motion is picked up outside the barrel with an optical detector illuminated at the same moment by laser beam. This signal is registered on the pressure curve.

See fig 2 and fig 3.

The so defined mean departure pressure $p_d \left[\frac{kgf}{cm^2}\right]$ equals 453 when ball powder is used and 510 when bofors powder is used.

The more dynamic character of ball powder probably justifies the lower measured mean departure pressure.

It is not excluded that for the same reason the real departure pressure for both propellants with normal propellant charge densities will be a bit lower, the dynamic character of the pressure curve being greater.

Consequently this choice implies following initial values :

p_d = 453 $\frac{kgf}{cm^2}$ (or 510)

C_d = 3,050 + 0,401 = 3,451 cm^3

v_d = 0

Z_d is deduced from the relation $p_d = \frac{f \cdot \overline{\omega} \cdot Z_d}{C_d - \overline{\omega}(\eta \cdot Z_d + (1 - Z_d)/\rho)}$

4. Choice of the parameters related to projectile and weapon.

– a. *The fictive mass* $\mu = m(1 + i)$

As the in former paragraph 1 cited value 0,07 of i is almost applicable to field artillery guns using projectiles provided with a driving band instead of a jacket and generally characterised by a rather short barrel, no reliable information on this value of i in the case of small caliber weapons is available.

Therefore the mean value of the fictive mass in question is determined on a semi-experimental way by integration of equation (1) of paragraph 1 namely, after transformation :

$$\mu = \frac{\sigma}{v_b} \int_0^{t_b} p\,dt \qquad (1')$$

Where the muzzle velocity v_b is experimentally determined and the integral $\int_0^{t_b} p\,dt$ is calculated starting from the experimentally registered pressure curve $p = f(t)$.

As a specific in bore velocity measuring device is not available, the muzzle velocity v_b is determined using the along the barrel distributed pressure measuring devices and the optical muzzle flash detector. Cfr fig 4, 5 and 6). Based on a great number of trials some points of the in bore velocity curve v = f(t) are experimentally determined. A polynomial compensation of these points finally gives by extrapolation the muzzle velocity v_b. See following table I.

Table I

	ball powder			bofors powder		
$\overline{\omega}$ (g)	2,93	2,80	2,60	2,92	2,80	2,60
v_b (m/s)	817,1	797,6	753,3	805,5	774,3	724,7

Application of equation (1') gives a mean value for μ : 12,46 g.
As m = 9,3 g one deduces easily the value of i : 0,34.

Conclusion : This value of i is thus sensibly higher than the value generally used in field artillery guns. This is nevertheless not so surprising as the work done against frictional resistance in a small caliber weapon should be noticeably higher due to a much larger common contact surface, namely the total jacket, on one side and to a much longer barrel, namely about 69 calibers long on the other side.

– b. *The initial percussion effect.*

The velocity measuring divices outside the barrel give by extrapolation the so called initial velocity v_o used in external ballistics and taking into account the effect of the initial percussion.

As the in (a) mentioned procedure furnishes the strictly muzzle velocity imparted to the projectile inside the gun v_b, the difference between both values is precisely produced by the initial percussion effect. Following differences in percentage have been enregistered in this manner :

Table II

	ball powder			bofors powder		
$\overline{\omega}$ (g)	2,93	2,80	2,60	2,93	2,80	2,60
$\Delta v = v_o - v_b$ [°/o]	4,21	4,02	3,43	4,11	4,10	3,63

Table II indicates that the effect of the initial percussion is not neglectable and that its order of magnitude is quite constant in question.

– *GENERAL REMARK* : Concerning the above paragraphs 4a and 4b we are very interested in results obtained in other laboratories by simular or other measuring techniques in order to verify if the applied procedures in question are sufficiently accurate.

5. Choice of the parameters related to the propellant.

– a. *General remarks on the two types of powder used :*

– *"ball powder"* Lot 418/82 manufactured by PRB. Defense Sector at Clermont-sous-Huy for munition caliber 7.62 mm NATO.

Granulometry indicates a mean diametre of the spherical shaped grains of 0,55 mm. The manufacturing process of "ball powder" leads by successively supplying of nitroglycerine (NG) and impregnation coating of dibutylphtalate (DBP) to different penetration depths of both compounds in the nitrocellulose (NC) matrix and even to variable percentages of these compounds with penetration depth.

The additive DBP in the outer covering decreases the combustion rate in the beginning and thus diminishes the vivacity A.

As spherical grain configurations are characterized by a degressive form function, this degressive character will be partially compensated during burning by increasing vivacity due, on the one hand, to a lower percentage of DBP and on the other hand to higher vivacity of respectively the double base (DB ≒ NG + NC) composition and the single base (NC) one.

A real problem is the incertitude about the effective penetration depth of both compounds DBP and NC and also about the radial percentage gradient of both compounds. The structure of ball powder can be determined by microhardness-tests (R. Couterier), hydrolytic dissolution (A. Sopranetti) and by adequate manometric bomb trials (E.H. Human).

– *propellant Bofors product* NC 1055 for small caliber weapons. The major compounds of this powder are NC (90,6 °/o), NG (4,6 °/o) and Diamylphtalate (2,9 °/o). The grains have been shaped into single perforated small sticks with a mean diametre of 0,73 mm, a web thickness of 0,32 mm and a mean length of 1,01 mm.

– b. *Determination of the powder parameters* f, η, A and α .

b.1. *Preliminary remarks.*

As no adequate small closed vessel (maximum volume of 100 cm^3) was available at the right time the first powder parameters used in the thermodynamic model were deduced from theoretical calculations.
Meanwhile, a first final study project was dealing with the practical realisation of the determination of the powder parameters using a Manometric Bomb M92BG type NATO, made in the Arsenal of Munition in Zwijndrecht (BE), an ameliorated version of the closed vessel type RARDE/B2/315/MA/5. (bomb volume : 700 cm^3). Its principal task consisted in making the appropriate computer algorithms for optimal exploitation of the closed vessel trials.
A second final cours work was dealing with the construction of an appropriate manometric bomb of about 100 cm^3 volume and more specifically with the determination of the ballistic parameters of respectively the two above mentionned propellants using the same computer algorithms as in the previous work.

b.2. *General remarks on the exploitation methods of closed vessel trials.*

1° – Concerning the determination of force f and covolume η by applying a linear regression technic it must be emphasized that in order to get statistically a minimum value of the correlation coefficient (0,9 at least), generally, depending on the confidence level fixed, a great number of closed vessel trials is necessary. Often 16 can be considered as an acceptable number.

2° – As the geometric form function $\varphi(Z)$ can always be formulated, it is important to calculate the *absolute vivacity* A based on following relations :

$$A = \frac{1}{p_{max} \cdot p^{\alpha} \cdot \varphi(Z)} \cdot \frac{dp}{dt} \qquad (6)$$

$$\alpha = \frac{\log\left[\left(\frac{dp}{dt}\right)_2 \cdot \varphi_1(Z)\right] - \log\left[\left(\frac{dp}{dt}\right)_1 \cdot \varphi_2(Z)\right]}{\log p_2 - \log p_1} \qquad (7)$$

where Z is supposed $= \frac{p}{p_{max}}$

α is supposed invariable between the two points

$$\left[p_1 , \left(\frac{dp}{dt}\right)_1\right] \quad \text{and} \quad \left[p_2 , \left(\frac{dp}{dt}\right)_2\right]$$

The discrete registered pressure versus time curve is compensated by an appropriate orthogonal polynomial, which on its turn is used to calculate the successive derivatives $\left(\frac{dp}{dt}\right)_i$.

Generally A is determined in a limited number of points (often 5) and the mean value is adopted as the best value of A. The same procedure permits the determination of α . If charbonniers law is used, α equals 1.

Note te difference between this absolute vivacity A and the so called *"dynamic vivacity"* defined as following :

$$\text{"dynamic vivacity"} = A \cdot \varphi(Z) = \frac{1}{p_{max} \cdot p^{\alpha}} \cdot \left(\frac{dp}{dt}\right) .$$

3° – A manometric bomb trial can be used for a pure experimental determination of the form function $\varphi(Z)$ starting from relation

$$\varphi(Z) = \frac{1}{A \cdot p_m \cdot p^{\alpha}} \left(\frac{dp}{dt}\right) .$$

An appropriate computer algorithm has been written for this purpose.

b.3. *Specific results deduced from closed vessel trials.*

– In order to test the different computer algorithms a great number of manometric bomb trials (volume 700 cm^3) has been made with different artillery propellants among which propellant N5470 with heptatubular grains.

It is worthwhile to mention here that the experimental determination of the form function $\varphi(Z)$ in accordance with the in paragraph 5.b.2. 3° cited method leads in normal conditions to a curve practically coinciding with the theoretical one. On the contrary, a pronounced difference between $\varphi(Z)_{exp}$ and $\varphi(Z)_{theor}$ would possibly indicate some combustion irregularity !

– Related to ball powder lot 418/82 a great number of manometric bomb trials (volume 96 cm^3) with different charge densities have been made.
Complementary also the rate of burn $r = \beta \cdot p^{\alpha} = \frac{V_o}{S_o} \cdot A \cdot p^{\alpha}$ has been determined. It must be noticed that the value α influences sensibly the value of vivacity A. Obvious is the choice of either a constant mean value of α deduced from the trials either $\alpha = 1$.
Fig. 7 represents the variation of A with pressure A = f(p).
Fig. 8 represents the variation of rate of burn r with pressure.
Both curves have been established for $\alpha = 0{,}877$.

– By a great number of simular manometric bomb trials this research has been extended respectively to 1° ball powder double base (NC + NG) without DBP and 2° ball powder single base (NC) without supplying NG.

You find comparative results concerning both parameters A and r on figures (9) namely A = f(p) and on (10) namely r = f(p).

Notice on figure 9 the appreciable variation of vivacity A with pressure for normal ball powder (NG + DBP).

Notice also that this variation is much more pronounced than for ball powder without DBP i.e. double base or single base.

Notice also that normal ball powder (NG + DBP) has a much lower mean value of vivacity A than the two other types.
Obiviously double base ball powder (NC + NG) has the highest mean value of vivacity A.

Notice finally on figure 10 that the rate of burn r is quite directly proportional to pressure rise.

6. Validity of the thermodynamic model. Fitting technic.

First of all, almost of the fitting of the thermodynamic model to the experimental results has been done before the powder parameters obtained by the above mentioned closed vessel trials were available. The fitting has been realised in two phases.

1°) Firstly the model has been fitted to the experimental maximum pressure p_{max} and muzzle velocitv $v_{b\,exp}$ only. Although other parameters can be used, vivacity A and force f bave been chosen as fitting parameters. Starting with the best estimated values of both fitting parameters, the sensitivity of p_{max} and v_b with respect to both parameters f and A are calculated with the aid of the model itself.

For the fitting itself an iteration procedure is applied and one, maximum two fitting iterations are necessary.
Figures 11 and 12 indicate the satisfying fitting result of the model after 1 step.
The same fitting procedure gives analogic results for the Bofors powder cfr fig 13 and 14.

2°) Secondly one tries to improve the fitting of the general shape of the theoretical pressure curve to the experimental one. Notice the specific change in pressure rise from a given moment on the pressure curve with ball powder (cfr fig 11). The pressure curve with bofors powder in contrary does not present this phenomenon. This specific phenomenon can be explained by the influence of the varying vivacity of ball powder with varying burning radius.

The fitting procedure uses first the fitted values of the preceding phase till the point of pronounced change in pressure rise, from where the vivacity is adapted linearly over a given time interval (or Z interval). Combined acting on the slope of linear variation and on the magnitude of applied interval conducts to a good shape fitting. Cfr. fig. 15.

This last procedure is rather specific and cannot be generalized. Obvious with more precise data on powder vivacity available (cfr paragraph 5.b.3.), the basic thermodynamic model should insert the variation law of vivacity with pressure and the fitting problem should be tackled differently.

The total work will be overdone in the future following these guidelines !

Conclusion : Although adequate fitting of the thermodynamic model gives quite satisfying results in accordance with the experiment, the real validity of this model remains restricted in so far its predicting capacity is concerned. Indeed, experience indicates the limiting predicting capacity of this model with changing initial data, due principally to strong influences of these data variations on phenomena the model is not integrally dealing with, such as inflammation, engraving, heat transfer, friction work.

Therefore, we decided in a first approach, to look more closely to the ignition phase : we 'll firstly analyze the flame front propagation generated by the percussion of the primary high explosive and secondly examine the inflammation build up of the powder bed.

7. Experimental study of the percussion effect of different primary explosive compounds. Flame front propagation in the combustion chamber.

Remark : As this study is going on we 'll only mention the experimental equipment used and some provisional results, without further interpretation.

– a. For the purpose of visualisation of the flame front propagation the IMACON-camera is used in a disposition with respect to the combustion chamber as indicated on figure 16. The combustion chamber made in clear polycarbonate is transparent and the manometric bloc is provided with an aperture. If necessary the chamber can be provided with a pressure measurement channel.

It is important to use, on the **one** hand, the right delay between the synchronisation pulse (= contact hammer percussion pin) and the moment of the first picture, on the other hand the adequate frame frequency (intervals of 5, 10 or 20 μS) in order to get the complete phenomenon with sufficient details for interpretation. Different types of percussion caps have been tested among which conventionnal metallic ones 5.56 mm and completely combustible ones applicable in caseless munition.

– b. *Some provisional results.*

The following pictures 17, 18 and 19 with a frame frequency of 50 kHz characterize the flame front propagation in an empty combustion chamber produced by a reference percussion disposition such as applicable for caseless munition. The mean propagation velocity deduced from a great number of trials is about 130m/s. Abviously several other important features such as ignition delay, reproducibility and variability in time and space can be simultaneously examined

Following two pictures 20 and 21 visualize the same phenomenon of an other type [with lead azide $Pb(N_3)_2$] suitable for caseless percussion disposition. The mean flame front propagation velocity is greater, about 190m/s probably due to the presence of $Pb(N_3)_2$. The variability of the phenomenon in velocity propagation is quite simular in both cases and so is the ignition time.

Pictures 22 and 23 visualize the phenomenon with the former reference percussion disposition with a bullet fitted at the beginning of the barrel. A remarkable difference is visible due to the presence of the bullet.

The same phenomenon with a conventional metallic percussion cap 5.56 mm is characterised by figures 24 and 25 respectively without and with a bullet. Notice the big difference between both phenomena in intensity and continuity of the flame spreading. The propagation velocity is obviously greater than in the former treated cases.

Conclusion : These provisional findings and results make it clear that further investigation in this research work will probably be very profitible to a better understanding of the critical ignition phenomenon in Interior Ballistics of small arms.

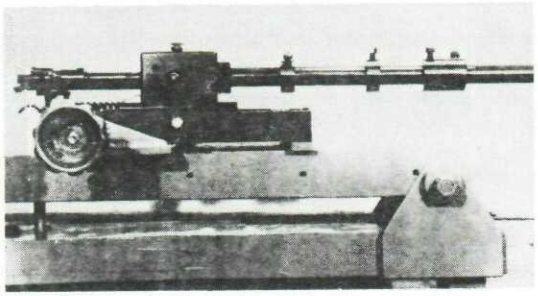

Fig.1:The BMCI.

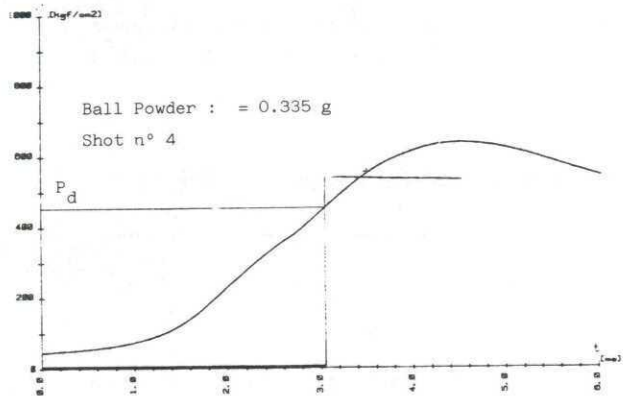

Fig.2:Determination of the departure pressure.

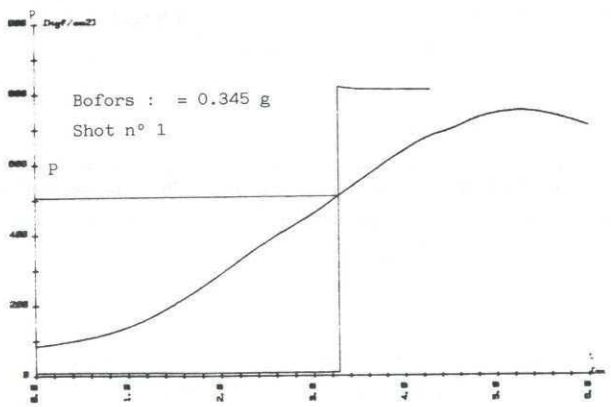

Fig.3:Determination of the departure pressure

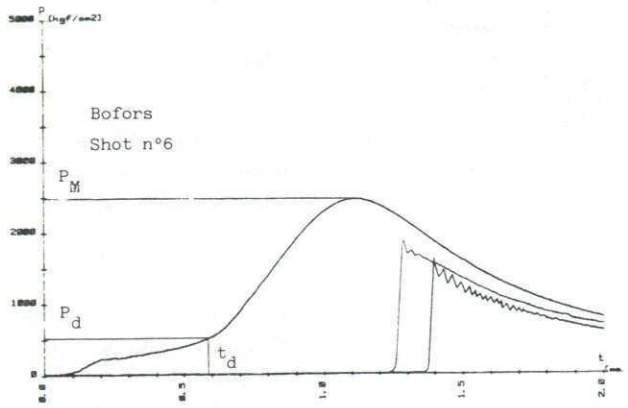

Fig.4:Simultaneous (P,t) recordings in different points of the barrel.

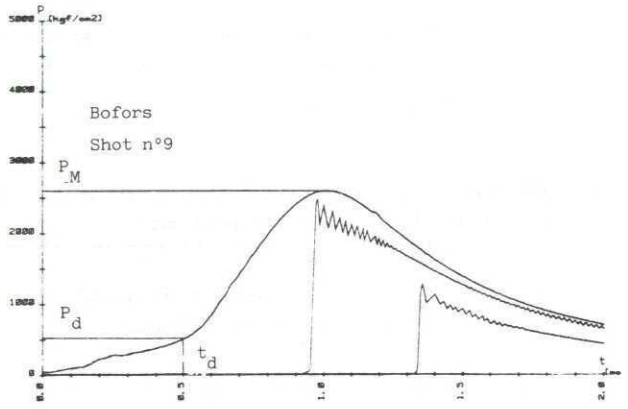

Fig.5

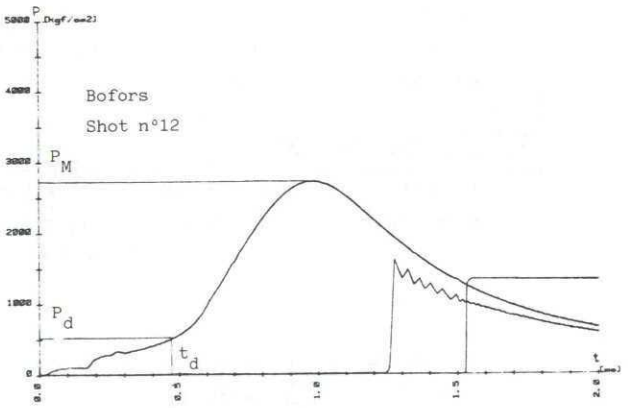

Fig.6

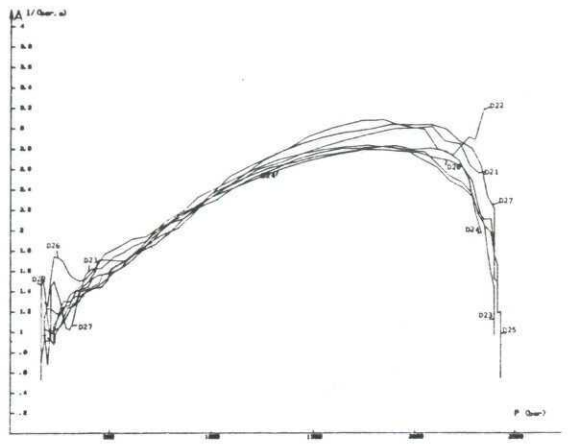

Fig.7: A=f(P) with ball powder BP418

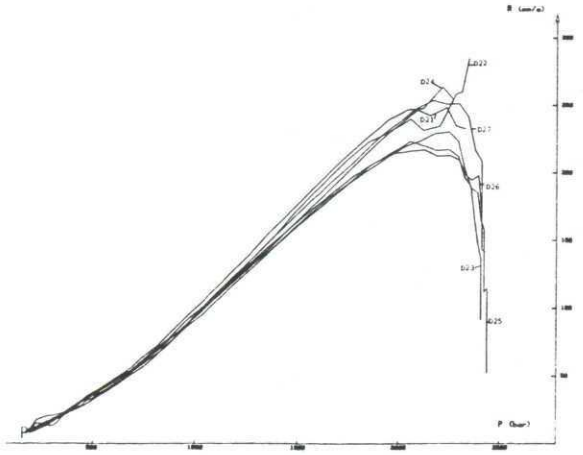

Fig.8: r=f(P) with ball powder BP418

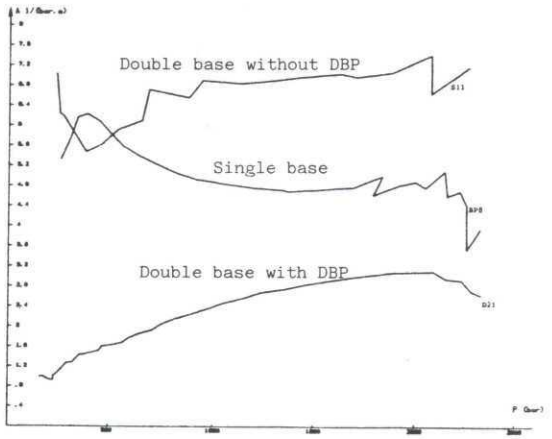

Fig.9: A=f(P)

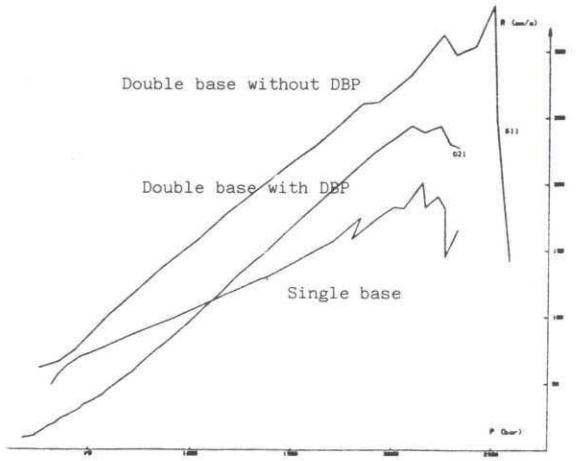

Fig.10: r=f(P)

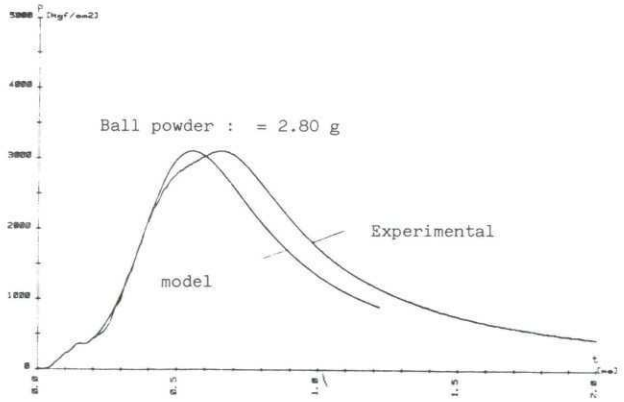

Fig.11: P=f(t)

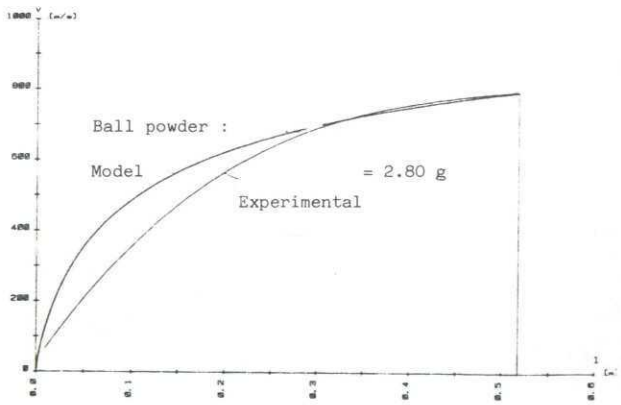

Fig.12: V=f(l)

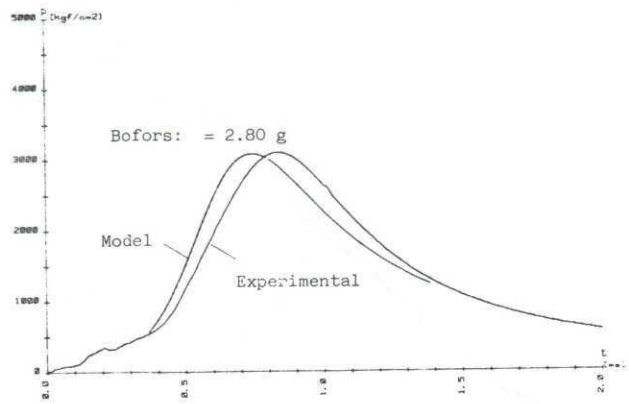

Fig.13

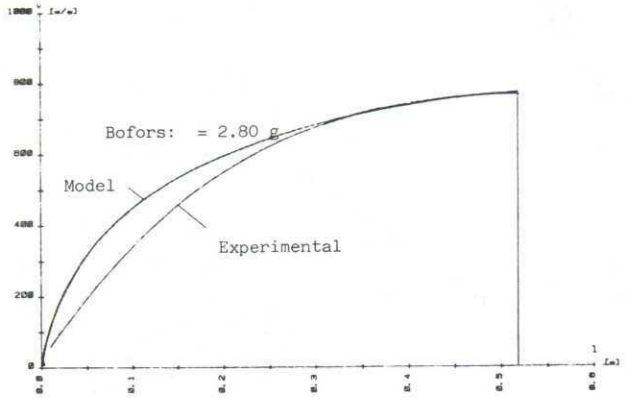

Fig.14

Fig.15: P=f(t) after fitting.

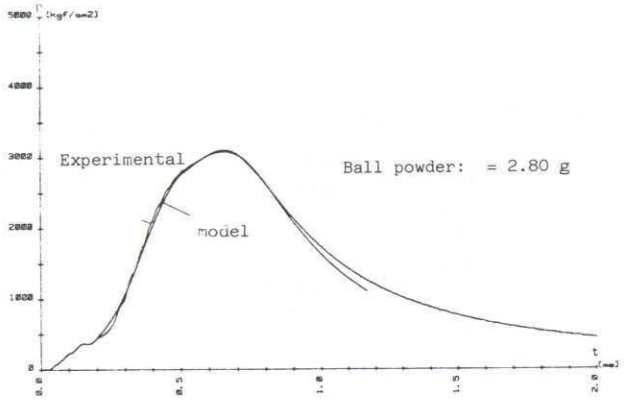

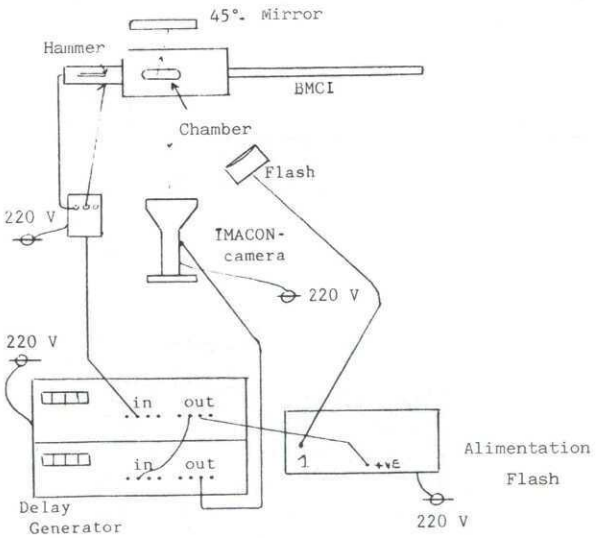

Fig.16: Experimental equipment with IMACON

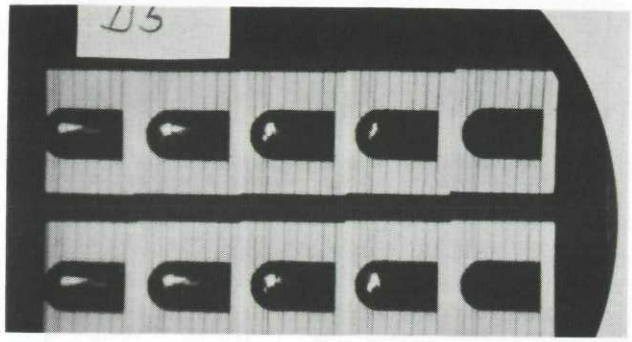

Fig.17

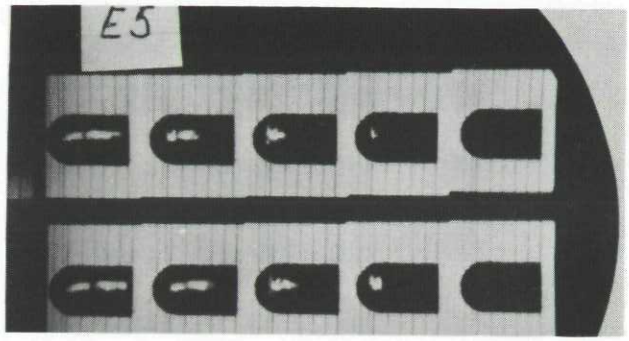

Fig.18

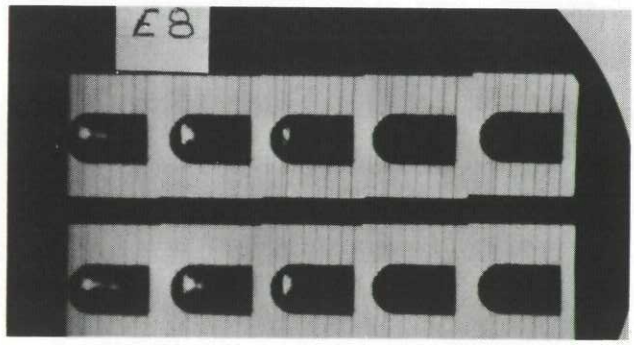

Fig.19

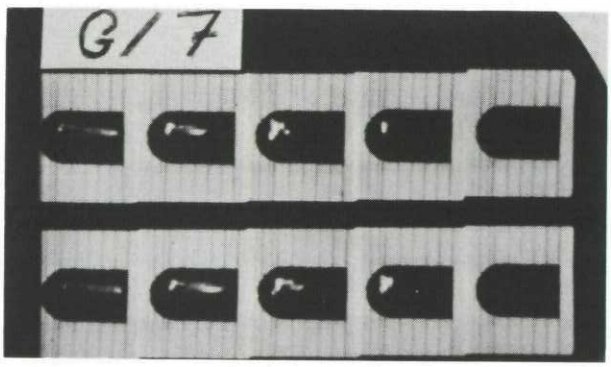

Fig.20

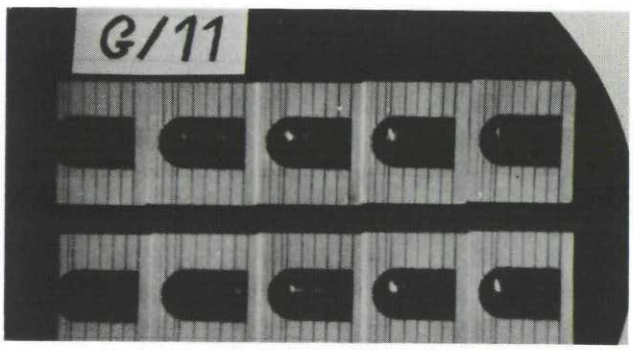

Fig.21

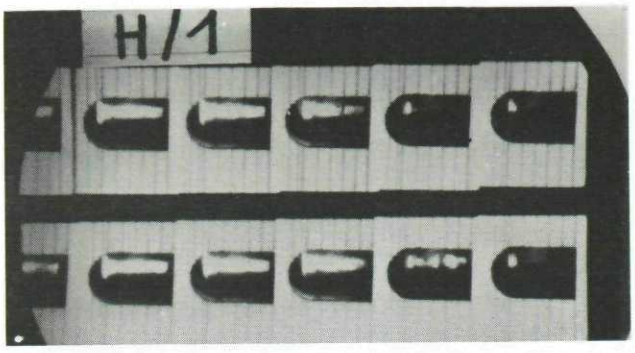

Fig.22

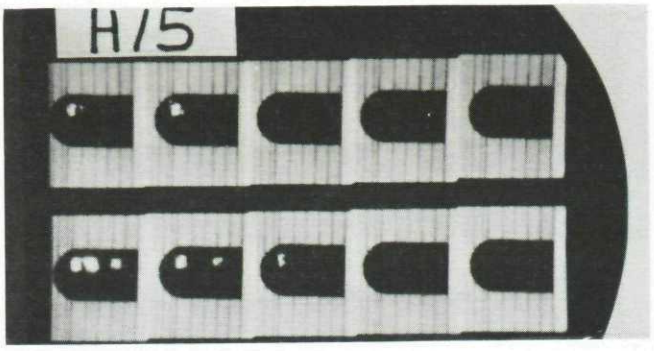

Fig.23

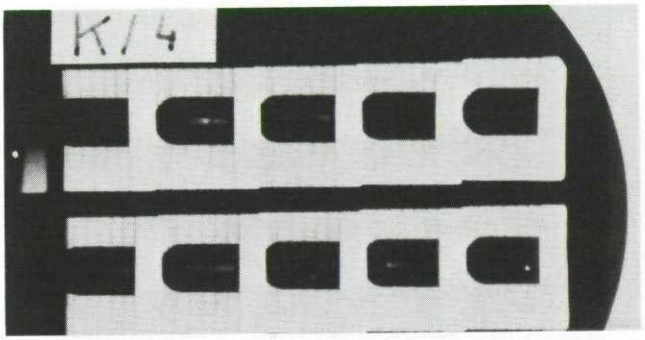

Fig.24

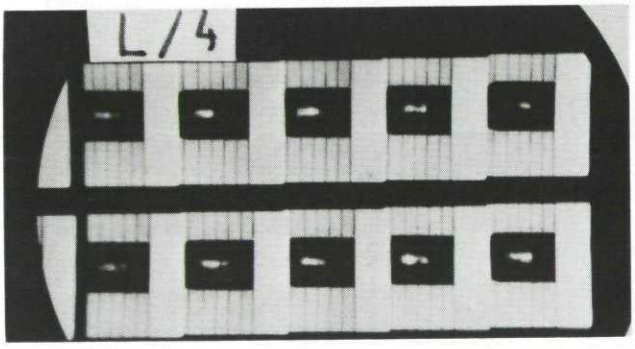

Fig.25

References.

1. STUDIE van de Inwendige Ballistiek van kleine wapens
   Final course work – 1981-1982 – Royal Military Academy (BE)
   OLt ROBBERECHT H. and OLt LECOCQ D.

2. STUDIE van de exploitatiemogelijkheden van een drukmeetketen toegepast op een klein-kaliber wapen.
   Final course work – 1982-1983 – Royal Military Academy (BE)
   OLt THIRY J.P.

3. STUDIE over de experimentele bepaling van de ballistische parameters van een propulsief kruit.
   Sep 83 - Eindstagewerk IMM - Munitie Arsenaal - Zwijndrecht (BE)
   Lt Ir D. HEMERYCK.

4. Ballistische parameters van kruit voor klein-kaliberwapens.
   Final course work – 1982-1983 – Royal Military Academy (BE)
   OLt DEWILDE K.

5. Technisch verslag van een experimentele studie van de werking van diverse types slaghoedjes.
   INTERN TECHNISCH VERSLAG - DEPARTMENT ARM & BAL.
   ROYAL MILITARY ACADEMY - APRIL 1985.

ETUDE EXPERIMENTALE DE L'ALLUMAGE D'UNE CHARGE PROPULSIVE PAR VISUALISATION DU PHENOMENE

Par Monsieur Claude BERTHOMMIER - ETABLISSEMENT TECHNIQUE DE BOURGES - Route de Guerry - Boite postale N° 712 - 18015 BOURGES Cedex - TEL. (48) 50.52.75.

RESUME

Dans le but de mieux connaître les phénomènes liés à l'allumage et à la combustion d'une charge propulsive pour munition de gros calibre, 3 dispositifs de visualisation ont été mis au point. Cette visualisation est rendue possible par la présence d'une douille translucide qui joue le rôle de la chambre du canon.

Le traitement des relevés expérimentaux fournis par les moyens de mesure permet d'atteindre la connaissance des grandeurs physiques (pression, déplacement et vitesse du front de flamme) au début de la combustion.

Il permet également de différencier des systèmes d'allumage et de comparer diverses configurations de charge. Deux exemples sont développés : le premier avec la comparaison de 2 allumeurs et le second sur un allumage programmé (programmation temporelle et spatiale, les points actifs de l'allumeur étant disséminés dans la charge).

DETAIL DE L'ETUDE EXPERIMENTALE

1) BUT DE L'ETUDE :

Cette étude a été développée afin de mieux connaître les phénomènes liés à l'allumage des poudres propulsives dans les munitions :

- de char (notamment à projectile flèche).
- d'artillerie de 155 mm

Elle doit permettre :

- la visualisation de l'allumage
- la détection des mouvements éventuels de grains de poudre
- l'amélioration de la connaissance des différents paramètres balistiques
- l'évaluation des contraintes subies par le projectile au départ du coup

La réalisation de ce programme s'est déroulée en 3 étapes :

- Simulateur 1 : dispositif simple sans projectile, calibre 105 mm (faisabilité)
- Simulateur 2 : appareillage avec départ de projectile, calibre 105 mm
- Simulateur 3 : simulateur pour charges de 155 mm

La visualisation est rendue possible par la présence d'une douille translucide en fibre de verre qui joue le rôle de la chambre du canon et qui se rompt à une pression d'environ 100 MPa pour une épaisseur de 10 mm.

2) SIMULATEUR 1

a) Description (planche 1)

Il est constitué essentiellement d'un bati métallique suffisamment robuste pour assurer l'étanchéité de la douille et qui reproduit la partie chambre de combustion du canon de 105 mm avec son système de mise à feu.

b) Instrumentation

- Cinématographie rapide : caméra 8000 images/seconde permettant de visualiser le développement de la flamme dans la douille.
- Radiographie éclair : deux clichés pendant la phase d'llumage, ceux-ci sont déclenchés par le premier mouvement des grains de poudre qui actionnent un contact (rupture d'une tige graphite). Ils permettent d'évaluer les instants de début de déplacement et les mouvements du lit de poudre.
- Pression piézoélectrique : sur une génératrice et au sommet de la douille, celle-ci donne l'allure de la montée en pression à l'intérieur de la charge.
- Synchronisation : de tous les moyens de mesure pour établir la chronologie des évènements.

3) SIMULATEUR 2

a) Description (Planche 1)

Il est composé à partir du 1er dispositif auquel sont adjoints :

- une partie représentative du début de l'âme rayée du canon de 105 mm
- un système destiné à guider et amortir le projectile après son démarrage.

b) Instrumentation

En plus des moyens décrits pour le simulateur 1, le freinage progressif du projectile permet son instrumentation :

- capteur de pression au culot
- accéléromètre
- vélocimétrie du projectile par la caméra

On notera que le départ du coup est reproduit fidèlement.

4) SIMULATEUR 3

Il est identique dans sa conception au simulateur 1 mais il reproduit la configuration des canons de 155 mm avec allumage soit par étoupille soit par système à induction.
L'instrumentation est celle du simulateur 1.

COMPARAISON DE 2 ALLUMEURS - EXEMPLE 1 -

1) DESCRIPTION

- le dispositif utilisé est le simulateur 2 (calibre 105 mm avec départ de projectile)
- le chargement propulsif est composé de poudre B
- allumage : **1er CAS** allumeur métallique avec poudre noire
  2ème CAS allumeur combustible à cordeau détonant et poudre noire

2) RESULTATS

a) Progression du front de flamme (Planche 2)

- 1er cas : l'allumage s'effectue tout d'abord en bas de la douille puis progresse lentement vers le haut (vitesse du front de flamme ≃ 300 m/s).
- 2ème cas : l'allumage s'effectue simultanément dans les 2/3 de la douille.

b) Développement de la pression (Planche 3)

- 1er cas : la pression apparait en premier au bas de la douille; la pression au culot du projectile augmente plus vite et dépasse même la pression en bas : c'est la mise en évidence d'ondes de pression.
- 2ème cas :la montée en pression se fait uniformément jusqu'à la rupture de la douille.

c) Accélération du projectile (Planche 3)

On notera la différence d'allure des courbes d'accélération :

- 2éme cas: l'accélération évolue régulièrement d'une manière homothétique à la pression des gaz
- 1er cas: Le surplus d'accélération est probablement dû au choc des grains de poudre sur le culot du projectile : en effet les radiographies de la planche 2 indiquent un mouvement des grains de poudre (vitesse des grains supérieurs d'environ 100 m/s).

3) ANALYSE

Les résultats précédents montrent clairement la différence de fonctionnement des 2 allumeurs. A l'évidence, l'allumeur 2 donnera les résultats balistiques les plus satisfaisants : meilleur développement de la pression et contraintes minimales pour le projectile.

ALLUMAGE PROGRAMME - EXEMPLE 2 -

1) DESCRIPTION

- le dispositif utilisé est le simulateur 1 (sans projectile)
- la douille en fibre de verre est remplaçée par une douille en polycarbonate se rompant à une pression de 300 bars.
- le chargement propulsif est composé de poudre B
- l'allumage est effectué par 6 petits allumeurs placés en 3 points de la charge (voir schéma ci-dessous.

1er CAS : l'allumage est simultané aux 3 emplacements

2ème CAS : l'allumage est fait de la manière suivante

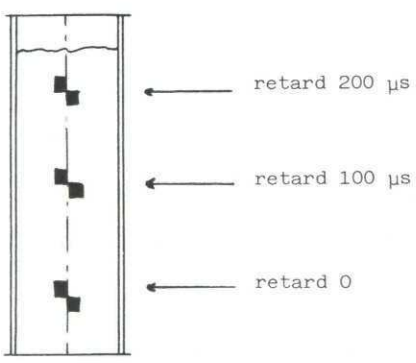

2) RESULTATS (Planche 4)

- 1er Cas : la simultanéité du fonctionnement des allumeurs est vérifiée sur les radiographies
- 2ème Cas : On distingue sur la planche 4 les allumages successifs et la progression du front de flamme qui en découle.

Cet exemple simple montre la possibilité d'étudier le comportement à l'allumage et la combustion de charges propulsives allumées d'une manière programmée.
(allumage en tête de charge, décalé dans le temps, avec des produits plus ou moins violents).

CONCLUSION

Les deux exemples précédents montrent à quel point ce moyen d'investigation en balistique intérieure est puissant. En effet, il apporte la connaissance de l'évolution de la plupart des grandeurs physiques au début de la combustion :

- pression dans la chambre et au culot du projectile
- progression du front de flamme
- déplacement éventuel du lit de poudre
- mouvement du projectile (déplacement, vitesse, accélération, contrainte, pression de forcement)
- corrélation des différents phénomènes

La connaissance de ces paramètres est également importante pour la validation des codes de calcul en balistique intérieure.

REFERENCES

- Note DAT/ETBS/CETAM N° 140/CT/CdB/80 - Dispositif expérimental d'étude de l'allumage d'une charge propulsive de gros calibre : définition du besoin.

- Procés verbaux d'essais DAT/ETBS/CE EBAI N° 129 du 10/11/81 et n° 144 du 6/09/83.

Cette étude a été conduite en collaboration avec les Etablissements GIAT/EFAB et SNPE/CRB.

PLANCHE 1

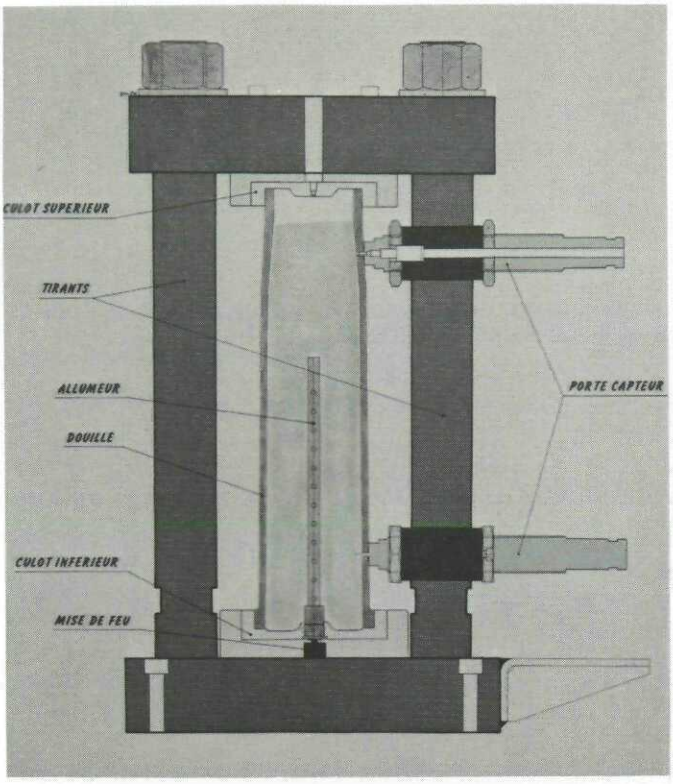

Fig. 1

Fig. 2

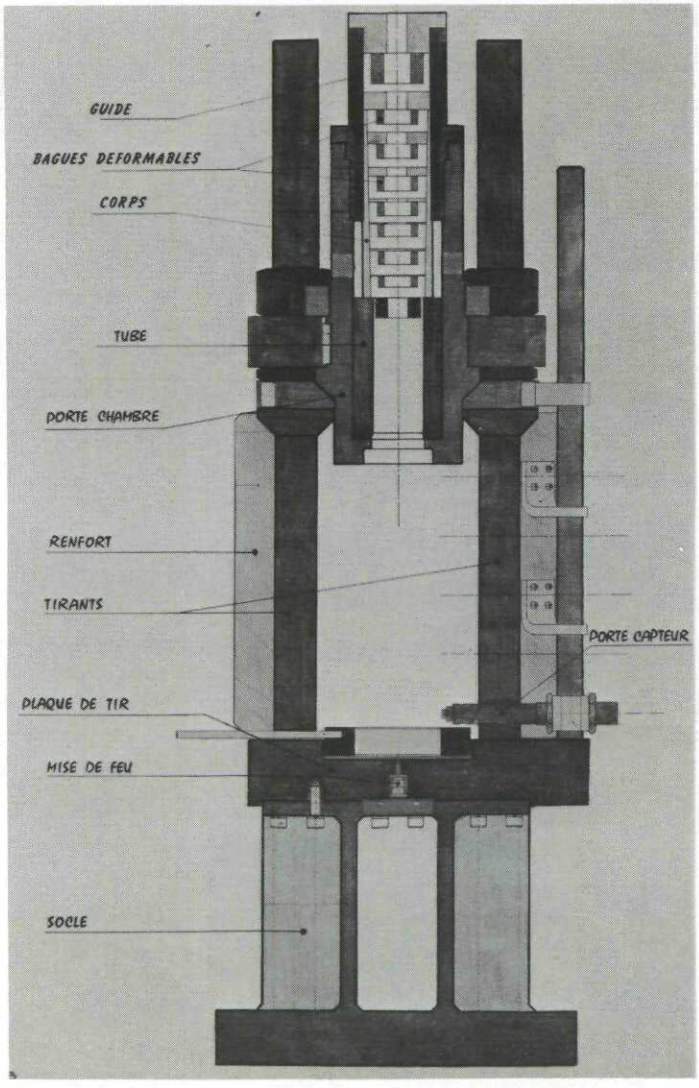

Fig. 3

Fig. 1 : Schéma du simulateur 1 (105 mm sans projectile).

Fig. 2 : Photo du simulateur 1 avec douille plexiglas (rupture à une pression de 30 MPa).

Fig. 3 : Schéma du simulateur 2

PLANCHE 2 - EXEMPLE 1 -

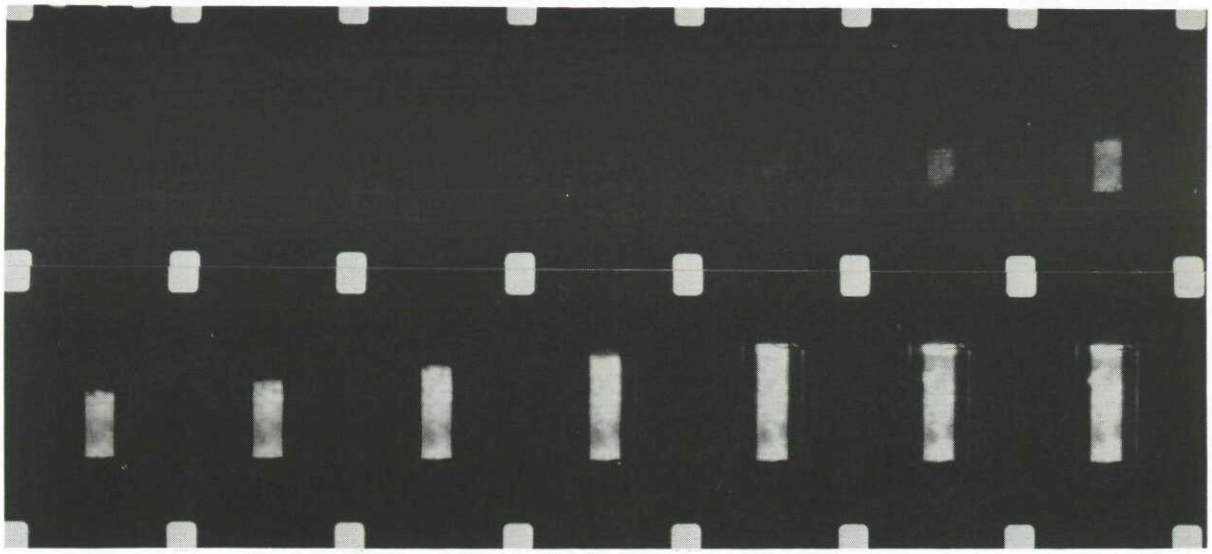

Progression du front de flamme : 1er cas

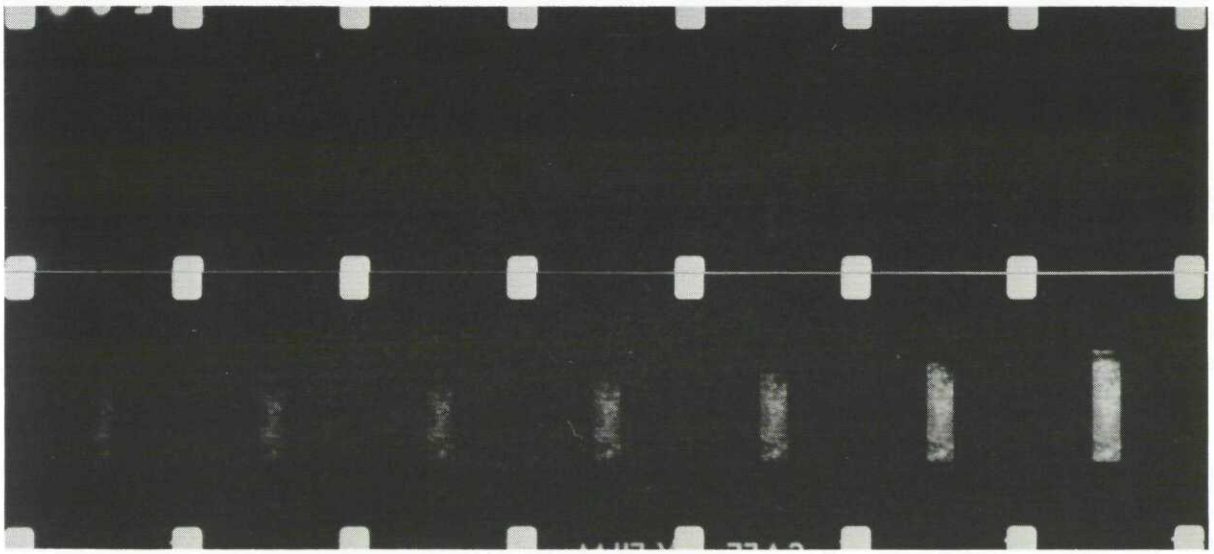

Progression du front de flamme : 2ème cas (0,12 ms entre 2 images)

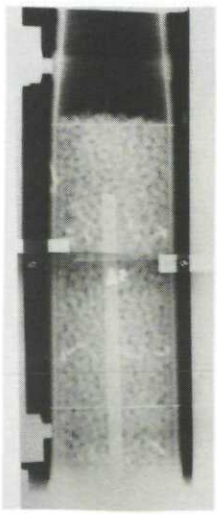

repos

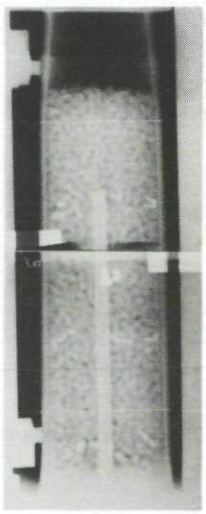

1er cliché

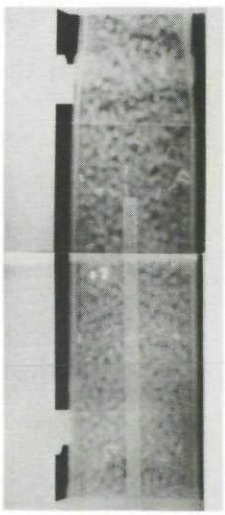

2ème cliché

Radiographies pendant l'allumage :
le mouvement des différentes couches
est repéré par des grains marqués

PLANCHE 3 - EXEMPLE 1 -

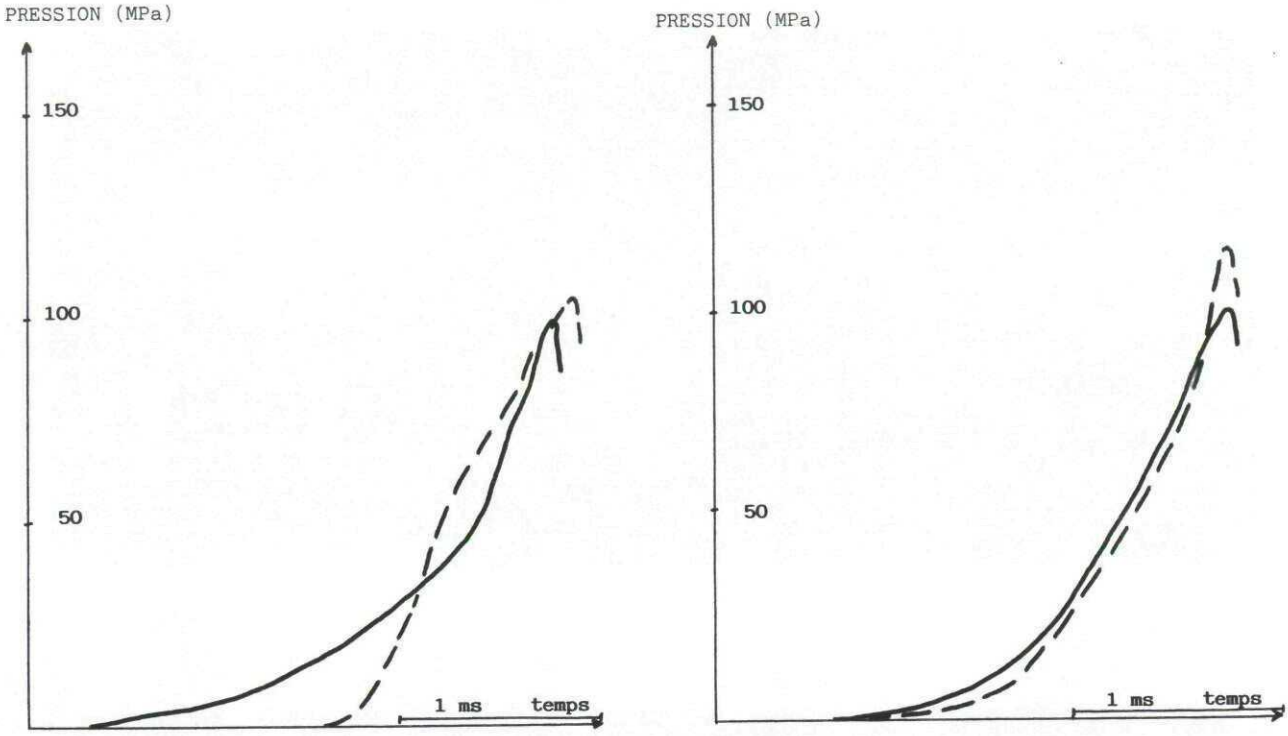

DEVELOPPEMENT DE LA PRESSION

1ER CAS

2ème CAS

Pression en bas de la douille

Pression au culot du projectile

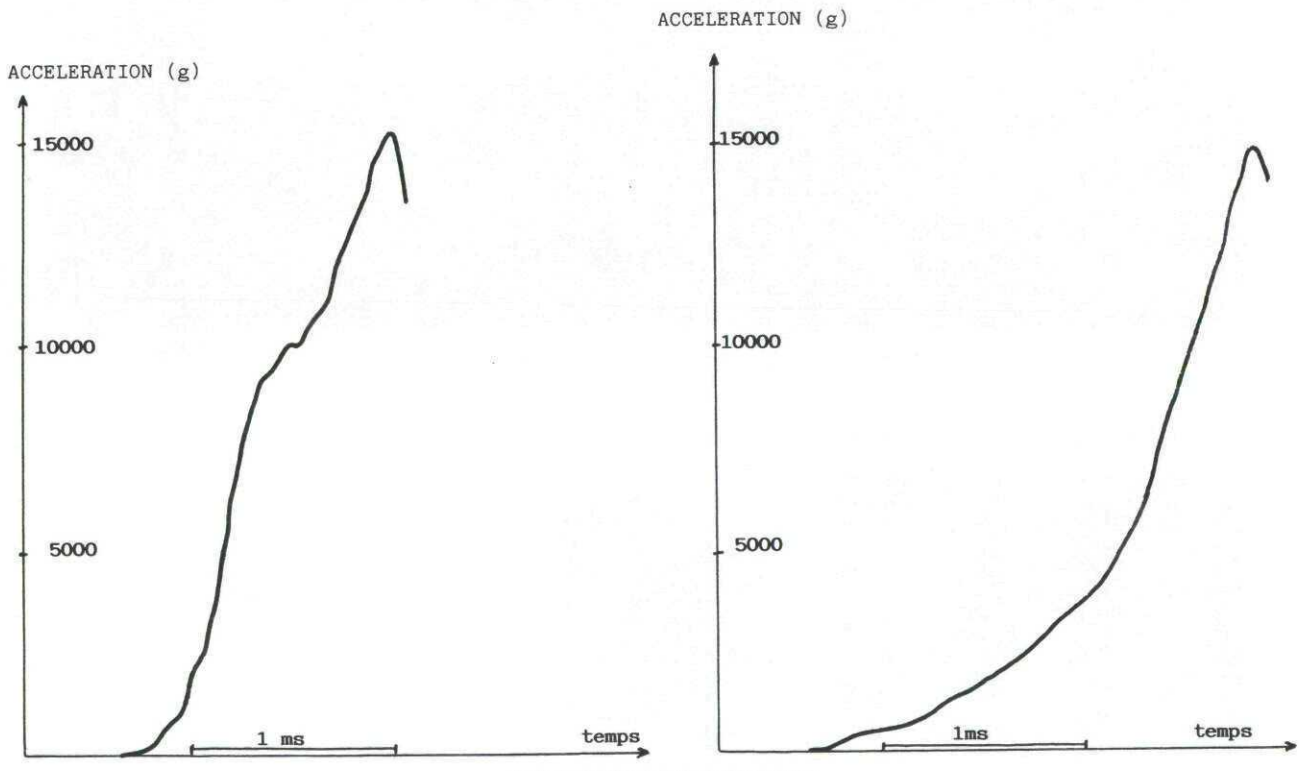

ACCELERATION DU PROJECTILE

1ER CAS

2ème CAS

PLANCHE 4 - EXEMPLE 2 -

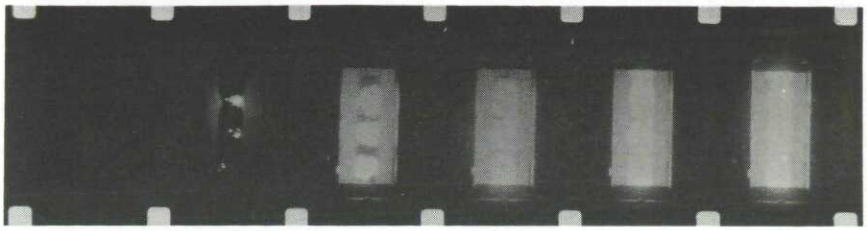

Progression du front de flamme : 1er cas, allumage simultané (0.17 ms entre 2 images)

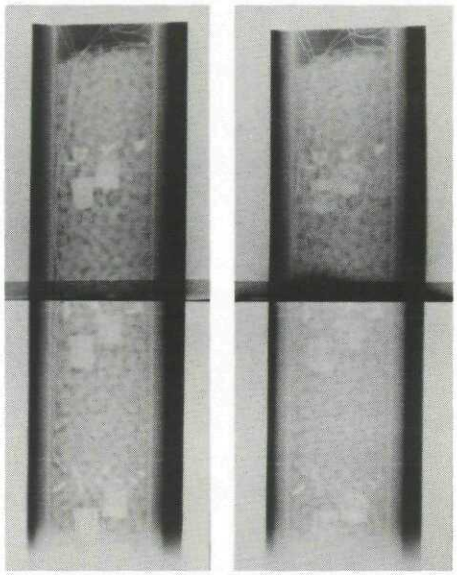

Radiographie pendant l'allumage, 1er cas.

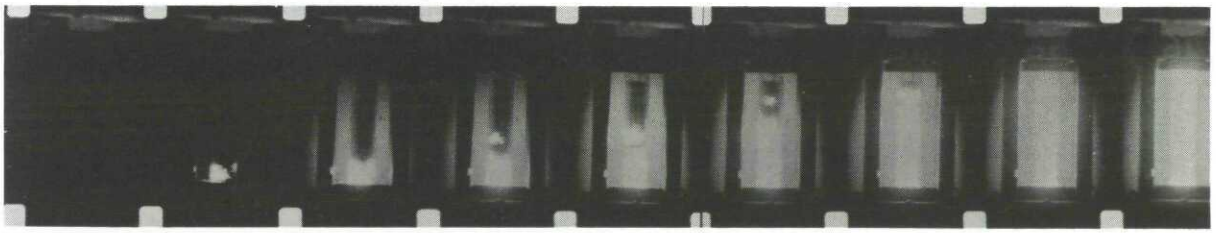

Progression du front de flamme : 2ème cas, allumage décalé (0.17 ms entre 2 images)

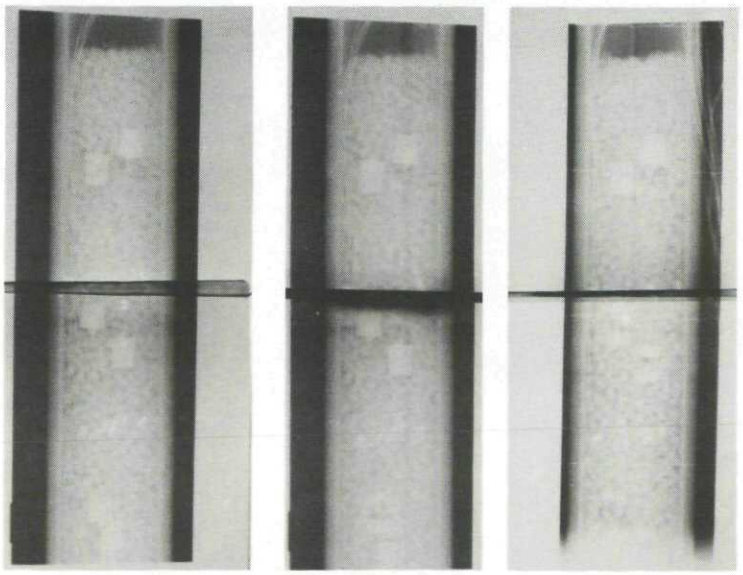

Radiographie pendant l'allumage
2ème Cas.

repos 1er cliché 2ème cliché

MEASUREMENT OF IMPORTANT BALLISTIC FLOW PROPERTIES BY SPECTROSCOPIC TECHNIQUES

Guenter Klingenberg

Fraunhofer-Institut für Kurzzeitdynamik, Ernst-Mach-Institut,
Abteilung für Ballistik (EMI-AFB), Hauptstrasse 18, D-7858 Weil am Rhein

SUMMARY

Considerable progress has been made in recent years in probing the gun interior ballistic cycle and the subsequent muzzle flow dynamics. With the amount of experimental research done, more detailed information has now been obtained to describe the many complexities of the flow phenomena which are associated with the discharge of a weapon. A survey of some of the experimental research is reviewed in this paper pointing out the capabilities as well as the limitations and constraints encountered in ballistic environments. The experimental diagnostics described includes spectroscopic techniques for measuring the temperature and gas velocity in reacting two-phase flows produced by the combustion of both solid and liquid propellants. These techniques are the emission and/or absorption methods, reversal and Abel inversion methods, and laser Doppler spectrometry. In particular, a novel intrusive emission gauge technique is described which permitted the thermometric probing of optically thick propellant gases in highly pressurized combustion chambers. Sample results of these measurements will be presented. In addition, efforts directed towards the adequate simulation of reacting ballistic flows by means of a gas gun simulator are described.

I. INTRODUCTION

In present day high performance gun systems, more information is required to understand important ballistic flow phenomena. The need to solve problems such as gun tube wear and erosion or muzzle blast and flash calls for a detailed and firm understanding of the physical and chemical processes that take place during the discharge of gun tube weapons. However, the complex interactions between the particle-laden flows and the chemical reactions occurring inside the bore and within the muzzle exhaust region impede severely the theoretical and experimental analysis [1,2,3]. Various numerical and analytical theoretical simulations of the gun interior ballistic flow and subsequent muzzle flow dynamics have been calculated in the past achieving much progress in the prediction of non-reacting single and two-phase flows [1,2,4]. However, there is no theoretical model available that describes all the details of realistic interior and transitional ballistic cycles. Existing numerical and analytical calculations have to rely on idealization of the flow in order to obtain solutions. These model solutions and the underlying assumptions are often inadequately verified by experiments, if at all. On the other hand, the salient probing of realistic ballistic flows, for other than routine pressure measurements, is limited as well by the harsh enrivonments encountered in real gun firings [1,3].

A critical assessment of the state-of-the-art of interior ballistic research, presented at the Sixth International Symposium on Ballistics in 1981 by Klingenberg and Banks [1], has identified major research gaps. Also, areas for future studies have been recommended. Recognizing that severe limitations and constraints are inherent in both the computational capabilities and the present day experimental techniques, recommendations have been made to pursue more well-controlled "benchmark" experiments and to develop computational methods interactively with these simulation experiments. If was proposed to perform the benchmark validation experiments on simulators that permit the generation of well-defined, well-controlled simplified flows beginning with one-phase, inert flows and advancing in stepwise fashion to more complex two-phase, reacting flows. Also, it was anticipated that the successful completion of these research efforts will allow one to isolate, identify, and understand important flow phenomena and enhance the chances of successfully modelling the physical events that occur in real ballistic flows.

The above recommendations have led to a resurgance of fundamental ballistic flow research and initiated simulation experiments that are presently under way at several European institutions [5,6]. These research efforts are summarized in Table 1. Simulations of reacting flows by means of a gas gun are under way at the Fraunhofer-Institute EMI-AFB (Ernst-Mach-Institut) and are based on the work of Lord [7]. This research program has been made possible through the support and sponsorship of the U.S. Government through its European Research Office of the U.S. Army. Since the gas gun is driven by the combustion of a prepressurized mixture of hydrogen and oxygen diluted with helium and, therefore, deals with simple gas phase chemistry, the gas gun simulator is expected to be an appropriate tool for the reproducible simulation of reacting gun interior and transitional ballistic flows [5,8]. A description of this simulation project concludes the present paper.

The main part of this paper is, however, concerned with the measurement of important ballistic flow properties by spectroscopic techniques. It reviews ballistic flow studies that have been conducted in the harsh environment of real gun firings or closed

SIMULATION EXPERIMENTS

INSTITUTE (COUNTRY)	FACILITY	MAXIMUM PRESSURE (MPa)	MAXIMUM TEMPERATURE (K)	FLOW STATUS	FLOW GOAL
IMPERIAL COLLEGE (UK)	COMPRESSION CHAMBER	0.9	——	INERT TWO PHASE	
INSTITUTE SAINT-LOUIS (FR/GR)	SHOCK TUBE	1.5 - 20	3000	INERT ONE PHASE	REACTING TWO PHASE
INSTITUTE SAINT-LOUIS (FR/GR)	LIGHT GAS GUN	350 - 400	3000	INERT ONE PHASE	INERT TWO PHASE
ERNST MACH INSTITUTE (GR)	GAS GUN	350 - 450	3000	REACTING ONE PHASE	REACTING TWO PHASE

Table 1: European Ballistic Simulation Experiments

bombs. To avoid unnecessary repetition, only the studies performed subsequently to the review by Klingenberg and Banks [1] will be covered in this paper. A novel intrusive emission gauge technique is described that permitted propellant gas temperature to be evaluated from emission data taken at discrete locations within the (a) combusting solid propellant charge of a 20-mm gun chamber [9,10,11,12], (b) radiating gun muzzle exhaust flow [3,13], and (c) combusting liquid monopropellant charge of a closed chamber [14,15]. Supplementary infrared emission measurements, performed inside the bore of the 20-mm gun tube, and emission-absorption measurements in the 20-mm gun muzzle exhaust flow yielded the complete temperature history of this particular gun system from ignition to shot ejection [6,16]. Beside of these spectroscpic techniques, reversal and Abel inversion techniques have been applied by Mach et al. and Klingenberg to measure temperature distributions in the muzzle flash of a caliber 7.62 mm gun [3,12,13,17,18,19]. 20-mm gun tube boundary layer studies by Mach [20] included the measurement of the temperature gradient that develops at the inner gun tube wall [20]. Gas temperature and convective heat flux in a reacting granular propellant bed of a large caliber Navy gun were determined by McLure [21] using an intrusive multi-wavelength pyrometer probe [21]. The novel laser-Doppler spectrometer, devised by Smeets [22,23,24], has been shown by Mach and coworkers [17,18,19,20,25-29] to be appropriate for the measurement of flow velocities of particle-laden ballistic flows. Some of this research work will be reviewed in greater detail pointing cut the capabilities as well as the limitations encountered in ballistic environments. It will be shown that the application of spectroscopic techniques is severely impeded by the extreme high opacity and/or the complex nature of the gun interior and transitional ballistic flow. The outcome of this experimental research stresses the importance of an appropriate simulation of the ballistic events. Prior to the description of these spectroscopic methods and to the presentation of sample results, the fundamentals of the spectroscopic methods for measuring gas temperature are presented.

II. FUNDAMENTALS

The use of emission and/or absorption spectroscopy for measuring gas temperature in radiating flows is a well-known and widely exploited technique. Excellent monographs by Tourin [30] and Roessler [31] cover this subject in detail. Since techniques based on emission/absorption measurements provice much higher signal levels than other laser-based methods, such as CARS (Coherent Anti-Stokes Raman Scattering), Raman or laser-induced fluorescence, they have been preferably used in ballistic flow studies. These emission and/or absorption methods include the (a) intrusive emission gauge technique (single-point emission measurement), (b) optical pyrometry (emission measurement), modified reversal method (emission and absorption measurements along a given optical path through the medium), and Abel inversion techniques [3]. In the cases (a) and (b), an optically thick medium is required to evaluate gas temperature from emission measurements. The main difficulty with the modified reversal method is its inability to provide spatially resolved measurements, since it yields only an average temperature along the given optical path. Therefore, the data evaluation presents difficulties, if gradients in the emitter concentration and temperature are encountered. Abel inversion of emission and absorption measurements along parallel lines-of-sight at various lateral distances from the center to the outer diameter of a cross-section through the flow field are required to provide information on two-dimensional temperature profiles. However, this technique is limited to flow fields of suitable axisymmetric properties. Optical tomography [32], a multi-angular absorption method, has the potential of measuring cross-sectional temperatures and species concentration even in highly non-symmetric flows giving a spatially resolved two-dimensional property field. Its feasibility in ballistic flows remains, however, to be demonstrated.

A. Radiation Laws

The above emission and/or absorption methods are based on the fundamental radiation laws [30,31]. In differential form, the spectral radiance, L_λ, of a source of temperature, T, emitted by this source per unit spectral wavelength, $\Delta\lambda$, per unit area of the source, ΔA, per unit solid angle, $\Delta\Psi$, about the source, per unit angle δ of the emitted beam is given by [30]:

$$L_\lambda(T) = \frac{\partial^3}{\partial\lambda\,\partial A\,\partial\Psi\cos\delta} \qquad (1)$$

When a radiant beam of spectral radiance, L_λ, is incident upon a medium, it can be attenuated by absorption, reflection, and scattering. If no scattering occurs, the fractions of an incident beam, which are absorbed, transmitted and reflected, are defined as spectral absorptance, $a_\lambda(T)$, spectral transmittance, $\tau_\lambda(T)$, and spectral reflectance, $r_\lambda(T)$. Evoking conservation of energy yields [31]:

$$a_\lambda + \tau_\lambda + r_\lambda = 1 \qquad (2)$$

where the subscript λ is used for denoting a function of wavelength, as customary in the field of optical spectroscopy [30].

A thermal radiator is a source in thermal equilibrium which emits radiation solely because of its temperature. The thermal radiator is called a "blackbody" if it absorbs all of the incident radiation [30], i.e., $a_\lambda(T) = 1$, and $\tau_\lambda(T)$, $r_\lambda(T) = 0$. At any wavelength λ, the spectral radiance of a blackbody, $L^b_\lambda(T)$, is given by the radiation law of Planck or by Wien's approximation:

$$L^b_\lambda(T) = c_1/\lambda^5[\exp(c_2/\lambda T)-1]^{-1} \text{ (Planck)} \quad \approx c_1/\lambda^5[\exp(c_2/\lambda T)]^{-1} \text{ (Wien)} \qquad (3)$$

where c_1, c_2 are the well-known radiation constants [30,31]. Wien's approximation is found to be accurate within 1 % for values of $T < 3000$ [μmK]. Therefore, this approximation is applicable in ballistics, since frequently $T < 3000$ K, and $\lambda < 1$ μm.

For a non-blackbody thermal radiator, the emitted spectral radiance, $L_\lambda(T)$, is related to that of a blackbody through its spectral absorptance, $a_\lambda(T)$, i.e., Kirchhoff's law [30,31]:

$$L_\lambda(T) = a_\lambda(T)\, L^b_\lambda(T) \qquad (4)$$

Therefore, if the spectral radiance and absorptance along a given optical path through the test medium is measured, the temperature can be evaluated using equation (4). However, an estimate on gas temperature can be also made, if only the spectral radiance, L_λ, is measured. This value approximates the true gas temperature, T, if the absorptance is so high that blackbody conditions are reached, i.e., $a_\lambda(T) \to 1$.

B. Brightness Temperature

In practice, the radiation source is characterized by the "brightness" temperature, $T_S(\lambda)$. For a given wavelength λ, the brightness temperature, $T_S(\lambda)$, is defined such that a blackbody at the brightness temperature $T_S(\lambda)$ has the same "brightness" or spectral radiance L^b_λ as the spectral radiance L_λ of the investigated source at the temperature T and the same wavelength λ, i.e.,

$$L_\lambda(T) = L^b_\lambda\,[T_S(\lambda)] \qquad (5)$$

With Wien's and Kirchhoff's equation, we obtain [3,31]:

$$\frac{1}{T} = \frac{1}{T_S(\lambda)} + \frac{\lambda}{c_2}\ln a_\lambda(T) \qquad (6)$$

which relates the gas temperature T of the radiation source to its brightness temperature $T_S(\lambda)$ and absorptance $a_\lambda(T)$. The brightness temperature is related to that of a calibrated source for which spectral radiance, L^*_λ, and brightness temperature, $T^*_S(\lambda)$, are known [31], by

$$1/T_S(\lambda) = 1/T^*_S(\lambda) - \lambda/c_2 \ln [L_\lambda(T)/L^*_\lambda(T)] \qquad (7)$$

Optical pyrometers which measure the brightness temperature are based on this equation.

C. Reversal Method

In the reversal method, applied to spectral lines, bands or continuum, an average temperature along some optical path through the medium is determined by measuring both the spectral radiance or emission and the absorptance along this path. In principal, the reversal technique is a null or balancing method. In its simplest form, the brightness temperature, $T_S(\lambda)$, of a background source is adjusted until the spectral radiance, L_λ, of the flame appears neither in absorption against the background source nor in emission superposed on the continuum emitted by the background source. It can be shown that at this reversal point the flame temperature, T, is the same as the brightness temperature,

$T_S(\lambda)$, of the background source. If we define $L_\lambda^1 = L_\lambda^b[T_S(\lambda)]$ as the spectral radiance of the backlight source, $L_\lambda^2 = [1-a_\lambda(T)]L_\lambda^b(T)$ as the spectral radiance of the non-absorbed radiation of the backlight source after it has passed the flame, and L_λ^3 as the spectral radiance emitted by the flame, we obtain

$$a_\lambda(T)\ L_\lambda^b(T) + [1-a_\lambda(T)]\ L_\lambda^b(T) = L_\lambda^b[T_S(\lambda)] \tag{8}$$

or

$$L_\lambda^b(T) = L_\lambda^b\ [T_S(\lambda)],\ \text{i.e.,}\quad T = T_S(\lambda) \tag{9}$$

Thus, the flame temperature is obtained by measuring the brightness temperature of the background source at the reversal point with a pyrometer.

However, in transient flows, a modified reversal technique is required which permits an approximate determination of the reversal point [3]. In this technique, the radiant flux with and without superimposed radiation of a background source is recorded photoelectrically, and the spectral radiances L_λ^2 and L_λ^3 are measured alternately by chopping the beam of the background source. The spectral radiance, L_λ^1, of the background source is determined before or after the flow occurs. Its brightness temperature is given, if we use a calibrated lamp such as a tungsten ribbon lamp [3]. Otherwise, we have to determine $T_S(\lambda)$ by means of an optical pyrometer. There we obtain the temperature from [3,31]:

$$1/T = 1/T_S(\lambda) + \lambda/c_2\ \ln\ [(L_\lambda^1 - L_\lambda^2)/L_\lambda^3] \tag{10}$$

with

$$a_\lambda(T) = (L_\lambda^1 - L_\lambda^2)/L_\lambda^3,\quad \text{or}\quad \tau_\lambda = L_\lambda^2/L_\lambda^1 \tag{11}$$

The error of the modified reversal method is particularly determined by the difference between T and $T_S(\lambda)$ and the emitter concentration expressed in terms of $a_\lambda(T)$:

$$|\Delta T/T| = [1/T - 1/T_S(\lambda)]^{1/2}/a_\lambda(T) \tag{12}$$

i.e., the error is small, if the brightness temperature of the background source is well adjusted to the flame temperature and a higher emitter concentration is present in the investigated gas volume [3].

D. Abel Inversion Technique

In radiating gases, the modified form of Kirchhoff's law can be used [31], i.e.,

$$L_\lambda^b(T) = \varepsilon_\lambda^*(T)/a_\lambda^*(T) \tag{13}$$

where ε_λ^* (W/cm^{4}ster) is the emission coefficient, and a_λ^* (cm^{-1}) is the absorption coefficient. These values are obtained from emission/absorption measurements which yield the optical thickness, D_λ, and the spectral radiance, L_λ, along a given optical path, ℓ, through the test section. The spectral absorptance, a_λ, spectral transmittance, τ_λ, and the optical thickness, D_λ, are given by [31]:

$$a_\lambda = 1 - \tau_\lambda = 1 - e^{-a_\lambda^*\ell} \tag{14}$$

$$D_\lambda = a_\lambda^*\ell = -\ln\ \tau_\lambda \tag{15}$$

The optical thickness, $D_\lambda(T)$, increases with the pathlength, ℓ, and the spectral absorption coefficient, $a_\lambda^*(T)$, which, in turn, is dependent upon the density of the absorbing chemical species and/or particles present in the test region. For large values of D_λ, th the gas is said to be optically thick. In this case, almost all of the incident radiation is absorbed so that $a_\lambda = 1 - \exp[-D_\lambda] \to 1$, and $L_\lambda \to L_\lambda^b$. Therefore, in optically thick gases, the measured spectral radiance, L_λ, permits an estimate on gas temperature [3].

In the Abel inversion technique, the lateral side-on distributions of $L_\lambda(y)$ and $D_\lambda(y)$ are determined from emission and absorption measurements along several optical paths at various lateral distances y from the center of the flow field. The modified form of Kirchhoff's law in terms of the radial and axial coordinates R and x yields [3]:

$$[\varepsilon_\lambda^*(R)/a_\lambda^*(R)]_x = L_\lambda^b\ [T(R)]_x \tag{16}$$

The side-on distribution of $D_\lambda(y)$ from the center of the flow field (y = 0) to its outer boundary ($y = R_a$) is given by the measured spectral transmittance $\tau_\lambda(y)$, through equation (15). In the axisymmetric case, we obtain

$$D_y = \pi \int_{|y|}^{R_a} a_\lambda^*(R)\ R\,dR\,(R^2-y^2)^{-1/2} \tag{17}$$

This equation is an Abel integration equation and can be inverted to yield [33]:

$$a_\lambda^*(R) = -1/\pi \int_{|y|=R}^{R_a} dD_\lambda(y)/dy\,[dy\,(y^2-R^2)^{-1/2}] \tag{18}$$

For optically thin gases, the measured side-on distribution of $L_\lambda(T)$ yields analogously

$$L_\lambda(y) = \pi \int_{|y|}^{R_a} \varepsilon_\lambda^*(R)\, R dR\, (R^2-y^2)^{-1/2} \qquad (19)$$

and the inverted integral equation is

$$\varepsilon_\lambda^* = -1/\pi \int_{|y|=R}^{R_a} d\, L_\lambda(y)/dy [dy\,(y^2-R^2)^{-1/2}] \qquad (20)$$

However, in gas flows with a high absorption coefficient, $a_\lambda^* > 3\ cm^{-1}$, the inversion of $L_\lambda(y) \rightarrow \varepsilon_\lambda^*(R)$ must be performed by means of the equation [33]:

$$L_\lambda(y) = 2\exp[-D_y(y)/2] \int_a^{R_a} R \cosh[\int_y^R a_\lambda^*(R')\, R'\, dR'\, (R'^2-y^2)^{-1/2}][RdR(R^2-y^2)^{-1/2}] \qquad (21)$$

We cannot invert equation (21) in a similar fashion, due to the dependence of the hyperbolic cosine. However, it can be solved by using a numerical solution given by Meiners [34]. From these solutions, the cross-sectional or radial temperature profile T(R) is derived [3,12,13,34].

E. Suppositions

The above relations are, however, derived by supposing that (a) radiation losses, due to reflection and scattering, are negligible, and (b) the system is in local thermal equilibrium (LTE). The first supposition depends on the type, size, and concentration of particles that are present in the investigated flow volume. For example, in the main radiating gun muzzle exhaust flow regions, most of the propellant combustion particulates exiting at the muzzle will be vaporized and/or consumed during the shock-heating and subsequently induced exothermic chemical reactions. The possible formation of soot would have a minor effect on the reflection and scattering. Therefore, this supposition is considered to be a reasonable approximation of the conditions that prevail in gun muzzle flash regions [3]. Local thermal equilibrium (LTE) exists if [30] (a) small gas volumes are of the same temperature, (b) the radiation is a function of temperature, (c) the particle mean free path is short compared to the gas test volume, and (d) energy transfer is mainly due to collisions and not to radiation. In transient flows, the relaxation time for LTE depends on the collision frequency and sometimes exceeds a characteristic flow time, giving a non-equilibrium condition. However, as long as the relaxation time is short in comparison with the flow residence time, the LTE assumption is good. This is commonly the case in ballistic flows, due to the high collision frequency [3].

On the other hand, non-equilibrium has been observed in chemically reacting gases or flames and in shock-heated gases [30]. Chemical processes may lead to the formation of an abnormally high population in the excited state of a molecular so that we have chemiluminescence. Apart from the chemical excitation which per se excludes LTE, it is possible that in chemically reacting flows there may be departures from thermal as well as from chemical equilibrium. The meaning of temperature then becomes doubtful and we have at best an effective temperature. For example, for non-equilibrium conditions, the line reversal gives only an effective electronic excitation temperature which is just a measure of the ratio of populations in the corresponding electronic states. Measurements of the excitation temperatures of the internal degrees of freedom in flames [30] and in the gun muzzle flash [3,13] have shown that quite often this excitation temperature substantially exceeds the equilibrium temperature. Therefore, the above suppositions remain to be assessed in every experiment.

III. TEMPERATURE MEASUREMENT

A. Emission Gauge Technique

Two different types of emission gauges have been designed and applied for intrusive temperature measurements in the combustion gases of solid and liquid propellants [9-16], Figures 1 and 2. The first design (Figure 1) consists of a bundle of 25 optical fibers arranged in parallel. The bundle is glued into the steel tube by epoxy. The diameter of a single fiber is 0.1 mm, and the diameter of the bundle is 0.5 mm. The surface area of the optical fiber bundle is 0.19 mm^2, and its opening angle at the end surface is 25°. To be able to screw this emission gauge into conventional pressure ports, both the diameter and the thread of the outer steel tube are adapted to the dimension of commercial pressure transducers. The design with the bundle of 25 fibers was selected from a trial-and-error approach. The goal was to achieve an optimum transfer of radiant energy in a high pressure environment. The design shown in Figure 1 withstands a maximum gas pressure of p = 300 MPa [9,10]. However, there are some limitations encountered in its application. At present, the commercial fiber optics available pass only visible light. Therefore, gas temperatures evaluated from the measured spectral radiance are limited to the range of $T \geq 1400$ K [9]. Also, this design cannot measure the influence of deposits which sometimes contaminate its end surface and then degrade the radiation measurement.

To overcome these difficulties, the emission gauge shown in Figure 2 was designed. In this design, a square rod of infrared (IR) transparent quartz with a cross-section of 6 mm^2 is glued into a steel tube by epoxy. The IR measurements extend the temperature

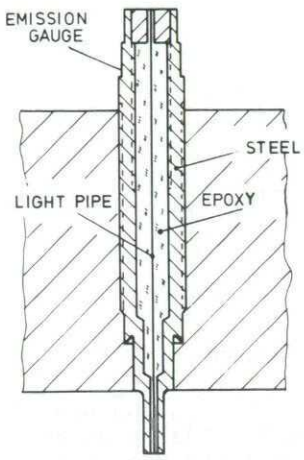

Fig. 1: Emission gauge (Type 1)

Fig. 2: Emission gauge (Type 2)

range to about 500 K. In addition, it permits the simultaneous measurement of both the emitted radiation and the effect of deposits, as a function of time, t. For this purpose, the upper end of the quartz rod is cut like a prism so that three surfaces are formed, the horizontal surface and the two surfaces which are turned at an angle of 45° with respect to the horizontal plane. Along the quartz rod, two opposite vertical surfaces are coated with silver. The other two vertical planes have been roughed to improve the adhesive sealing by epoxy between this quartz rod and the steel tube. The effect of deposits at the end surface of the gauge can be determined by coupling a laser beam into one of its upper end 45° surfaces. As the laser beam passes through the quartz rod, it experiences total reflection at both the coated vertical planes and at the end or flow facing surface, provided the length of the rod is adequately designed. The total reflection at the end surface is attenuated if deposits contaminate it during the measurement period. This attenuation is dependent on the thickness of the deposit layers. Thus, the contamination of the end surface can be taken into account, if a relationship is established between the attenuation and the layer thickness by a calibration method. In this calibration method, the end surface of the gauge is contaminated by residual combustion products in layers of variable concentrations [11].

A typical application of these emission gauges is shown in the schematic drawings of Figures 3 and 4. The two different emission gauges are placed into the combusting solid propellant charge. The light generated during the combustion is transmitted through the emission gauge. In Figure 3, it is divided into four beams which pass different interference filters and are then recorded by photomultipliers. Thus, the light emitted by the combustion gases is recorded simultaneously at four different wavelengths. In Figure 4, the quartz rod functions as a light pipe and transmits the emitted radiance. In addition, the effect of deposits at the end side of the gauge is determined by measuring the attenuation of the total reflection of an incident laser beam, Figure 4.

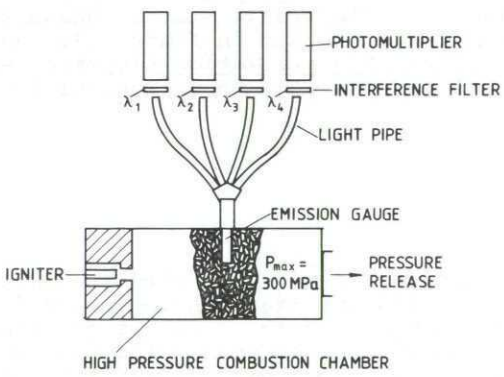

Fig. 3: Application of emission gauge (Type 1)

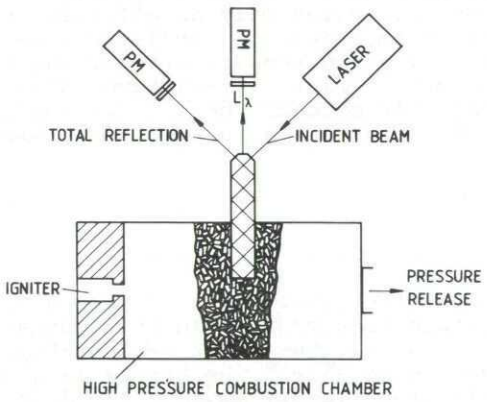

Fig. 4: Application of emission gauge (Type 2)

In order to evaluate the brightness temperature, $T_S(\lambda)$, from the measured spectral radiance, L_λ, the emission gauge setup used is calibrated by comparing the L_λ-signals, recorded in terms of the photomultiplier voltage U(t), to the L_λ^*-signals of a calibration source of brightness temperature $T_S^*(\lambda)$. A schematic of such a calibration procedure is shown in Figure 5. In this case, a tungsten ribbon lamp is used as a calibration source. In this calibration procedure, the chopped light of the tungsten ribbon lamp is focused on a scattering foil which is located at the end surface of the emission gauge setup. This scattering device simulates the real test site conditions in the combusting propellant bed where the light enters the gauge end surface from all directions. In order to avoid calibration errors, the calibration beam is adapted to the opening angle of the end surface of the emission gauge. Then the spectral radiance, L_λ^*, of the tungsten ribbon lamp of brightness temperature, $T_S^*(\lambda)$, is related to the spectral radiance, L_λ, measured

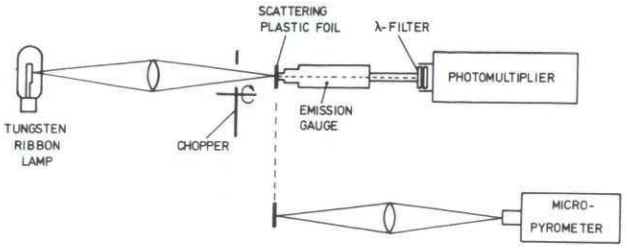

Fig. 5: Schematic of calibration procedure

in the combustion gases. A micropyrometer is used to measure the effective brightness temperature of the tungsten ribbon lamp at the scattering plastic foil. Thus, the brightness temperature, $T_S(\lambda)$, at the test site is evaluated.

For optically thick gases, $a_\lambda \to 1$ or $T_S(\lambda) \to T$, the emission gauge measures the spectral radiance emitted in the vicinity of the end surface of the gauge and yields an estimate of local propellant gas temperature histories. For example, in the combustion chamber of a caliber 20-mm test fixture gun, the spectral absorptance, a_λ, at λ = 589 nm is of the order of $a_\lambda > 0.94$ [9]. In this case, the spectral radiance measured by the emission gauge stems from the optically thick flow layer at the end surface and the evaluated brightness temperature $T_S(\lambda)$ approximates the true gas temperature T [9,10]. Sample results of the measurements with both emission gauges and the setups of Figures 1 and 2 are shown in Figures 6 and 7.

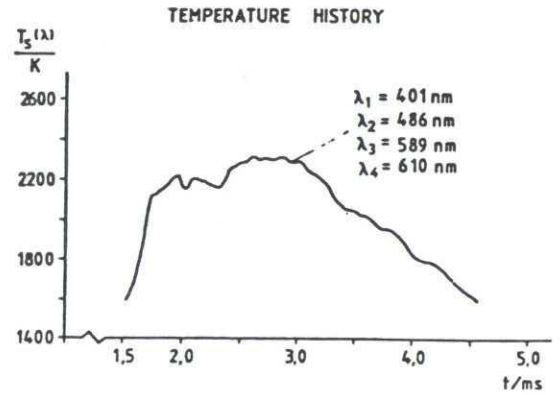

Fig. 6: $T_S(\lambda)$ vs. t (emission gauge type 1) at four wavelengths λ_1 to λ_4

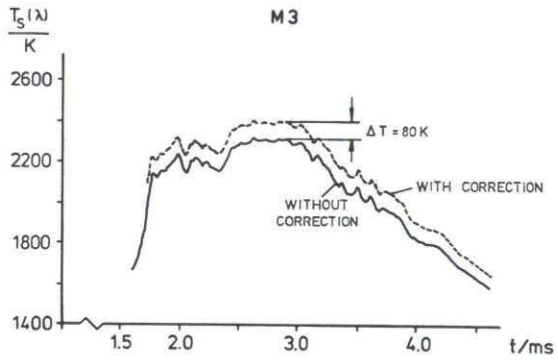

Fig. 7: Comparison of $T_S(\lambda)$ vs. t obtained with both emission gauges

In Figure 6, the results obtained with the emission gauge of type 1 by probing the combustion of a solid propellant charge show that equal $T_S(\lambda)$ vs. t recordings were measured at the wavelengths λ_1 = 401 nm, λ_2 = 486 nm, λ_3 = 589 nm, and λ_4 = 610 nm. It is therefore reasonable to assume that the radiance approaches blackbody conditions and that local thermal equilibrium prevails in the highly pressurized combustion gases. Figure 7 compares this result to the measurement with the type 2 emission gauge where a correction could be evaluated to account for the effect of deposits. Obviously, in the combustion chamber, this effect results in a temperature correction of ΔT = 80 K. In this case, the effect of deposits is small. However, the precipitation of combustion residues increases with the flow expansion as, for example, in the gun tube flow [33]. Then, the correction factor becomes more important.

Since the combustion of liquid gun propellants produces also opaque gases, the emission gauge technique could be used to determine temperature histories [14,15]. A schematic of the setup used in the liquid propellant combustion chamber is shown in Figure 8. In this experiment, the liquid monopropellant NOS-365, a hydroxyl ammonium nitrate (HAN) based liquid propellant, was investigated. Figure 9 shows a sample result of these experiments. It compares the temperature histories obtained by two different methods, i.e., with the (a) emission gauge technique, and (b) the modified reversal method. The good agreement between the two data sets confirms that the assumption of optical thick radiation is realistic.

The emission gauges were also used to obtain an estimate of local temperature in the intermediate flash of the caliber 7.62 mm rifle [3,13]. A schematic of the setup is shown in Figure 10. Figure 11 presents sample results obtained again by the reversal and the emission gauge technique. In this technique, the emission gauges are placed into the radiating gun intermediate flash at an axial distance from the muzzle of x = 15 cm and at lateral distances from the main flow axis of y = 1 cm and 7 cm. In Figure 11, good agreement was achieved between the reversal and the emission gauge data. However, the temperature measured at the wavelength of the resonance line of sodium (λ = 589 nm)

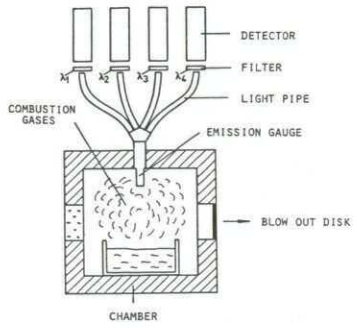

Fig. 8: Schematic of test setup used in the probing of liquid propellants

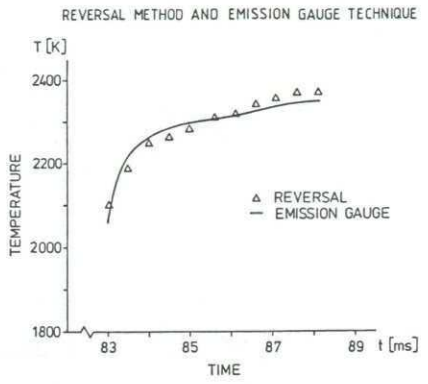

Fig. 9: T vs. t in the combustion gases of NOS-365 as obtained by the reversal and emission gauge technique

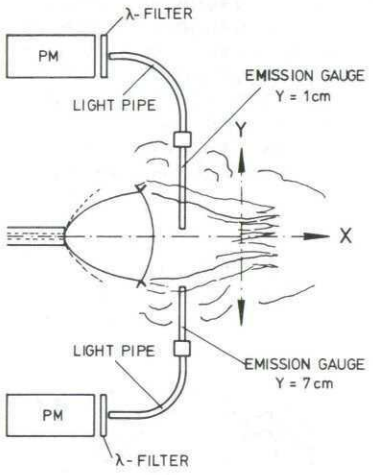

Fig. 10: Intrusive probing of the 7.62 mm intermediate flash

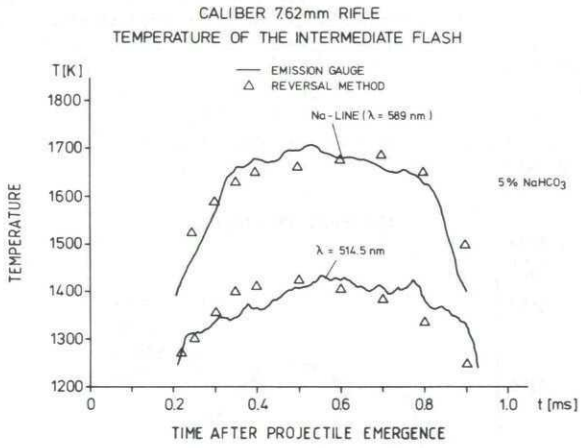

Fig. 11: T vs. t as obtained by reversal and the emission gauge technique at λ = 589 nm and λ = 514.5 nm

exceeds substantially the temperature measured in the continuum (λ = 514.5 nm). As will be shown later, such significant temperature differences were also measured when the Abel inversion technique was applied. Therefore, these results show that radiation emitted by the sodium atoms is not in thermal equilibrium [3,13].

B. Temperature History of the 20-mm Cannon from Ignition to Shot Ejection

The above results have shown the excellent potential of these emission gauges for the intrusive probing of opaque, particle-laden, ballistic flows. With this technique, local measurements of the spectral radiance emitted during the combustion of solid gun propellants in a 20-mm gun chamber have been made [9,10,16]. In these experiments, four of the emission gauges shown in Figure 1 have been used for intrusive temperature measurements at the igniter vent and within the 20-mm gun chamber, i.e., at locations M1 to M4. In addition, six saphire windows were mounted at locations M5 to M10 into bores along the 20-mm gun tube, to record the spectral IR-radiance emitted by the opaque tube flow at λ = 3,6 µm. The measurement also included the probing of the intermediate flash by reversal methods. A schematic of the setup is shown in Figure 12.

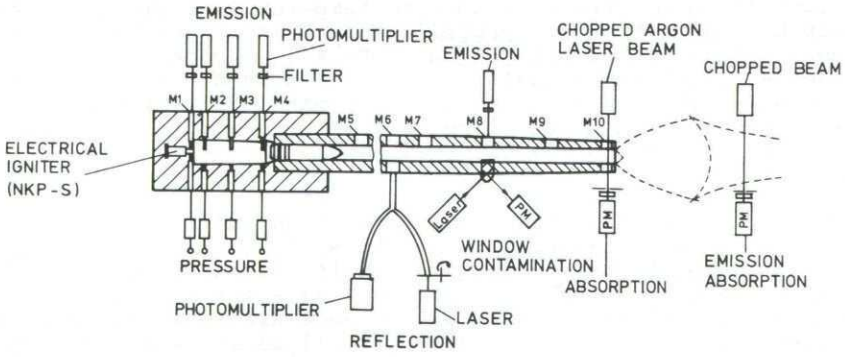

Fig. 12: Experimental setup used for temperature measurements in the 20-mm cannon

To account for the reflectance, r_λ, as well as for the contamination of the optical windows during the measurement period, these data were also measured using a laser reflection method and a prism-shaped window. These methods have been used in earlier gun tube experiments and are well described in references 16 and 33.

As a sample result, Figure 13 shows the local distribution of maximum T-data from ignition to shot ejection as evaluated from these measurements.

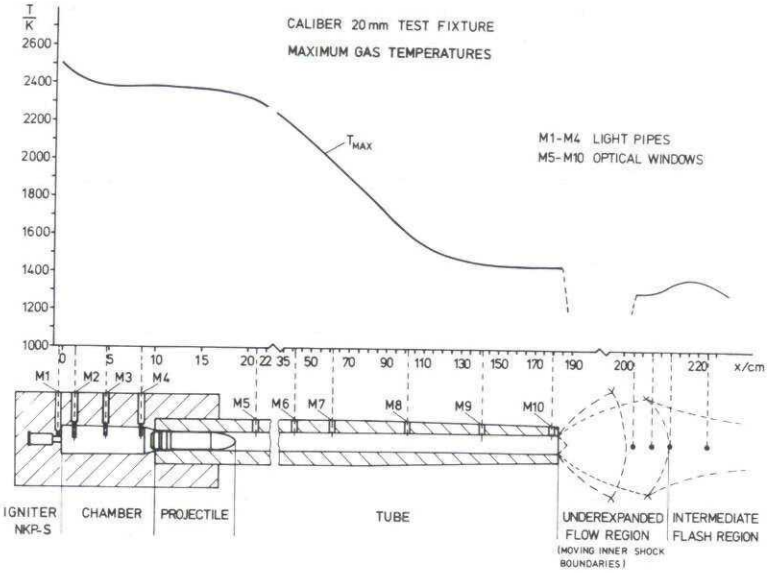

Fig. 13: Maximum temperatures in the interior ballistic flow of a 20-mm cannon

However, these measurements have also shown that severe limitations are encountered in the probing of gun tube flows, since the absorptance of the particle-laden flow is extremely high. Even the beam of a powerful laser could only penetrate the tube flow at location M10, i.e., in the vicinity of the muzzle, see Figure 12. The measured absorption data reveal that the measured emission is representative of a thin gas layer near the wall of the gun tube. That is, the radiation emitted in the visible and near infrared region is similar to a blackbody radiator for small penetration depths of about 3 mm at λ = 3.6 µm [16,33]. Since a temperature decrease is expected to occur in the wall layer, the emission data and the evaluated temperatures may already represent this temperature decrease, Figure 14, see also reference [20].

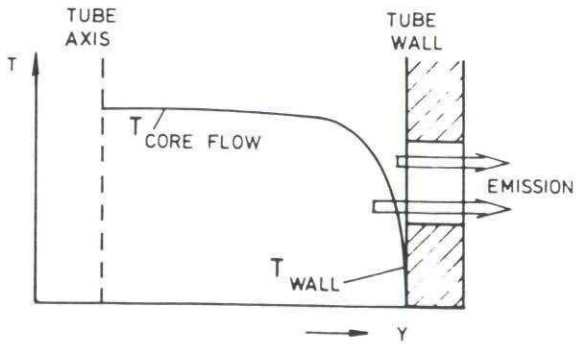

Fig. 14: Schematic of in-bore gas temperature gradient

The high absorptance of the combustion gases in real gun firings obviously prevent the measurement of radially or spatially resolved temperatures in gun tube flows. On the other hand, temperatures could be evaluated in the combusting propellant bed by means of the emission gauges, since the radiation approximates blackbody conditions.

C. Gun Muzzle Flash Studies

Gun muzzle flash and its suppression by alkali salts additives has been intensively investigated in the past; however, a fundamental understanding of the underlying suppressant mechanism is still lacking [3,5,13,18]. Three main radiating flow areas develop during the discharge of a gun into ambient air [3,5]. These flow areas are usually referred to as primary, intermediate, and secondary flashes [3,5]. The primary flash, located at the muzzle, is of small spatial extent and low radiation intensity. It represents the hot gas-particle flow exiting at the muzzle. The intermediate flash is a more extensive region of greater radiation intensity commencing farther from the muzzle downstream behind the inner shock disc which terminates the underexpanded supersonic region of the gun muzzle blast field. The secondary flash is known to commence as an extension of the intermediate flash and develops upstream and downstream covering the turbulent gas plume

which forms the muzzle exhaust flow field. It is much more extensive and of much higher radiation intensity than the intermediate flash [13,18].

To investigate the effect of alkali salts, added to the gun propellant as chemical flash reducers, a series of experiments have been conducted by using three different alkali salts and varying the percentage of these additives in a stepwise fashion [3,13]. The alkali salts were added to the propellant charge of a caliber 7.62 mm gun in steps of 0.5 wt.% raising the percent of (a) KNO_3 to 2.0 wt.%, (b) K_2CO_3 from 0.5 wt.% to 5 wt.%, and (c) $NaHCO_3$ from 0.5 wt.% to 10 wt.%. In these experiments, both the intensity of the emitted radiation and the temperature in the intermediate flash region was determined by means of the reversal and Abel inversion method.

The principle of the reversal method is shown in Figure 15. In this technique, the radiant flux of a monochromatic laser beam, chopped by an acusto-optic coupler, is used as a background source. The laser beam is scattered at the diffuser and forms a point-like radiation source. This source is focused by two identical lenses, L_1 and L_2, into

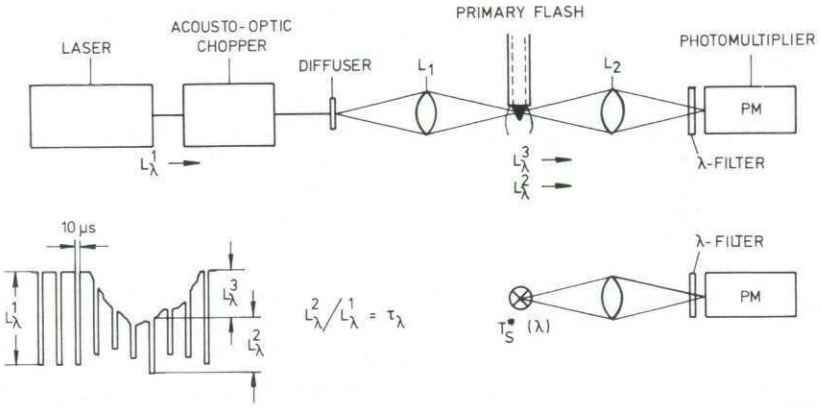

Fig. 15: Experimental setup for modified reversal measurements

the flow and then onto the photomultiplier (PM). The signal wave train is also shown in Figure 15. The spectral radiance of the background source, L_λ^1, is measured before the flow commences and gives together with the traversed portion, L_λ^2, the transmittance, along the given optical path, i.e., $L_\lambda^2/L_\lambda^1 = \tau_\lambda$. Substituting $a_\lambda = 1-\tau_\lambda$ in equation (6) yields the average temperature along this path. To calibrate the measurement, a calibration lamp is put at the location of the event. Then, the spectral radiance L_λ^* for $T_S^*(\lambda)$ of this lamp is related to the measured photomultiplier signals. In these experiments, the light of the background source was divided into three beams by beam splitters in order to measure simultaneously the reversal temperatures at three wavelengths along parallel optical paths [3].

Sample results of these reversal measurements are shown in Figures 16 and 17. The measured temperature, T, is normalized to the measured muzzle exit temperature, T_m, since the gun muzzle exit properties are dependent on the amount of alkali salts added to the propellant charge [3].

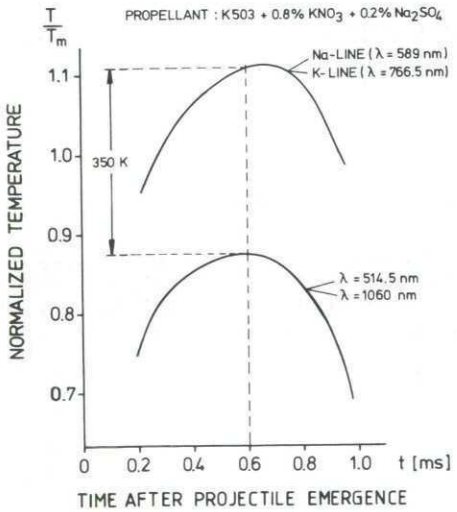

Fig. 16: T/T_m vs. t in the intermediate flash of the 7.62 mm rifle (results of two tests; propellant K 503 with 0.8 wt.% KNO_3 and 0.2 wt.% Na_2SO_4)

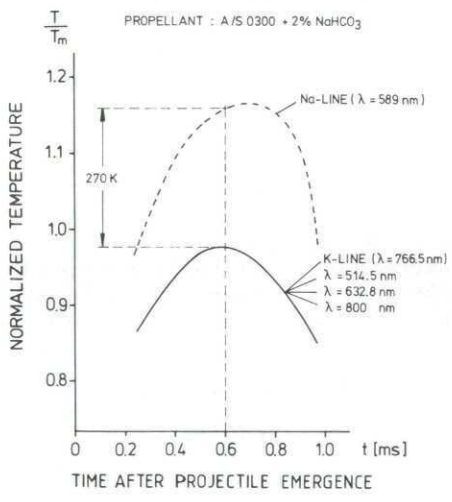

Fig. 17: T/T_m vs. t in the intermediate flash of the 7.62 mm rifle (results of three tests; propellant A/S 0300 with 2 wt.% $NaHCO_3$)

The normalized temperatures show a significant temperature difference between the data taken in the resonance line wavelength of the alkali added to the propellant charge and the data taken in the other wavelengths. Obviously, the inclusion of alkali salts as chemical flash reducers results in an excitation of these alkali atoms in the intermediate flash region so that the measured temperatures exceed the temperatures measured at the other wavelengths.

Abel inversion measurements as well as the data measured by means of the emission gauge technique (see Figure 11) confirm the occurrence of this temperature anomaly [3]. In the Abel inversion technique, the side-on measurements of $L_\lambda(y)$ and $D_\lambda(y)$ were made in a single firing. The principle of the experimental setup used is shown in Figure 18.

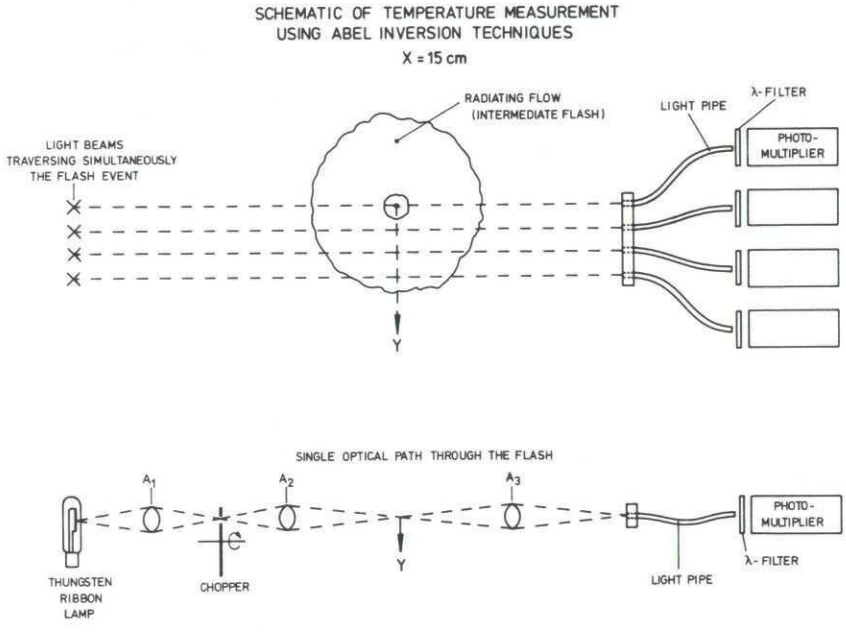

Fig. 18: Abel inversion setup for probing the 7.62 mm gun intermediate flash

In this technique, several light beams pass a cross-section of the 7.62 mm intermediate flash at an axial distance from the muzzle of x = 15 cm. A calibrated tungsten ribbon lamp is used as a background source. The tungsten light is focused and chopped and then divided in several beams by beam splitters, which simultaneously pass through the intermediate flash at various optical paths and equal lateral distances from the main flow axis. On the detector side, light pipes feed the signals to the photomultipliers which record alternately the emission and absorption so that $L_\lambda(y)$ and $D_\lambda(y)$ can be determined.

The inversion of the $L_\lambda(y)$- and $D_\lambda(y)$-data yields the radial distribution of both the emission and absorption coefficients, ϵ^*_λ and a^*_λ, and, therefore, the radial or cross-sectional temperature distribution T vs. R. Sample results of these measurements are shown in Figures 19, 20, and 21. Figure 19 confirms the temperature anomaly that occurs in the resonance line wavelength of the sodium atom. The temperature data taken at the other wavelengths show a decrease of temperature with the percent of alkali salt added, Figure 20. This is also shown in Figure 21 which compares the temperatures measured in the continuum by reversal and Abel inversion techniques. Since the radiation intensity emitted by the intermediate flash decreases also significantly with the percent of alkali salts added to the propellant charge [3,13], it is reasonable to conclude [3] that

- the chemical inhibition reaction caused by alkali salts commences in the intermediate flash region
- these reactions result in the continued excitation of the alkali atoms above equilibrium temperature, if they are involved in the chemical flash inhibition reaction
- spectroscopic temperature measurement in the resonance line wavelength of these alkali species yield, therefore, an effective electronic excitation temperature which substantially exceeds the equilibrium temperature
- temperatures measured at other wavelengths approximate the equilibrium gas temperature
- the radiant intensity and temperature of the intermediate flash decreases with the percent of alkali salt added to the propellant charge as flash reducers
- the inhibition of secondary muzzle flash is presumably due to the decrease of temperature by alkali salts in the intermediate flash region.

The above results of temperature measurements have enhanced the understanding of gun interior and transitional ballistic flows. However, the diagnosis and quantitative

characterization of non-equilibrium conditions in chemically reacting muzzle flows and the chemical inhibition of gun muzzle flash is still an unsolved problem.

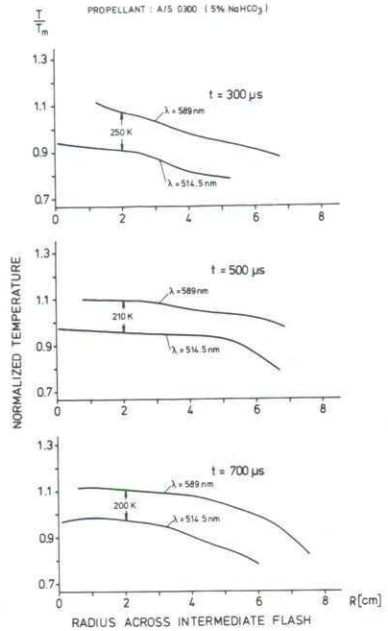

Fig. 19:
Cross-sectional temperature profiles T/T_m vs. R at x = 15 cm obtained by Abel inversion measurements at λ = 589 nm and 514.5 nm in the intermediate flash of the 7.62 mm rifle when firing the propellant A/S 0300 with 5 wt.% of $NaHCO_3$ added to the propellant charge

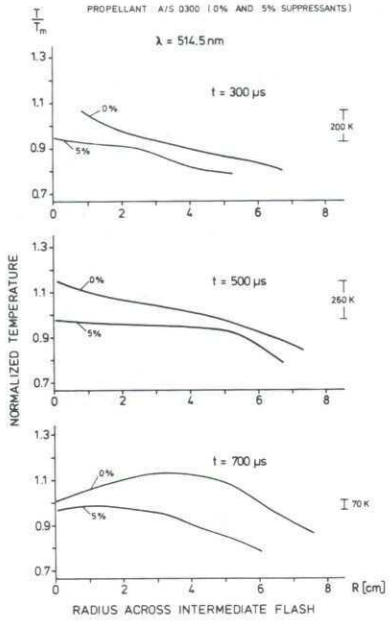

Fig. 20:
Cross-sectional temperature profiles T/T_m vs. R at x = 15 cm obtained by Abel inversion measurements at λ = 514.5 nm in the intermediate flash of the 7.62 mm rifle when firing the propellant A/S 0300
(a) without adding alkali salts (0%)
(b) with 5 wt.% of $NaHCO_3$ (5 %) added to the propellant

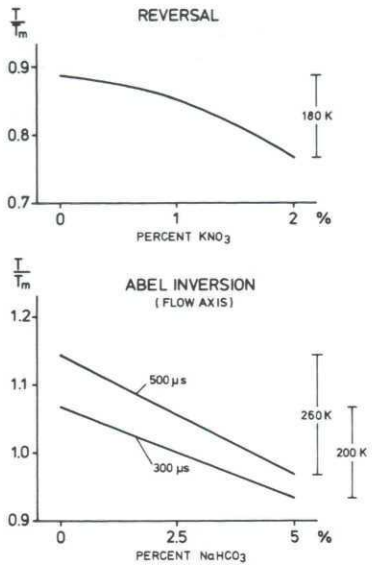

Fig. 21:
T/T_m vs. wt.% of added alkali salts at x = 15 cm obtained by reversal and Abel inversion measurements in the continuous radiation of the intermediate flash of the 7.62 mm rifle

IV. FLOW VELOCITY MEASUREMENTS

A. Laser Doppler Velocimeter as Devised by Smeets

Smeets' laser Doppler velocimeter is well described in references [22,23] and [24]. This Michelson type of spectrometer is more appropriate for the measurement of flow velocities in particle-laden ballistic flows than other laser Doppler techniques [27,28,29]. The method is based on a phase-stabilized Michelson interferometer as a sensitive spectrometer, Figure 22.

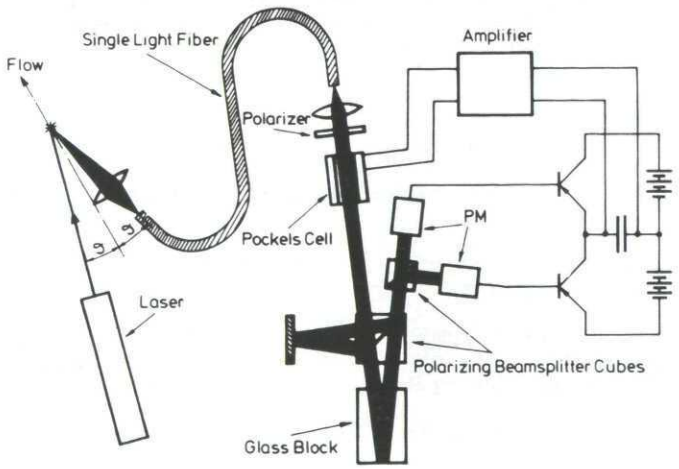

Fig. 22: Schematic of Smeets' laser Doppler velocimeter [22]

In this technique, a monochromatic laser beam is focused into the flow. When the laser light is scattered by a cloud of flow-borne particles that pass through the test volume, a continuous signal, proportional to the wavelength changes of the laser light is generated in the velocimeter. Thus, a near real-time velocity signal of the motion of the flow-borne particles is obtained. If the sizes of flow-borne particles are small enough to

neglect particle lag ($\leq$ 1 μm), then the gas velocity can be deduced from the recorded velocity signal. In ballistic flow studies, the response is measured in milliseconds [27].

The velocity signal is generated by the Michelson spectrometer. For this purpose, the scattered and Doppler-shifted laser light is introduced into a fiber optic cable (single light fiber) that delivers the signal to the Michelson spectrometer. It is linearly polarized and traverses through the Pockels cell and the beam splitter cube. The beam splitter divides the signal into two beams of equal intensity that are linearly polarized parallel and vertical to the plane of the Michelson interferometer. The glass block in one of the legs produces an optical path difference which accounts for the wavelength sensitivity. Then the two beams are recombined and pass through a second beam splitter cube. Thus, both the beams that arrive at the two photomultipliers (PM) have complementary interferences. The interferometer is adjusted to indefinite fringe spacing so that the photocathodes of the photomultipliers are uniformly irradiated. The radiant fluxes of the two exiting beams, P_1 and P_2, are given by [22,23]:

$$P_1 = P_0 \cos^2[\pi\Delta\ell/\lambda] \quad ; \quad P_2 = P_0 \sin^2[\pi\Delta\ell/\lambda] \tag{22}$$

where $\Delta\ell$ denotes the optical path difference between the two beams, λ the wavelength, and P_0 the incident radiant flux. For $\Delta\ell \ll 1$, the interference becomes sensitive to small wavelength changes so that shifts of $\Delta\lambda/\lambda = 10^7$ can be resolved.

The two mutually perpendicular, polarized beams which receive a large $\Delta\ell$ within the Michelson interferometer can be additionally phase-shifted in the Pockels cell. This results in a small contribution, $d\Delta\ell$, which is proportional to the applied voltage. A fast acting phase stabilization can be realized so that the ratio $\Delta\ell/\lambda$ is kept strictly constant. A wavelength change, $d\lambda$, which occurs during the scattering at the moving particles is then automatically compensated by a $d\Delta\ell$ within the Pockels cell so that

$$\Delta\ell/\ell = (\Delta\ell_o + d\Delta\ell)/(\lambda_o + d\lambda) = \text{constant}, \quad \text{or} \quad d\lambda\ell = (\Delta\ell_o/\lambda_o)d\lambda \tag{23}$$

since the Doppler shift of the scattered radiation produces rather small wavelength changes, i.e., $d\lambda/\lambda << 1$.

The phase stabilization is achieved with a simple electrical circuit, see Figure 1. The electro-optical system maintains a phase at which there are equal radiant fluxes to both of the PM's photocathodes. Concurrently, the photo currents are equal and both transistors pass the same current. A sudden change in the wavelength, λ, alters the phase for an instant which, according to equation (22), leads to a difference in the two radiant fluxes. The resulting difference current in the transistor circuit causes a variation in the charge and voltage of the capacitor. The capacitor is connected with the Pockels cell through a DC amplifier. Thus, the voltage, U, and the correlated optical path difference, $d\Delta\ell$, of the Pockels cell are instantly shifted until the phase is restored. Since the Pockels cell effect is linear, the variation of its voltage with time, U(t), follows proportionally the change in the optical path difference, $d\Delta\ell$, and, according to equation (23), proportionally $d\lambda$. Therefore, the recording of U(t) yields the velocity history, $U_P(t)$, of the particles which pass the test volume and scatter the incident monochromatic laser light.

B. Sample Results of Velocity Measurements

Measurements in gun tube flows are impeded as well, due to the extremely high absorptance of the particle-laden in-bore flow. Mach [20] has reported on in-bore measurements using a relatively particle-free propellant charge in the 20-mm cannon at low loading densities. The experimental setup and the results obtained in the middle of the gun tube are shown in Figures 23 and 24. In this experiment, two single-point measurements were made simultaneously by using two sets of velocimeters, i.e., in the main flow axis and in the wall layers, Figure 23. At a distance of 2 mm from the inner tube wall, the flow

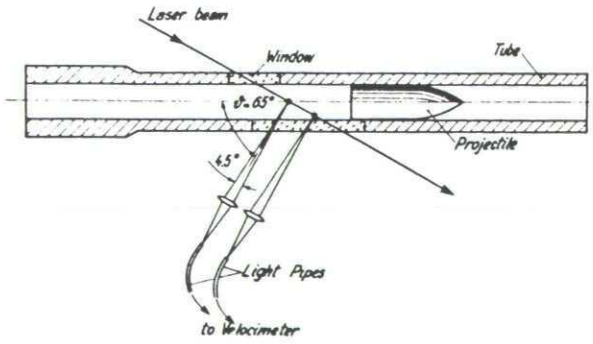

Fig. 23: Schematic of velocity test setup [20]

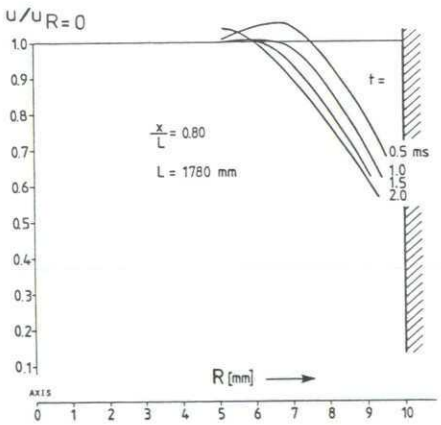

Fig. 24: Radial profiles of normalized velocity [20]

velocity which, in Figure 24, is normalized to the values in the main flow axis (R = 0), is decreased by a factor of 0.4 showing the radial velocity gradient that exists in such gun tubes.

Smeets' velocimeter is, however, an appropriate tool for probing the more transparent gun muzzle exhaust flow fields [25,26,27]. A sample result of the velocity measurements in the intermediate flash region of the 7.62 mm rifle is shown in Figure 25.

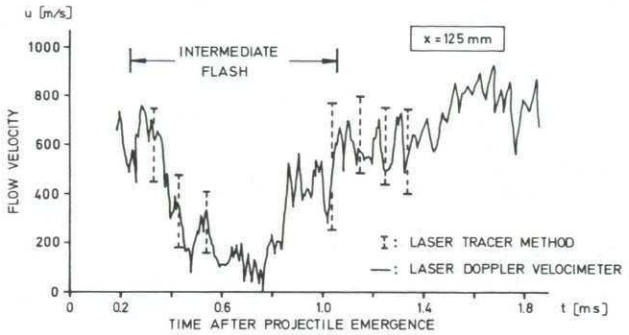

Fig. 25: Axial flow velocity vs. time as measured in the 7.62 mm gun muzzle blast field at z = 125 mm by both the laser-tracer and laser-Doppler velocimeter methods

In Figure 25, the data evaluated from the motion of a laser tracer [35] are compared to the data obtained by the laser-Doppler velocimeter. Both data sets show good agreement. In the flow region where the intermediate flash has developed, the flow velocity is sharply reduced. This drastic change of flow velocity has a duration of about 0.5 ms, allowing time for chemical processes to take place. It is in this region where a chemical suppressant can be most effective [3,6].

Another sample result of flow velocity measurements in the muzzle blast field of a 20-mm cannon is shown in Figure 26.

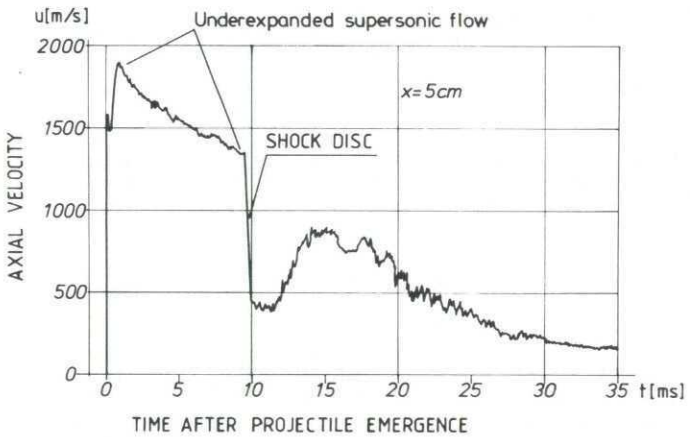

Fig. 26: Axial velocity vs. time at x = 5 cm in the muzzle blast field of a 20-mm cannon [27]

In this single-point measurement, the flow velocity decreases in the underexpanded supersonic flow region from about 1900 m/s to 1400 m/s. Then, a sharp velocity decrease is measured as the shock front passes the measuring point ($t \approx 10$ ms). For times $t > 12$ ms, the velocity increases, due to the reestablished flow expansion. However, this expansion is disturbed by the intermediate flash causing a velocity descent as in the case of the 7.62 mm rifle [27].

Simultaneous measurements of both the axial and lateral velocity components, u_x and u_y, permitted the evaluation of the velocity vector. By combining the results of various firings and comparing them with shadowgraphs of the flow yielded the velocity vector projections throughout the flow field [27], see, for example, Figure 27.

In this velocity vector measurements, the direction and the magnitude of the flow is given. Figure 27 shows the high flow velocities prevailing in the supersonic region of the flow. After the propellant flow has passed the inner shock disc, the magnitude of the velocity vector is small. Downstream it increases with the axial distance x. However, in the vicinity of the turbulent gas plume boundary, the flow is decelerated again, due to the restraint caused by the outer blast wave [3,13].

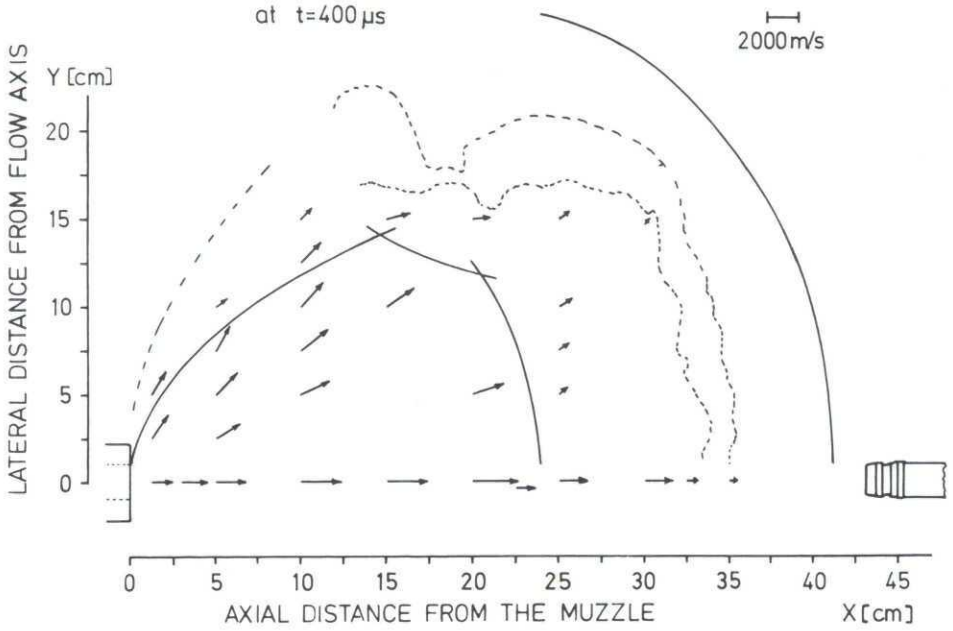

Fig. 27: Velocity vector projections in the 20-mm gun muzzle blast field at time t = 400 µs after projectile emergence

V. SIMULATION EXPERIMENTS

The objective of the gas gun simulation experiments, performed by Klingenberg and Schmolinske [8] at EMI-AFB, is to investigate two-phase, chemically reacting flows. For this purpose, a gas gun driven by the combustion of a prepressurized mixture of hydrogen and oxygen diluted with helium is used. Lord [7] using a similar device had obtained maximum chamber pressures of about 350 MPa.

The gas gun has been assembled in two stages. The first stage is the combustion chamber shown in Figure 28. It consists of a two liter chamber that is either closed by a solid retainer or a diaphragm (blow-out disc). The solid retainer holds the pressure until a 100 % combustion is achieved. The second stage includes a projectile and a gun tube, Figure 28. An adaptor permits the mounting of either 20 mm or 40 mm gun tubes, Figure 28.

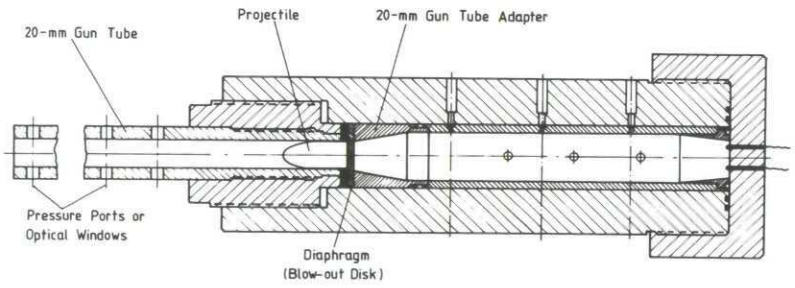

Gas Gun Chamber with Diaphragm, Projectile and Gun Tube (20-mm or 40-mm Barrel)

Fig. 28: Gas gun with projectile and tube

A sample result of pressure measurements for the first stage testing is shown in Figure 29. It shows that for a total charge pressure of 48 MPa a maximum chamber pressure of about 350 MPa was achieved. This is the value that was reported by Lord [7] for the gas mixture 3 H_2 + O_2 + 8 He.

Current plans are to test the second stage of the gas gun using the 20-mm tube measuring pressure, temperature and flow velocity in the reacting flow. Since we are dealing with simple gas phase chemistry, the gun simulator is expected to be a tool for the reproducible generation of gun muzzle flash. Therefore, it is planned to address not only interior ballistics but also the phenomena of muzzle flash and its suppression. Future plans will include the study of the role of both inert and reacting particles.

The importance of the simulation experiments outlined above lies in the ability to

(1) identify the governing processes,

(2) isolate the effect of a single variable, and

(3) establish equivalence between different sources of data.

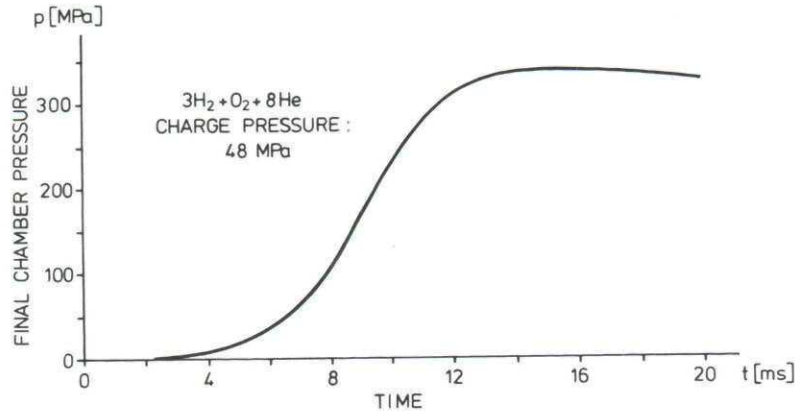

Fig. 29: Chamber pressure history

VI. REFERENCES

[1] G. Klingenberg, and N.E. Banks, "Review of Interior Ballistic Research: State-of-the-Art of Computational and Experimental Efforts", Proc. 6th International Symposium on Ballistics, Orlando, Fla., October 1981

[2] E.M. Schmidt, "Survey of Muzzle Blast Research", Proc. 5th International Symposium on Ballistics, Toulouse, France, April 1980

[3] G. Klingenberg, "Experimental Diagnostics in Reacting Muzzle Flows", Fraunhofer-Institut für Kurzzeitdynamik, Weil am Rhein, EMI-AFB Report E 12/84, 1984

[4] J.A. Schmitt, and R. Heiser, "Predictions of Special Interior Ballistic Phenomena with a New Multi-Dimensional Multi-Phase Code with Heat Transfer", Proc. 8th International Symposium on Ballistics, Orlando, Fla., October 1984

[5] G. Klingenberg, "Overview on European Interior Ballistic Simulation Experiments", Proc. of the DEA-G-1060 Germany/United States Ballistic Research and Development Meeting, Naval Weapons Center, China Lake, CA, April 1985

[6] J.M. Heimerl, G.E. Keller, and G. Klingenberg, "Muzzle Flash Kinetics and Modelling", Fraunhofer-Institut für Kurzzeitdynamik, Weil am Rhein, EMI-AFB Report No. 1/85, 1985

[7] M.E. Lord, "Performance of a 40-mm Combustion-Heated Light Gas Gun Launcher", Arnold Engineering Development Center, Report AEDC-TN-60-176, October 1960

[8] G. Klingenberg, and E. Schmolinske, "Simulation Experiments on Reacting Two Phase Ballistic Flows - Gas Gun Simulator", Fraunhofer-Institut für Kurzzeitdynamik, Weil am Rhein, EMI-AFB Report No. E 15/83, 1983

[9] G. Klingenberg, "Temperature History of the 20-mm Gun Interior Ballistic Flow From Ignition to Shot Ejection", Proc. 8th International Symposium on Ballistics, Orlando, Fla., October 1984

[10] G. Klingenberg, "Investigation of Two Different Propellants during the Ignition and Combustion in a 20-mm Gun Chamber", J. Propellants, Explosives, Pyrotechnics 10, 1985, pp. 31-38

[11] G. Klingenberg, "Invasive Spectroscopic Technique for Measuring Temperature in Highly Pressurized Combustion Chambers", Proc. 16th International Congress on High Speed Photography and Photonics, Strasbourg, France, August 1984

[12] G. Klingenberg, and H. Mach, "Spectroscopic Temperature Measurements in Interior Ballistic Environments", Proc. 10th International Congress on Instrumentation in Aerospace Simulation Facilities, St. Louis, France, September 1983, ICIASF'83 Record 83CH1954-7, pp. 271-281

[13] G. Klingenberg, and J.M. Heimerl, "The Effect of Chemical Flash Suppressants on Intermediate Flash", Proc. 8th International Symposium on Ballistics, Orlando, Fla., October 1984

[14] G. Klingenberg, "Experimentelle Untersuchungen an monergolen flüssigen Rohrwaffentreibmitteln", Fraunhofer-Institut für Kurzzeitdynamik, Weil am Rhein, EMI-AFB Report No. E 3/85, 1985

[15] G. Klingenberg, "Spectroscopic Temperature Measurements in the Reaction Gases of the Liquid Monopropellant NOS-365", Proc. of the DEA-G-1060 Germany/United States Workshop on Liquid Propellants, Pfinztal-Berghausen, FRG, May 1985

[16] G. Klingenberg, "Temperature History of the Interior Ballistic Flow of a 20-mm Cannon", Journal of Ballistics, Vol. 8, No. 2, 1985

[17] H. Mach, "Measurements of Two-Phase Exhaust Flow Parameters of a Small Caliber Gun Associated with Muzzle Flash Phenomena", Proc. 7th International Symposium on Ballistics, The Hague, The Netherlands, April 1983

[18] J.M. Heimerl, and G. Klingenberg, "Gun Muzzle Flash and Its Suppression", Proc. 7th International Symposium on Ballistics, The Hague, The Netherlands, April 1983

[19] H. Mach, U. Werner, and M. Masur, "Messungen an der Zwei-Phasenströmung im Anströmbereich eines Gewehres vom Kaliber 7.62 mm", German-French Research Institute, St. Louis, France, ISL Report No. R 110/84, 1984

[20] H. Mach, "New Experimental Technique for Probing Gun-Barrel Boundary Layers", Proc. 8th International Symposium on Ballistics, Orlando, Fla., October 1984

[21] D.R. McLure, "Measurements of Gas Temperature and Convective Heat Flux in a Reacting Granular Propellant Bed", PhD-Thesis, The Pennsylvania State University, Dpt. of Mechanical Engineering, University Park, PA, August 1984

[22] G. Smeets, and A. George, "Instantaneous Laser-Doppler Velocimeter Using a Fast Wavelength Tracking Michelson", J. Rev. Sci, Instrum., Vol. 49, 1977, p. 1589

[23] G. Smeets, and A. George, "Michelson Spectrometer for Instantaneous Doppler Velocity Measurements", J. Phys. E.: Sci. Instrum., Vol. 14, 1981, pp. 838-845

[24] G. Smeets, and A. George, "Laser-Doppler Velozimeter mit einem Michelson-Spektrometer", German-French Research Institute, St. Louis, France, ISL Report No. R 109/84, 1984

[25] H. Mach, U. Werner, and H. Masur, "Vermessung des instationären Geschwindigkeitsfeldes im Ausströmbereich einer Rohrwaffe vom Kaliber 20 mm mittels eines Laser-Doppler-Interferometers", German-French Research Institute, St. Louis, France, ISL-Report No. R 128/81, 1981

[26] G. Klingenberg, H. Mach, and G. Smeets, "Probing of the Unsteady Reacting Muzzle Exhaust Flow of 20-mm Gun", AIAA/ASME Third Joint Thermophysics, Fluids, Plasma and Heat Transfer Conference, St. Louis, Missouri, June 1982, 82-HT-34

[27] G. Klingenberg, H. Mach, and G. Smeets, "Flow Field Measurements of an Unsteady Reacting Muzzle Exhaust Flow", Journal of Heat Transfer, Vol. 105, Nov. 1982, pp. 884-888

[28] H. Mach, H.J. Schaefer, and G. Klingenberg, "Laser Anemometry Applied to Unsteady, Two-Phase, Reacting Propellant Flow", International Symposium on Applications of Laser-Doppler Anemometry to Fluids Mechanics, Lisbon, Portugal, July 1982 (ISL Report No. CO217/82, 1982)

[29] H. Mach, H.J. Schaefer, U. Werner, and E. Sommer, "Vergleichende Messungen mit dem Laser-Interferenz-Velozimeter und dem Streifenanomometer an der Schwadenströmung eines Gewehres", German-French Research Institute, St. Louis, France, ISL Report No. R 123/83, 1983

[30] R.H. Tourin, "Spectroscopic Gas Temperature Measurement", Elsevier Publ. Company, Amsterdam - London - New York, 1966

[31] F. Roessler, "Temperaturmessungen", in F. Vollrath and G. Thomer "Kurzzeitphysik", Springer, Wien, 1967, pp. 436-497

[32] S. Ray, and H.G. Semerjian, "Laser Tomography for Simultaneous Concentration and Temperature Measurement in Reacting Flows", AIAA 18th Thermophysics Conference, Montreal. Canada, June 1983, AIAA-83-1583

[33] G. Klingenberg, and H. Mach, "Experimental Study of Non-Steady Phenomena Associated with the Combustion of Solid Gun Propellants", Proc. 16th Symposium (International) on Combustion, The Combustion Institute, Philadelphia, PA, 1976, pp. 1193-1200

[34] D. Meiners, "Spektroskopische Methoden zur Messung der Temperatur in Plasmen mit Selbstabsorption", BMWB, Report K-72-22, November 1972

[35] G. Klingenberg, and G.A. Schröder, Combustion and Flame 27, 1976, pp. 177-187

DISCUSSION

M.Summerfield, US

Your paper describes a variety of experimental techniques, mainly of spectroscopic or radiometric nature, for determining various interior ballistic characteristics of a gun. You add to this the methods for studying the state of the gas in the emerging jet. There would be great interest in knowing the state of reactedness of the combustion gas inside a gun. At present, in all the predictive ballistic codes, especially the NOVA Code and its derivatives, the assumption is made, without any experimental verification whatever, that the so-called burned propellant gas is completely burned; that it is completely inert chemically. Yet, in Paper 21 of the AGARD Meeting on Smokeless Propellants, Dr Beckstead shows experimentally that, if only about 5% of the total heat release leaves the burning surface, stability can turn into instability, driven by the pressure-dependent exothermicity of the still-reacting gases in the core. If the same process occurs in a gun, then those codes would be inaccurate for predicting wave motions and we would have to develop new codes. But we do not know the composition of the gases at all, not in the slightest, by direct measurement. The question is, can a determination of the state of reactedness be made inside the barrel? If it cannot be made there, due to severe pressure broadening of the lines and virtually black-body conditions as you say in your paper, then can measurements as functions of time of such characteristics be made at the muzzle, in the primary jet, not including the secondary flash, so that inferences can be made about the internal flow? Have direct gas sampling techniques as a function of time for barrel gases ever been tried, and can they work successfully for the purpose intended?

Author's Reply

As has already been pointed out in a review paper [1] on interior ballistic flow research, given by the author at the 6th International Symposium on Ballistics at Orlando, FL, in 1981, the interior ballistic flow of solid propellant guns is indeed a still-reacting flow. In general, only 50 per cent of the combustibles are burned during the in-bore passage and about 50 per cent of the unburned gas-particle mixture is existing at the muzzle. These expelled combustibles are reacting in the muzzle exhaust flow field if mixing with ambient air occurs and the ignition temperature in the flow field is high enough so that secondary flash can take place. Experimental techniques for probing the gas-particle flow inside the bore and at the gun muzzle exit included (a) X-ray visualization of the flow using X-ray transparent gun tubes, (b) optical measurements through specially designed windows, (c) mass spectrometry of the in-bore and muzzle flow gases, and (d) direct sampling of the gases in the muzzle exhaust region [1, 2, 3]. However, every experiment is limited to some extent by the hostile gun environment. Nevertheless, from the results of these investigations we know that the in-bore flow is a reacting flow. It reacts in the gaseous phase and contains burning particulates that move up to the muzzle. For example, an increase of soot formation in the wall layers was measured by optical means [3] and radial flow gradients were observed to occur across the tube. Therefore, the author concluded that the in-bore flow of guns is affected by the exothermic reaction sequence occurring in the gun tube. At present we do not know, for example, whether observed gun failures are due to combustion instabilities or other phenomena. The described simulation experiments on reacting flows were initiated to close the gap that exists between the modeling and experimental interior ballistic capabilities. The objective is to lay the foundation for improved theoretical codes that include the chemistry of the reacting in-bore flow of guns.

---

[1] G.Klingenberg and N.E.Banks, *Review on Interior Ballistics Research: State-of-the-Art of Computational and Experimental Efforts*, Proceedings of the 6th International Symposium on Ballistics, Orlando, FL, 27—29 October 1981, pp 94—105.

[2] G.Klingenberg and J.M.Heimerl, *Investigation of Gun Muzzle Exhaust Flow and Muzzle Flash*, Fraunhofer-Institüt für Kurzzeitdynamik, EMI-AFB Report 1/82, 1982.

[3] G.Klingenberg and H.Mach, *Experimental Study of Non-Steady Phenomena Associated with the Combustion of Solid Gun Propellants*, Proceedings of the 16th Symposium (International) on Combustion, The Combustion Institute, Philadelphia, 1976, pp 1193—1200.

MODELLING THE BEHAVIOUR OF ADDITIVES IN GUN BARRELS

by
N Rhodes and J C Ludwig
CHAM Ltd
Bakery House
40 High Street
Wimbledon
SW19 5AU
London

SUMMARY

A mathematical model which predicts the flow and heat-transfer in a gun-barrel is described. The model is transient, two-dimensional and equations are solved for velocities and enthalpies of a gas-phase, which arises from the combustion of propellant and cartridge case, for particle additives which are released from the case; volume fractions of the gas and particles. Closure of the equations is obtained using a two-equation turbulence model. Preliminary calculations are described in which the proportions of particle additives in the cartridge case has been altered. The model gives a good prediction of the ballistic performance and the gas-to-wall heat transfer. However, the expected magnitude of reduction in heat-transfer when particles are present is not predicted. The predictions of gas flow invalidate some of the assumptions made regarding case and propellant behaviour during combustion and further work is required to investigate these effects and other possible interactions, both chemical and physical, between gas and particles.

INTRODUCTION

The impregnation of additives, such as talcum powder, into combustile cartridge cases has been found to reduce gun-barrel wear. Wear reductions of the order of 25-fold have been reported (1), although the reasons why additives should have such a marked effect is not clearly understood. Convective heat-transfer during firing, and erosion caused by the propellant gases, are thought to be the main factors contributing to wear. The presence of particle additives in the flow and their effect on boundary layer structure, reduction of transport gradients near the wall, reduction of turbulence levels and hence mass transport to the wall and possible chemical effects are likely reasons for the observed wear reduction.

The purpose of the present paper is to report on a collaborative experimental and theoretical study aimed at achieving a clearer understanding of the effects of additive particles on propellant gas flow and associated fluid-to-wall heat transfer. An earlier part of the study focussed attention on the behaviour of particles in the relatively simpler flow obtained in a shock tube, so that a basic understanding of the interactions between the particle and gas flows could be arrived at. In the experimental situation considered in this earlier study, ref (2), measurements were made of the heat-transfer to a flat plate after the passage of a shock wave. Measurements were made in both clean and dusty flows, and in the latter, a laser-attenuation technique was used to deduce particle concentration profiles.

A two-dimensional, two-phase mathematical model of this flow situation was developed. The application of this model, (3), showed that the velocity and thermal boundary layers were approximately doubled in thickness when particles were present. The heat transfer rate compared well with experimental data for both clean and dusty flows, the latter showing a marked reduction in heat pulse, and the predicted particle behaviour was in good qualitative agreement with the laser-attenuation measurements. It was concluded that the model describing the particle behaviour was sufficiently well validated for this case to merit testing it in a more detailed gun barrel model.

Present Contribution

The present paper describes the main features of a two-dimensional, two-phase transient model of a gun-barrel flow. As in the previous study, a general-purpose fluid flow computer code, PHOENICS, (4) is used to provide the solutions to the partial differential equations governing the fluid and particle behaviour. However, in contrast with the earlier shock studies where the geometry was extremely simple, the gun-barrel model includes many additional features which affect the flow, including:

* Variations in barrel geometry due to the forcing cones.
* Geometrical features of the projectile, including the penetrator rod, sabot and driving band.
* The projectile motion and associated frictional effects
* The propellant charge and its combustion.
* The initial distribution of particle additives and their rate of release.
* Leakages past the driving band and stabiliser band.
* The rise in barrel surface temperature.

Thus, as shown in Figure 1, virtually all the major features which might be important are represented in the model.

Separate equations are solved for the pressure, which is assumed common to both phases, the velocities of the gas and particles in the two coordinate directions and the enthalpies and phase volume fractions. The effects of turbulence are represented by use of a two-equation model (5) in which additional equations are solved for the turbulence kinetic energy and its rate of dissipation are solved.

The model has been used to predict the flow in a 120mm tank gun. Using values of numerical parameters which have been found to give grid and time-step independent results, calculations have been performed for cases with no additives, to establish a benchmark case. The model was then used to investigate the effects of talcum powder additives on the flow, and the heat transfer to the gun-barrel wall. Talc loadings of 10%, 20% and 30% by total weight of the case were studied.

The most debatable feature of the model concerns the assumptions made about the rate of release of additives, and the behaviour of the propellant and combustible cartridge case during the ballistic cycle. In the absence of any more detailed knowledge, the following simple assumptions have been made for preliminary studies.

* The propellant charge and cartridge case is assumed to remain in its original position throughout the transient.
* The rate of release of additives is in proportion to the amount of cartridge case burnt. The location of release is therefore governed by the initial distribution of talc.

The results of the calculations indicate that the first assumption is rather implausible, due to the high gas velocities which would transport unburnt propellant and case. This re-distribution of material would then affect the location of additive release.

MATHEMATICAL REPRESENTATION

Governing Differential Equations.

The flow in the gun-barrel is treated as transient and two-dimensional. The independent variables are thus the distances in the radial and axial directions, r and z, and time, t.

The dependent variables are represented in PHOENICS by the general, two-phase, three-dimensional transient conservation equation:

$$\frac{\partial(\rho_l R_l \phi)}{\partial t} + \mathrm{div}\,(\rho_l R_l \vec{u}_l \phi + j_\phi) = S_\phi \qquad 1;$$

here the subscript 'l' denotes the phase in question (1 for gas, 2 for particles) and:

ϕ = the dependent variable;

ρ = the density;

R = the volume fraction ($R_1 + R_2 = 1.0$);

u = the vector velocity;

J_ϕ = the diffusive flux vector; and

S_ϕ = the source of ϕ per unit volume

The variables which have been solved for in this study are:

v_1, v_2 = velocity of gas and particles in the radial, r, direction;

w_1, w_2 = velocity of gas and particles in the axial, z, direction;

h_1, h_2 = stagnation enthalpies of gas and particles;

k = turbulent kinetic energy of the gas;

ϵ = rate of dissipation of k; and

R_1, R_2 = volume fractions of gas and particles.

The pressure, p, which is presumed common to both phases, does not appear explicitly as the subject of a conservation equation. It is deduced indirectly from a combination of the phase continuity equations. The volume fractions are also calculated from the phase continuity equations, which are obtained by setting $\phi=1$ in equation 1.

The diffusive flux vector, J_ϕ, is written as:

$$j_\phi = -\Gamma\phi \ \mathrm{grad}\ \phi \qquad 2;$$

where $\Gamma\phi$ is the exchange coefficient for the variable.

In PHOENICS, the diffusive flux vectors for the continuity equations are taken to be zero.

The above equation set is closed by a series of auxiliary relationships linking the fluid properties and exchange coefficients to the dependent variables and the pressure.

The auxiliary relations have been described previously in reference (3), and therefore attention will be concentrated on details relating to the gun-barrel model.

Barrel and Projectile Geometry

The geometry of the barrel is defined by a set of formulae which give the radius at any distance from the breech. Thus the forcing cones, for example, are defined by the initial and final radii, and the corresponding axial distances. The taper of the barrel in these regions is allowed for by adjusting the volumes, face areas and radii of the finite-difference cells as a function of z.

The profile geometry is defined by blocking off appropriate cells in the finite-difference grid.

Projectile Motion

Motion of the projectile is accounted for by allowing a region of the grid, located between the charge and the projectile, to stretch as a function of time. The grid is thus a three-part grid; a fixed portion representing the charge; a stretching region to accommodate projectile motion; and a non-stretching moving section representing the projectile. The actual motion of the projectile is calculated from the pressure on the base of the projectile, and the resistance to motion.

Propellant and Combustible Case

No allowance has been made in the present calculation for movement or break-up of the propellant or case. They are assumed to remain in their original position throughout the transient. The propellant and combustible cartridge case occupy a known volume of the finite-difference cells at the start of the transient. As combustion proceeds, their volume diminishes. The buring rates of case and propellant are not calculated by the model at present. The fraction of each charge burned at any point in time is supplied as input data, the values being generated using a version of the Baer-Frankle lumped-parameter ballistics code (6).

The initial talc distribution can be defined by specifying the local percentage by weight of talc in each cell containing combustible case may be specified. The model then calculates the total percentage by weight of talc present. This allows the input of highly non-uniform talc distributions. Alternatively, the total percentage by weight of talc is specified, and the cells to contain talc are labelled. The model calculates the local mass percentage required to uniformly distribute the specified amount of talc among the specified cells.

Driving Band Leakage

(a) The Leakage Gap and Gap Closure

A small gap is assumed to exist initially between the nylon driving band and the barrel wall. High pressure gas escapes through this gap from the chamber into the saddle region. The gap is assumed to be a uniform annulus.

The size of the gap decreases linearly until complete closure when the rear edge of the driving band reaches a specified position. The size of the gap is given by a simple function of the input geometrical variables.

(b) Wall Friction and Heat-Transfer Rate in the Leak Region

The wall functions described in reference (3) are not used in the leakage region. Instead, the wall shear stress is estimated from a correlation for flow between parallel plates. The correlation used for the friction factor is:

$$f = \frac{24}{Re} \text{ for } Re \leq 6000 \qquad 3;$$

$$f = \frac{0.085}{Re^{1/4}} \text{ for } Re > 6000 \qquad 4;$$

The wall shear is then

$$\tau\omega = 0.5\ f\ \rho_{gm}\ W_g^2 \qquad 5;$$

where:

ρ_{gm} = Near wall mean gas density

W_g = Gas velocity in the leak region.

The wall heat-transfer rate is calculated from the shear stress using the simple Reynolds analogy:

$$\dot{q}_w'' = \frac{\tau_\omega}{W_g} (h_g - h_w) \qquad 6;$$

where:

h_g = Gas enthalpy in leakage gap
h_w = Gas enthalpy at wall temperature

Talc is also allowed to pass through the gap, but with no wall shear-stress or heat-transfer acting.

Stabiliser Band Leakage

The nylon stabiliser band at the front of the sabot is only a clearance fit within the rifling, and never forms a gas-tight seal. Gas and particles are allowed to escape whenever the pressure in the saddle is higher than the pressure ahead of the projectile. The mass outflow rates are calculated assuming choked nozzle flow (7).

$$\dot{m}_{g_{out}} = R_1\ A_{out}\ P_{IN} \left[\frac{2\gamma}{1-\gamma} \frac{1}{RT_{IN}} \left\{ \left[\frac{P_{OUT}}{P_{IN}}\right]^{\frac{\gamma+1}{\gamma}} - \left[\frac{P_{OUT}}{P_{IN}}\right]^{2/\gamma} \right\} \right]^{1/2} \qquad 7;$$

$$\dot{m}_{Tout} = \dot{m}_{gout} \frac{\rho_T R_2}{\rho_g R_1}$$

where:

P_{IN} = Pressure in saddle region
T_{IN} = Temperature in saddle region
P_{out} = Pressure ahead of projectile
A_{out} = Out flow area = free area of rifling grooves

Barrel Wall Temperature

The rise in temperature of the barrel wall surface is calculated assuming that the barrel is an infinite medium. A derivation of the expression shown below may be found in Rohsenow and Hartnett (8).

$$\Delta Tw = \left[\frac{\Delta H}{\pi/4\ \rho_S C_{ps} k_S\ t}\right]^{1/2} \qquad 8:$$

where:

ΔH = Total heat input to the barrel wall at that point

$\rho s, C_{ps}, k_S$ = Properties of the wall,

t = total elapsed time

The actual wall surface temperature at any time is then:

$$T_w = T_{w_o} + \Delta T_w$$

Where: T_{wo} = barrel temperature before firing.

This calculation is performed only along the barrel wall, but not on the breech, or on the projectile surface. These are assumed to remain at the original barrel temperature, T_{wo}. Along the barrel wall, the updated temperature, T_w, is used in the calculation of the wall heat transfer rate.

Finite-Domain Equations

The calculation domain is divided into a number of grid cells. A staggered grid is used in which the velocities are stored at the centres of cell faces to which they are normal. All other variables are stored at the centres of the cells themselves.

The velocity locations have their own surrounding cells, which act as control volumes over which the differential momentum equations are integrated, to yield the corresponding finite-domain equations for velocity. The continuity equations are integrated over control volumes surrounding the grid points.

The result of the integration is a set of finite-domain equations of the general form:

$$\phi_p = \frac{\Sigma a_l \phi_l + b}{\Sigma a_l - c} \qquad 9:$$

where Σ denotes summation over the neighbouring grid points. The coefficients a_i represent the effects of convection and diffusion; $(b + c\phi_p)$ contains the integrated source term for the cell, and, for the momentum equations, the pressure term. The use of upwind differencing in evaluating the convection terms ensures that the coefficients a_i are always positive, as required for numerical stability.

The finite-domain equations are solved using the IPSA algorithm of Spalding (9,10). For a complete description of the solution procedure the reader is directed to these references.

PRESENTATION OF RESULTS

Physical Situation

The main features of the modelled gun-barrel are shown in Figure 1. the barrel comprises a chamber of uniform radius followed by two forcing cones having tapers of 8^o and 1^o respectively, then a further section of uniform radius up to the commencement of rifling. From the C of R to the muzzle, a mean radius is calculated, taking into account the geometry of the rifling.

The projectile represented is of the Armour Piercing Fin Stabilised Discarding Sabot (APFSDS) type. It consists of a central penetrator rod, surrounded by a sabot, which is discarded when the projectile leaves the muzzle. The sabot is a clearance fit within the lands of the rifling. The gap between the projectile and barrel is sealed by a nylon driving band, which is compressed as the projectile is forced up the barrel. A gas-tight seal is only formed once the projectile has moved some distance up the barrel. Initially, obturation is poor and some gas will escape past the driving band. At the front of the sabot is a stabilising band, also of nylon, which centres the projectile in the barrel. This does not form a gas-tight seal at any stage of the ballistic cycle. At the rear end of the penetrator rod are six evenly spaced fins, which are covered by a fin-protect case, made of a combustible material. The propellant charge is composed of many long perforated sticks of propellant material. These are contained within a combustile case, which is impregnated with talc. The talc may be uniformly distributed throughout the case, or it may be locally concentrated in key areas. The firing sequence is initiated when an igniter charge is fired into the base of the propellant charge. This ignites a pad of black powder which in turn ignites the end of the propellant sticks in a more or less uniform fashion across the chamber diameter.

The flame then spreads up the sticks until they are completely ingited.

No attempt is made at present to model this process, and the calculation starts with the whole charge ignited. The initial gas temperature is taken to be the adiabatic flame temperature of the igniter pad, and the initial pressure that generated by the ignition process. Both temperature and pressure are assumed to be uniform throughout the chamber at the start of the calculation. The initial presure is 3.38 MPa, and the initial temperature is 2000 K. The projectile is initially at rest, and the gas within the chamber is also stationary.

Computational Details

The calculation domain is bounded by the wall and the breech end of the gun barrel which present impervious boundaries. At the stabilizing band, a constant pressure boundary is imposed. The grid size used for the reported calculations was 30 x 60 cells in the radial and axial directions respectively. The time-steps employed were 25μS until start of projectile motion, and thereafter 10μs.

Four runs are reported below, run 1 with no talcum powder additives, and runs 2 to 4 with 10%, 20% and 30% total weight of talc respectively. The talc is concentrated in the forward half of the combustible case.

Discussion of Results

Figures 2 to 5 show the projectile motion history in terms of travel, velocity, acceleration and base pressure respectively. The values of the parameter at the time of the peak Baer-Frankle pressure are also shown. The peak base pressure is reached about 0.5 ms before the Baer-Frankle prediction, and the other parameters show the same trend. Figure 6 shows the mean gas temperature within the chamber as a function of time. This again shows good agreement with the Baer-Frankle prediction. This is to be expected, since the burning rate used in the PHOENICS model is that predicted by the Baer-Frankle code thus implying that the equation of state and resistance to motion are correctly set up in the model.

Wall heat-transfer rates at three locations along the breech are shown in Figure 7. These locations are at the front end of the charge, at the initial position of the trailing edge of the driving band, and at the commencement of rifling respectively. The corresponding wall surface temperatures are shown in Figure 8.

Initially heat-transfer rate and surface temperature are highest at the front of the charge. Once the projectile starts to move, the peak heat-transfer rate moves down the barrel. There is no heat transfer at C of R until the projectile has passed, when the heat-transfer rate rises sharply. Once the peak value has been passed at around 4.0 msec, the heat-transfer rates fall quite rapidly and become very similar at all three locations. The surface temperature peaks somewhat later, reaching a value of 1150 K at 7.0 ms at C of R.

Axial distributions of wall heat-transfer rates and surface temperature are shown in Figure 9 and 10. The heat-transfer profiles rise to a peak immediately behind the projectile and move gradually down the barrel. At 8ms it is well past the C of R. The peak surface temperature reached is just below 1200 K.

Figure 11 shows radial profiles of axial gas velocity at 1ms. Within the charge, the core profile is fairly flat, although the influence of the penetrator rod can be seen near the axis. Between the end of the charge and the penetrator rod the core profile is again flat, but the velocity is about half of that in the charge due to the increased volume available. At small radii, the increasing influence of the penetrator rod can be seen, and at the barrel wall, the velocity reduces and exhibits a reverse velocity in front of the case due to a small flow recirculation in this region.

Figures 12 shows axial profiles of axial velocity at a radius of 3.0 cm, at 1 msec intervals between 5.0 and 8.0 msec and shows that as the projectile begins to move more rapidly, the velocity profiles become more or less linear, from zero velocity at the breech to projectile velocity immediately behind the projectile.

Axial profiles of gas temperature in the core flow region (at y = 3.0 cm) at 1 msec intervals from 1.0 to 8.0 msec are shown in Figure 13 and 14. The temperature profile remains flat in the propellant sticks, rising to a peak of 3250 K at 3.0 msec. This is below the adiabatic flame temperature of the propellant. As the projectile then accelerates away, the temperature throughout the barrel gradually falls. The peak temperature is always just behind the projectile. The highest value reached is 5000 K at 4.0 msec. These high temperatures are due to compression heating of gas released earlier. In spite of these high local temperatures, the mean chamber temperature, as shown in Figure 6, does not to exceed 3300 K.

Effect of Additives

Axial profiles of talc volume fraction for Runs 2 to 4 are shown in Figure 15. As expected, an increase in talc loading in the case increases the near wall particle density.

This effect is also seen in Figure 16 which shows the radial talc volume fractions for Run 18 only, at 0.64 m at 1ms intervals from 1 to 7ms. The concentration of talc by the wall builds up to a peak by 4.0 msec, and then falls rapidly. By 7.0 msec there is a small amount of talc by the wall, then a clear region with no talc, and then another region of talc. At this time the case has been fully burned for over 1 msec, so this must represent the remains of the talc being swept down the barrel.

Radial profiles of axial gas velocity for runs 1 and 3 at 0.64 m and 3.0 msec are shown in Figure 17. By the wall, and within the boundary layer generally, the presence of talc leads to higher velocities and thinner boundary layers. The core flow velocity can be seen to be slightly lower. This reflects the behaviour seen in Figures 2 to 5, where the effect of talc is to slightly reduce the projectile base pressure and hence the projectile acceleration and velocity. This is because some of the energy of the propellant is being absorbed by the talc particles, and does not contribute to the pressure on the projectile.

Radial profiles of gas temperature for runs 2 to 4 at 0.64m at 3ms are shown in Figure 18. The 'dusty' runs show a higher gas temperature than the 'clean' run, the temperature increasing with talc loading. This increase is a result of thermal equilibrium having been reached by the particles, and their specific heat being about half

that of the gas. Consequently, they cannot absorb as much heat as an equivalent mass of gas.

Despite the presence of talc, the heat fluxes to the wall are not greatly reduced. At 0.34m along the breech, just within the talc region, there is a small but systematic reduction in heat-transfer rate between 4.0 and 6.0 msec, Figure 19. Before this time, particle loadings near the wall are small, and afterwards the case is fully burnt, and all the particles have been swept away. During this time, there is a fairly high loading of cold particles close to the wall, and a small reduction in heat-transfer rate is seen.

The behaviour at monitoring locations further down the barrel is not so simple. For example at 63 m, Figure 20, the heat-transfer rates are sometimes lower and sometimes higher than in the case with no talc. Overall, the heat-pulse at these locations is higher.

CONCLUDING REMARKS

The predicted two-phase flow and heat-transfer in the gas and to the wall are in good quantitiative agreement with available direct evidence for the case with no particles. In particular, the ballistic behaviour and the wall surface temperature and heat-transfer rate are well predicted.

A small heat pulse reduction, which increases with increasing talc loading, is seen at the start of the talc region. However, the general flow conditions over much of the barrel are apparently such as to reduce, or even reverse the cooling effect of the particles.

Ward and Brosseau (11) have shown that additives reduce the measured heat pulse by ≈ 10%. They have also shown that the reduction is very sensitive to the exact location and configuration of the additive with respect to the propellant and projectile. Hence we may conclude that either:

* The talc is being released in the wrong place, and possibly at the wrong rate;

* Under gun-barrel conditions, particles cause heat-pulse reduction by other mechanisms.

Considering these points in turn, the representation of the charge and combustible case is a very simplified one, and may not represent the physical situation in enough detail. The burning rate of the case is an uncertain quantity, and the rate of release of talc from the case even more so.

The high velocities found in the propellant ($\approx 300\ ms^{-1}$) would give rise to large shear forces on the sticks and case, which would tend to break them up and move them about the chamber. This may bring talc bearing material into closer contact with the rear of the projectile and hence help reduce heat-transfer rates around the C or R.

Many alternative mechanisms of heat-transfer rate reduction have been suggested. These include:

* Endothermic chemical reactions in the boundary layer;
* Promotion of atomic reassociation further away from the wall,
* The creation of a thin insulating layer on the barrel surface; and,
* The effect of particles on near-wall turbulence structure.

None of these mechanisms have been included in the model, though in a high-pressure reactive flow they may be significant. The present model is, of course, a necessary first step in examining alternative mechanisms of wear reduction, since the distribution and conditions of additives must first be known before assumptions regarding their physical behaviour can be usefully tested.

The model can also provide useful insight into the flow behaviour within the gun barrel by giving information such as:

* Heat-transfer rate and surface temperature distributions along the barrel wall;
* Talc distributions within the barrel;
* Temperature distributions within the barrel;
* Passage of pressure waves up and down the barrel;
* Flow patterns around the back of the projectile; and,
* Leakage effects.

Further work is now required to investigate the effects of charge break-up and its motion during the ballistic cycle, and the consequences in terms of particle release rate and location. The incorporation of physical models which account for other wear reducing mechanisms should also be carried out in a systematic way in order to determine whether such effects are important.

ACKNOWLEDGEMENT

This work was carried out under contract for the Royal Armament Research and Development Establishment, Procurement Executive, Ministry of Defence.

REFERENCES

1. D C A Izod and R G Baker, "Gun Wear: An Account of recent UK Research and New Wear Mechanisms", Seventh Int. Symposium on Ballistic paper S2.5 (1983).

2. G T Roberts, R A East and N H Pratt, "Heat Transfer in Flows with Particulate Additives - A Shock Tube Study". Seventh Int. Symposium on Ballistic paper S1.4 (1983).

3. J C Ludwig, N Rhodes, D G Tatchell, "Numerical Modelling of the Flow of a Hot Particle-Laden Gas", Seventh Int. Symposium on Ballistics, paper S1.3 (1983).

4. D B Spalding, "A General-Purpose Computer Program for Multi-dimensional One- and Two-phase Flows", Mathematics and Computers in Simulation, North Holland, Vol XXIII, pp 267-276, (1981).

5. F H Harlow and Nakamaya, "Transport of Turbulent Energy Decay Rate". Los Alamos Scientific Laboratory, U. of California, L 3854, (1968).

6. P G Baer and J M Frankle, The Simulation of Internal Ballistics Performance of Guns by Digital Computer Program. BRL Report 1183, (1962).

7. G F C Rogers and J P Mayhew, Engineering Thermodynamics Work and Heat Transfer. Longmans, London, (1967).

8. W M Rohsenow and J P Hartnett, Handbook of Heat Transfer. McGraw-Hill Book Co. (1973).

9. D B Spalding, "Numerical Computation of Multiphase Fluid Flow and Heat Transfer". Recent Advances in Numerical Methods in Fluids, Vol I, Editors: Taylor C and Morgan K, Pineridge Press, pp 139-167 (1981).

10. D B Spalding, "Development in the procedure for numerical computation of multiphase-flow phenomena with interphase slip, unequal temperature, etc". Second International Conference on Numerical Methods, Maryland University, USA. (1981).

11. J R Ward and T L Brosseau, Reduction of Heat-Transfer to High Velocity Gun Barrels by Wear-Reducing Additives. AIChE-ASME Heat-Transfer Conference, Salt Lake City, Aug 15-17, (1977).

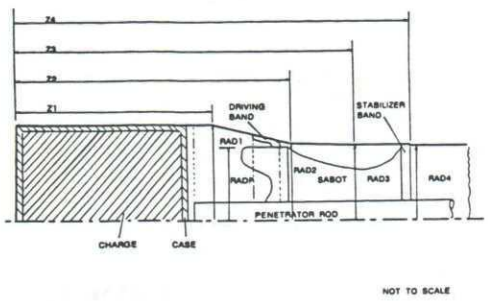

FIGURE 1 AXIAL CROSS SECTION OF BARREL AND PROJECTILE WITH SIMPLIFIED CHARGE AND NO FIN-PROTECT CASE

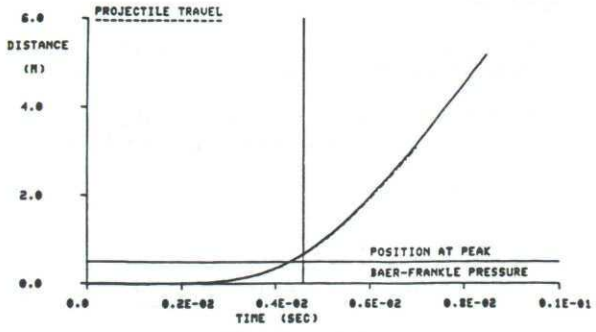

FIGURE 2 PROJECTILE MOTION TIME HISTORIES FOR RUNS 1 TO 4

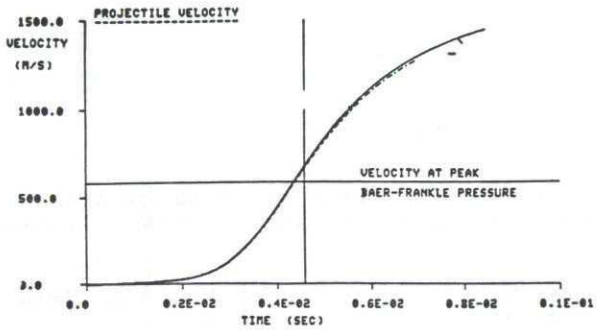

FIGURE 3 PROJECTILE VELOCITY TIME HISTORIES FOR RUNS 1 TO 4

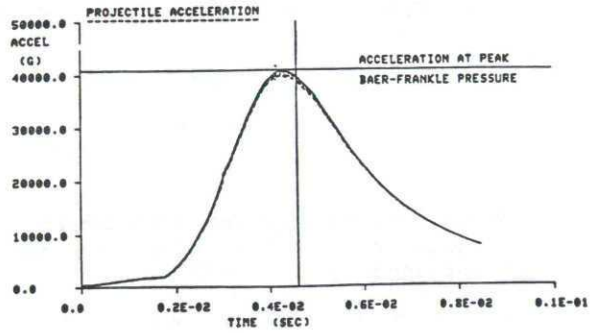

FIGURE 4 PROJECTILE ACCELERATION TIME HISTORIES FOR RUNS 1 TO 4

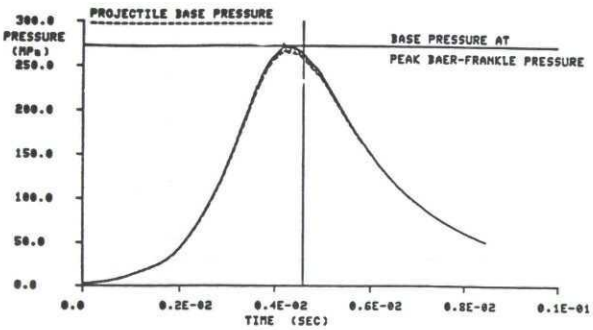

FIGURE 5 PROJECTILE BASE PRESSURE TIME HISTORIES FOR RUNS 1 TO 4

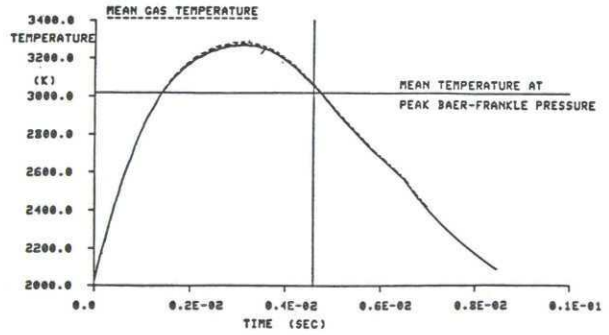

FIGURE 6 WALL HEAT-TRANSFER RATE TIME HISTORIES AT Z=0.63m, 0.76m AND 0.97m FOR RUNS 1 TO 4

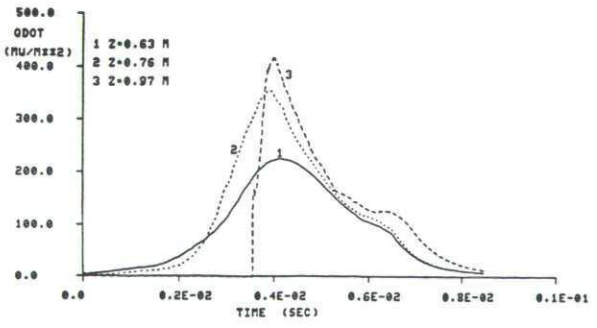

FIGURE 7 WALL HEAT-TRANSFER RATE TIME HISTORIES AT Z=0.63m, 0.76m AND 0.97m FOR RUN 1

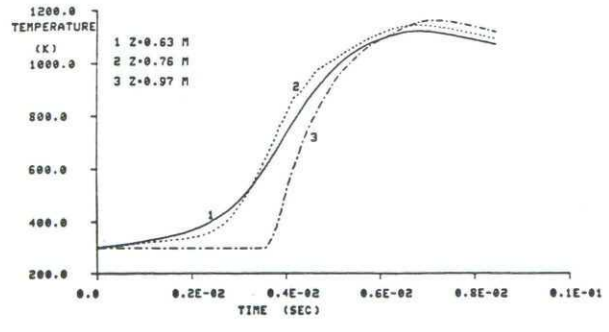

FIGURE 8 WALL SURFACE TEMPERATURE TIME HISTORIES AT Z=0.63m, 0.76m AND 0.97m FOR RUN 1

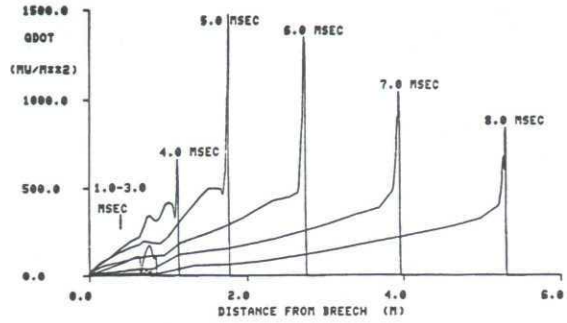

FIGURE 9 AXIAL PROFILES OF WALL HEAT-TRANSFER RATE FOR RUN 1

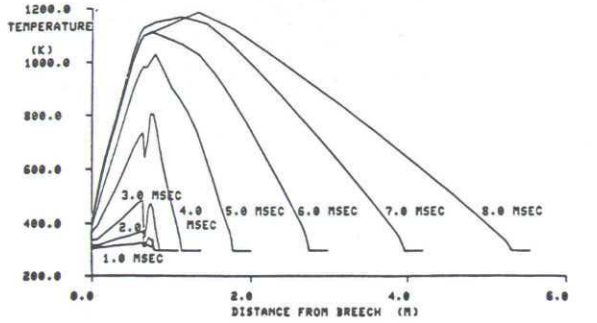

FIGURE 10 AXIAL PROFILES OF WALL SURFACE TEMPERATURES FOR RUN 1

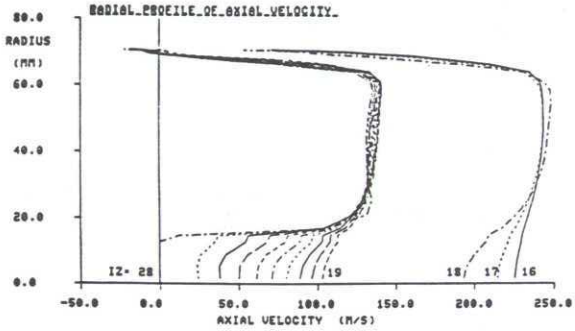

FIGURE 11 RADIAL PROFILES OF AXIAL GAS VELOCITY AT VARIOUS AXIAL LOCATIONS AT 1.0msec FOR RUN 1

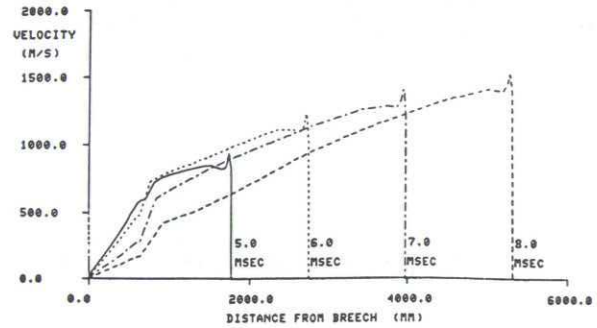

FIGURE 12 AXIAL PROFILES OF AXIAL GAS VELOCITY AT A RADIUS OF 30mm FOR RUN 1

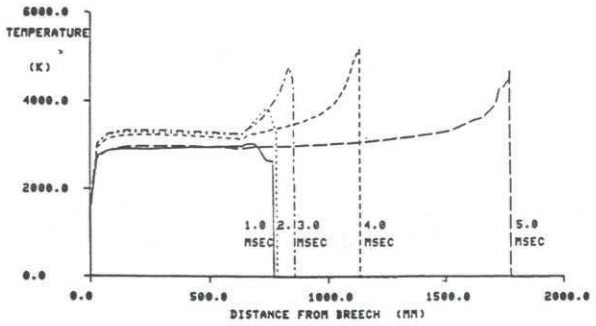

FIGURE 13 AXIAL PROFILES OF GAS TEMPERATURE AT A RADIUS OF 30mm FOR RUN 1

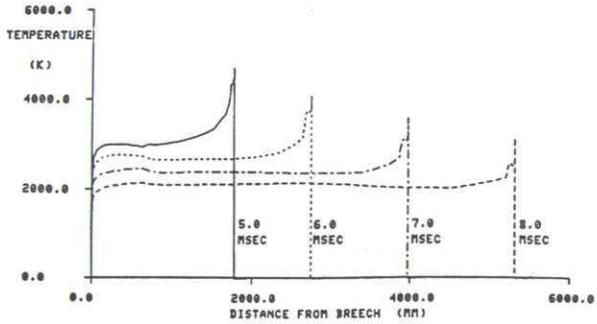

FIGURE 14 AXIAL PROFILES OF GAS TEMPERATURE AT A RADIUS OF 30mm FOR RUN 1

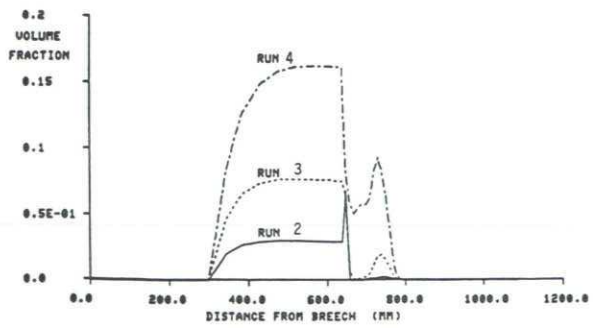

FIGURE 15 AXIAL PROFILES OF NEAR-WALL TALC VOLUME FRACTION AT 3.0msec FOR RUNS 2 TO 4

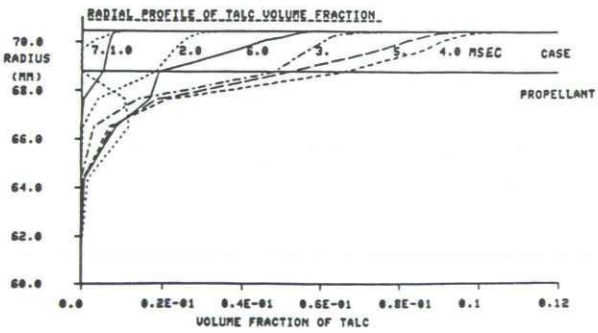

FIGURE 16 RADIAL PROFILES OF TALC VOLUME FRACTION AT Z=0.64 AT VARIOUS TIMES FOR RUN 2

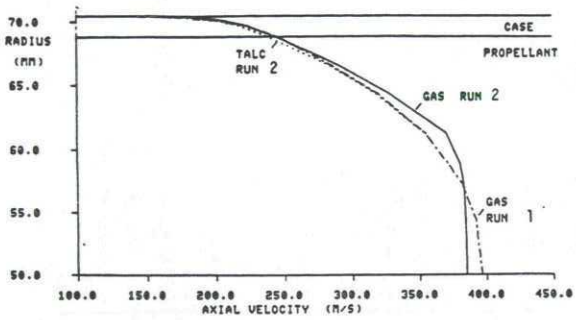

FIGURE 17 RADIAL PROFILES OF AXIAL GAS AND TALC VELOCITY AT Z=0.64 AT 3.0msec FOR RUNS 1 AND 2

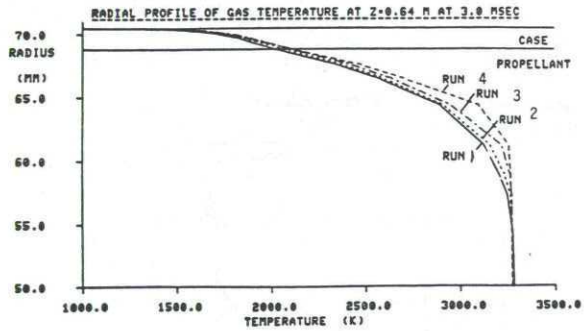

FIGURE 18 RADIAL PROFILES OF GAS TEMPERATURE AT Z=0.64m AT 3.0msec FOR RUNS 1 TO 4

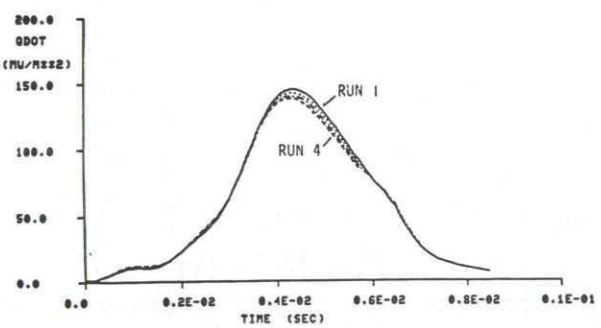

FIGURE 19 WALL HEAT-TRANSFER RATE TIME HISTORIES AT Z=0.34m FOR RUNS 1 TO 4

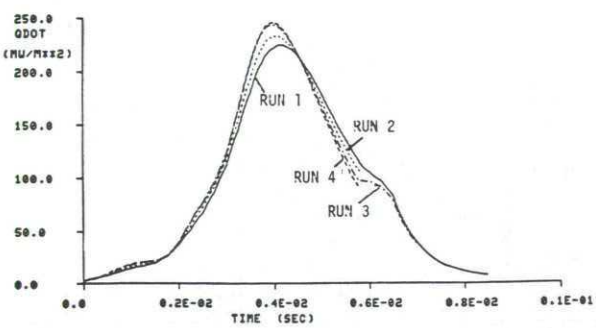

FIGURE 20 WALL HEAT-TRANSFER RATE TIME HISTORIES AT Z=0.63m FOR RUNS 1 TO 4

DISCUSSION

B.Zeller, Fr

What is the volume of this code? That is, how many instructions does it have on the computer you use?

Author's Reply

We did a study of the effects of grid size and time step because, of course, it's a transient process, and produced results which we felt were independent of these numerical parameters. The typical sort of grid sizes were 20×30 or 30×40, which we found were reasonable. The computer time? Is that your question? or the size of the program? (Mr Zeller's question was not answered.)

M.Summerfield, US

This paper does not shed much light on the mode of action of talc additive as a barrel wear reducer. The mathematics does not reveal the mechanism that the authors embedded in their analysis. From the text, one can perhaps guess that the talc is assumed by the authors to participate mainly by being a heat sink for part of the energy released by combustion, thus reducing the heat transfer slightly. Is this inference correct? If the authors had shown the relations used, if any, for the ways in which the particles interact with the gas, some inferences might have been drawn. Thus, is it assumed that the particles lag the turbulent gas motions, thus suppressing the near-wall turbulence by viscous drag? Do the particles add to the main gas so as to alter the computation of average gas properties, such as gas constant, R? Do they alter the boundary layer structure in some way? We note that the authors state that whatever mechanisms are contained in this theory are not successful, but that it might lead to alternative better hypotheses in future work; but what are the hypothetical mechanisms that are found to be unsuccessful?

Author's Reply

In order to grasp the full complexity of the model, it is essential to study Reference (3), which describes the development of the physical basis of the gas/particle interactions which are incorporated in the mathematics. In summary, it should be emphasized that conservation equations of the form of Equation (1) are solved for the velocities and enthalpies of the gas and particulate phases. Coupling between the phases occurs through heat transfer and inertial effects, and the physical properties of the mixture are affected locally according to particle number density.

The model was developed and tested by comparison with shock tube experiments. Reference (3) describes the success of the model in predicting boundary layer thickening, heat-transfer reduction and particulate dispersion in the boundary layer, which develops in a shock tube. When this model is applied in the gun-barrel environment, the reduction in heat-transfer observed in the shock-tube experiments is not predicted, largely due to the great change in gas conditions between the two cases. Nevertheless, the assumptions used to describe the gas/particle interactions are deemed to be valid although clearly incomplete. A number of additional mechanisms are mentioned in the paper which should be tested in the model. However, close collaboration between modellers and experimentalists is required to throw light on the very complex physics occurring in a gun barrel.

R.Mesnil, Fr

I would like to know whether in your model, not now maybe but in the future, you can take into account the various reasons for erosion, that is, the level of pressure at which the gun operates, the flame temperature of the propellant which is used, and also maybe the chemical aspects which will have to be taken into account according to the different propellants that you use. Do you think you'll be able to separate the various types of erosion or wear and what the main factors are for explaining a type of erosion or wear?

Author's Reply

The purpose of the modelling study is to obtain a clearer understanding of the physical processes occurring in a gun barrel. When the physics are well described by the model, then it can be used to predict the effect of all parameters. At the present stage, the model predicts the gross ballistic parameters well, and provides much information on the flow behaviour. Attention needs to be focused on the details of the chemistry, and suitable physical laws included in the model in order that the above questions can be answered fully. Incorporating the physical laws is a minor task, assuming, of course, that they are known.

NOVEL IGNITION SYSTEMS FOR HEAVY CALIBRE GUNS.

C N Bowden, G G Cook and P S Henning.
Royal Armament Research and Development Establishment,
Fort Halstead,
Sevenoaks, Kent, TN14 7BP, UK.

SUMMARY.

In recent years there has been a trend towards steadily rising gun pressures, especially in direct fire weapons and this has caused many functional problems to arise with conventional vent tube ignition systems. To overcome these problems and to allow the process of gun development to continue, the UK has been carrying out a programme of research into a number of novel ignition systems for heavy calibre guns. These include: spark ignition, laser ignition and electrical impulse ignition.

A number of different spark plug configurations have been evaluated. Extensive trials have been carried out on the ignition characteristics of black powders and black powder substitutes using an experimental 4J Neodymium laser. Work has also been carried out on the development of high pressure sapphire windows. A study into methods of charge ignition by electrical impulse techniques has also been carried out.

1. INTRODUCTION.

In recent years in the UK, there has been a design trend for both direct and indirect fire guns, towards separated ammunition with stick propellant charges contained in combustible cartridge cases. With this design layout, ignition is traditionally achieved by means of separately loaded vent tube cartridges, which are either percussion or electrically ignited. At the same time,there has also been a trend towards significantly higher operating pressures and higher rates of fire which has caused problems with sealing the vent tubes, with maintaining the mechanical integrity of the cartridge cases, with preventing vent hole erosion, and with loading the cartridges quickly and reliably. It is the opinion of many British gun designers that the current state-of-the-art represents the design limit of vent tube ignition systems and that alternative methods of ignition have to be provided to allow the process of system performance improvement to continue.

To establish the most suitable alternative, the UK has been carrying out a systematic review of novel methods of igniting gun propelling charges. As a design principle for this study, it was considered necessary to retain the concept of separately loaded ammunition and any alternative ignition method must have the ability to ignite the propelling charge under the following criteria:

a. It must be capable of igniting charges repeatedly for at least 250 rounds and desirably for the life of the barrel or breech mechanism.
b. It must satisfactorily ignite the charge despite the fact that there can be considerable variations in its initial position in the chamber relative to the breech.
c. It is desirable that wherever possible, a new system should be capable of igniting the range of charges which are currently in service.

In the study covered by this paper, the following ignition methods have been reviewed:

i. Spark ignition.
ii. Laser ignition.
iii. Electrical impulse ignition.

This paper describes some of the initial trials that were carried out to prove the feasibility of each method. In each case the aspect of the system which was considered to be the most critical was studied experimentally in detail.

We will discuss each of these methods in turn in the following sections of the paper:

2. SPARK IGNITION.

2.1 Spark System Layout.

Spark ignition appears to offer the benefit of very large amounts of power being available for charge ignition at a well defined point in the gun, utilising relatively low cost, well proven technology. The system also permits considerable simplification of the gun breech design.

Spark ignition was previously studied at RARDE during the 1960's (Ref.1 and 2) by Price and Miles who used a similar experimental layout to the one which is proposed for this study, shown schematically in Fig.1. The spark plug is situated in the wall of the

gun chamber. The spark is made to penetrate an insulant layer covering a conducting band on the combustible charge case material,from whence it passes along a conducting track to the point of ignition. The gun powder igniter pad may be ignited by a match head fuse or by means of a secondary spark igniting pyrotechnic material. The electrical energy is returned to earth through a physical contact between an outer conducting track on the charge container and the gun barrel.

The work of Price and Miles indicated that this layout could successfully ignite large calibre gun systems. The problem which they did not successfully solve, however, was the design of a spark plug which could endure the gun environment for an acceptable number of firing cycles without insulator fracture or erosion. They found that the ceramic materials which were available at the time, were too brittle to withstand the heavy cyclic loads whilst insulants which had the inherent toughness to withstand the pressure environment could not withstand erosion by the hot gases.

2.2 Spark Plug Evaluation Trials.

It was decided that the present review of spark ignition (Ref. 3) would start at this point. The work of Price and Miles was considered as an adequate demonstration of the feasibility of igniting heavy calibre guns by spark, thus allowing the present work to be directed towards evolving a spark plug design which could withstand the gun environment. This was considered to be the most critical aspect of applying this method of ignition to a practical gun application.

Improved ceramic materials, which have become available since Price and Miles carried out their studies, offer some prospect of success. However, in the same period, there has been a considerable increase in maximum gun pressures with a consequent exacerbation of the previous sealing and insulator brittleness problems. The current research programme has been directed towards evaluating the performance of modern ceramic materials under simulated gun conditions, using a special purpose vented vessel (Fig 2). The mechanical integrity of the candidate materials was tested "passively" by repeated pressurisations in the vessel which was ignited by means of a separate electric vent tube system. It is necessary for the spark plug to survive the high pressures in the gun chamber and to tolerate the conductive effects of debris deposits on the surface of the insulating material.

Rapid rates of fire is probably the most important feature of the heavy calibre gun environment which the vented vessel shown in Fig 2 does not simulate. To simulate typical rates of fire, a special vented vessel was produced with multiple charges which could be fired in a predetermined sequence. The vessel could be preloaded with up to 10 propellant charges, each with its own means of ignition, nine of these propellant charges were located in specially designed holders housed in radial borings in the vessel. A fusehead was situated at the end of each holder which was closed by an aluminium burst disc. The restriction to flow in the holder ensures that the combustion pressure exceeds the pressure in the main chamber of the vessel. By allowing the burster disc rupture pressure to be greater than the main chamber pressure, the charges can be isolated until required . The first charge to be ignited was located in the main chamber of the vessel and again initiated by an electric fusehead.

The propellant used in the rate of fire evaluation was NC30, a single based propellant with a flame temperature of 3240K. The ceramic sample for assessment was located in the remaining radial location and, to simulate maximum erosion effects, the sample was always located adjacent to the vent orifice.

The spark plug design which was used for most of the evaluations, is shown in Fig 3a and follows quite closely the design of Price and Miles. Later the design was changed to take advantage of the properties of modern glass ceramics. After firing, the change of electrical resistance of the spark plug insulators was monitored and the recovery of electrical properties with time was noted.

The criteria used for judging the spark plug designs can be summarised as follows:

a. The plug materials and seals should sustain a limited number of pressurisations to 620 MPa.
b. The plug materials and seals should sustain 500 firing cycles at a pressure of 360 MPa.
c. The electrical insulation properties of the ceramic materials should sustain 500 firing cycles at a pressure of 360 MPa.
d. The spark plug should be able to sustain burst rates of fire of up to one round every 5 secs.

2.3 Ceramic Materials Reviewed.

So far during this study five ceramic materials have been assessed. These are:

a. Polycrystalline alumina.
b. Single crystal alumina(ie sapphire)
c. Hot pressed silicon nitride.
d. Silicon aluminium oxynitride (Sialon).
e. Glass ceramic (lithium alumino silicate).

The polycrystalline alumina ceramics were chosen as a starting point to correlate with the work of Price and Miles. The commercially available alumina ceramic used in this work was Deranox 995 which is made up of 99.5% aluminium oxide and 0.5% magnesium oxide. The Deranox ceramic is manufactured by a sintering process and has a residual porosity of approximately 5%. For the present application, the porosity has several disadvantages. Firstly, the strength of the ceramic is a function of the pore size and so is subject to variability. Secondly, the porosity allows combustion products and debris to penetrate and so impair the electrical insulation properties of the material. These problems may be overcome by manufacturing the insulators from fully dense single crystal alumina (i.e. sapphire).

Hot pressed silicon nitride is manufactured from elemental silicon which is compressed in a graphite mould and allowed to react with nitrogen gas at elevated temperature over an extended period of time. The material used in this work had a mean residual porosity of 0.2%. The second nitride based ceramic which was considered was Sialon, a silicon aluminium oxynitride. Sialon is stronger than hot pressed silicon nitride and should be a suitable candidate material.

Glass ceramics, only recently available in the UK, differ from conventional ceramics in that they are manufactured by the de-vitrification of a glass. The end result is a material that is fully dense with glass occupying intercrystalline sites. The presence of glass in place of voids is preferred as it represents a significant increase in strength over a porous ceramic and in addition, the absence of porosity will help prevent the ingress of debris. The glass ceramics used in the present assessment were all based on a lithium alumino silicate system. The strength of the ceramic, although considerably lower than that of silicon nitride, is reproducible. Another significant advantage of glass ceramics is that bonding to metals is an established technology. The spark plug which was used for evaluation, took advantage of this fact and had a bonded central electrode(Fig 3b).

2.4 Experimental Results.

2.4a. Mechanical Assessment.

Both polycrystalline and single crystal alumina spark plugs(Fig 3a)fractured repeatedly when subjected to pressures of 620 MPa in the vessel shown in Fig 2. Only one sample of polycrystalline alumina survived the life assessment test of 500 pressurisations to 360 MPa. This test piece revealed an additional problem in that the insulator was eroded by the combustion products. At this point further assessment of alumina was abandoned as it was apparent that spark plugs of this material were unlikely to survive reliably in the gun environment.

During its evaluation, the strength of silicon nitride proved adequate. There were no insulator failures observed at pressures up to 620 MPa. The main problem encountered during the evaluation was the destruction of the copper compression seals. During the life assessment tests, in which the plugs were exposed to 500 consecutive firings at 360 MPa, it was found necessary to replace the copper compression seals after approximately 50 firings. When exposed to pressures in excess of about 550 MPa the seals needed replacing after each firing. Silicon nitride was not seriously eroded by the products of combustion during the life assessment trial.

Sialon (silicon aluminium oxynitride) was initially assessed in the form of cylindrical test specimens. These were subjected to gun conditions using the vented vessel (Fig 2). Sialon proved to be a very brittle material and when exposed to rapid pressuration it fractured catastrophically. Further assessment of Sialon was abandonned.

As mentioned earlier, the principle advantage of glass ceramics is that ceramic-to-metal bonding is an established technology. Thus the evaluation plugs were manufactured with bonded central electrodes. Trials showed that these plugs were a significant improvement on alumina but they were still unable reliably to withstand pressurisation to 620 MPa without failure. Mechanical failure took the form of chipping of the ceramic rather than catastrophic fracture. However, in several isolated cases, sections of significant size were removed thus rendering the design unacceptable at gun pressures. During the endurance test, in which the spark plugs were exposed to 500 consecutive firings at 360 MPa erosion of the ceramic by the products of combustion was minimal.

The results of these tests were sufficiently encouraging to warrant further evaluation of the glass ceramic material. It was felt that the established and reliable ceramic-to-metal bonding techniques provided the opportunity of incorporating the insulator into a metal housing which could give it adequate support. Consequently a composite spark plug (Fig 3c) was designed. The housing and electrode were made of Fecraloy to match the linear thermal expansion of the ceramic. As yet, this spark plug has not been evaluated over 500 firings but the early results in which the plug has been exposed to 620 MPa were encouraging with no failures of either the ceramic or the seals.

2.4b. Electrical Assessment.

The quiescent resistance values (after drying in an oven)for the range of materials which were tested are shown in Fig(4) as a function of the number of firings. Alumina shows a steady decay from 10^{11} ohms to 10^{8} ohms. The glazed alumina which was introduced to prevent impregnation by combustion debris,is of particular interest. The resistance

increases initially which corresponds to a period in which the surface glaze cracks and is removed along with the adhering debris. Thereafter the resistance decays in a similar fashion to the unglazed alumina. The glass ceramic exhibits a curious effect at around 100 exposures. A white glass-like deposit (the original ceramic being blue) became apparent after 30 exposures during which the resistance slowly dropped. At around 100 exposures the rate of decrease was arrested, coinciding with the start of the subsequent erosion of the white deposit and with a recovery in the resistance across the plug. Of all the materials tested, silicon nitride exhibited the most favourable characteristics.

The change of resistance with time after firing, is also a spark plug characteristic which is of interest to the gun designer. Fig(5a) and (5b) show typical results for two different ceramic materials. Fig (5a) shows the recovery of resistance as a function of time across a silicon nitride insulator which has been fired only once and one which has been fired 500 times. For the clean plug, little effect is seen on the resistance after approximately 45 minutes but for the fouled plug, recovery to a steady value takes approximately 2.5 hours. Fig (5b) shows a similar result for the glass ceramic spark plug.

2.4c Thermal Assessment.

As mentioned earlier, the rate of heating of the ceramic insulator as a function of the rate of fire was determined. So far this evaluation has only been carried out on alumina. The temperature was recorded using a chromel/alumel thermocouple embedded 0.5 mm below the surface of a 10 mm diameter cylindrical sample of the alumina ceramic. Fig(6) shows the results of the experiments. The temperatures in the ceramic were continuously recorded and the values plotted represent the maximum temperatures reached after 8 consecutive firings at the appropriate rate. It will be observed that at the higher rates of fire the temperatures in the surface layers of the ceramic will approach the auto-ignition temperature of the charge containment material. This is a factor which will need to be kept in mind when a gun ignition system is designed.

3. LASER IGNITION.

3.1 Laser System Layout.

Laser ignition (Ref.4,5 and 8) appears to offer the benefits of large amounts of power impinging upon the charge in a well defined near-parallel beam of radiation, thus reducing the problems arising from the uncertainty in charge position. In order to deliver the laser energy to the propelling charge within the gun chamber, it is necessary to design a window which is capable of withstanding gun pressures and which is transparent to the chosen laser wave length. The laser must provide sufficient power to penetrate the charge and igniter containment materials through a window partially obscured by combustion debris. In order to avoid surface damage to the windows by dissipation of the laser energy in the contamination layer, specific steps must be taken to minimise the build-up of propellant debris on the window surface.

From a survey of potential window materials with the required strength for operation at gun pressures and transparent to useful laser wavelengths, sapphire was chosen as the most suitable and cost effective. Sample sapphire windows were subjected in a test vessel to multiple exposure cycles of burning gun propellant at a pressure of 500 MPa. Fig (7) shows the measured light transmission properties of sapphire in both the clean and the contaminated condition. Between 0.28 and 0.90 micrometres there are additional losses caused by scattering from debris on the window. The results also indicate that the attenuation caused by debris tends to approach an equilibrium value as the number of exposures to the combustion products increases.

This evaluation of the transmission properties of sapphire in both the clean and fouled condition, led to the choice of neodymium glass as the most suitable laser for the application. This laser system operates at 1.06 micrometres in the near infra-red region and so operates away from the region where the debris causes additional scattering.

Having chosen the window and the most appropriate laser system, the layout of the overall system (Fig 8) can now be designed. It was decided that the laser cavity would be fixed to the gun cradle and the laser beam passed axially back along the side of the gun. A mirror system would be used to pass the beam through drillings in the breech assembly, turning the beam through 180 degrees so that it enters the chamber through the sapphire window on the centre line of the barrel. In the system studied the laser would be required to ignite those components of the ignition train which, in British practice, is currently incorporated in the base of the separated charge. This usually consists of a powder ignition charge contained in a cloth bag which, in turn, ignites the main propellant charge. In addition the laser, in some cases, may have to penetrate the base of a combustible cartridge case.

Several areas of the above design layout were considered to be critical to the feasibility of applying laser ignition to heavy calibre guns and these were the ones which were addressed in this initial study. The first critical area is the determination of the exact physical conditions required for a laser to reliably ignite the combustible materials commonly used in gun charge systems. As a preliminary to gun ignition trials, detailed ignition tests on various igniter materials using a 4J neodymium laser have been carried out in the laboratory. These ignition trials and the design and manufacture

of the laser required for gun trials has been carried out by International Research and Development Co Ltd (Newcastle-upon-Tyne, England) under contract to RARDE. The second critical area is the design of a suitable window which will allow the laser energy to enter the gun chamber repeatedly, even when fouled with combustion debris and which will survive the aggressive gun environment to give an acceptable component life.

3.2 Assessment of Laser Ignition Energies.

The experimental test arrangement is shown in Fig 9. An angled microscope eyepiece unit was combined with suitable lenses to form a viewing system. The viewing/focusing optics were mounted on a channel-section chassis bolted to the front of the laser head with the laser beam being introduced to the optical axis by a deflector mirror. An in-head energy monitor was incorporated in the laser to enable the output to be continuously recorded during the experiments. The optical pick-up head consisted of a beam splitter diverting approximately 5% of the laser output to a remote detector unit containing a photodiode and associated electronics. The integrated output from the photodiode gave a measure of the pulse energy. A small 1mW helium-neon laser was used to align the optical system with the test samples.

The materials which were assessed included the following:

a. Blackpowder.
b. Blackpowder + 5% graphite.
c. Substitute powder.
d. Lead dinitroresorcinate (LDNR).

The tests were all performed in air at atmospheric pressure. The beam diameter at the point of ignition was set by altering the distance between the sample and the laser focusing lens. No attempt was made to specify energy densities. Instead the beam energy was simply recorded for each measurement and the focused beam diameters were defined purely in terms of the optical geometry. The approach, adopted by some workers,of increasing the incident laser energy until ignition occurred was found to be inadequate. Thresholds obtained by applying multiple shots until ignition occurred were invariably lower than the true first shot threshold. An ignition probability curve was required to describe the behaviour properly.

Fig 10 gives the ignition energy characteristics for blackpowder. The curves show the ignition probability as a function of the laser pulse energy for a number of different beam diameters. The ignition threshold energy is defined as the minimum energy required to give an ignition probability of unity. There is some anomalous behaviour with gunpowder. Firstly, the ignition threshold energy increases as the beam is concentrated to smaller diameters and secondly, the curves contain unusual dips. These phenomena are attributed to the generation of extremely energetic reactions at the point of laser impingement resulting in the burning material being rapidly dispersed before continuous burning can be established.

The ignition characteristics of blackpowder with 5% graphite added as a retardant are shown in Fig 11. They show a trend similar to that of blackpowder in which the threshold energy increases as the beam is concentrated. However, no anomalous dips are present in the ignition probability curve and the thresholds are much lower than for blackpowder.

Fig 12 shows ignition characteristics of substitute powder. As would be expected threshold energy decreases as the beam is reduced in diameter. However, at the lowest beam diameter, anomalous behaviour is again exhibited with the curve showing an increased energy threshold.

Fig 13 shows the limited results at present available for lead dinitroresorcinate (LDNR). The ignition thresholds are extremely low in comparison to the other materials and difficulty was experienced in making accurate measurements at these low energy values.

3.3 Assessment of the Effect of Pulse Duration.

The work reported above was carried out at a constant laser pulse duration of 1.5 msec. A study was carried out to assess the influence on the ignition threshold of variation in the laser pulse duration. The results for blackpowder are given in Table 1, for a beam diameter of 2 mm.

TABLE 1.

The Ignition Threshold of Blackpowder as a Function of Pulse Duration.

Pulse Duration (msec)	Ignition Threshold (J)
1.0	3.8
1.7	2.6
2.3	1.5
3.0	0.1
4.5	0.1

From these results it can be seen that there is a sharp fall in the ignition threshold energy when the pulse duration is increased from 2.3 to 3.0 msec. It is this value which represents the optimum pulse duration for the ignition of blackpowder.

3.4. Assessment of the Laser Window Design.

The design of a suitable laser window was the second critical area of a laser ignition system which was addressed in this study. A window system was designed and extensively tested under simulated gun conditions in a vented vessel. In this design, the sapphire window was first bonded into a metal holder of Nilo 42 using the well established moly-manganese system for bonding alumina based ceramics to metals. The window holder assembly was then electron beam welded into a housing.

In the assessment trials, window assemblies have been pressurised to 960 MPa without leakage. However, some distortion of the Nilo 42 holder was noted. The design is considered to have adequate strength up to 650 MPa. An initial assessment was carried out which consisted of 100 consecutive firings at 650 MPa in a vented vessel. These results gave an indication that windows with an acceptable design life could be produced.

Studies were also carried out into ways of reducing the amounts of combustion debris deposited on the surface of the windows. Tests showed that the debris trap concept shown in Fig 14 can significantly alleviate the window fouling problem. In this system, the pressurising gases are forced to enter an expansion chamber through a restricting orifice. The flow pattern tends to direct the debris towards the wall of the expansion chamber where they impinge and adhere. The experimental assessment allowed the optimum dimensions of the debris trap to be determined. Fig 15 shows the effect of a typical debris trap on the deposition of contamination on a sapphire window. The propellant which was used for these tests was single base NC30 and the maximum combustion pressure was 360 MPa. The results show a reduction in transmission of approximately 30% which can be compared to a reduction of nearly 75% when the windows are unprotected.

4. ELECTRICAL IMPULSE IGNITION.

4.1 Initial Assessment.

The evaluation of electrical impulse ignition (Ref.6,7 and 8) commenced with an overall assessment of a variety of methods of obtaining electrical coupling between the components of the ignition train situated in the charge and those situated in the breech assembly. There are two basic types of system. The first type is the contacting method in which a contact or probe is used to form a direct electrical connection from outside the gun to the ignition train in the propelling charge. The second variety is the non-contacting type in which the electrical energy is transferred to the charge by means of either capacitive, magnetic or electro-magnetic coupling. This gives a total of four systems to be evaluated which we will discuss in turn.

A brief study of the contacting method revealed some serious problems. Maintaining the reliability of the electrical contact on repeated firing seems a very difficult task as the surface of the contact within the breech assembly would rapidly become fouled and eroded by combustion products. As a comparatively high voltage would be required, debris contamination of the insulating material would rapidly reduce the system reliability.

The capacitive method of electrical coupling is shown in Fig 16a. Coupling is achieved at high frequency between an insulated drive plate at the gun breech and a consumable pick-up plate in the propellant charge. To obtain the maximum electrical coupling, the largest possible electrode area should be used. Thus the breech bolt itself has to be used as the input capacitance probe and this means that an insulating obturator pad has to be developed to electrically insulate the bolt from the gun structure. The receiving electrode in the end of the charge can be a foil or metallised disc. The coupling capacity varies inversely with the charge to bolt separation. Calculation has shown that significant charge-to-breech separation distances can be tolerated by using a combination of increased input power and higher frequency. The optimum combination of these parameters needs practical investigation. However, the indications are that it should be possible to couple across moderate separation distances.

The magnetic coupling method is shown in Fig 16b. The bolt is again the most convenient point from which a magnetic field may be initiated. In order to project a magnetic field into the chamber, the bolt has to be made of a non-magnetic material. Tests were performed on a 1/7 scale model in which the bolt was manufactured from a non-magnetic austenitic stainless steel with a magnetic core of mild steel. Tests were undertaken to establish the characteristics of the energy transfer process which were then used to calculate the behaviour of the full scale system. Unless some unforeseen circumstance should alter the performance at full scale, the tests indicate that it will be very difficult to obtain sufficient energy at the igniter for charge-to-breech separations of greater than 25mm.

The electro-magnetic coupling method is shown in Fig 16c. In this system, a wave which is launched from some form of antenna in the breech, travels along the chamber which acts as a waveguide. With the waves propagating, little attenuation should be experienced provided that the frequency is suitably related to the diameter of the tube.

For typical large calibre guns the frequency will be in the range 1.6 GHz to 4 GHz. Higher frequencies are possible and could be advantageous. An antenna of the type shown in Fig 16c presents a low impedance to the generator but once matching sections are provided high launch efficiencies are possible. Initial tests with the antenna produced a transfer efficiency of 30% under some conditions. An initial estimate indicates that an input power of 2 Watts should be required which should not present too many difficulties in the frequency band under consideration. Considerable work will be required to optimise the transmit and receive antennas.

4.2 Further Assessment of Electrical Impulse Methods.

From the initial assessment it was felt that two systems looked attractive. They were electro-magnetic coupling and capacitive field coupling. Magnetic field coupling was considered to be the least attractive. Delays in obtaining hardware for capacitive field coupling tests resulted in the electro-magnetic system being the first system chosen for further study.

Work is in hand to optimise the design of the electro-magnetic launch antenna. In order to withstand the high pressures, glass ceramics are under consideration as the dielectric material which surrounds the launch antenna. A frequency of 2.05 GHz is being used with the gun chamber operating in the TM01 wave guide mode of oscillation.Slot antennas are being considered for the receiving antenna in the charge. The detailed results of this study will be reported in a later paper.

5. CONCLUSIONS.

A number of important conclusions may be drawn from the assessment work on novel ignition systems which has been carried out so far:

a. Spark ignition of heavy calibre guns has been shown to be feasible and several ceramic materials have been identified as showing promise for spark plug service which could overcome the failure problems previously experienced with spark ignition. Further advances are being sought with the encapsulation of the insulator/central electrode into a strong metal support.

b. Laser ignition of commonly used gun ignition materials has been shown to be possible and the laser parameters for reliable ignition have been established. A laser window design has been defined which offers the prospect of being able to withstand the severe gun environment without being obscured by combustion debris. When laser penetration of charge containment materials has been demonstrated, laser ignition will be alone among the systems under consideration in being "backwards compatible" with existing charge designs. This could allow laser ignition to be fitted to a system designed to fire current in-service charges and it could also be a compelling advantage when system interoperability is required.

c. From the results of the studies carried out so far electro-magnetic means of ignition shows promise.

6. REFERENCES.

1. Price, J R, unpublished ARDE Report, 1960.
2. Miles, E N, unpublished RARDE Report, 1968.
3. Henning, P S, unpublished RARDE Report, 1984.
4. Tuck, D, unpublished IRD Report, 1981.
5. Henning, P S,unpublished RARDE Report, 1984.
6. Fitz, P J, unpublished Marconi Report, 1980.
7. Fitz, P J, unpublished Marconi Report, 1984.
8. Henning, P S, unpublished RARDE Report, 1982.

7. ACKNOWLEDGEMENTS.

The authors wish to acknowledge the assistance of several colleagues in carrying out this work. Mr D Tuck of International Research and Development Co Ltd (Newcastle upon Tyne) for the work on laser ignition. Mr P Fitz of Marconi Research Laboratories (Chelmsford) for the work on electrical impulse ignition.

SPARK IGNITION CONCEPT

Fig. 1

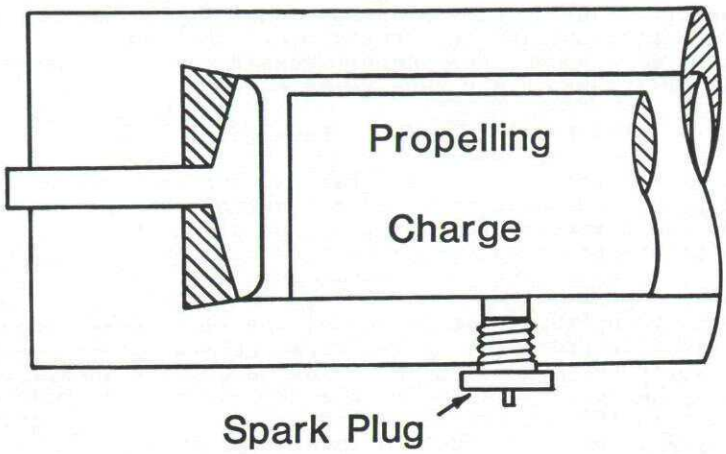

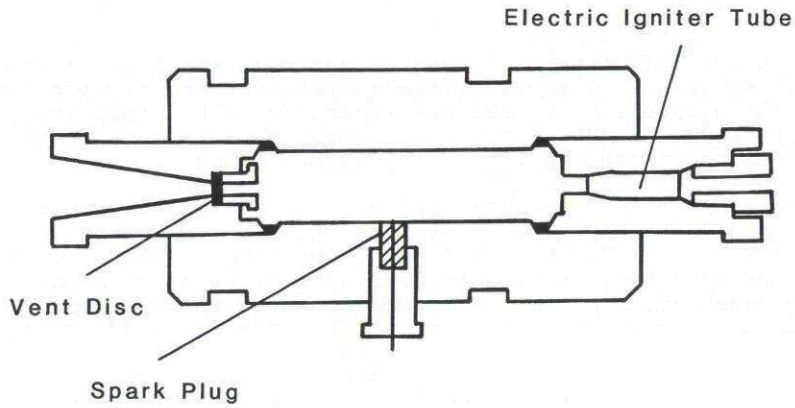

Fig. 2

VENTED VESSEL GUN SIMULATOR

EXPERIMENTAL SPARK PLUGS

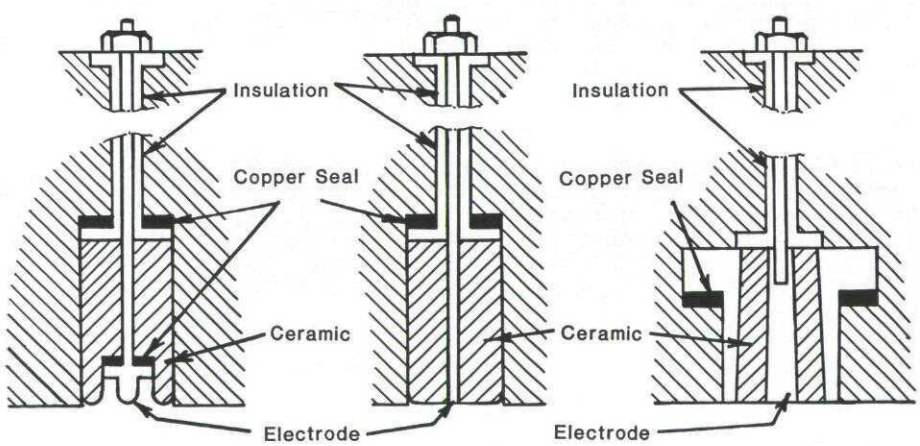

Fig. 3

a. Multipiece Spark Plug

b. Glass Ceramic Spark Plug

c. Composite Spark Plug

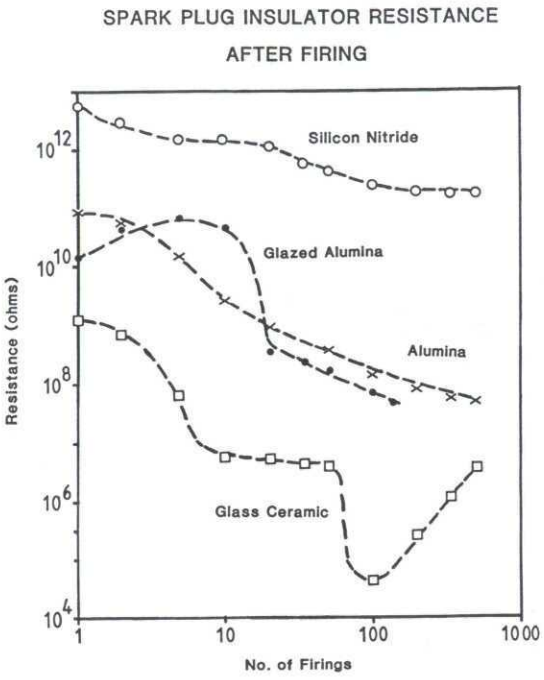

Fig. 4

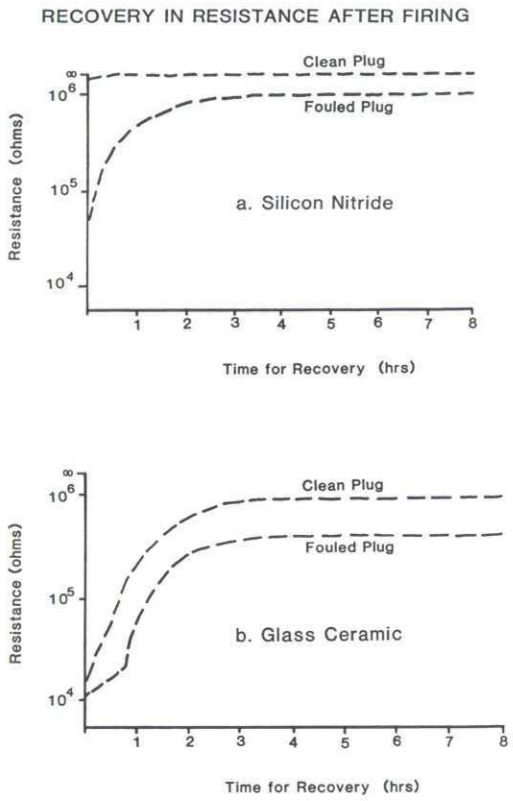

Fig. 5

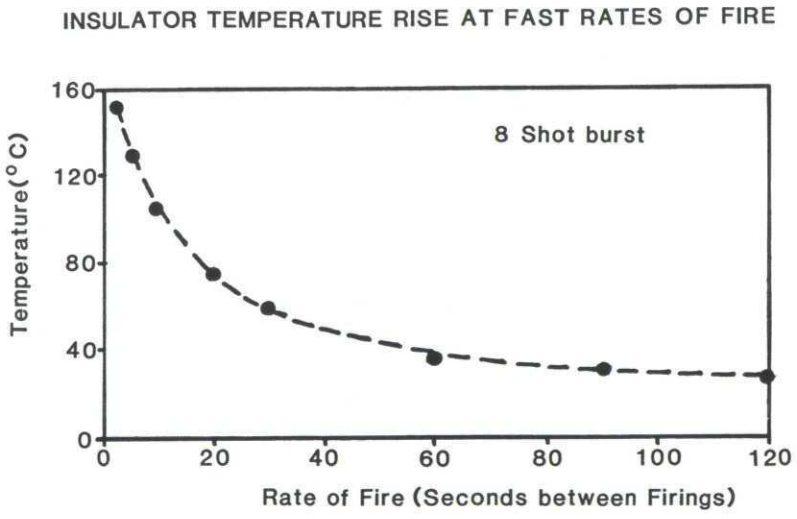

Fig. 6

LIGHT ATTENUATION OF SAPPHIRE

CONTAMINATED BY COMBUSTION PRODUCTS

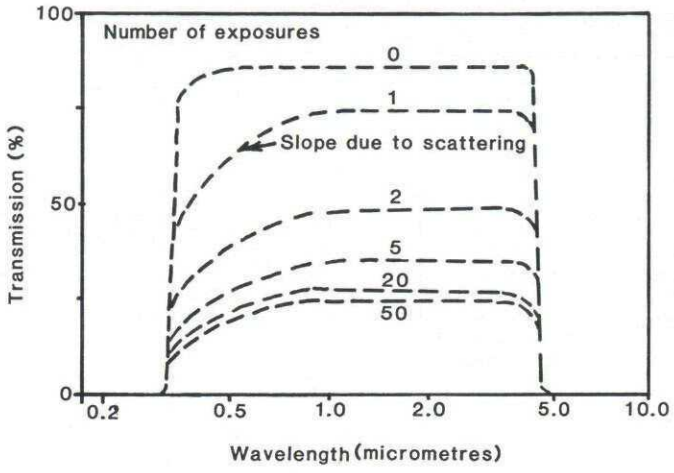

Fig. 7

LASER IGNITION SYSTEM LAYOUT

Fig. 8

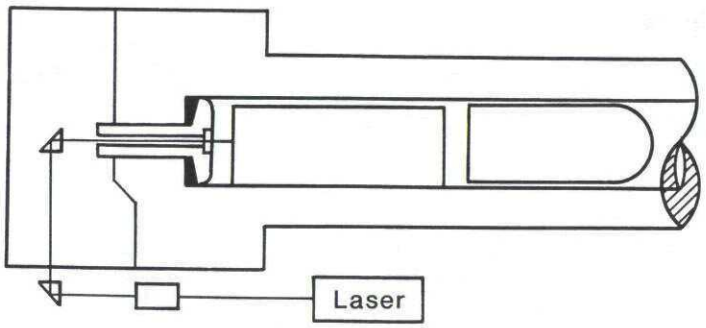

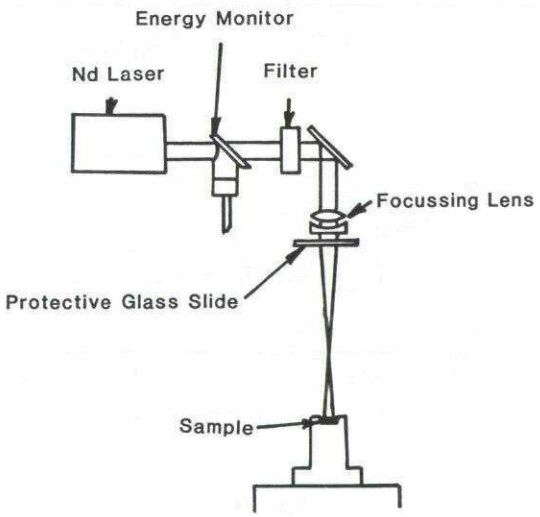

Fig. 9

SCHEMATIC OF LASER IGNITION APPARATUS

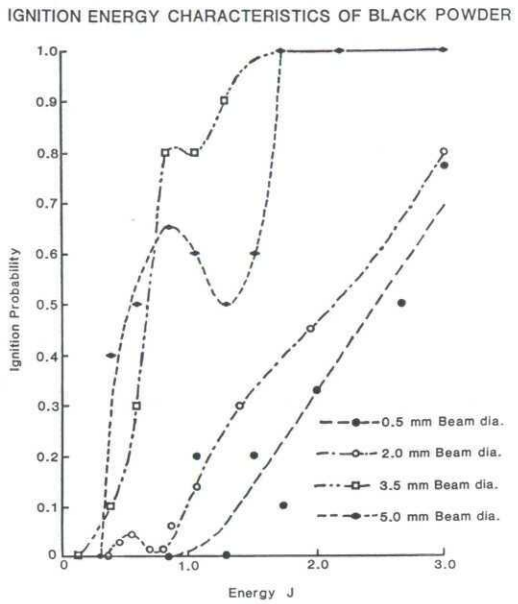

Fig. 10

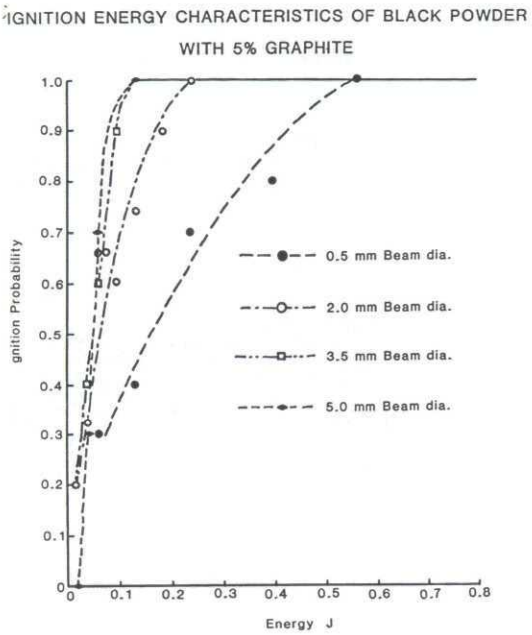

Fig. 11

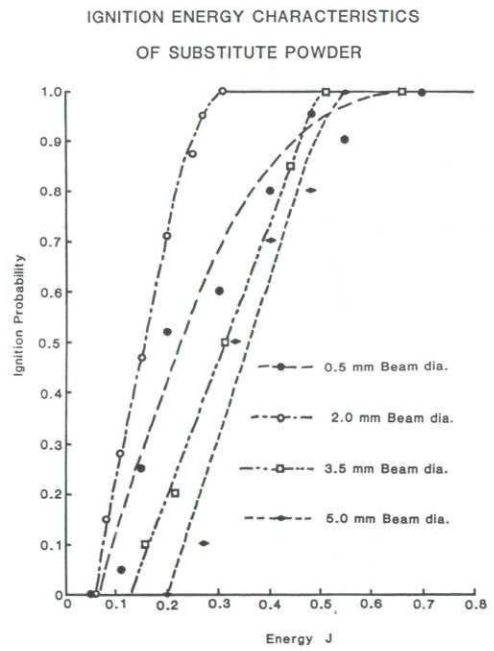

Fig. 12

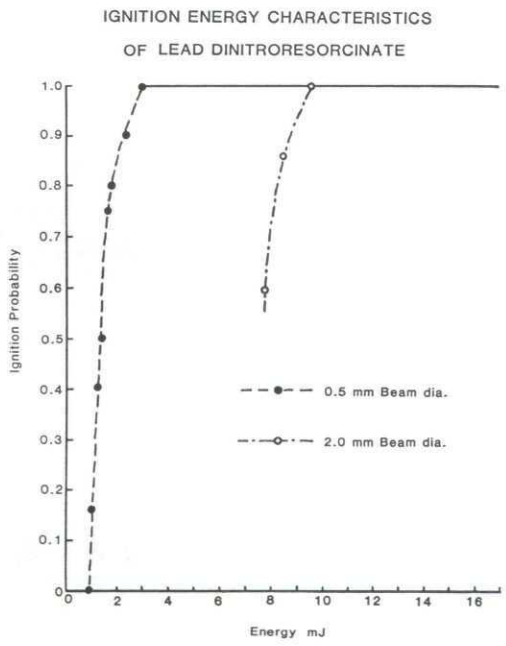

Fig. 13

LASER WINDOW LAYOUT

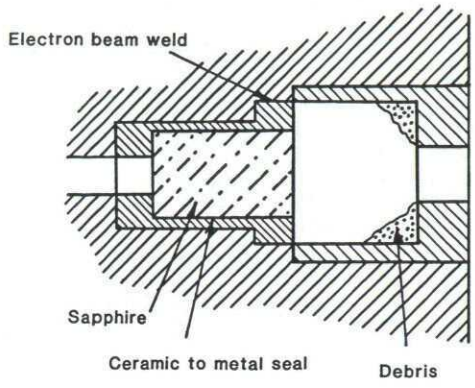

Fig. 14

LIGHT ATTENUATION OF SAPPHIRE
WHEN PROTECTED BY A DEBRIS TRAP

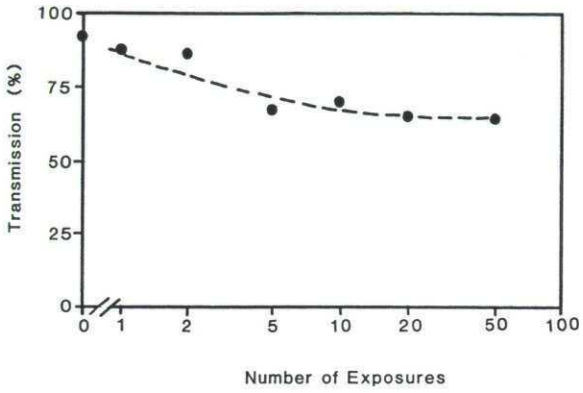

Fig. 15

ELECTRICAL IMPULSE IGNITION SYSTEM

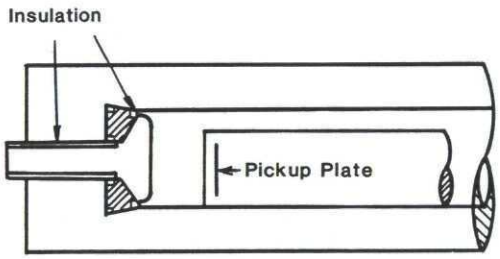

a. Capacitive Coupling

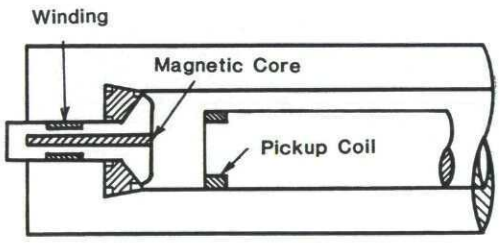

b. Magnetic Coupling

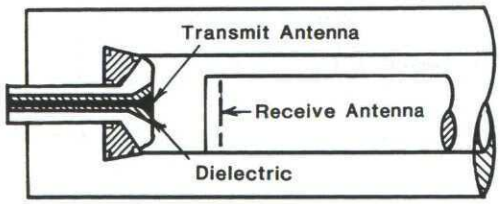

c. Electromagnetic Coupling

Fig. 16

IGNITION OF HIGH-PERFORMANCE GUN AMMUNITION

by
Dr. Horst Penner
Head, R+D-Dept. Ammunition

Dynamit Nobel AG
Kronacher Str. 63
8510 Fuerth

Germany

S u m m a r y

Modern high-performance cartridges are designed for high loading densities of propelling charges. Sometimes they exceed the normal filling density of the propellant grains. This paper discusses the conditions for fast and complete ignition and presents a new group of primers for 105 mm-rounds which will ignite the propelling charge in an optimum manner.

L e g e n d

a	:	Thermal conductivity of propellant
c	:	Specific heat of propellant
$\dot{q}$	:	Heat flow
t	:	Time
x	:	Unidimensional path coordinate
α	:	Heat transmission coefficient; primer ignition fumes - propelling charge
Δ	:	Laplace operator
$\partial/\partial t$	:	Partial differential operator
ϑ	:	Temperature
ϑ_o	:	Temperature of primer ignition fumes
ϑ_{amb}	:	Initial temperature of propellant
ϑ_s	:	Temperature of propellant surface
λ	:	Thermal conductivity of propellant
ϱ	:	Propellant density
τ	:	$= \frac{\alpha^2}{\varrho c \lambda} \cdot t$
Φ	:	Gaussian error function

I n t r o d u c t i o n

Propelling charges of any type of ammunition have always been ignited by the flash of a priming charge. In the course of historical developments ranging from the flintlock rifle to intercontinental ballistic missiles, this principle has not changed much except that ignition systems have become more effective and more complex. It is therefore amazing that the very definition of the ignition process has not yet been possible on the basis of a standard formula. For this reason, this paper establishes the following thesis:

> "The ignition of a propelling charge is to be understood as a process in which the propellant surface is heated to a temperature at which the propellant molecules may be thermally decomposed and the decomposed molecule fractions recombine as they release thermal energy. The ignition process is completed when the propellant burns under steady conditions, i.e. if the recombination energy is sufficient to maintain the propellant surface at the decomposition temperature!"

In order to meet these requirements, an ideal primer must be designed to

- produce hot matter (primer proper) [step 1]
- transfer this matter to the propellant [step 2]
- distribute this matter throughout the propelling charge [step 3]
- heat the propellant surface up to the decomposition temperature [step 4]

- and maintain the propellant surface at this temperature until sufficient recombination energy is available.

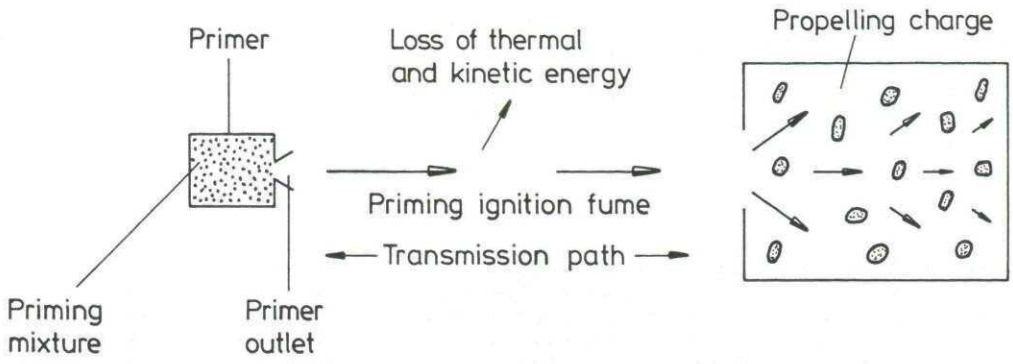

Thus the ignition process is essentially a problem of unsteady thermodynamics.

The ignition process

The discussion of the individual process steps should best be started in step 4, i.e. heating of the propellant surface. For the unidimensional case of a semi-infinite propellant layer, this process in the propellant interior is described by means of the differential equation of unsteady thermal conduction:

$$\Delta \vartheta_{(x,t)} - \frac{1}{a} \cdot \frac{\partial \vartheta_{(x,t)}}{\partial t} = 0 \qquad (1)$$

This differential equation cannot be solved without initial and marginal conditions. The initial condition is easy to identify. At the beginning of the ignition process, the entire propelling charge is at ambient temperature [ϑ_{amb}], whereas the temperature of the hot primer ignition fumes prevails in the area forward of the propellant [ϑ_o], 2400 K for example.

Definition of the marginal conditions requires a greater amount of simplification. Let us assume that it is permissible to apply the Newton statement for the heat flow,

$$\dot{q} = \alpha \cdot \left(\vartheta_o - \vartheta_s \right) \qquad (2)$$

where α is to describe the heat transmission coefficient of a hot gaseous medium to a solid (propellant) wall.

The solution would then be as follows:

$$\vartheta_{(x,t)} = \left(\vartheta_o - \vartheta_{amb}\right) \cdot \left\{ 1 - \Phi\left(\frac{\alpha x}{2\lambda\sqrt{\tau}}\right) - e^{\left(\frac{\alpha x}{\lambda} + \tau\right)} \cdot \left[1 - \Phi\left(\frac{\alpha x}{2\lambda\sqrt{\tau}} + \sqrt{\tau}\right)\right]\right\} \qquad (3)$$

Using experimental and theoretical numbers, the solution can be represented graphically as shown below. However, the solution is limited to gaseous primer ignition fumes only.

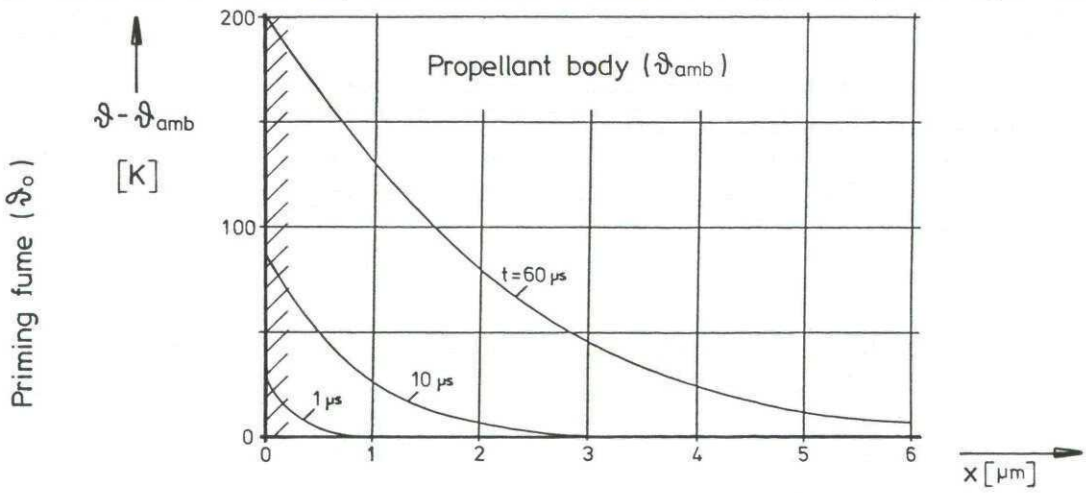

Without going into details at this point, the solution can be interpreted as follows:

- The time phase required to heat the propellant surface to the necessary decompotion temperature of appr. 470 K for nitrocellulose propellants is about 60 µs.

- During this time phase, a propellant layer of appr. 6 µm thickness is heated.

- The pulse thermal power transmitted during the heating process is about 100 MW for the propelling charge of a tank gun!

These considerations alone clearly illustrate the extreme functional requirements to be met by a primer. Considerable thermal power must be generated and transferred during very short periods of time. At the same time, time-dependent functioning must be controlled with precision.

However, before the heating process of the propellant can start, the primer ignition fumes should be distributed in the propelling charge (step 3). It stands to reason that this condition in gaseous primer ignition fumes can hardly be distinctly seperated from the propellant heating phase. It should be remembered that, due to the boundary layer characteristic of heat transmission from the primer ignition fumes to the propellant, there is a strong dependence on the flow velocity, which has the effect that the propellant is heated not after but during the distribution of the primer ignition fumes in the propelling charge. This dependence on the heat transmission rate is the reason why primer ignition fumes with high gas content cannot ignite a propelling charge with time and local constancy. Propellant grains located at a greater distance from the primer are always ignited by such fumes later and also more slowly because, in addition to a lower propagation rate, there are also temperature losses due to cooling such that the fume temperature and heat transmission will be lower for more distant propellant grains.

All efforts to achieve uniform distribution of primer ignition fumes with high gas content in the propelling charge in terms of time and location are bound to fail because of the physical properties of the propelling charge. It should be taken into account that the propelling charge represents a considerable flow resistance for the primer ignition fumes which increases with increasing density of the propellant granules in the cartridge case (choke). This results in pressure gradients in the direction of flow such that the propellant is subjected to a mechanical compression load. The propellant grain will break up under extreme conditions. It will no longer burn in accordance with the laws of predetermined grain geometry. As a consequence, there are erratic pressure increases of the propelling gas which, in turn, may furthermore increase the pressure gradients to explosive or detonative conditions similar to a chain reaction.

In addition to these choking effects, the propellant - particularly at the primer nozzle, where the fume flow rate is particularly high, is subjected to erosion. In those areas, heating of the propellant becomes impossible, because surface layers are eroded away even before or during the heating process such that the remaining propellant body remains cool. It is only after a considerable reduction in the fume flow rate deeper inside the propelling charge that ignition conditions are restored. However, the eroded propellant material may by that time have undergone a detonative reaction similar to a dust explosion.

In order to avoid these effects, a reduction in flow velocities would initially seem like a conceivable approach. Of course, the ignition process would then slow down because of the slower heat transmission from the ignition fumes to the propellant. But not only that! As you know, the propelling charge (in conventional types of ammunition) is placed in a sealed container. During the ignition process, the container is filled with the primer ignition fumes and the pressure goes up. This pressure, however, acts against the flow and decelerates the propagation rate. The heat transmission is thus reduced and the ignition process slowed down. This effect increases in intensity with decreasing availability of free volume for gas propagation, i.e. with closely packed propellant or high charge density.

In extreme cases, the ignition process is diminished to such an extent until the primer has burned out such that there can be no further convective heating of the propellant surface take place. In these cases, the propellant will only "smolder". The result is the formation of an explodable gas-air mixture which may detonate even after an extended period of time and so can cause erratic pressure rises.

These facts are not new. Consequently, primers which generate mainly gaseous fumes are rare or unpopular in practical applications.

The following conclusions can therefore be drawn for primers producing hot gaseous fumes:

- They are not suitable for a uniform ignition of propelling charges in terms of location and time.

- Critical (high) pressure conditions cannot be excluded with high loading densities of propellant.

- The optimal range between high- and low-vivacity ignition is extremely limited.

Conditions with primer ignition fumes of low gas content are more favourable. In those cases, the significance of the gases is more or less limited to the role of a transfer medium for hot particles (e.g. slag) and condensable vapours (e.g. reaction products of low boiling point). They heat the propellant surface through direct contact between the condensed particles. The boundary layer characteristic of heat transmission is now of subordinate significance. The problems involved with the local distribution of the particles in the propelling charge nevertheless remain.

Conclusion:

- Time-dependent control of an ignition process is facilitated if the primer ignition fumes contain condensed or (more favourable) condensable portions.

The second process step of the ignition model includes the fume transfer to the propelling charge. The transfer medium is the hot gas generated by the primer. At the same time, it is also partially an ignition energy carrier. This dual function of the primer ignition fumes now has the effect that all thermal and flow losses during transfer at the same time weaken the ignition effect, with the weakening effect increasing with increasing gas content of the fumes. The amount of the energy loss also depends on the design of the cartridge. It is difficult to estimate its magnitude. However, since the functional characteristics of the ignition process are determined by the amount of these losses, they should be kept at a low level and - above all - regular and uniform.

All of these effects are determined by the primer itself (step 1). It produces hot matter which ignites the propellant and at the same time generates the flow medium required to carry the energy to the propelling charge. Furthermore, it determines the initial pressure level in the propelling charge and thus regulates its burning rate and therefore the maximum gas pressure level and barrel time. Heavy demands are placed on uniformity; these demands increase with increasing performance requirements for the cartridge. In this respect, normal primers with casted priming mixtures have a few drawbacks:

- The flame temperature of most primer ignition fumes is too low
- The flow rate of the igniting fumes is too high
- The primer interior pressure is too high
- The time-dependent pattern of the generated quantity of matter is too irregular
- The mass ratio of permanent gases and condensed or condensable reaction products is not optimal
- The reaction times are not optimal

Primer of new design

DYNAMIT NOBEL has now developed by order of the german BWB a new series of primers, the DM 102 series, which has been significantly improved with respect to these characteristics. They are suitable for tank main gun ammunition with consolidated propellant charges and particularly qualified for ammunition with upgraded performance.

Their design characteristics are:

- High-energy priming mixture based on boron and potassiumnitrate. The flame temperature of this pyrotechnic mixture runs up to 2.483 K (calculated for a pressure of 50 bars) and is therefore appr. 500 degrees above the flame temperature of normal black powder. Furthermore, the content of permanent gases is low; in fact, it is only 9% compared to 39% for black powder. The greatest advantage of the ignition mixture, however, is considered to be its high proportion of condensable reaction elements, of which more than 72% are available in vapour form at the temperature of the isobar flame. The reason why the ignition energy is particularly high lies in the fact that the heat of the condensable elements, condensed on the propellant surface, can be utilized for heating up the propellant. By comparision, black powder contains only about 9% condensable elements, but 52% particles already condensed and therefore capable of acting on the propellant in only small areas. (See following list).

Thermodynamic data for primer mixture
(Calculated for 50 bar pressure)

Type of primer mixture	Flame temperature	Permanent gas content	Condensed elements	Condensable elements
Black powder Y 593	1.994 K	39.2 %	52.1 %	8.7 %
Primer mixture 953 (Bor/KNO_3)	2.483 K	9.0 %	18.8 %	72.2 %

- Defined burning behaviour of priming mixture in the priming charge. This characteristic has been achieved by using geometrically exact molded bodies from the priming mixture. They are torus-shaped pellets stacked on top of one another like columns in the primer housing. They are burning in layers similar to the solid grains of a propelling charge. Their burning characteristic is therefore slightly degressive but considerably less than with loosely packed grains of usual priming mixtures. A reduction in degressive burning behaviour considerably reduces the danger inherent in the time interval between heating of the propellant surface and the delayed initiation of the propellant flame formation. In this time interval, when the time curve of the ignition energy often undergoes a sharp decline, the heat transmission to the propellant surface is not sufficient to maintain the surface temperature. This results in extinction conditions causing irregular gas pressure curves and, in extreme situations, carbonization gas deflagration.

- The pressure in the primer housing is extremely low. The peak pressure is below 60 bars if the primer burns in the atmosphere. The values for different types of known primers are several times as high. Through design action, the pressure reduction is achieved by the relatively small surface of the primer mixture pellets and low confinement. The natural confinement of the pellet column is also reduced by a castellated design of the stacked-up pellets such that the fumes can escape without hindrance. The low pressure also reduces the discharge velocity from the primer housing. The problem of propellant erosion and associated dust explosions as well as excessive mechanical compression by the pressure gradient in the propelling charge is greatly reduced. The primer has been tested without any difficulty even in triple-based propellants which are susceptible to brittle fracture at low temperatures.

- The primer ignition fumes have a long range of effectiveness and a particularly homogeneous distribution in the propelling charge. Both characteristics are due to the high proportion of condensable reaction products and the low interior pressure. It should be recognized that cooling of the fumes as a result of expansion when leaving the primer outlet is on the one hand drastically reduced by the low interior pressure, whereas these and other cooling losses are on the other hand offset by continuous condensation of fume elements.

- Local homogeneity of the ignition is supported by the internal structure of the primer which is empty inside the pellet column. The whole column is therefore almost simultaneously ignited by the flame of the primary ignitor, i.e. time and local fluctuations of the escaping fumes are very low both in a circumferential and axial direction. The homogeneity of the ignition process manifests itself in a slightly increased efficiency of the fired projectile. Due to the good homogeneity of the ignition, the unfavourable thermodynamic conditions of propellant not simultaneously set on fire will have been reduced to normal conditions towards the end of the propellant burning process only. As compared with a primer of standard design, it will be possible to either increase projectile velocities or reduce propellant weight and/or peak gas pressure.

- Further design characteristics:

  Watertightness of complete primer housing.

  Beyond this, insensitivity of burning characteristics of priming mixture to humidity.

  Compatibility with electromagnetic hazards of battlefield

  Design of the sealing plug screw as to permit trouble-free ignition of complex charge configurations, particularly with projectile tail sections fitted with guidance fins and inserted in the propelling charge.

[For primer drawing see next page]

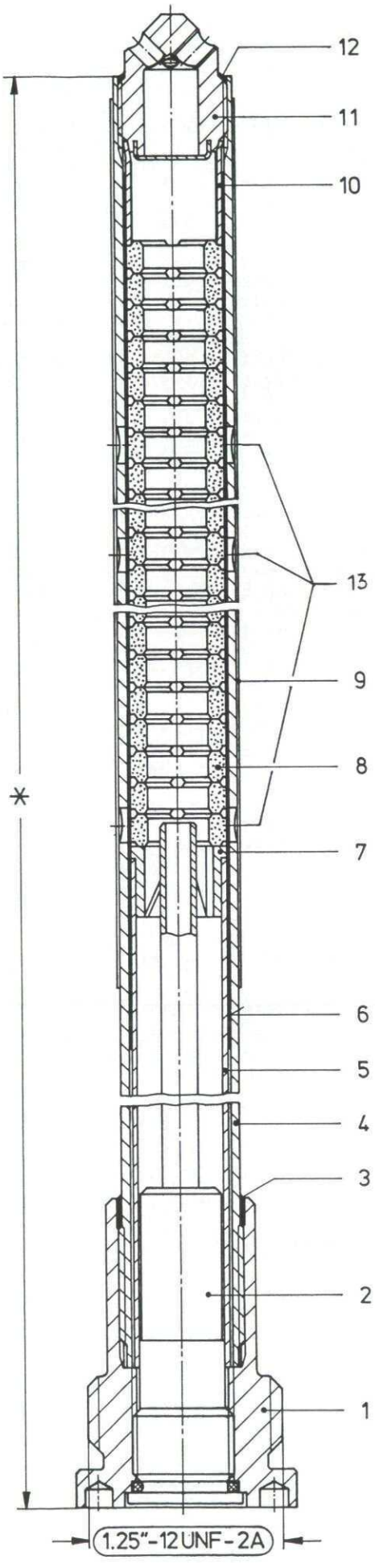

*

For cartridge 105mmx617, DM 33
length 365 mm

For cartridge 105mmx617, DM 68
length 317 mm

For cartridge 105mmx617, DM 23
length 379 mm

L e g e n d

13: Vent holes

12: Sealing

11: Closing screw

10: Spacer (2)

9: Heat-shrinkable tubing (2)

8: Priming mixture pellets

7: Centering device

6: Heat-shrinkable tubing (1)

5: Spacer (1)

4: Primer tube

3: Sealing

2: Primary igniter

1: Primer body

DISCUSSION

P.Ramette, Fr

You have indicated that the new primers developed by Dynamit Nobel are based on boron and potassium nitrate. Could you indicate the percentage of each of these components?

Author's Reply

The percentages of ingredients are about 70 percent boron and 30 percent potassium nitrate and a small amount of binder (polyurethane).

COMBUSTION SOUS HAUTES PRESSIONS CONFRONTATION THEORIE-EXPERIENCE

D. GRUNE, M. SAMIRANT

Institut Franco-Allemand de Recherches de Saint-Louis (ISL)
Rue de l'Industrie 68301 SAINT-LOUIS, France

Résumé

A la suite d'un important désaccord (30-50%) constaté entre les valeurs théoriques et expérimentales au cours de la mesure de la pression de combustion de poudres jusqu'à 1500 MPa nous avons entrepris une confrontation des techniques expérimentales entre plusieurs laboratoires. Les résultats de ces mesures étant comparables,nous avons étudié l'influence de la composition des gaz de combustion. Cette composition s'est révélée conforme à la théorie. Nous avons alors mesuré la déformation de la bombe manométrique au cours du tir. Complétée par une variation probable du covolume à haute pression cette déformation permet d'expliquer les importants écarts enregistrés. Ces résultats sont applicables à toutes les bombes manométriques.

I - Introduction

Les canons futurs à hautes performances exigent des propergols capables de développer des pressions élevées tout en conservant l'intégrité de leurs propriétés mécaniques et physico-chimiques. Pour s'assurer d'un comportement prévisible jusqu'à des pressions de 700 à 800 MPa, il convient d'étendre la gamme des mesures expérimentales jusqu'à 1000 MPa. L'ISL a développé une bombe manométrique capable de travailler de façon routinière jusqu'à 1000 MPa et permettant de nombreux essais jusqu'à 1500 MPa (fig. 1). Après mise au point de l'appareil et de sa chaîne de mesure, il a été utilisé systématiquement avec la plupart des poudres classiques [1] ainsi qu'avec des poudres à base de nitramines fabriquées à l'ISL [2]. A partir de la mesure piézoélectrique de la variation de la pression en fonction du temps sont calculés les paramètres habituels des poudres: force, vitesse de combustion, vivacité dynamique, exposant adiabatique de pression... L'équation d'état utilisée est celle du viriel. Simultanément, l'ICT présentait des résultats de calculs de pression de combustion déduits de données de la physique fondamentale. Là comparaison théorie-expérience faisait apparaître un important désaccord.

II - Désaccord théorie-expérience

Sur la base des valeurs mesurées avec la bombe, l'équation d'état des gaz de combustion peut être exprimée, entre 300 et 1000 MPa,par une équation du viriel à trois termes. A partir de la composition chimique de la poudre, en utilisant des fonctions potentielles du type Lennard-Jones, l'ICT calcule les deuxième et troisième termes de l'équation du viriel [3, 4]. La comparaison des résultats obtenus pour une poudre GB Pa 125/05 conduit à des valeurs expérimentales inférieures de 30% vers 1000 MPa et de 50% vers 1500 MPa aux valeurs théoriques. Les causes de ces écarts peuvent être nombreuses, et l'ensemble des résultats théoriques a été confirmé au cours d'une collaboration avec le LLNL [5] par l'utilisation de modèles de calcul différents qui ont fourni des valeurs semblables. Les erreurs expérimentales peuvent provenir de la non-linéarité des capteurs piézoélectriques utilisés dans les gammes de pressions élevées. On peut également soupçonner la composition réelle des gaz de combustion au cours d'un tir et enfin le comportement mécanique de la bombe. L'ISL a alors lancé un programme de travail pour élucider cette différence. Les pertes de chaleur aux parois n'ont pas été envisagées, leur influence ayant déjà fait l'objet d'études systématiques.

III - Campagne d'essais comparatifs

Trois laboratoires, le BICT, l'ETBS et l'ISL ont entrepris une série de mesures de pression dans la gamme 400 à 650 MPa avec des bombes de conception et de volume variables (200, 400 et 700 cm^3) et une série de capteurs de différentes origines: Kistler, AVL, Brosa, utilisés successivement par chaque laboratoire qui conservait sa chaîne de mesure propre et sa méthode habituelle d'étalonnage. Tous les tirs étaient effectués à partir d'un même lot de poudre BTu 85. Les résultats sont parfaitement comparables, et les écarts pour chaque densité de chargement tombent à l'intérieur du domaine d'incertitude probable. Même dans ce domaine de pressions modérées l'écart entre théorie et expérience reste important, variant de 13% pour 350 MPa à 17% pour 600 MPa. Les résultats complets de ces essais sont publiés sous la référence [6].

IV - Etude de la compositon des gaz de combustion

L'analyse des gaz est effectuée par spectroscopie de masse et chromatographie après détente des produits de combustion dans une enceinte sous vide. Lors des premiers essais, cette détente avait lieu à travers une tuyère de faible section. La température de figeage obtenue était de 1500 à 1700 K, et l'énorme érosion de cette tuyère apportait des perturbations évidentes à la compositon du mélange, tant par réaction chimique avec les produits d'ablation que par combinaison à la surface des particules solides.

Afin de réduire cette érosion, la section d'écoulement a été augmentée d'un facteur 225 en utilisant une membrane de rupture en acier dont la pression d'ouverture est réglée par l'épaisseur (fig. 2). La durée de détente est réduite de ± 1 s à 0,8 ±/ms et il n'y a plus d'érosion notable. La température de figeage atteint 2000 K. Les figures 3 et 4 montrent les résultats obtenus, en bonne conformité avec les calculs théoriques. L'écart le plus important se remarque sur les dérivés oxygénés; il manque environ 1% d'oxygène sous forme d'espèces gazeuses. L'estimation de la quantité de matière érodée à partir de mesures sur des tuyères de diamètre croissant, permet d'évaluer la quantité d'oxygène fixée en particulier sous forme de Fe_2O_3. Cette correction faite, l'accord théorie-expérience est excellent et ces phénomènes ne permettent pas d'expliquer les écarts de pression relevés.

V - Etude du comportement de la bombe

Le seul paramètre pouvant être encore mis en cause est le comportement mécanique de la bombe. Ce phénomène a été étudié en dernier lieu, car la méthode habituelle de définition des bombes manométriques en calculant la tension dans chaque couche métallique, était considérée comme fiable. Cependant, un calcul simplifié proposé par J. KURY du LLNL [5] montrait que si une partie du métal avait un comportement élasto-plastique on obtenait une variation de volume expliquant largement les erreurs de mesure. Nous avons repris à l'ISL un calcul complet de la déformation de la bombe en contrainte triaxiale avec un comportement élastique pur et obtenu une variation de volume importante mais inférieure à la précédente; la figure 5 résume les trois hypothèses possibles. Pour trancher entre ces possibilités nous avons calculé, dans les divers cas, le déplacement d'un point de la paroi de la bombe situé dans une des ouvertures de mesure bouchée par une pièce en acier pour la circonstance et mesuré le déplacement de ce même point par vélocimétrie laser Doppler. La figure 6 décrit la méthode utilisée. Le vélocimètre ISL [6, 7] permet, grâce à une correction asservie à la longueur d'onde instantanée de l'émission laser, de mesurer des vitesses très faibles. Les résultats sont reportés sur la figure 7; ils confirment l'hypothèse du comportement élastique. Les variations de volume correspondantes y sont sont, également indiquées. Ce comportement qui se retrouve pour toutes les bombes manométriques, doit donc être pris en compte dans les mesures à très haute pression.

VI - Discussion des résultats

Après correction de la variation de volume des bombes au cours des essais comparatifs, il reste une différence de 8% entre la théorie et l'expérience (fig. 8). Le tableau I rassemble les résultats des mesures et ceux de calculs effectués au BRL [9]. Les valeurs de pression de la première ligne sont calculées avec les valeurs standards des rayons moléculaires, celles de la seconde ligne avec une variation de 3% de ces rayons. Il nous apparaît hautement probable qu'une telle variation est réelle; des études sont en cours à l'ISL pour le vérifier grâce à des propergols fournissant des gaz à deux composants, ce qui simplifie les calculs théoriques.

VII - Conclusion

La prise en compte du comportement mécanique des bombes à haute pression est maintenant intégrée à nos protocoles de mesures des caractéristiques des poudres. Remarquons néanmoins que lors des mesures de routine seule la pression maximale est fortement altérée par cette déformation. La figure 9 montre les écarts entre les valeurs calculées et celles mesurées pour une poudre hypothétique de force f = 1 MJ/kg et avec un covolume η = 1 cm^3/g. Dans le domaine courant, 300 à 600 MPa, les erreurs sur ces derniers paramètres ne dépassent pas quelques pour-cent et sont inférieures à l'incertitude des mesures.

Bibliographie

[1] D. GRUNE, W. DANIELS, F. VINCENT
ISL - Rapport technique RT 506/80, (1980)

[2] D. GRUNE
ISL - Rapport CO 203/83, (1983)

[3] F. VOLK, H. BATHELT
Propellants and Explosives 1, p. 7 - 14, (1976)

[4] F. VOLK (ICT)
Communication personnelle

[5] J. KURY (LLNL)
Communication personnelle

[6] D. GRUNE
ISL - Rapport CR 84/3-5, (1984)

[7] G. SMEETS, A. GEORGE
J. Phys. E: Sci. Instrum., Vol. 14, p. 38-45, (1981)

[8] G. SMEETS, G. MATHIEU
ISL - Rapport R 123/83,(1983)

[9] E. FREEDMAN (BRL)
Communication personnelle

		Pression en fonction de la densité de chargement			
		0,301 g/cm³	0,338 g/cm³	0,374 g/cm³	0,410 g/cm³
Pressions calculée (MPa)	Rayon moléculaire Standard	422,5	496,2	573,3	656,2
	97% du rayon Standard	409,3	478,8	551,2	628,7
Pressions	mesurées (MPa)	403,4	470,5	543,5	627,4

Tableau I: Comparaison des pressions mesurées et calculées

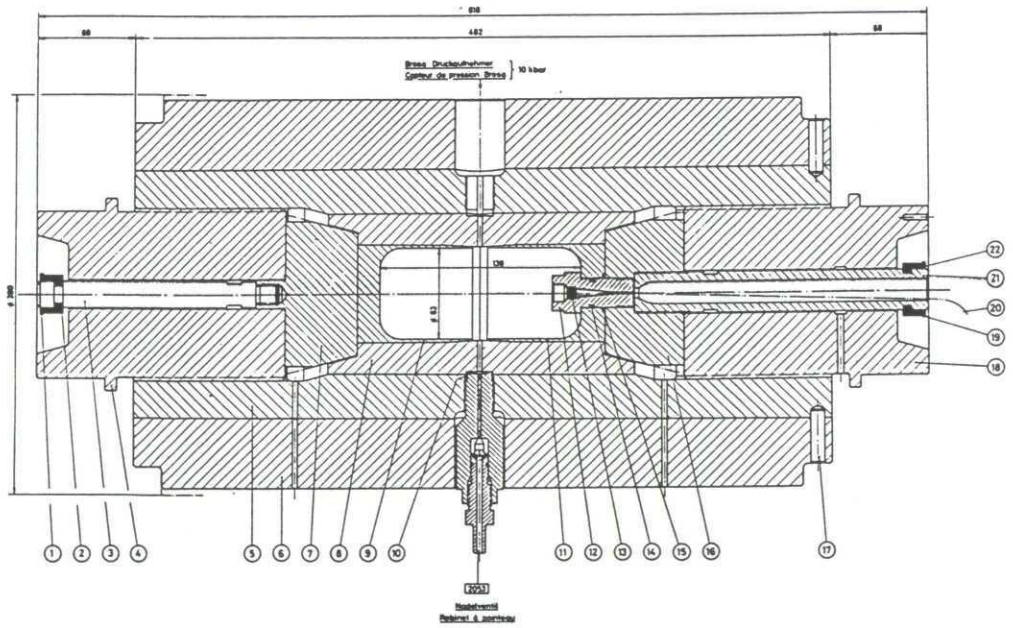

Fig. 1: Bombe haute pression (Type ISL, 400 cm³, 10 000 bar)
Dessin d'ensemble et de principe

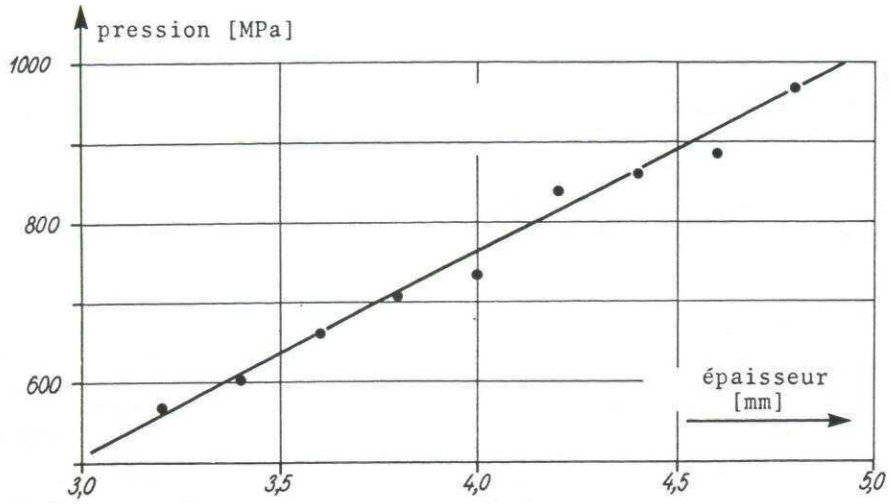

Fig. 2: Pression maximale en fonction de l'épaisseur de la membrane

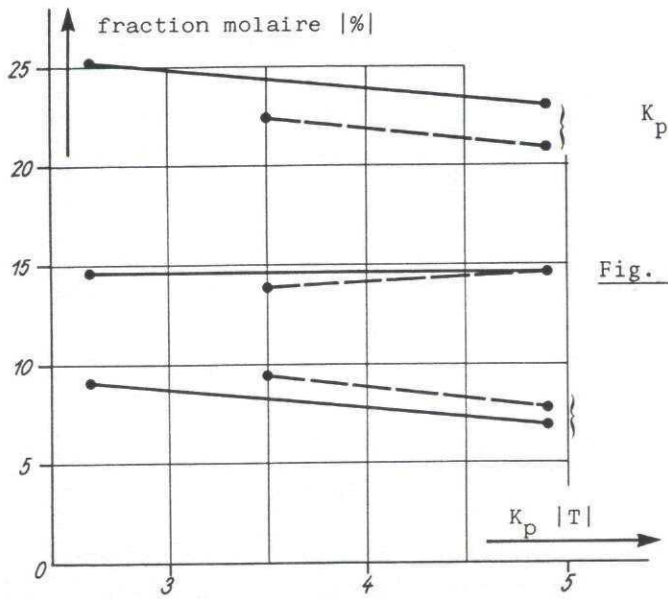

$$K_p[T] = \frac{[H_2O] \times [CO]}{[H_2] \times [CO_2]}$$

Fig. 3: Fraction molaire de CO_2 N_2 et H_2 après combustion de GB Pa 125 trait continu calculs ICT, trait interrompu mesures ISL

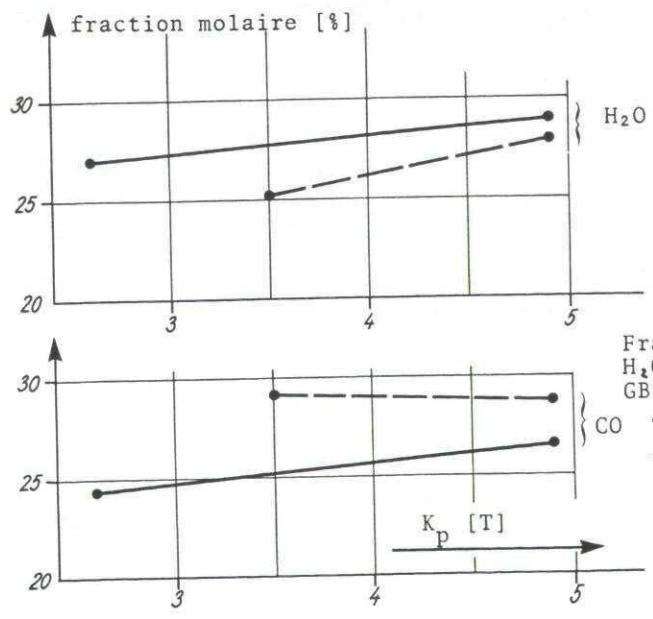

Fig. 4

Fraction molaire de CO et H_2O après combustion de GB Pa 125.

Trait continu: calculs ICT

Trait interrompu: mesures ISL

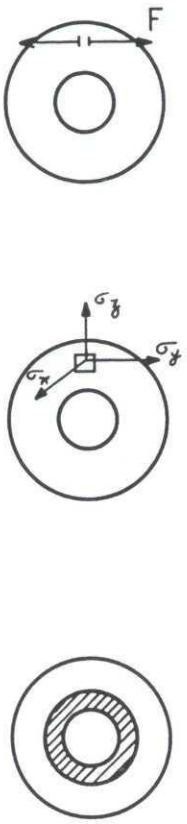

Fig. 5: Trois comportements possibles de la bombe
1 classique $\Delta V = 2\%$
2 élastique $\Delta V = 5\%$
3 plastique $\Delta V = 15\%$
pour p = 7 kbar

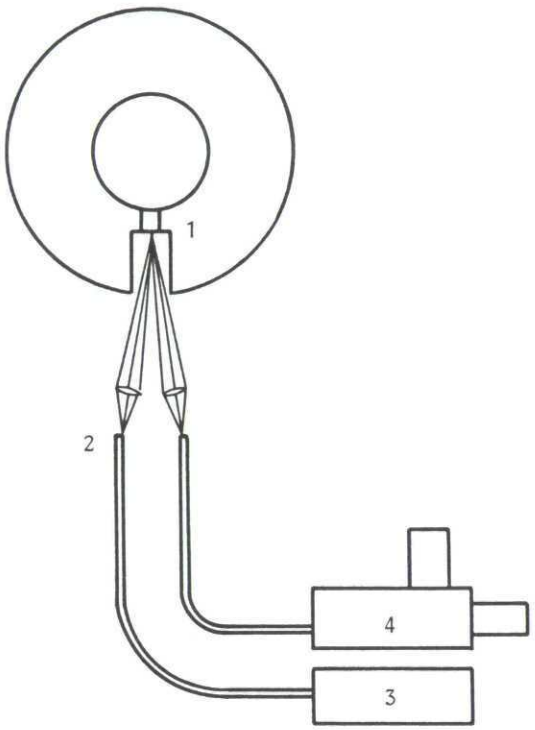

Fig. 6: Mesure de la variation de volume de la bombe par vélocimétrie laser Doppler
1 point de mesure
2 fibres optiques
3 laser
4 vélocimètre

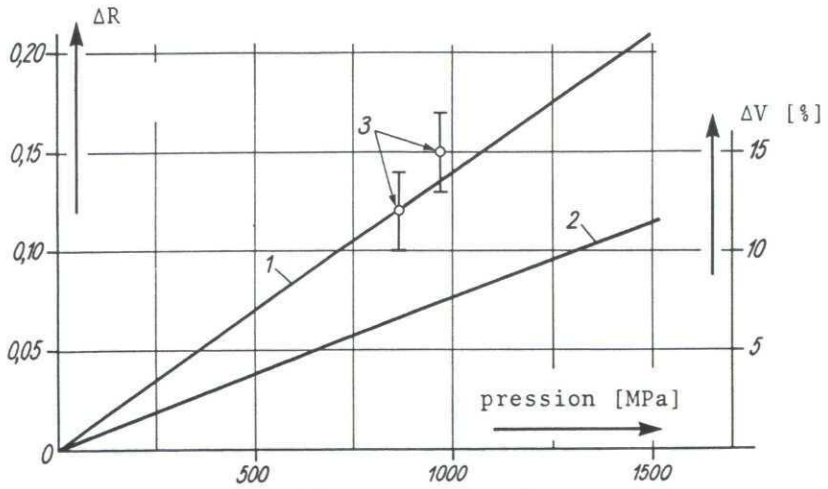

Fig. 7: Variation des dimensions de la bombe en fonction de la pression
1 variation de R calculée
2 variation de V calculée
3 mesures de R

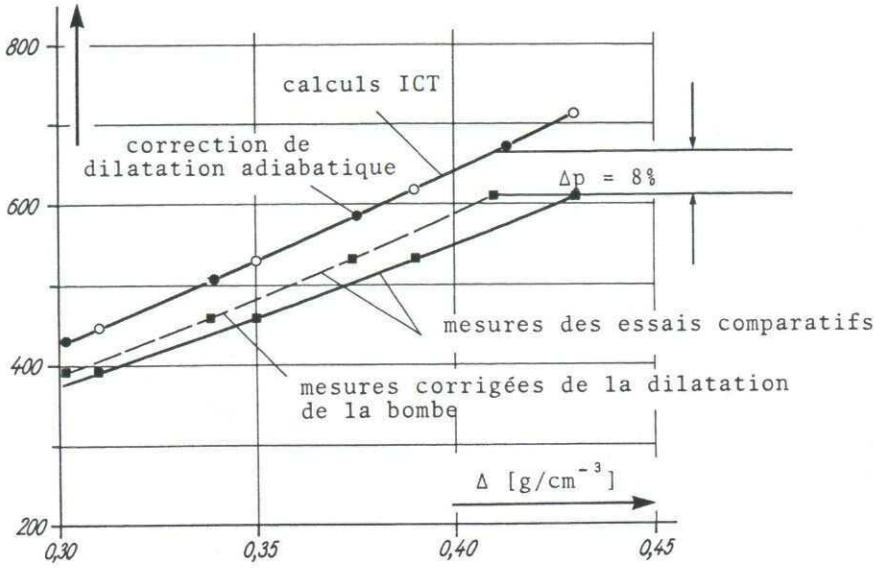

Fig. 8: Pression en fonction de la densité de chargement (BTu 85)

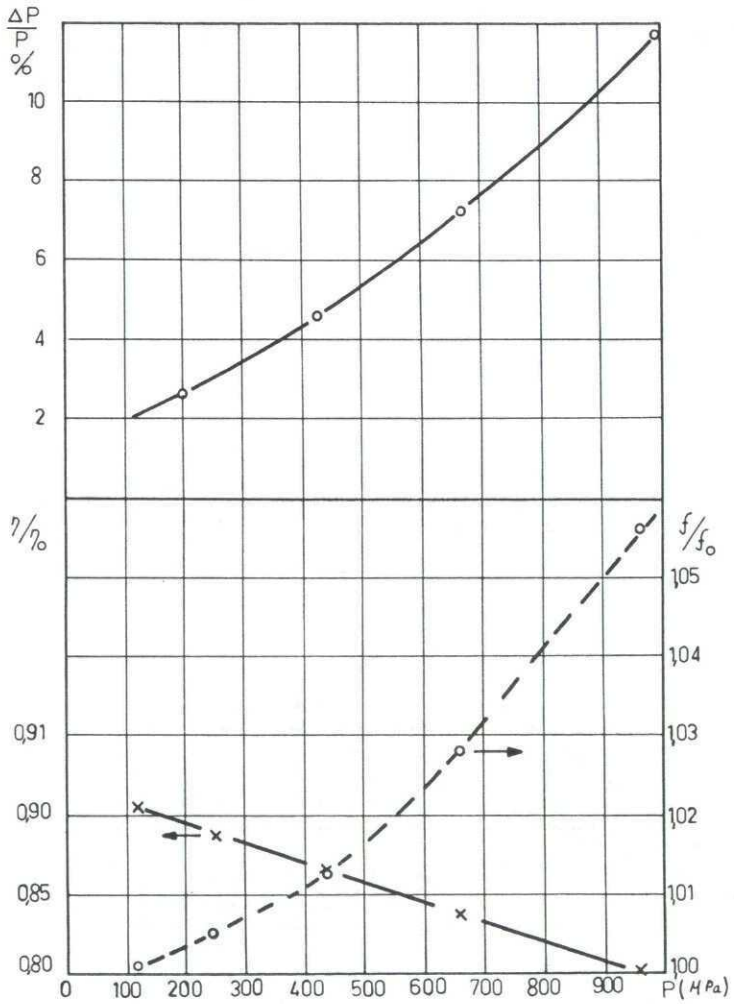

Fig. 9: Erreur entraînée par la variation de volume de la bombe sur la mesure de différents paramètres: pression p, covolume η force f

DISCUSSION

M.Summerfield, US

As the authors say, there is a major discrepancy between the measured pressure of a closed chamber firing and the theoretically predicted value. They say that, in seeking an explanation, the principal unresolved question was whether the bomb volume expanded sufficiently at 100—200 kpsi to explain the lower pressure measured. They claim that the volume of a typical bomb can expand by as much as 15 per cent at a pressure of 100 kpsi, and presumably, the dimensions would return to their original values afterward, that is there would be no deformation. It is difficult to understand such a large volume expansion. If we assume that a bomb can be represented as a thick-walled sphere, and that the tensile stress of the inner surface is perhaps 30 kpsi (a conservative designer would not want much more), then the linear stretch of the inner surface would be 0.1 per cent for steel, and so the volume would expand by only 0.3 per cent. Indeed, their geometry is not a sphere, and the wall stress I assumed might be too conservative by a factor of two. But the authors claim 15 per cent. Can they explain the difference between my value and theirs? Theirs seems much too large.

Author's Reply

As can be seen from Figure 7, the increase in volume at 1000 MPa is only 7.5 per cent. This increase comprises radial and axial extension (change in diameter = 3.19 per cent; change in length of pressure bomb = 1.06 per cent).

The high pressure bomb is a multi-layer shrinking construction with great hardness (interior liner: R = 160 daN per square mm) and only allows the application of the high pressures at still elastic deformation. In a distance of 54 mm from the axis of the pressure bomb and at a load of 1000 MPa, a difference in the radius of 0.14 mm is calculated. At this point, the measurement showed 0.15 ± 0.02 mm. These data can also be taken from Figure 7.

REPORT DOCUMENTATION PAGE

1. Recipient's Reference	2. Originator's Reference	3. Further Reference	4. Security Classification of Document
	AGARD-CP-392	ISBN 92-835-0388-0	UNCLASSIFIED

5. Originator Advisory Group for Aerospace Research and Development
North Atlantic Treaty Organization
7 rue Ancelle, 92200 Neuilly sur Seine, France

6. Title INTERIOR BALLISTICS OF GUNS

7. Presented at the Propulsion and Energetics Panel 66th (B) Specialists' Meeting, held in Florence, Italy 9—10 September 1985.

8. Author(s)/Editor(s)	9. Date
Various	January 1986
10. Author's/Editor's Address	**11. Pages**
Various	222

12. Distribution Statement This document is distributed in accordance with AGARD policies and regulations, which are outlined on the Outside Back Covers of all AGARD publications.

13. Keywords/Descriptors

Ballistics
Grain behaviour
Guns
Gun Barrel
Ignition of gun propellants
Liquid propellant guns
Solid gun propellants
Triple-base powder

14. Abstract

The Conference Proceedings contains 16 unclassified papers.

The Technical Evaluation Report, and an Introduction by the Programme Committee Chairman, are included at the beginning of the Proceedings. Questions and answers of the discussions follow each paper. The Specialists' Meeting was arranged into the following sessions: Overview (1); Liquid Propellant Guns (3); Characteristics of Solid Gun Propellants (3); Gun Barrel Erosion (3); Low Vulnerability Propellants for Guns (2); Experimental and Test Techniques in Interior Ballistics (5); Gun Ignition Systems (2); New Problems in Guns (1); and Travelling Charge Gun Theory (1).

The meeting was intended to provide research scientists, development engineers and application specialists with a broad overview of advancing technology and experimental techniques in interior ballistics of liquid and solid propellant guns. The achievements were discussed in the Technical Evaluation Report, in which several conclusions were also drawn and recommendations made for future explorations.

AGARD Conference Proceedings No.392
Advisory Group for Aerospace Research and Development, NATO
INTERIOR BALLISTICS OF GUNS
Published January 1986
222 pages

The Conference Proceedings contains 16 unclassified papers presented at the Propulsion and Energetics 66th (B) Specialists' Meeting on Interior Ballistics of Guns, which was held 9—10 September 1985 in Florence, Italy.

The Technical Evaluation Report, and an Introduction by the Programme Committee Chairman, are included at the beginning of the Proceedings. Questions and answers of the discussions follow each paper. The Specialists'

P.T.O.

AGARD-CP-392

Ballistics
Grain behaviour
Guns
Gun barrel
Ignition of gun propellants
Liquid propellant guns
Solid gun propellants
Triple-base powder

AGARD Conference Proceedings No.392
Advisory Group for Aerospace Research and Development, NATO
INTERIOR BALLISTICS OF GUNS
Published January 1986
222 pages

The Conference Proceedings contains 16 unclassified papers presented at the Propulsion and Energetics 66th (B) Specialists' Meeting on Interior Ballistics of Guns, which was held 9—10 September 1985 in Florence, Italy.

The Technical Evaluation Report, and an Introduction by the Programme Committee Chairman, are included at the beginning of the Proceedings. Questions and answers of the discussions follow each paper. The Specialists'

P.T.O.

AGARD-CP-392

Ballistics
Grain behaviour
Guns
Gun barrel
Ignition of gun propellants
Liquid propellant guns
Solid gun propellants
Triple-base powder

AGARD Conference Proceedings No.392
Advisory Group for Aerospace Research and Development, NATO
INTERIOR BALLISTICS OF GUNS
Published January 1986
222 pages

The Conference Proceedings contains 16 unclassified papers presented at the Propulsion and Energetics 66th (B) Specialists' Meeting on Interior Ballistics of Guns, which was held 9—10 September 1985 in Florence, Italy.

The Technical Evaluation Report, and an Introduction by the Programme Committee Chairman, are included at the beginning of the Proceedings. Questions and answers of the discussions follow each paper. The Specialists'

P.T.O.

AGARD-CP-392

Ballistics
Grain behaviour
Guns
Gun barrel
Ignition of gun propellants
Liquid propellant guns
Solid gun propellants
Triple-base powder

AGARD Conference Proceedings No.392
Advisory Group for Aerospace Research and Development, NATO
INTERIOR BALLISTICS OF GUNS
Published January 1986
222 pages

The Conference Proceedings contains 16 unclassified papers presented at the Propulsion and Energetics 66th (B) Specialists' Meeting on Interior Ballistics of Guns, which was held 9—10 September 1985 in Florence, Italy.

The Technical Evaluation Report, and an Introduction by the Programme Committee Chairman, are included at the beginning of the Proceedings. Questions and answers of the discussions follow each paper. The Specialists'

P.T.O.

AGARD-CP-392

Ballistics
Grain behaviour
Guns
Gun barrel
Ignition of gun propellants
Liquid propellant guns
Solid gun propellants
Triple-base powder

Meeting was arranged into the following sessions: Overview (1); Liquid Propellant Guns (3); Characteristics of Solid Gun Propellants (3); Gun Barrel Erosion (3); Low Vulnerability Propellants for Guns (2); Experimental and Test Techniques in Interior Ballistics (5); Gun Ignition Systems (2); New Problems in Guns (1); and Travelling Charge Gun Theory (1).

The meeting was intended to provide research scientists, development engineers and application specialists with a broad overview of advancing technology and experimental techniques in interior ballistics of liquid and solid propellant guns. The achievements were discussed in the Technical Evaluation Report, in which several conclusions were also drawn and recommendations made for future explorations.

ISBN 92-835-0388-0

Meeting was arranged into the following sessions: Overview (1); Liquid Propellant Guns (3); Characteristics of Solid Gun Propellants (3); Gun Barrel Erosion (3); Low Vulnerability Propellants for Guns (2); Experimental and Test Techniques in Interior Ballistics (5); Gun Ignition Systems (2); New Problems in Guns (1); and Travelling Charge Gun Theory (1).

The meeting was intended to provide research scientists, development engineers and application specialists with a broad overview of advancing technology and experimental techniques in interior ballistics of liquid and solid propellant guns. The achievements were discussed in the Technical Evaluation Report, in which several conclusions were also drawn and recommendations made for future explorations.

ISBN 92-835-0388-0

Meeting was arranged into the following sessions: Overview (1); Liquid Propellant Guns (3); Characteristics of Solid Gun Propellants (3); Gun Barrel Erosion (3); Low Vulnerability Propellants for Guns (2); Experimental and Test Techniques in Interior Ballistics (5); Gun Ignition Systems (2); New Problems in Guns (1); and Travelling Charge Gun Theory (1).

The meeting was intended to provide research scientists, development engineers and application specialists with a broad overview of advancing technology and experimental techniques in interior ballistics of liquid and solid propellant guns. The achievements were discussed in the Technical Evaluation Report, in which several conclusions were also drawn and recommendations made for future explorations.

ISBN 92-835-0388-0

Meeting was arranged into the following sessions: Overview (1); Liquid Propellant Guns (3); Characteristics of Solid Gun Propellants (3); Gun Barrel Erosion (3); Low Vulnerability Propellants for Guns (2); Experimental and Test Techniques in Interior Ballistics (5); Gun Ignition Systems (2); New Problems in Guns (1); and Travelling Charge Gun Theory (1).

The meeting was intended to provide research scientists, development engineers and application specialists with a broad overview of advancing technology and experimental techniques in interior ballistics of liquid and solid propellant guns. The achievements were discussed in the Technical Evaluation Report, in which several conclusions were also drawn and recommendations made for future explorations.

ISBN 92-835-0388-0

AGARD
NATO OTAN
7 RUE ANCELLE · 92200 NEUILLY-SUR-SEINE
FRANCE
Telephone (1) 47.45.08.10 · Telex 610176

DISTRIBUTION OF UNCLASSIFIED AGARD PUBLICATIONS

AGARD does NOT hold stocks of AGARD publications at the above address for general distribution. Initial distribution of AGARD publications is made to AGARD Member Nations through the following National Distribution Centres.Further copies are sometimes available from these Centres, but if not may be purchased in Microfiche or Photocopy form from the Purchase Agencies listed below.

NATIONAL DISTRIBUTION CENTRES

BELGIUM
Coordonnateur AGARD — VSL
Etat-Major de la Force Aérienne
Quartier Reine Elisabeth
Rue d'Evere, 1140 Bruxelles

CANADA
Defence Scientific Information Services
Dept of National Defence
Ottawa, Ontario K1A 0K2

DENMARK
Danish Defence Research Board
Ved Idraetsparken 4
2100 Copenhagen Ø

FRANCE
O.N.E.R.A. (Direction)
29 Avenue de la Division Leclerc
92320 Châtillon

GERMANY
Fachinformationszentrum Energie,
Physik, Mathematik GmbH
Kernforschungszentrum
D-7514 Eggenstein-Leopoldshafen

GREECE
Hellenic Air Force General Staff
Research and Development Directorate
Holargos, Athens

ICELAND
Director of Aviation
c/o Flugrad
Reyjavik

ITALY
Aeronautica Militare
Ufficio del Delegato Nazionale all'AGARD
3 Piazzale Adenauer
00144 Roma/EUR

LUXEMBOURG
See Belgium

NETHERLANDS
Netherlands Delegation to AGARD
National Aerospace Laboratory, NLR
P.O. Box 126
2600 AC Delft

NORWAY
Norwegian Defence Research Establishment
Attn: Biblioteket
P.O. Box 25
N-2007 Kjeller

PORTUGAL
Portuguese National Coordinator to AGARD
Gabinete de Estudos e Programas
CLAFA
Base de Alfragide
Alfragide
2700 Amadora

TURKEY
Department of Research and Development (ARGE)
Ministry of National Defence, Ankara

UNITED KINGDOM
Defence Research Information Centre
Station Square House
St Mary Cray
Orpington, Kent BR5 3RE

UNITED STATES
National Aeronautics and Space Administration (NASA)
Langley Research Center
M/S 180
Hampton, Virginia 23665

THE UNITED STATES NATIONAL DISTRIBUTION CENTRE (NASA) DOES NOT HOLD STOCKS OF AGARD PUBLICATIONS, AND APPLICATIONS FOR COPIES SHOULD BE MADE DIRECT TO THE NATIONAL TECHNICAL INFORMATION SERVICE (NTIS) AT THE ADDRESS BELOW.

PURCHASE AGENCIES

Microfiche or Photocopy
National Technical
Information Service (NTIS)
5285 Port Royal Road
Springfield
Virginia 22161, USA

Microfiche
ESA/Information Retrieval Service
European Space Agency
10, rue Mario Nikis
75015 Paris, France

Microfiche or Photocopy
British Library Lending
Division
Boston Spa, Wetherby
West Yorkshire LS23 7BQ
England

Requests for microfiche or photocopies of AGARD documents should include the AGARD serial number, title, author or editor, and publication date. Requests to NTIS should include the NASA accession report number. Full bibliographical references and abstracts of AGARD publications are given in the following journals:

Scientific and Technical Aerospace Reports (STAR)
published by NASA Scientific and Technical
Information Branch
NASA Headquarters (NIT-40)
Washington D.C. 20546, USA

Government Reports Announcements (GRA)
published by the National Technical
Information Services, Springfield
Virginia 22161, USA

Printed by Specialised Printing Services Limited
40 Chigwell Lane, Loughton, Essex IG10 3TZ

ISBN 92-835-0388-0